Interreg Euro-MED

Co-funded by the European Union

FRED

Title of document:

Preliminary data collection and processing study

Work package 1

Defining and implementing tools for wildfire prevention and mitigation

Activity 1.1

Implementation methodology

Deliverable 1.1.1

Preliminary data collection and processing study

Project full title:	Fire free MED
Mission:	Protecting, restoring and valorising the natural environment and heritage – Natural heritage
Priority:	Greener MED
Specific objective:	RSO 2.4 Promoting climate change adaptation and disaster risk prevention, resilience, taking into account eco-system-based approaches

Partner in charge: Democritus University of Thrace, School of Agricultural Science and Forestry

Partners involved: Democritus University of Thrace, School of Agricultural Science and Forestry, University of Rijeka, Faculty of Maritime Studies, Fire rescue service Sežana, Rocca di Cerere UNESCO Global Geopark, The Municipality of Ulcinj, RGO Communications Ltd., The National Park UNA, Public fire brigade of the Town of Mali Lošinj, Centre of Integrated Geomorphology for the Mediterranean Area, CIMBAL – Intermunicipal Community of Baixo Alentejo

Status: Draft

Distribution: Public

Date of production: 28.05.2024

Revision chart and history log

Author in charge	Status	Date of production
Name Surname	draft/final/N version	DD.MM.YYYY
Panteleimon Xofis	V0.1 (draft)	30.06.2024
Alexandros Timoleon	V0.1 (draft)	30.06.2024
Stavros Chatzigiovanakis	V0.1 (draft)	30.06.2024
Giuseppe Mancino	V0.2 (draft)	12.07.2024

Antonio Falciano	V0.2 (draft)	12.07.2024
Panteleimon Xofis	V0.3 (draft)	19.07.2024
Alexandros Timoleon	V0.3 (draft)	19.07.2024
Stavros Chatzigiovanakis	V0.3 (draft)	19.07.2024
Gabriele Freni	V0.3 (draft)	19.07.2024
Marcello Troia	V0.3 (draft)	19.07.2024
Marianna Gallina	V0.3 (draft)	19.07.2024
Peter Lah	V0.3 (draft)	19.07.2024
Sofia Martins	V0.3 (draft)	19.07.2024
Sara Balcazar	V0.3 (draft)	19.07.2024
Peter Lah	V0.3 (draft)	19.07.2024
Antonio Falciano	V0.4 (draft)	29.07.2024
Stavros Chatzigiovanakis	V0.5 (final)	30.07.2024
Alexandros Timoleon	V0.5 (final)	30.07.2024
Panteleimon Xofis	V0.5 (final)	30.07.2024

Table of Contents

List of Figures

List of Tables

List of abbreviations and terms

Abbreviation	Definition
API	Application Programming Interface
CDO	Climate Data Operators
CHM	Canopy Height Models
CORINE	Coordination of Information on the Environment
COSMO	Consortium for Small-scale Modeling
CS	Coordinate System
DEM	Digital Elevation Model
DTM	Digital Terrain Model
EEA	European Environment Agency
ECMWF	European Centre for Medium-Range Weather Forecasts
EFFIS	European Forest Fire Information System
FARSITE	Fire Area Simulator - model development and evaluation
FRED	Fire Free MED
FDI	Fire Danger Index
FI	Fire Intensity
FWI	Fire Weather Index
GDAL	Geospatial Data Abstraction Library
GIS	Geographical Information System
GRIB	General Regularly distributed Information in Binary form
HI	Human Index
MISTRAL	Meteo Italian Supercomputing Portal
NDVI	Normalized Difference Vegetation Index
NetCDF	NETwork Common Data Form
OBIA	Object-Based Image Analysis
PH	Pyric History Index
ROS	Rate of Spread

TIN	Triangulated Irregular Network
UAS	Unmanned Aircraft System
UTC	Coordinated Universal Time
WKT	Well-Known Text
WMO	World Meteorological Organisation
WSL	Windows Subsystem for Linux

1. Introduction

The Mediterranean area is in deep need of transnational harmonisation of tools and practices designed to monitor and manage natural disasters and risks induced by human activities, creating a common approach to preventing climate change effects, particularly fires.

In that context, the main objective of the FRED project is to implement advanced ICT/UAS (Unmanned Aircraft System) remote sensing tools for climate change adaptation, disaster risk prevention and mitigation in the wildfire segment. The project's main result will be a significant increase in the prevention capacity of relevant authorities in the most endangered fire-prone areas.

FRED involves six piloting areas in different MED countries (Croatia, Portugal, Slovenia, Italy, Bosnia and Herzegovina and Montenegro.) It indirectly connects stakeholders/beneficiaries through capitalising results and subsequent transferring of the specific, efficient and pragmatic tools for wildfire prevention and mitigation that will be implemented in this project. This is why, this deliverable- Capitalization paper – lessons learnt from past projects- is of vital importance for the successful development of the project.

The paper includes methodologies, tools and synergies from different projects already implemented by some of the partners in the consortium.

2. Purpose of the document

This document is aimed at providing all the necessary details regarding the pilot areas which will be studied and analyzed for this project. The preliminary data that have been collected, are crucial for the analysis of each area and will be great help to this project. Wildfires are phenomena that occur in specific “habitats” and under specific conditions. These are primarily characterized by the availability of enough fuel to sustain a fire, the presence of ignition sources, including human activities and particular topographical futures that can either support the spread of a destructive fire or help contain and suppress it. In order for the analysis of each area to happen, it was important that the data collection was aimed at gathering information and data regarding factors which can affect wildfires. For example, Digital Elevation Models (DEM) and Canopy Height Models (CHM) were collected for each pilot area, as they can directly and indirectly be used in a wildfire analysis. Another important dataset to gather was the roads and buildings of every area, a resource that will later play an important role. Further details regarding the preliminary data collection process will be thoroughly discussed in the subsequent chapters. These chapters will provide an in-depth explanation of the methods, procedures, and techniques employed during the initial data gathering phase.

In this paper particular attention is also given into the noteworthy ecological futures of each pilot area, which are of considerable conservation importance. These locations face various risks and threats, particularly from wildfires and have also detailed pyric histories. Understanding the pyric history of each study area and using the data that occurred from these wildfires will be useful and will provide valuable insights into “where” and “when” wildfires occur. Additionally, a furthermore analysis of the pilot areas will be provided and will give various important information about each of the areas. The deliverable includes six Geo-Databases, each corresponding to one of the six pilot areas, which will aid in this planning process. The data will be classified into two categories: Remote sensing data, encompassing images obtained from Planet, Sentinel, and Landsat satellites and geospatial data, consisting of various types such as road networks, building footprints, canopy height models, aspect models, and similar datasets.

3. Pilot Areas

As previously stated, the project will concentrate on six specific regions within the Mediterranean, serving as pilot areas for our initiatives. These regions encompass the following European countries: Croatia, Slovenia, Montenegro, Bosnia and Herzegovina, Italy, and Portugal. For each region a specific selection of areas named pilot areas is made, where the project will concentrate its efforts and attention (Figure 1). The selection of these areas is strategic, allowing for a diverse representation of the Mediterranean basin and facilitating comprehensive testing and analysis of our project's methodologies and objectives across different cultural and geographical landscapes.

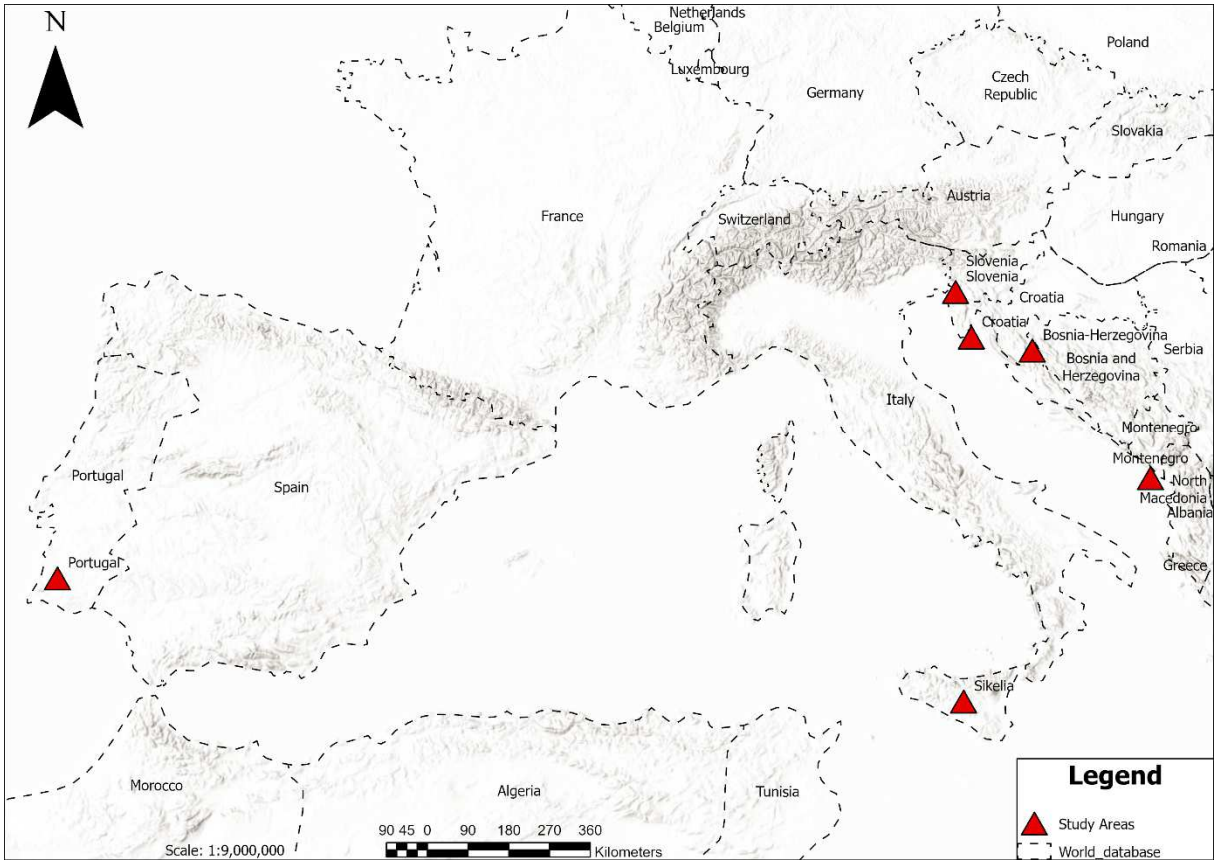

Figure 1. Map that showcases the location of the different pilot areas across Europe.

3.1. Mali Lošinj and Cres islands - Croatia

Croatia is a country situated in the northwestern part of the Balkan Peninsula and is an ecologically significant country due to its rich biodiversity and numerous protect areas. The country boasts a wide range

of diverse landscapes, featuring a long Adriatic Sea coastline with over a thousand islands. It is also home to eight national parks and 444 protected areas in general, which are encompassing 9% of the country. This project places special emphasis on the islands of Cres and Lošinj, two scenic islands situated in the northern Adriatic Sea within Croatia's Kvarner Gulf, which form the country's designated pilot area (Figure 2).

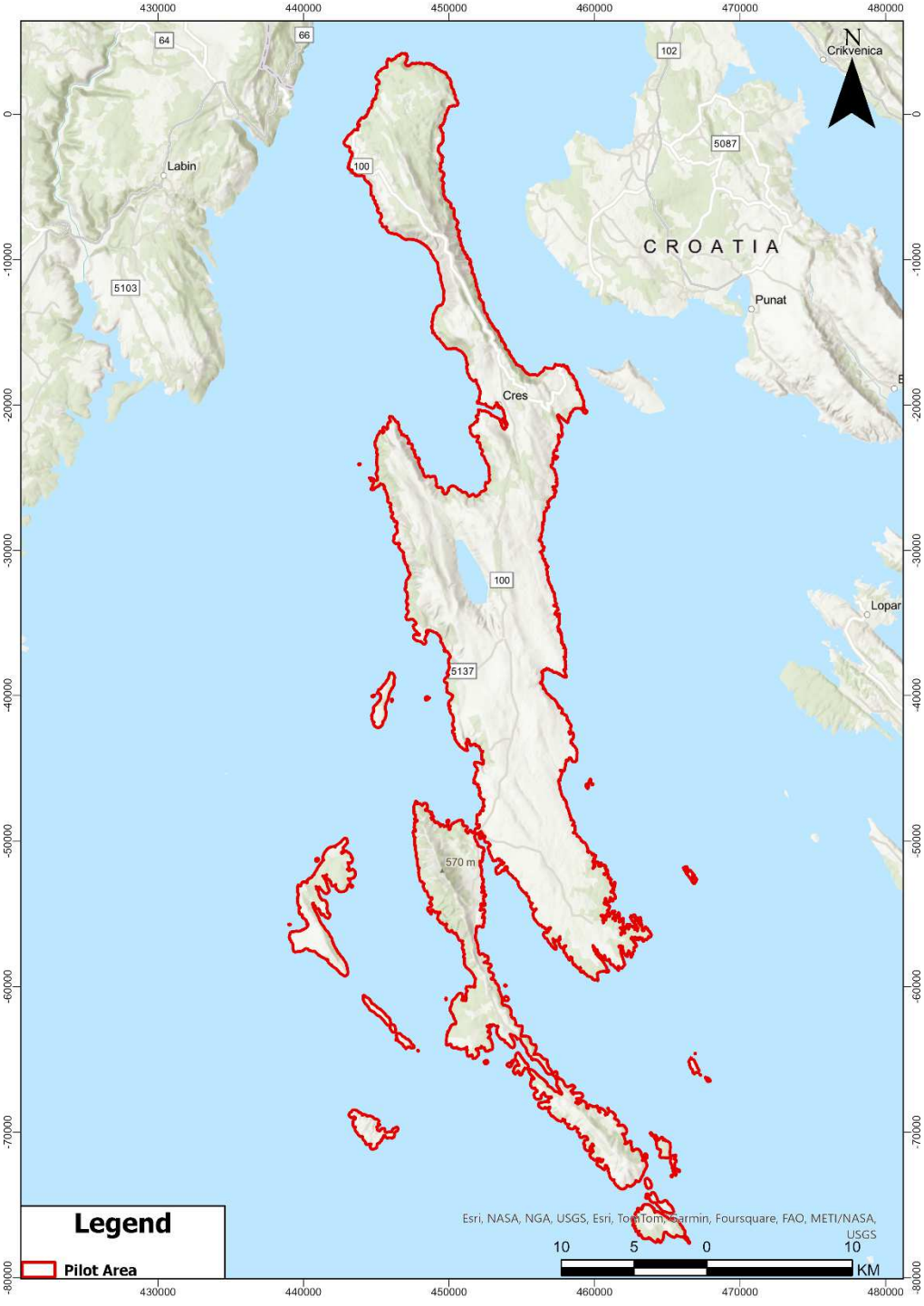

Figure 2. Pilot area of Croatia.

Regarding wildfires, Croatia experiences frequent wildfires, particularly during the hot, dry summer months. These fires are most common in the coastal and island regions where Mediterranean vegetation is prevalent. Because of the rich and complex vegetation, which consists of dense forests, dry grasslands and numerous shrubs, combined with strong winds and dry periods, the whole area is very prone to wildfires. According to the country's reports from National Fire Services (Milijenko, et al. 2023), 245 fires occurred in the country during the year 2022 which burned 24.225 ha of forest and other land owned by the Republic of Croatia and private forest owners (Figure 2). Valuable graphs are also being provided, from the analysis of which some useful information can be gathered. For Croatia it occurs that the annual average of burnt areas is around 13.600 ha (Figure 3), the annual average fire occurrences is around 248 fires (Figure 4) and the average annual fire size is around 48 ha (Figure 5).

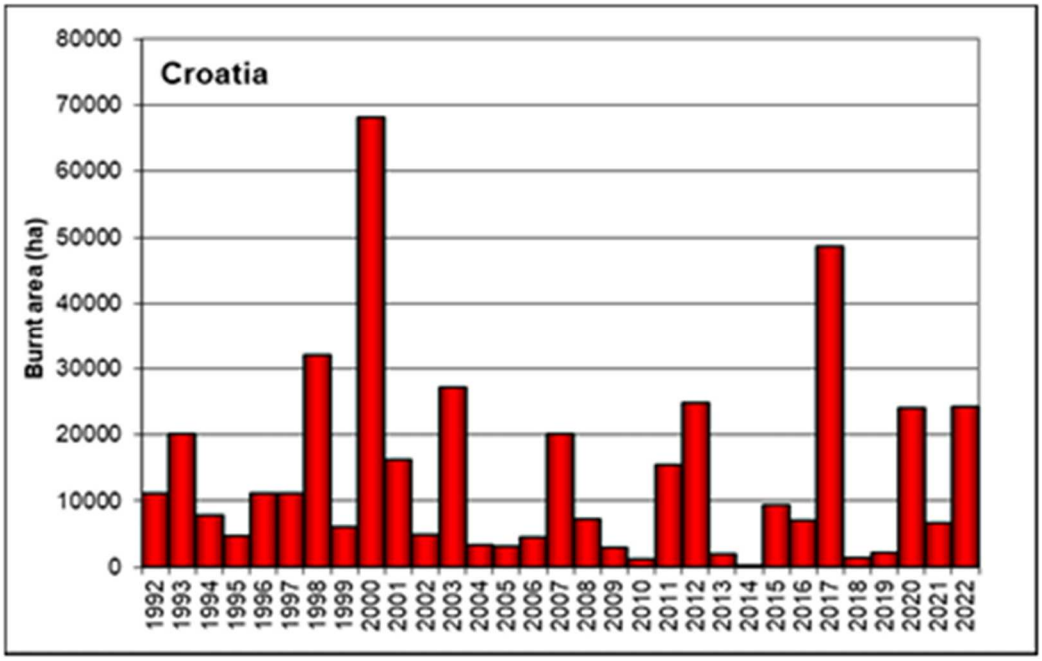

Figure 3. Annual burnt areas in Croatia based on reports from the National Fire Services for the period 1992-2022 (Milijenko, et al. 2023)

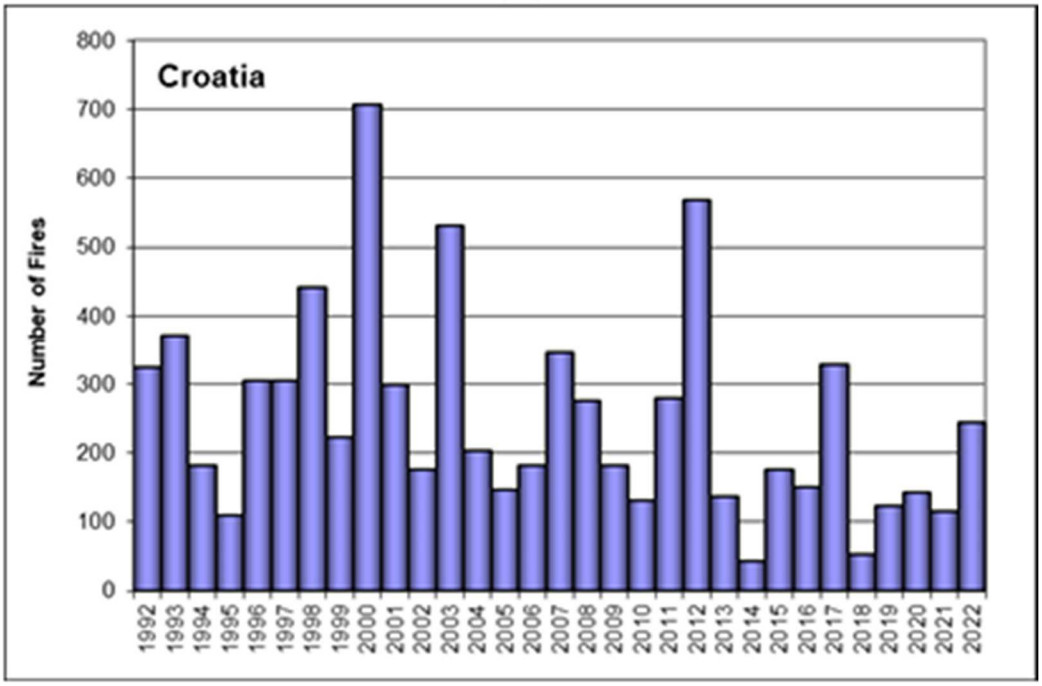

Figure 4. Annual fire occurrences in Croatia based on reports from the National Fire Services for the period 1992-2022 (Milijenko, et al. 2023).

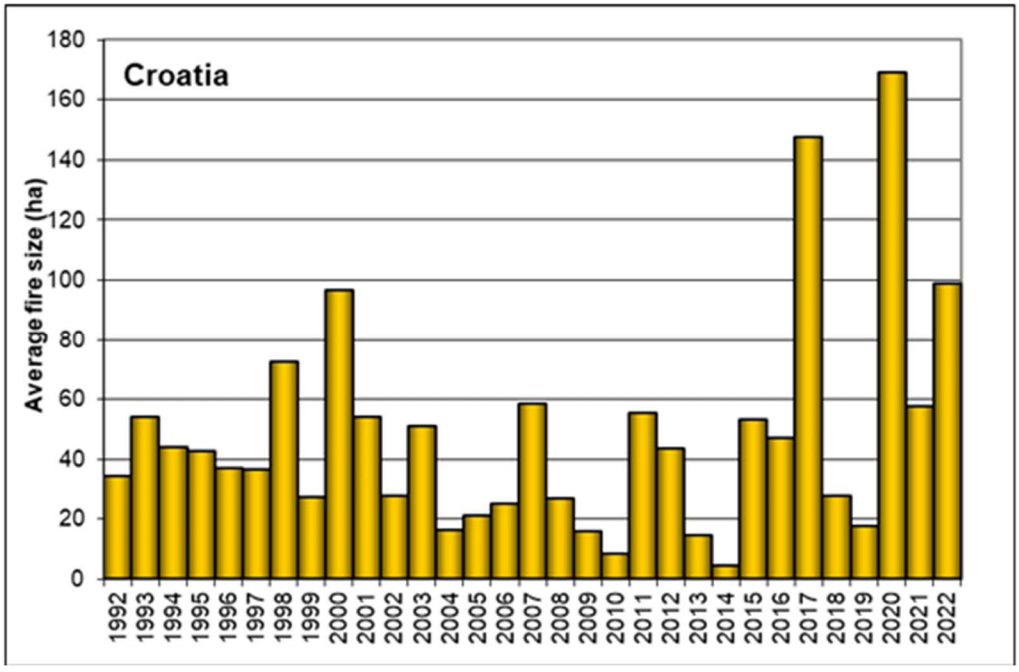

Figure 5. Annual average fire size in Croatia based on reports from the National Fire Services for the period 1992-2022 (Milijenko, et al. 2023).

3.1.1. Geographical Location and administration

The island of Cres is the larger of the two islands., characterized by its rugged terrain, dense forest and the extensive coast. It covers an area of 405,78 km^2 and reaches a maximum elevation of 650 m at Gorice. In the Southern part of the island, a canal separates the island of Cres from the island of Lošinj. The two islands are connected by a small bridge at the town of Osor. The largest settlement of the island is Cres and it consists of 2.716 people.

Regarding Lošinj, it is a significantly smaller with an area of 74,36 km^2 and it reaches a maximum elevation of 588 m at the mountain Televrin. It is the 11^{th} largest Adriatic island by area. The largest settlement of the island is Mali Lošinj with a population of 7.537 people.

3.1.2. Climatic conditions

The climatic conditions of these areas are influenced by the diverse geography, which includes mountains, plains, forests, and an extensive coastal zone. The country of Croatia is divided into two main climate regions: Mediterranean and Continental, with further variations within these zones. The meteorological dataset was generated by the CRU TS dataset, which was initially created and has since been continuously enhanced and managed through funding from various supporters, notably the UK's Natural Environment Research Council (NERC) and the US Department of Energy. Ongoing support is now facilitated by the UK National Centre for Atmospheric Science (NCAS). According to the Ombrothermic diagram which is constructed for the period 1980-2022 (Figure 6), during the summer the average temperatures of the islands Cres and Lošinj range from 21,14 °C to around 23,99 °C and the average precipitation varies from around 48,69 mm to 79,51 mm. In the winter, the average temperatures of the islands range from 6,26 °C to 7,3 °C and the average precipitation from 81,1 mm to 112,84 mm. It also occurs that the hottest month is July with a temperature of 23,99 °C and the coldest month is January with a temperature of 6,26 °C while the wettest month seems to be November with a precipitation of 145,87 mm and the driest July with a precipitation of 48,69 mm.

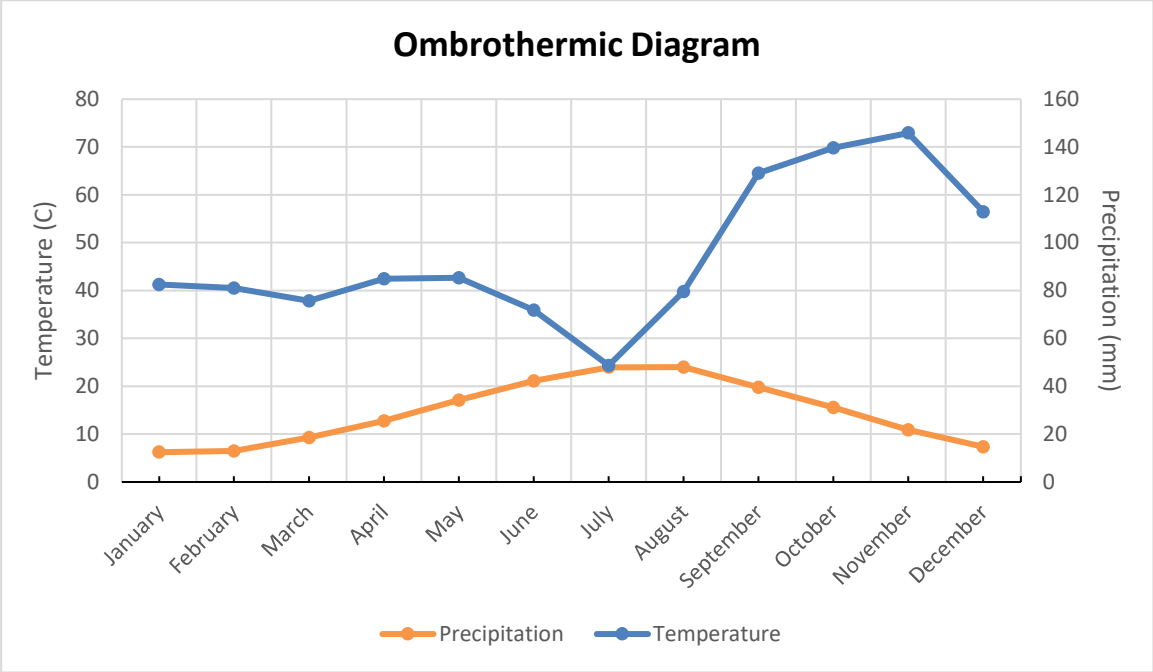

Figure 6. Ombrothermic Diagram of the islands Cres and Lošinj for the years 1980-2022 based on the CRU TS dataset (Harris et al. 2020).

3.1.3. Land uses

In terms of land uses, the pilot area of Croatia showcases a wide variety of different land uses across its landscape. Both islands exhibit a diverse array of land use patterns, creating a landscape characterized by a mix of different uses. This diversity highlights the unique and multifaceted nature of the islands' terrains and their adaptation to various land use practices.

The different land uses of the area, occur by analyzing the CORINE (Coordination of Information on the Environment) Land Cover map. This map is a detailed inventory of land cover across Europe, developed by the European Environment Agency (EEA). It classifies and maps land cover into various categories such as forests, grasslands, wetlands, urban areas, and agricultural lands. The map provides comprehensive spatial data that illustrates the distribution and extent of different land cover types within a specific region or country. It is created using satellite imagery and other geographic data sources, allowing for consistent monitoring and comparison over time. The CORINE Land Cover map is widely used for environmental assessments, spatial planning, biodiversity monitoring, climate change studies, and policy-making. It serves as a valuable tool for understanding landscape dynamics, identifying land use changes, assessing habitat fragmentation, and supporting sustainable land management practices across Europe and beyond.

Upon examining Figure 7, it becomes evident that Broad-leaved forests dominate the pilot area, occupying the largest portion at 25,1% of the total area. Transitional woodland-shrub areas follow closely behind, covering 17.6% of the total area. Pastures constitute the third most significant land use, occupying 12,3% of the total area. While there are several other land uses present in these islands, many of them occupy less than 1% of the total area, with a few ranging from 4% to 8%. The total area is 51.577,71 ha.

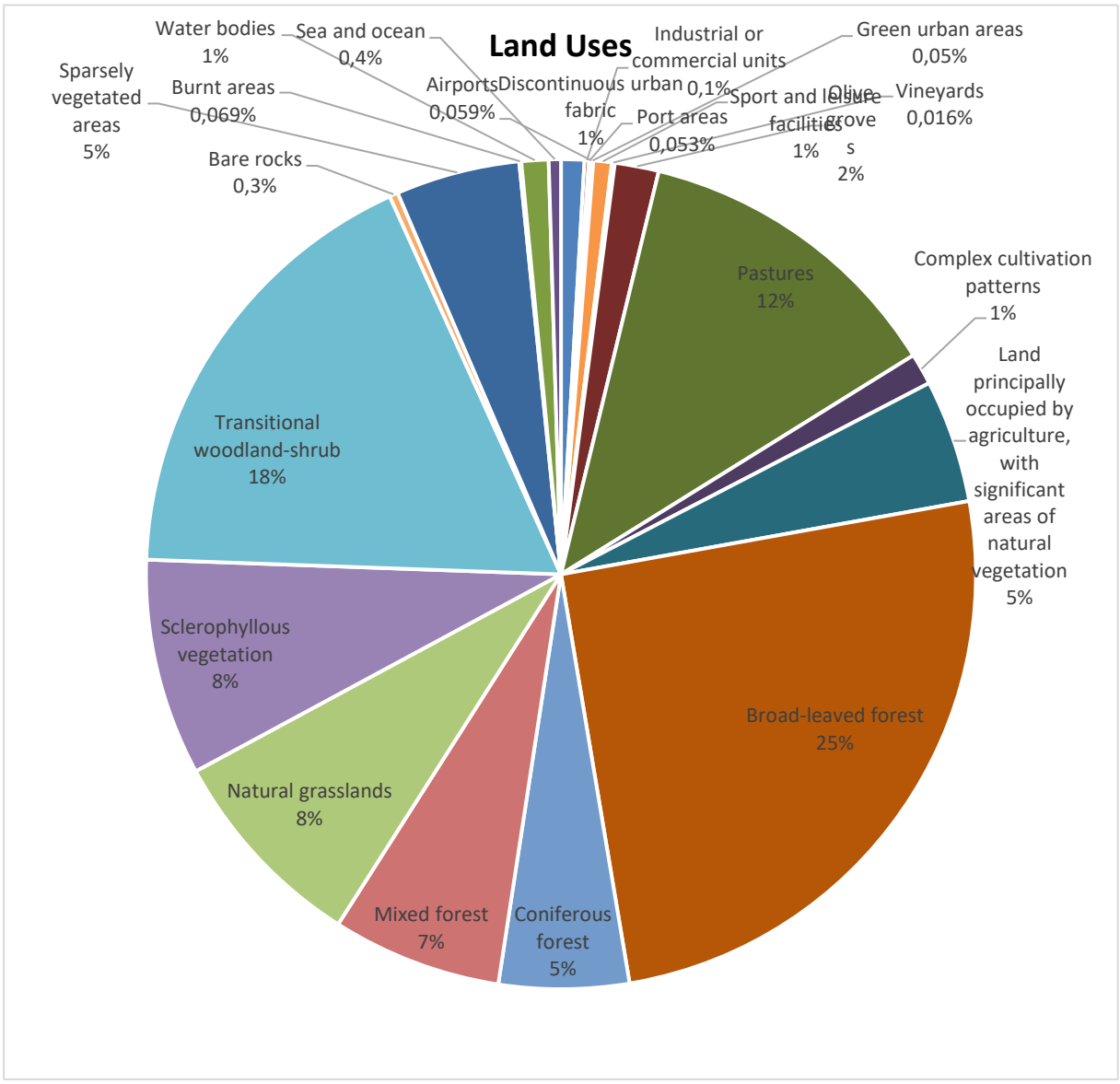

Figure 7. Percentage cover of different land use types that occupy the pilot area in Croatia based on the CORINE land cover.

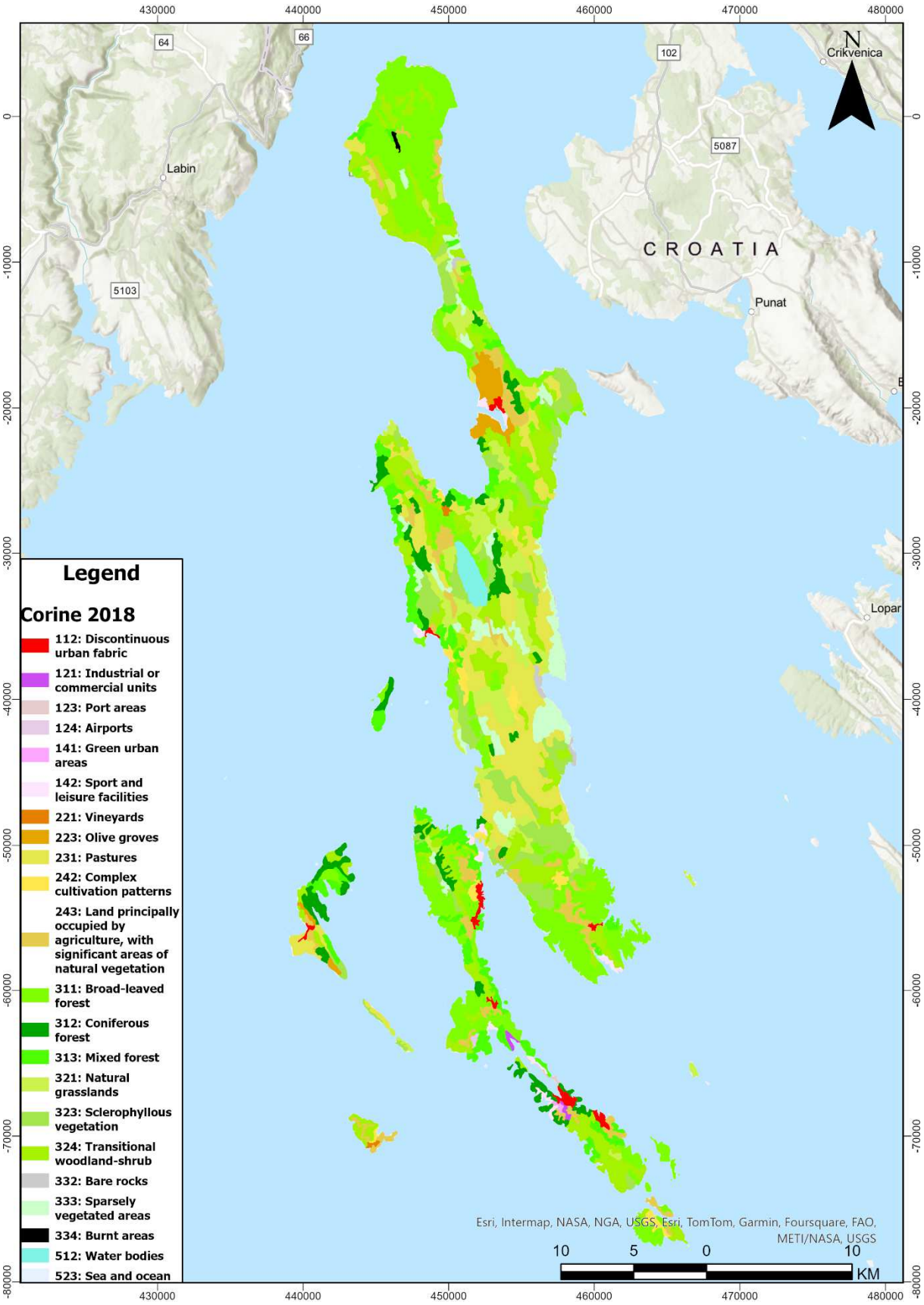

Figure 8. CORINE land cover map of the pilot area in Croatia.

3.1.4. Flora and vegetation

The islands of Cres and Lošinj have a unique and diverse composition of flora and vegetation across all over their area. It is interesting to note that on the islands there are around 1.500 different plant species, some which are very rare and endangered.

The northern region of Cres, known as Tramuntana, features enchanting forests filled with tall, ancient Mediterranean oaks (Quercus ilex), chestnuts (Castanea sativa) and hornbeams (Carpinus sp.). The landscape here is also marked by numerous caves, pits and ponds. The interior of the island is filled with pastures, olive groves and vineyards while dense maquis, rich with yellow weaver's broom (Spartium junceum) covers the western part of the island. The southeastern region is characterized by a sum-Mediterranean climate and flora, where thick bushes and maquis transform into forests. Additionally, the entire island of Cres is adorned with shrubs of sage and immortelle. The island's vegetation remains vibrant throughout all four seasons, with different plants blooming in succession.

The mild climate of Lošinj Island is evident in its diverse plant life. Research has identified 1.018 plant species on the island, with 939 being native. Among these, 230 are medicinal herbs. Additionally, around 80 exotic plant species were brought from different parts of the world by masters and sailors of the the island, who planted them in their home gardens. The unique climate allows for plants from southern Dalmatia and Sicily to thrive here. Dense pine forests around Mali Lošinj form a green belt that shields the town and harbor from the northern winds. Near Čikat, these woods gradually transform into a park. Today Lošinj's thick pine forests are a symbol of the island and an important asset for tourism and the Čikat area has been designated as a natural park.

According to the Ministry of Culture, the pilot area in Croatia comprises 25 different habitat types (Figure 9). The most prevalent habitat type is forests, covering 31.407,2 hectares and making up 60.8% of the total area. Other significant habitats include Eastern Adriatic stony pastures of the sub-Mediterranean zone, which span 8.692,539 hectares (16,8% of the total area), stands of sharp-needle pine covering 5.943,527 hectares (11,5%), and olive groves, which occupy 2.008,24 hectares (3,8%). As already mentioned, there are also other habitat types occupying the area but those are not as largely abundant as the ones already mentioned and each habitat's area is less than 800 ha. Many of these habitats are also under the protection of the Natura 2000 network, with the largest one being the Eastern Adriatic stony pastures of the sub-Mediterranean zone. From the 25 different habitat types, the 16 are under the protection of the Natura 2000 network and their most

important characteristics are presented below with a descending classification, from the types that occupy the larger areas to those who occupy the smallest.

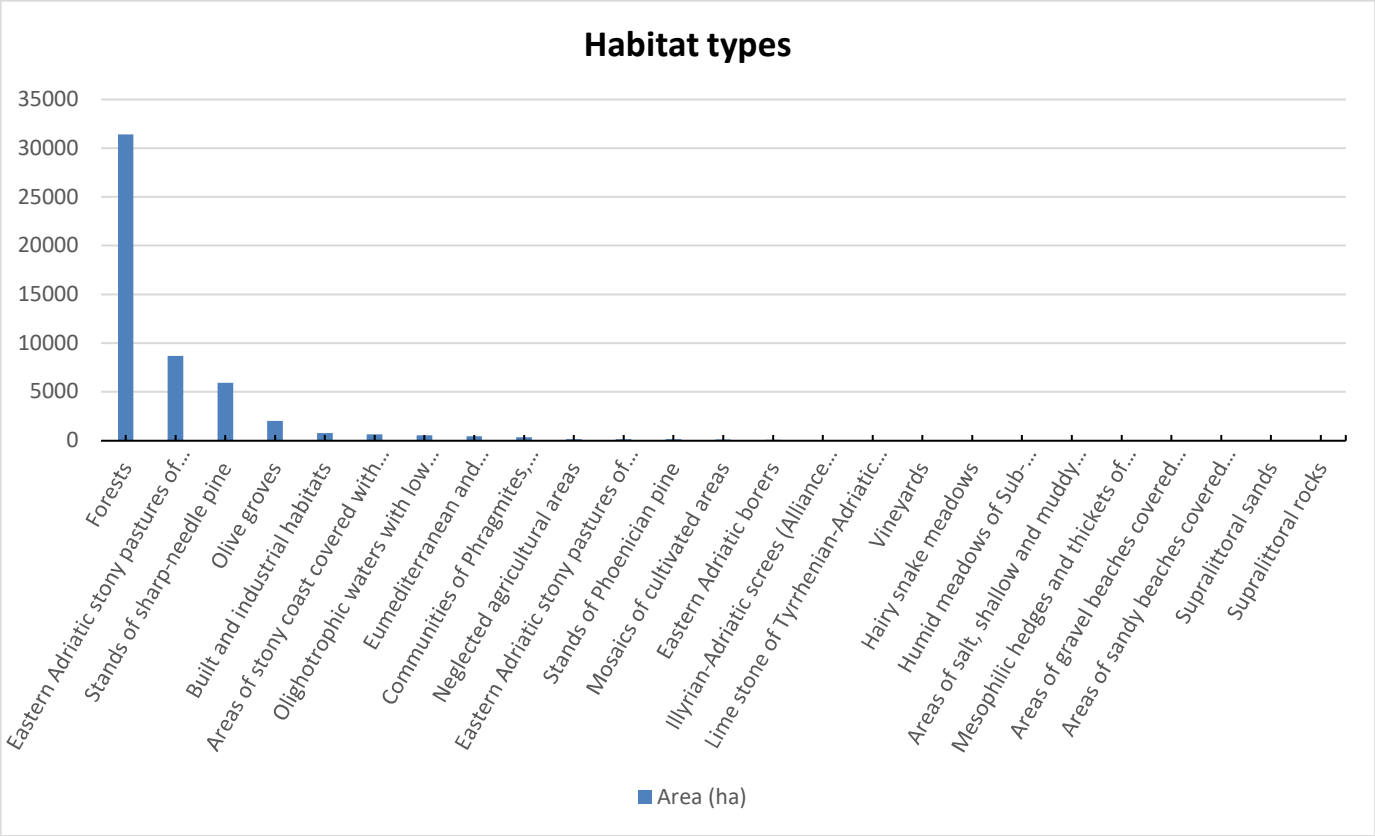

Figure 9. Habitat types of the Cres and Lošinj islands.

- **Habitat type 62A0**

  Xeric grasslands in the sub-Mediterranean zones of Trieste, Istria, and the Balkan Peninsula coexist with the steppic grasslands of the Festucetalia valesiacae (6210). These grasslands develop in areas with less continental influence than the steppic grasslands and include more Mediterranean elements. Some of the present communities include: Carici humilis-Centaureetum rupestris, Genisto holopetalae-Caricetum mucronatae, Chrysopogono-Centaureetum cristatae, and Danthonio-Scorzoneretum villosae.

- **Habitat type 5210**

  Mediterranean and sub-Mediterranean regions feature evergreen sclerophyllous bushes and scrubs, primarily centered around

arborescent junipers. Mixed dominance in these areas can be identified using combinations of Palaearctic codes. Some of the subtypes are: Pal. 32.131: Arborescent matorral dominated by Juniperus oxycedrus s.l., Pal. 32.132: Arborescent matorral dominated by Juniperus phoenicea s.l. and Pal. 32.133: Arborescent matorrals of Greece, Anatolia and the Near East, dominated by Juniperus excelsa or Juniperus foetidissima.

- **Habitat type 1240**

  The vegetated cliffs and rocky shores are characteristic of the Mediterranean region, the temperate eastern Atlantic along the southwestern Iberian Peninsula, and the Black Sea. These areas support unique plant communities classified under Crithmo-Limonietalia, showcasing a diverse range of flora adapted to these harsh coastal environments.

- **Habitat type 6220**

  The meso- and thermo-Mediterranean regions feature xerophilic, predominantly open grasslands composed of short grasses rich in therophytes. These annual grasslands thrive in oligotrophic soils that are base-rich, often calcareous. The perennial communities in these habitats fall under the Thero-Brachypodietea class, specifically the Thero-Brachypodietalia order and Thero-Brachypodion alliance. This type of grassland is considered a priority habitat within the Natura 2000 network due to its ecological significance and the unique biodiversity it supports.

- **Habitat type 6450**

  This habitat type corresponds to areas along large rivers with calm sections that freeze each winter, this habitat type is influenced by spring flooding. The traditional practice of managing these areas as hay meadows has generally been abandoned. This habitat includes regions that have not yet become heavily overgrown with trees and bushes.

- **Habitat type 62A0**

  The xeric grasslands found in the sub-Mediterranean regions of Trieste, Istria, and the Balkan Peninsula exist alongside the steppic grasslands categorized under Festucetalia valesiacae (6210). These grasslands thrive in areas with lower continentality compared to the steppic grasslands, incorporating a stronger Mediterranean character. Within this habitat, one can find diverse communities such as Carici

humilis-Centaureetum rupestris, Genisto holopetalae-Caricetum mucronatae, Chrysopogono-Centaureetum cristatae, and Danthonio-Scorzoneretum villosae.

- **Habitat type 8130**

  Slopes with warm exposures in the Alps and Pyrenees, as well as on calcareous substrates in the Pyrenees, Mediterranean mountains, hills, and lowlands, and occasionally on sunny middle European uplands or lowlands, are characterized by screes. The vegetation in these areas falls under the Androsacetalia alpinae p., Thlaspietalia rotundifolii p., Stipetalia calamagrostis, and Polystichetalia lonchitis orders. This habitat includes several subtypes some of which are the following: Pal. 61.31: Peri-Alpine thermophilous screes, known as Stipion calamagrostidis and Leontodontion hyoseroidis. These are typically coarse, unstabilized, sunny calcareous screes found at montane and subalpine levels in the Alps, as well as in uplands and lowlands across western and central middle Europe. Pal. 61.32: Provençal screes, also known as Pimpinello-Gouffeion screes. These are screes found in Mediterranean southern France, characterized by species such as Gouffeia arenarioides, Ptychotis heterophylla, Linaria supina, Centranthus ruber, and Crucianella latifolia. Pal. 61.33: Pyreneo-Alpine thermo-siliceous screes, known as Senecion leucophyllae and Taraxacion pyrenaici screes. These screes occur in the Pyrenees and Alpine regions, characterized by their thermo-siliceous nature.

- **Habitat type 8210**

  The vegetation found in crevices of limestone cliffs spans from the Mediterranean region to the Euro-Siberian plain, extending to alpine levels. This vegetation primarily falls under the Potentilletalia caulescentis and Asplenietalia glandulosi orders. There are two distinct levels within this habitat: a) thermo- and meso-Mediterranean (Onosmetalia frutescentis) featuring species like Campanula versicolor, Campanula rupestris, Inula attica, Inula mixta, and Odontites luskii and b) montane-oro-Mediterranean (Potentilletalia speciosae), which includes endemic species such as Silenion aurticulatae, Galion degenii, and Ramondion nathaliae. This habitat type exhibits significant regional diversity, hosting numerous endemic plant species as indicated in botanical studies.

- **Habitat type 6410**

  Molinia meadows occur from plain to montane levels on soils that are generally wet and nutrient-poor in nitrogen and phosphorus. They

result from extensive management practices, which may include late-season mowing, or they may represent a degraded stage of formerly drained peat bogs. These meadows can be categorized into two subtypes: Pal. 37.311: Found on neutral to alkaline or calcareous soils with a fluctuating water table, these meadows are relatively rich in species (Eu-molinion). The soil may occasionally be peaty and experience drying in summer. Pal. 37.312: Occurring on more acidic soils typical of Junco-Molinion (Juncion acutiflori), these meadows are often species-poor or found on degraded peat soils.

- **Habitat type 1310**

  Formations primarily composed of annual plants, particularly Chenopodiaceae like Salicornia or various grasses, thrive in periodically flooded muds and sandy soils of both coastal and inland salt marshes. These habitats are classified under Thero-Salicornietea, Frankenietea pulverulentae, and Saginetea maritimae. Some of the subtypes are: Pal. 15.11 - Glasswort swards (Thero-Salicornietalia): These include annual plants such as glasswort (Salicornia spp., Microcnemum coralloides), seablite (Suaeda maritima), and occasionally saltwort (Salsola spp.), which colonize periodically flooded mud flats in coastal salt marshes and inland salt basins. Pal. 15.12 - Mediterranean halo-nitrophilous pioneer communities (Frankenion pulverulentae): These formations consist of annuals adapted to saline conditions, including plants like Frankenia pulverulenta, Suaeda splendens, Salsola soda, Cressa cretica, Parapholis incurva, P. strigosa, Hordeum marinum, and Sphenopus divaricatus. They colonize salt muds in the Mediterranean region, enduring temporary inundation and extreme dry spells.

- **Habitat type 1410**

  The Juncetalia maritimi encompasses various Mediterranean communities, classified into several subtypes. Pal. 15.51 refers to tall rush saltmarshes where Juncus maritimus and/or J. acutus dominate. Pal. 15.52 describes short rush, sedge, and clover saltmarshes (Juncion maritimi), along with humid meadows located behind the shoreline that are abundant in annual plant species and Fabaceae like Trifolion squamosi. Pal. 15.53 denotes Mediterranean halo-psammophile meadows (Plantaginion crassifoliae), which thrive in sandy coastal environments characterized by specific plant communities.

- **Habitat type 1420**

  The perennial vegetation found in saline marine mudflats (schorre) primarily consists of shrubs, predominantly distributed in Mediterranean-Atlantic regions. These communities include plants such as Salicornia, Limonium vulgare, Suaeda, and Atriplex. This vegetation type falls under the Sarcocornetea fruticosi class.

- **Habitat type 1210**

  Communities composed of annuals or a mixture of annuals and perennials thrive in accumulations of drift material and nitrogen-rich gravel. These habitats are classified under Cakiletea maritimae p.

- **Habitat type 2110**

  Coastal formations found along the Atlantic, North Sea, Baltic Sea, and Mediterranean represent initial stages of dune formation. These formations consist of ripple patterns or elevated sandy surfaces on the upper beach, or a fringe of vegetation extending seaward at the base of taller dunes.

- **Habitat type 1140**

  Sandy and muddy coastal areas of oceans, connected seas, and lagoons that are exposed during low tide, typically lacking vascular plants but often covered by blue-green algae and diatoms. These habitats are crucial feeding grounds for wildfowl and waders. Note that eelgrass communities (Palaearctic 11.3) are part of this habitat type.

- **Habitat type 1170**

  Rocky substrates and biogenic concretions, whether submerged or exposed during low tide, emerge from the seafloor in the sublittoral zone, sometimes extending into the littoral zone where distinct plant and animal communities thrive in uninterrupted bands. These reefs typically host diverse benthic communities of algae and animal species, including encrustations and coral-forming concretions. In the northern Baltic regions, shallow waters are dominated by filamentous algal zones with significant seasonal changes, especially on gently sloping shores. Fucus vesiculosus thrives at depths ranging from 0.5 to 6 meters in the sublittoral zone. Below the Fucus zone, a red algae zone emerges at depths around 5 to 10 meters.

3.1.5. Fauna

The Cres-Lošinj archipelago is renowned for its diverse fauna, housing hundreds of different animal species. These islands varied habitats, from dense forests and scrublands to rocky coastlines and freshwater lakes, support numerous species of birds, mammals, reptiles and amphibians. Notably, they are home to several endemic species of insects and small mammals. Their rich biodiversity makes then an important area for wildlife conservation and ecological study.

They are home to small game such as rabbits, hares and stone martens and also has an abundance of partridges, snipes and pheasants. Among the birds of prey, the Griffon Vulture, known locally as "Orel," is particularly significant, with a wingspan reaching up to 2.8 meters. This animal is an endangered species roaming in the area and it is important to pay special attention to its conservation. That is why these endangered birds are taken care of by the Rescue Centre for Griffon Vultures in Beli. The traditional practice of keeping sheep, which graze freely throughout the year, has helped sustain the ecosystem but the introduction of non-native species like fallow deer, mouflons and boars has caused some disruption. Sheep farming methods have remained unchanged since ancient times, with sheep moving between fields separated by dry stone walls to allow pastures to recover. This practice has also supported the griffon vulture, which feeds exclusively on carrion.

Interestingly enough, no poisonous snakes have been recorded in the area, although non-poisonous snakes and lizards are present. Geckos are also present in the area, which are small lizards of the Gekkonidae family and they are also a protected species. The surrounding sea is rich in marine life, with prevalent blue fish and various shellfish, prawns, calamari and octopi. White fish such as dentex, sea bass, John Dory, and red scorpionfish are less common. Annual spear fishing competitions are held in Mali Lošinj, and seagulls nest along the coast. The clear, unpolluted waters of the Cres-Lošinj archipelago are also home to the common bottlenose dolphin, one of the best-studied colonies in the Mediterranean, with research conducted by the Blue World Institute.

Another interesting thing about the islands is that they host a broad variety of butterflies. 77 different species of butterflies have been recorded in the island of Cres, which ranks it in the second place in terms of abundance among all explored Adriatic islands.

3.1.6. Spatial data

As already mentioned at the start of the paper, each pilot area will be also followed by a Geo-Database which will include spatial data regarding the area and that will aid further in the project. In this chapter, geospatial data maps will be introduced first, followed by remote sensing data maps. The geospatial data maps will encompass various types, including an aspect map, slope map, TIN map, Canopy Height Model (CHM) map, tree cover density map, a roads and buildings map and finally an NDVI map for all seasons. Subsequently, remote sensing data maps will be presented, featuring images from the Sentinel-2 satellite across all seasons. These maps illustrate the data that will be incorporated into Croatia's final Geo-Database, providing invaluable insights for the analysis of the region.

- **Aspect**

An aspect map provides a detailed representation of a terrain (or any continuous surface) by illustrating the direction (aspect) of its slopes. In this type of map, aspect categories are represented by different colors such as red, orange, yellow, and so on. The degree of slope is conveyed through the saturation or brilliance of these colors, where steeper slopes are depicted with brighter colors. This approach creates a visually informative map, with the colors displayed as shown on the right. By analyzing the colors, you can identify patterns in the landscape, such as predominant orientations of hillsides, valleys, and other landforms.

In the pilot area of Croatia, through analyzing the Aspect map (Figure 10), it is understood that on average the slopes in this area tend to face more south-southwest and also east-northeast. This indicates also that this area is a part of a varied landscape with hills, valleys and potentially complex topography. The different types of slopes can influence the types of vegetation and also create microclimates in the area. Slopes can also affect wildfires and the spread of those, so it is important to notice the change in slopes in this area.

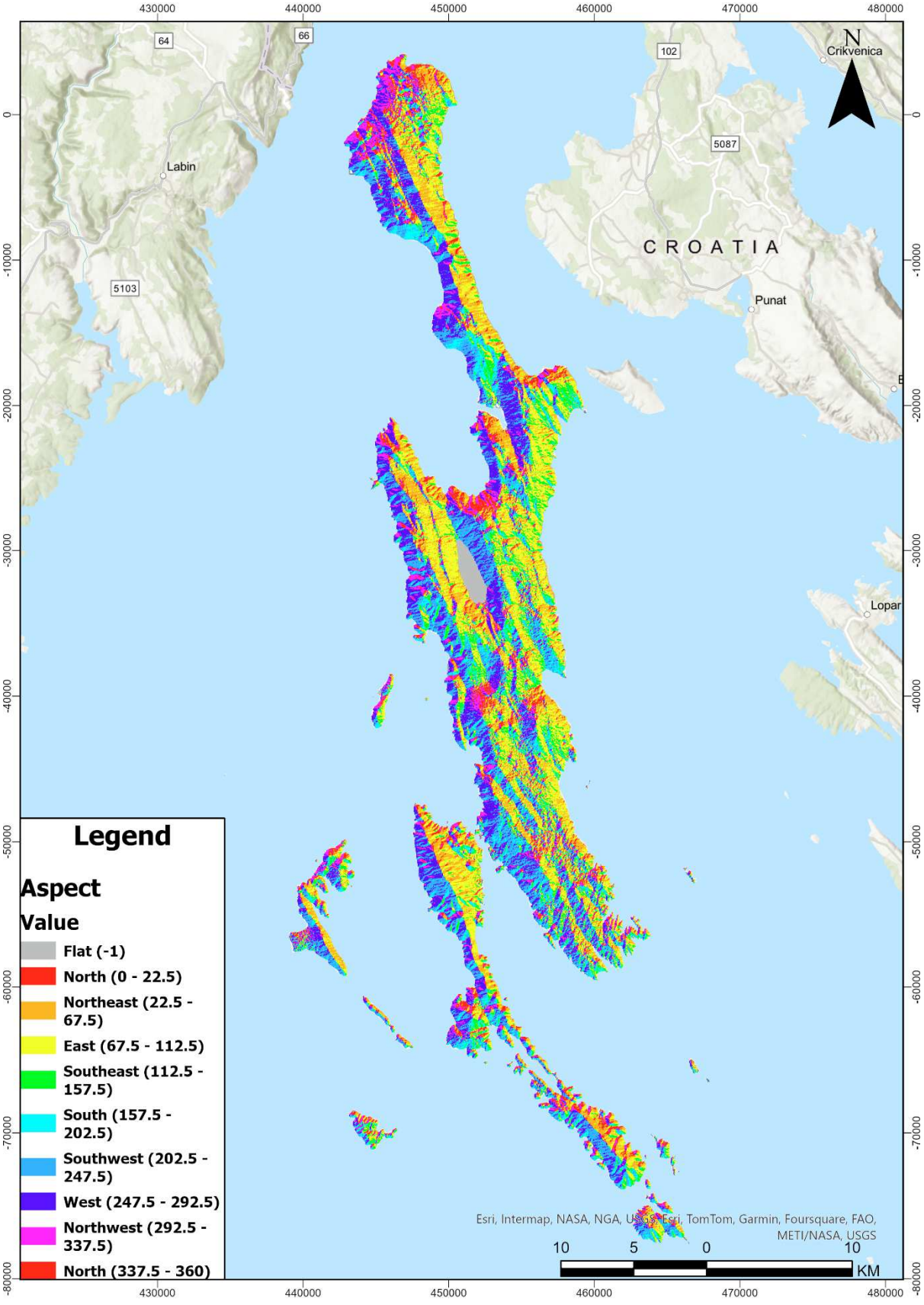

Figure 10. Aspect map of the pilot area in Croatia.

- **Slope**

A slope map is a thematic map representing the steepness or incline of terrain, calculated from topographic or digital elevation data and expressed in degrees or percentage. It uses color gradients to show different steepness levels, with flatter areas in lighter colors and steeper areas in darker colors. Derived from digital elevation models (DEMs) or topographic maps, slope maps are essential for urban planning, construction, agriculture, environmental management, hydrology, and recreational planning. They help identify suitable areas for building, farming, and understanding erosion patterns, water flow, and runoff. Steeper slopes, shown in darker colors, are more prone to erosion and may require special management, while gentler slopes, in lighter colors, are more suitable for various land uses. Slope maps are created by collecting elevation data, calculating slope using GIS software, and visualizing the data with a color gradient to highlight different levels of steepness across the terrain. Slope maps together with aspect maps can be a great representation of the landscape in an area and can also be helpful into facing wildfires and predicting their spread.

For the pilot area of Croatia, through analyzing the slope map (Figure 11), we can understand that there are plenty of gentler slopes which are represented in light brown to white color but there are also plenty of steep slopes as well, which are represented in dark brown color. The slope map together with the aspect map can really provide insights about the complexity of the landscape for this area and they can be helpful tools in the prevention of a wildfire.

Figure 11. Slope map of the pilot area in Croatia.

- **Geomorphology**

All of the geomorphology maps will be constructed through Triangulated Irregular Network (TIN) models. These models generate continuous surfaces, like terrain elevation or temperature gradients. This surface is depicted as a collection of facets created by linking data points at nodes to form adjacent triangles. TINs are usually displayed using color-shaded relief to illustrate elevation, with shaded relief simulating sunlight illuminating the earth's surface. Adding color enhances the visibility of ridges, valleys, and hillsides, showing their respective heights. Viewing data in this manner can help clarify the locations of other map features. Tin can be used to display any one of three surface characteristics: slope, aspect, and elevation on your map and you can simulate shaded relief. You can also display contour lines representing lines of elevation change.

In this specific map, the geomorphology of Croatia is being shown (Figure 12). Although the highest point in the area is relatively modest, examining the map provides a clearer perspective on the elevation variations within the region. The map reveals that, despite the overall low peak, there are notable changes in elevation in certain areas. This detailed visualization helps to better understand the topography and the significant shifts in height that occur throughout the landscape.

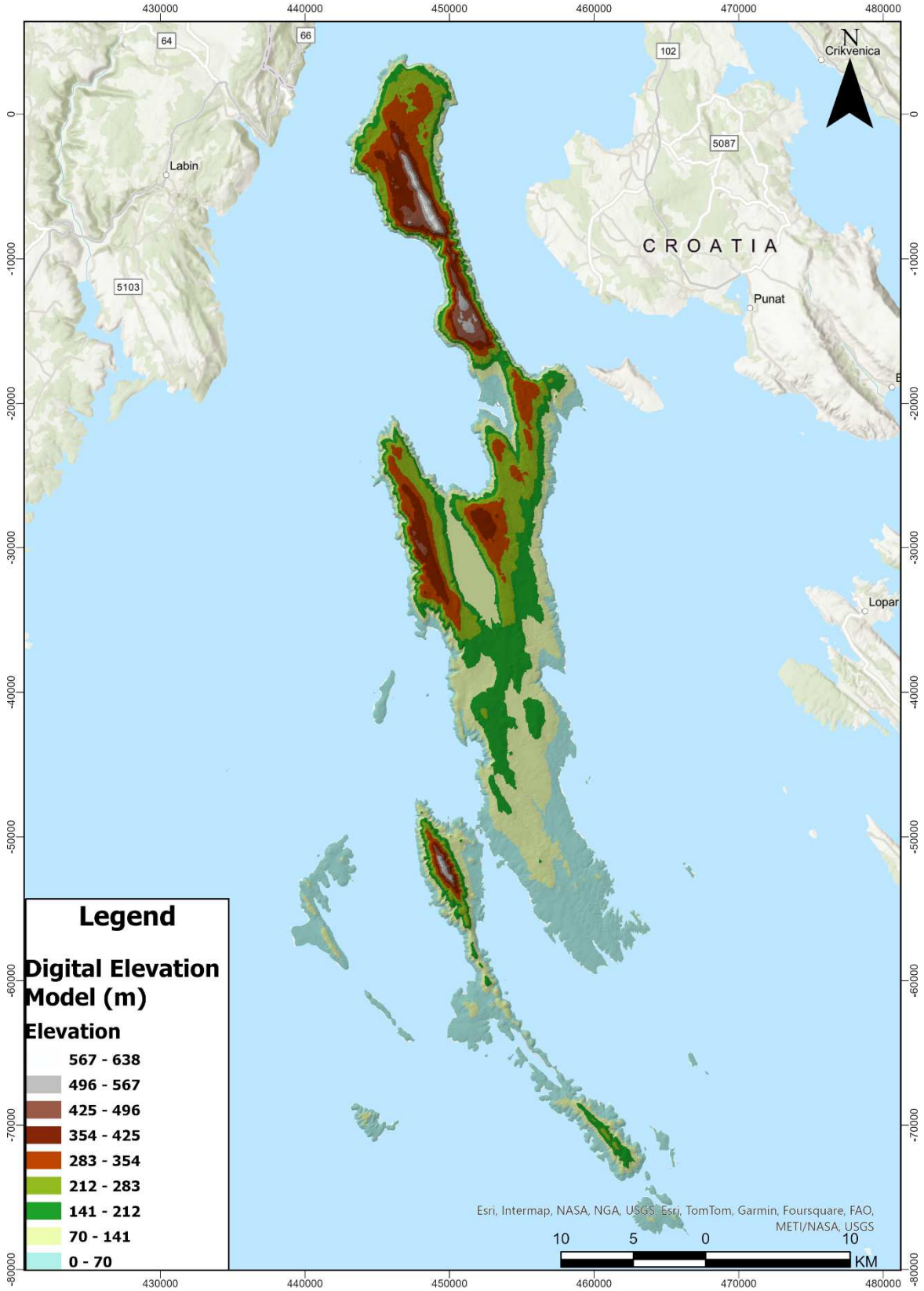

Figure 12. Geomorphology map of the pilot area in Croatia.

- **Canopy Height**

A canopy height model (CHM) map is a specialized type of map that represents the height of vegetation, particularly trees, above the ground surface. It is created by subtracting the ground elevation data (digital terrain model or DTM) from the top-of-canopy elevation data (digital surface model or DSM). This map visually depicts the vertical structure of vegetation, highlighting the height variations across different areas. A CHM is essential for ecological studies, forest management, and environmental monitoring, as it provides detailed information about the biomass, canopy density, and forest health. By showing the distribution and height of vegetation, CHM maps help in understanding habitat diversity, assessing carbon storage, and planning conservation strategies. A CHM is also really useful for studying wildfires. CHMs provide valuable spatial information about the vertical structure of vegetation, including tree heights and canopy density. This data is crucial for understanding how wildfires spread and behave in different types of forested landscapes. By integrating CHM data with fire behavior models, researchers and fire managers can better predict fire behavior, assess potential fire hazards, and plan effective fire management strategies such as prescribed burns or fuel reduction treatments. Therefore, CHMs play a significant role in enhancing the accuracy and effectiveness of wildfire management and mitigation efforts.

Upon examining the canopy height model (CHM) for Croatia (Figure 13), it becomes evident that a significant portion of the region is predominantly forested, which also agrees with earlier findings from the land use section. Additionally, flat areas likely corresponding to grasslands or urban developments are discernible. Notably, a distinct red area on the map indicates the presence of a lake, explaining the absence of forest cover in that specific region.

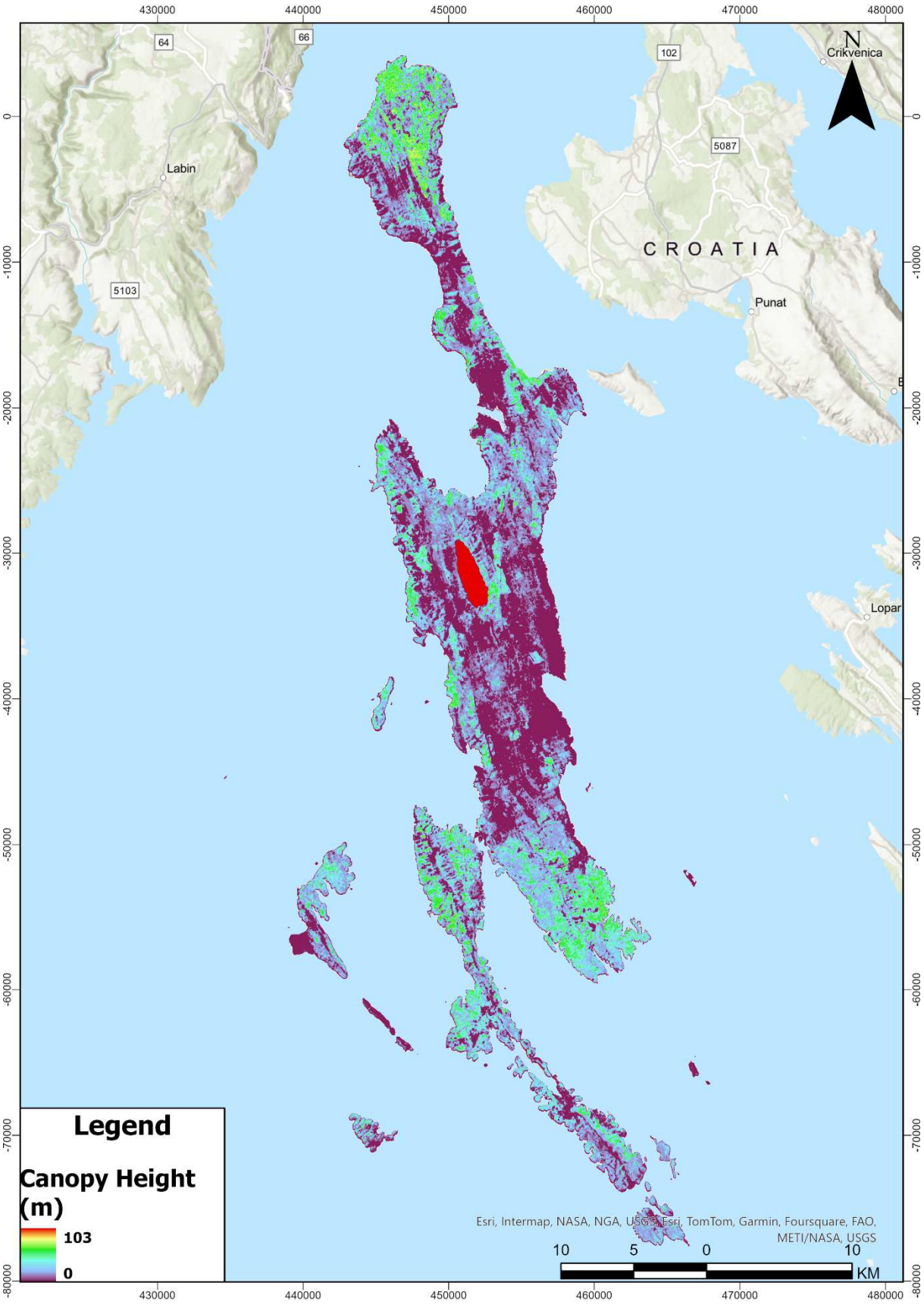

Figure 13. Canopy Height Model of the pilot area in Croatia.

- **Tree cover density**

A tree cover density map is a visual representation that shows the extent and density of tree canopies across a specific geographical area, typically derived from satellite imagery and remote sensing data. These maps use various techniques to classify and quantify the amount of vegetation cover present, ranging from sparse to dense forests. They are invaluable tools for environmental monitoring, allowing researchers and policymakers to track changes in forest cover over time, assess habitat quality and biodiversity, and understand the carbon storage capacity of forests. Moreover, they are important data that can be used in predicting different things about wildfires, for example how wildfires might spread across a landscape. Integrating tree cover density maps with fire behavior models allows for more accurate wildfire risk assessments and helps prioritize areas for fire prevention measures, such as fuel reduction treatments or prescribed burns. Therefore, tree cover density maps play a significant role in enhancing wildfire management strategies and improving overall preparedness for fire events.

As already noted from the CHM map, it is clear that a large portion of the area is covered by forest. That also occurs from the tree cover density map (Figure 14), through the analysis of which it is understood that except from flat areas or urban regions, the rest of the pilot area is covered by an extent tree network. This factor could significantly impact the forthcoming analysis of wildfires, given that trees are among the most critical fuel components influencing wildfire propagation.

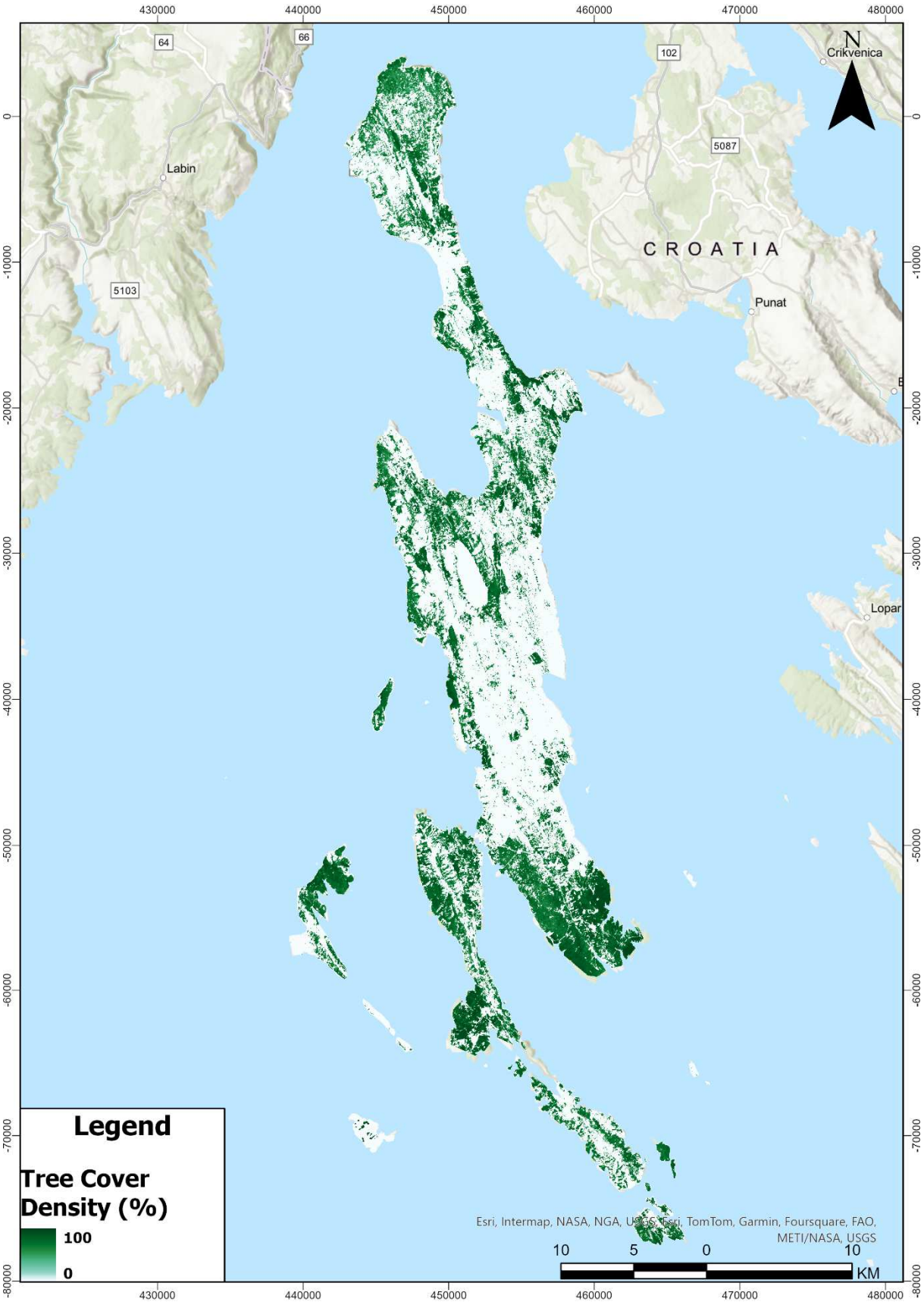

Figure 14. Tree cover density map of the pilot area in Croatia.

- **Roads and buildings network**

A roads and buildings map provides a comprehensive view of the infrastructure and urban layout within a specific area. It typically displays the network of roads, highways, streets, and pathways, detailing their connectivity and hierarchy. Additionally, such maps depict the distribution and types of buildings, including residential, commercial, industrial, and public structures. This information is crucial for urban planning, transportation management, and emergency services, as it helps identify access points, traffic flow patterns, and areas of congestion. A roads and buildings map also plays a pivotal role in the analysis and prediction of wildfires by providing critical spatial information about the built environment and infrastructure. Such maps help identify urban areas, residential neighborhoods, industrial zones, and commercial districts, which are crucial for assessing the potential impact of wildfires on populated areas. Understanding the layout of roads and highways allows fire management teams to plan evacuation routes and access points for firefighting equipment. Moreover, the distribution of buildings and their proximity to vegetation can indicate areas of higher fire risk or vulnerability. Integrating this information with wildfire spread models enables more accurate predictions of fire behavior and potential paths of fire spread. Additionally, the map aids in prioritizing areas for wildfire prevention strategies, such as creating firebreaks, implementing building codes, and conducting community outreach for fire preparedness. Overall, a roads and buildings map enhances the effectiveness of wildfire analysis, planning, and mitigation efforts by providing essential spatial context and infrastructure details.

By analyzing the roads and buildings map of the pilot area in Croatia, an extensive road network stretching all over the area of the islands can be noted (Figure 15). This network consists of many different types of roads, from primary and secondary to track and service roads and they can all be used for future wildfire planning. Several of these road networks may be designated as emergency routes for fire incidents, providing essential access for fire trucks during emergencies. This designation is highly beneficial and critical when responding to sudden wildfires that require immediate attention.

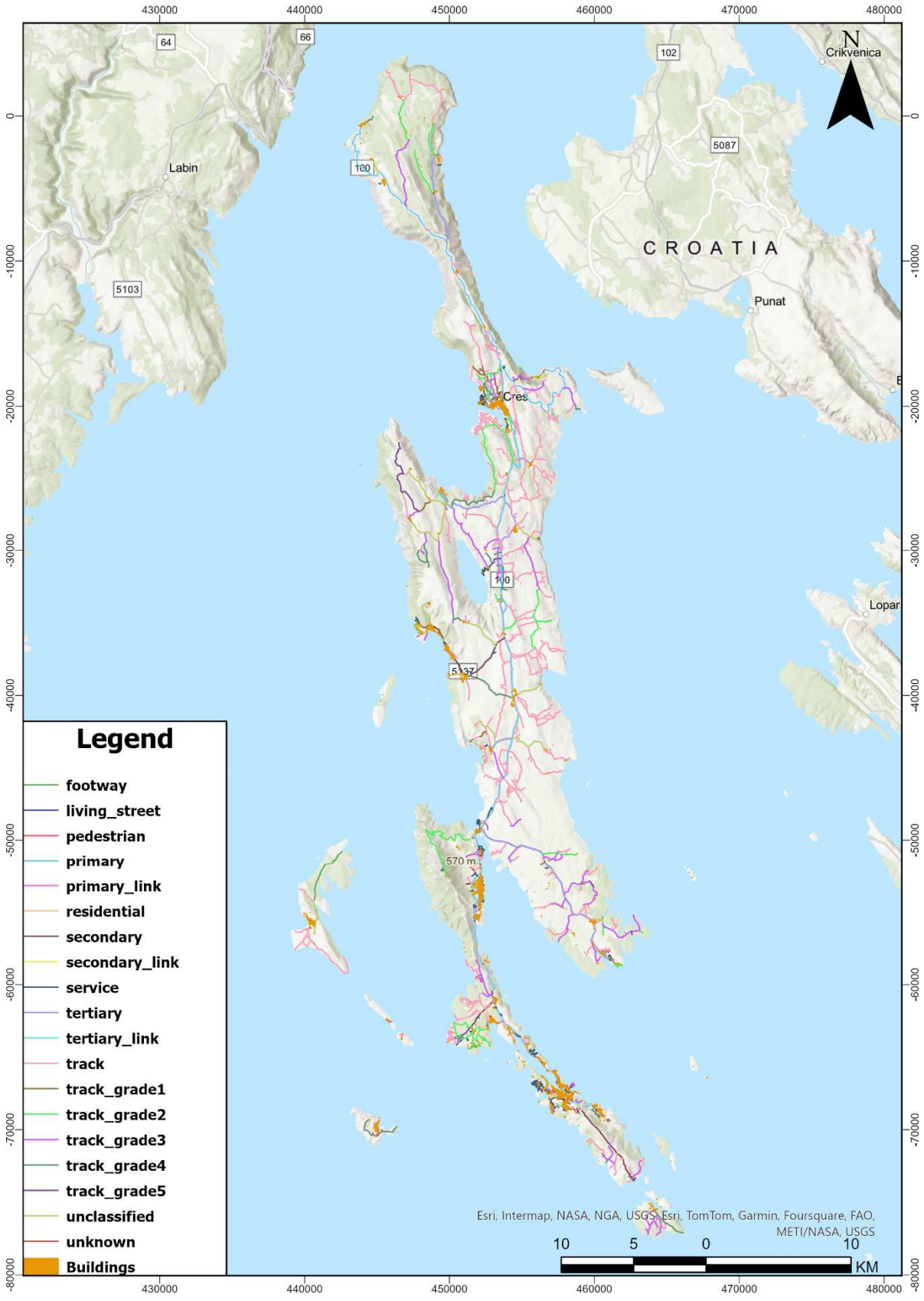

Figure 15. Roads and buildings map of the pilot area in Croatia.

- **NDVI**

The NDVI (Normalized Difference Vegetation Index) is a numerical indicator derived from satellite imagery that measures the density and health of vegetation in a specific area. It calculates vegetation greenness by comparing the reflectance of near-infrared (NIR) and red bands. Higher NDVI values indicate denser, healthier vegetation, while lower values signify sparse vegetation or non-vegetated surfaces like bare soil or water bodies. For predicting and mitigating wildfires, NDVI serves several critical purposes. High NDVI values indicate areas with abundant, potentially flammable vegetation, which can help identify regions at greater risk of wildfires. Conversely, low NDVI values may highlight areas with sparse vegetation or drought-stressed plants, which could influence fire behavior differently. By monitoring changes in NDVI over time, fire managers can track seasonal vegetation growth, identify fuel accumulation patterns, and predict where wildfires are most likely to ignite and spread rapidly. This information allows for proactive measures such as targeted fuel reduction treatments, prescribed burns, and strategic deployment of firefighting resources to mitigate fire risk and protect vulnerable areas effectively. Therefore, NDVI plays a crucial role in wildfire prediction, planning, and response by providing actionable insights into vegetation conditions and fire potential across landscapes.

Obtaining NDVI (Normalized Difference Vegetation Index) data for all seasons of an area is highly beneficial for gaining comprehensive insights into wildfire management and mitigation strategies. NDVI data across seasons provides a detailed temporal perspective on vegetation dynamics, highlighting seasonal variations in vegetation density, health, and moisture content. This information is crucial for assessing fuel loads, the amount and flammability of vegetation available to burn across different times of the year. By studying the different NDVI maps of the pilot area in Croatia, it is noted that throughout all of the seasons high NDVI values are present (Figure 16). This data can be crucial for future wildfire prevention planning and it should be noted that many areas are prone to wildfires because of their high fuel load. Below the algorithm for the calculation of NDVI is presented:

$$Normalised\ Difference\ Vegetation\ Index\ (NDVI) = \frac{(NIR - RED)}{(NIR + RED)}$$

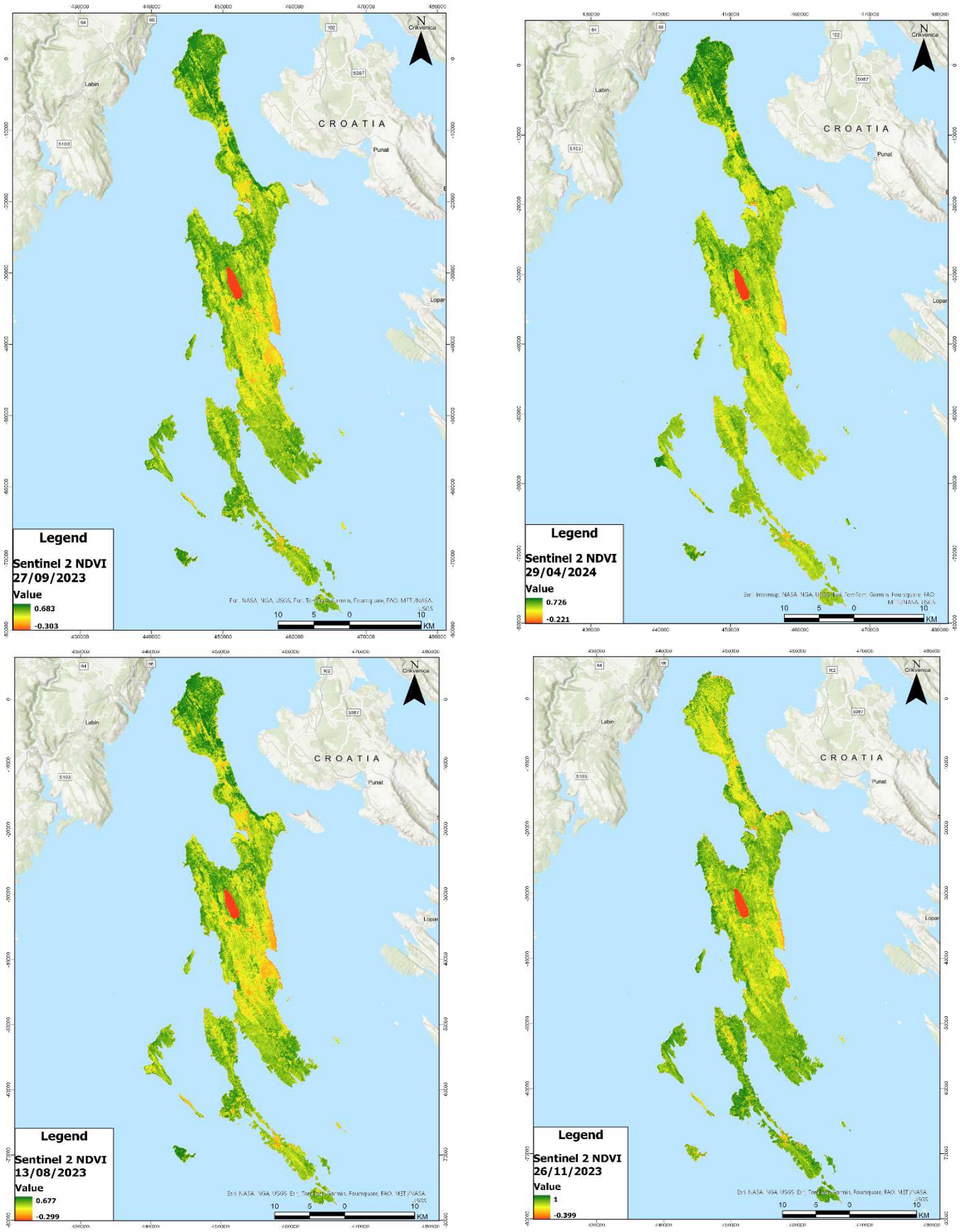

Figure 16. NDVI maps that cover all four seasons for the pilot area of Croatia. The autumn NDVI map is displayed at the top left, the spring NDVI map at the top right, the summer NDVI map at the bottom left, and the winter NDVI map at the bottom right.

- **Sentinel 2 images**

The Sentinel 2 satellite is part of the European Space Agency's (ESA) Copernicus program (formerly known as GMES, Drush et al. 2012), designed to provide high-resolution optical imagery for various Earth observation applications. Sentinel 2 carries a multispectral sensor capable of capturing images in 13 spectral bands, ranging from visible to shortwave infrared wavelengths. Sentinel 2 is a constellation of two polar-orbiting satellites that deliver multispectral data at spatial resolution of up to 10m in the visual and near infrared bands and a great thematic resolution at 20 and 60 m spatial resolution, and with a revisiting frequency of 5 days. Table 1. Spectral and Spatial characteristics of Sentinel 2 images. shows the spectral and spatial characteristics of Sentinel 2 images.

These images are instrumental in monitoring and preventing wildfires due to their ability to provide detailed and frequent observations of vegetation conditions and land cover dynamics. These images can detect changes in vegetation health and density, which are crucial indicators of wildfire fuel availability and susceptibility. By analyzing Sentinel 2 data over time, fire managers can monitor vegetation growth patterns, identify areas of high biomass accumulation (potential fuel sources), and assess vegetation stress due to factors like drought or disease, all of which influence wildfire behavior. Moreover, the satellite's multispectral capabilities allow for the detection of subtle changes in land surface temperatures and moisture content, which are critical factors in fire spread and intensity. This information enables early detection of fire-prone areas and supports proactive wildfire prevention measures such as fuel management strategies (e.g., prescribed burns, fuel breaks) and emergency response planning. By integrating Sentinel 2 imagery into wildfire management workflows, authorities can enhance preparedness, response efficiency, and community safety in fire-prone region.

For the pilot area of Croatia, four different Sentinel 2 satellite images are collected, which cover the total area over four seasons (Figure 17). This can help analyzing and studying the vegetation changes in the islands of Cres and Lošinj, something that can prove crucial for the analysis of previous fires and the prevention of future ones.

Spectral Band	Band description	Wavelength range (nm)	Spatial Resolution (m)
Band 1	Coastal aerosol	433–453	60
Band 2	Blue	458–523	10
Band 3	Green	543–578	10
Band 4	Red	650–680	10
Band 5	Red Edge 1	698–713	20
Band 6	Red Edge 2	733–748	20
Band 7	Red Edge 3	773–793	20
Band 8	Near Infrared	785–900	10
Band 8A	Narrow Near Infrared	855–875	20
Band 9	Water vapour	395–955	60
Band 10	Shortwave infrared-Cirrus	1360–1390	60
Band 11	Shortwave infrared 1	1565–1655	20
Band 12	Shortwave infrared 2	2100–2280	20

Table 1. Spectral and Spatial characteristics of Sentinel 2 images.

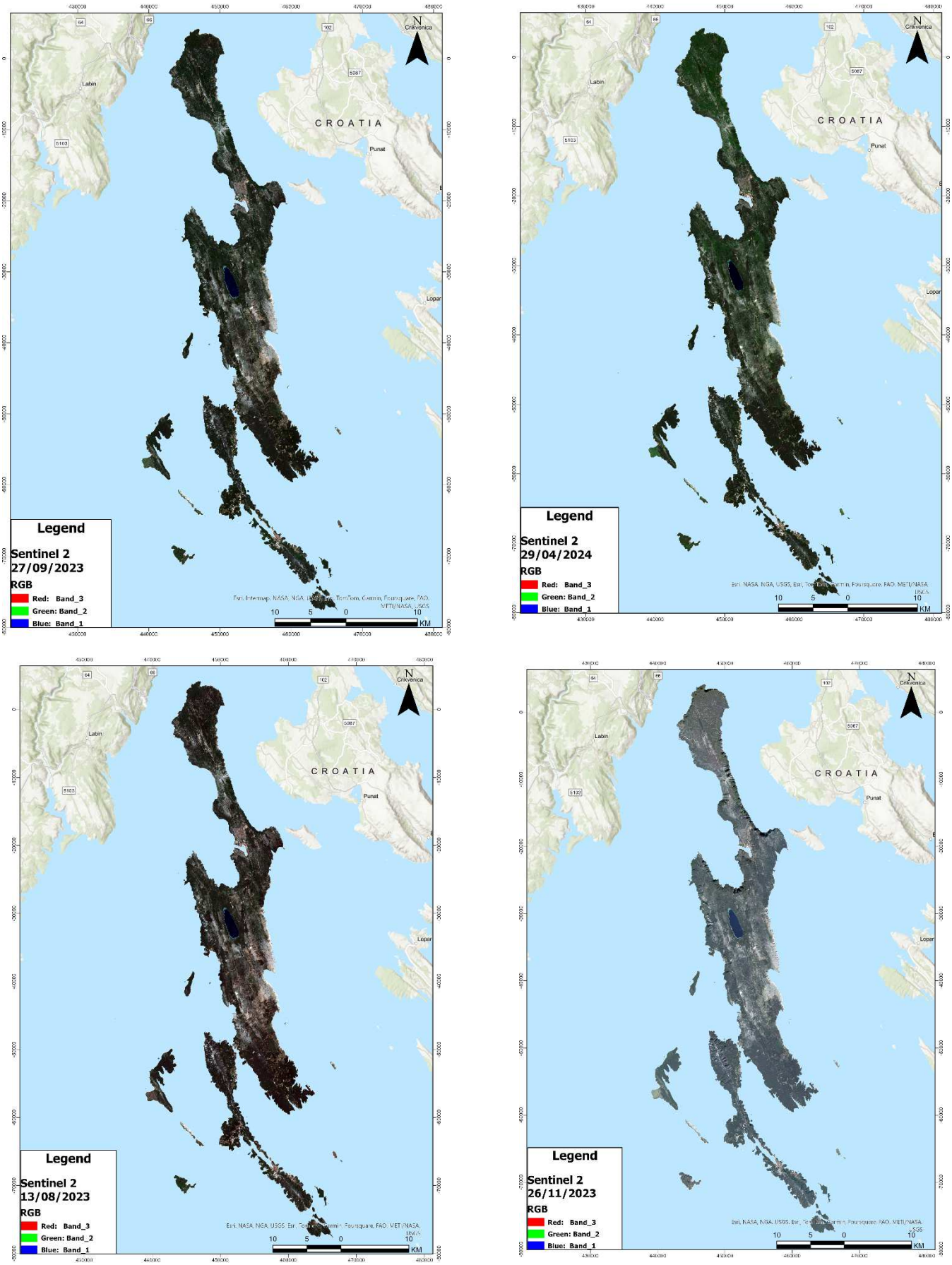

Figure 17. Sentinel 2 satellite images (true color combination) that cover all four seasons for the pilot area of Croatia. The autumn Sentinel 2 image is displayed at the top left, the spring one at the top right, the summer one at the bottom left, and the winter one at the bottom right.

- **Planet image**

Planet Labs, a private Earth imaging company, operates a fleet of small satellites known as CubeSats, which capture high-resolution, frequently updated satellite imagery of the entire planet. These satellites, collectively called the PlanetScope constellation, consist of hundreds of small, lightweight satellites that provide daily coverage of the Earth's landmass. Planet's imagery is valuable for a wide range of applications, including agriculture, forestry, environmental monitoring, urban planning, and disaster response. With resolutions ranging from 3 to 5 meters, Planet's satellite images offer detailed views that help track changes in land use, monitor crop health, assess the impacts of natural disasters, and support climate change research. The frequent revisits and high temporal resolution of Planet's imagery make it a crucial tool for timely and accurate geospatial analysis, enabling users to make informed decisions based on up-to-date visual data of the Earth's surface. Table 2 shows the spectral and spatial characteristics of Planet images.

It is crucial to note that Planet images differ from Sentinel 2 satellite images. Planet images lack mid-infrared channels, resulting in lower spectral analysis capabilities and a reduced ability to identify features with high discriminative power compared to Sentinel 2. Nonetheless, Planet images offer a significantly higher spatial resolution (3m) than Sentinel 2, enabling more precise delineation of vegetation polygons during the segmentation phase. Therefore, the combined use of both types of satellite images is an important factor for the analysis of an area.

Spectral Band	Band description	Wavelength range (nm)	Spatial resolution (m)
Band 1	Coastal blue	431–452	3
Band 2	Blue	465–515	3
Band 3	Green 1	513–549	3
Band 4	Green 2	547–583	3
Band 5	Yellow	600–620	3
Band 6	Red	650–682	3
Band 7	Red Edge	697–713	3
Band 8	Near Infrared	845–885	3

Table 2. Spectral and Spatial characteristics of Planet images.

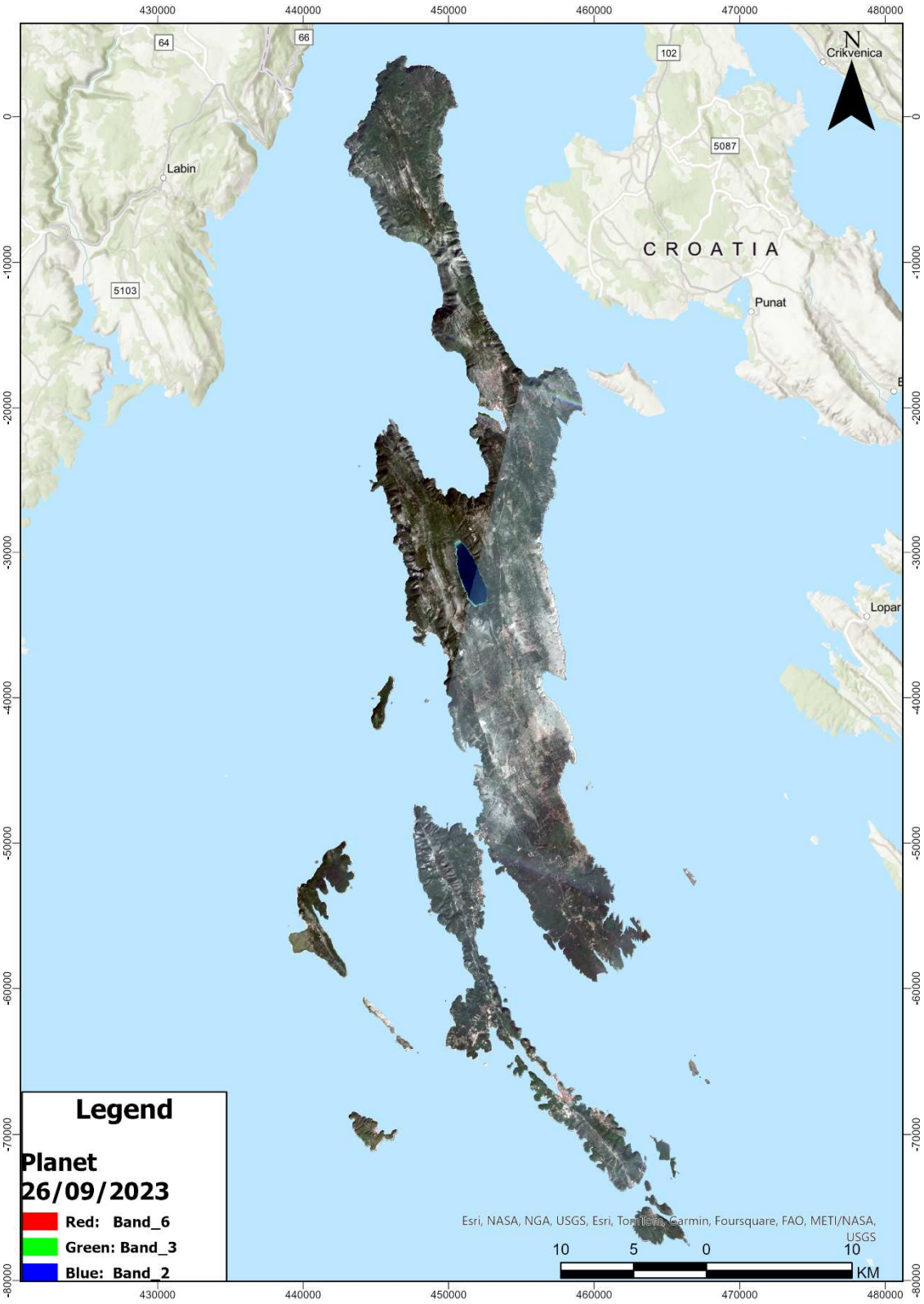

Figure 18. Planet image captured during autumn for the pilot area of Croatia.

3.2. Sežana – Slovenia

Slovenia is located in Central Europe or South-Eastern Europe, at the junction of the Alps, the Dinaric Mountains, the Pannonian Plain and the Mediterranean. The north-western part of the country is dominated by the Alps. The Karst landscape stretches towards the sea. A large biodiversity can be found in a relatively small area. This is largely the result of the interplay of different types of climate, geological structures and large differences in altitude. Covering an area of approximately 20.271 km^2, Slovenia ranks among the smaller European countries in term of population, with approximately 2.1 million people. The natural parks of Slovenia represent the most valuable part of the Slovenian territory from the point of view of long-term preservation of natural values, biotic diversity and special landscape features. Protected areas of nature are protected in one national park, three regional parks, 34 landscape parks, 66 nature reserves and over 1.200 natural monuments, which together cover 13% of the Slovenian territory. In addition, Slovenia has 2 geoparks, several botanical gardens and 144 monuments of designed nature. This project places special emphasis on the Karst and Brkin region, located in the southwest of Slovenia, which forms the country's pilot area (Figure 19).

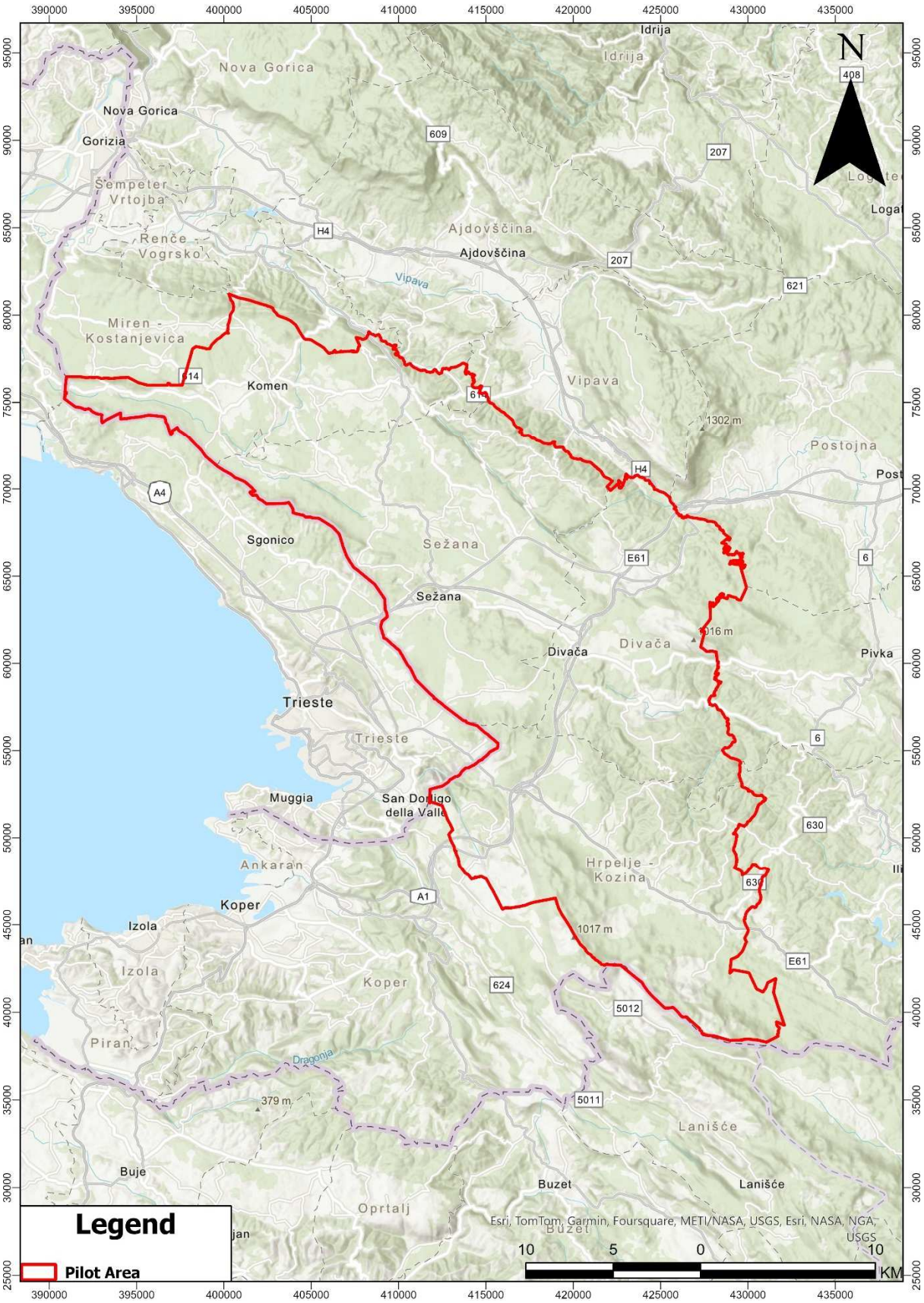

Figure 19. Pilot area of Slovenia.

The number and area of fires in Slovenia fluctuates greatly between years (Figure 20 and Figure 21) as the incidence depends on the weather conditions in the individual year. In Slovenia, the western, sub-Mediterranean part of the country is most at risk. It is expected that climate change will contribute to a greater fire risk in the eastern parts of Slovenia as well.

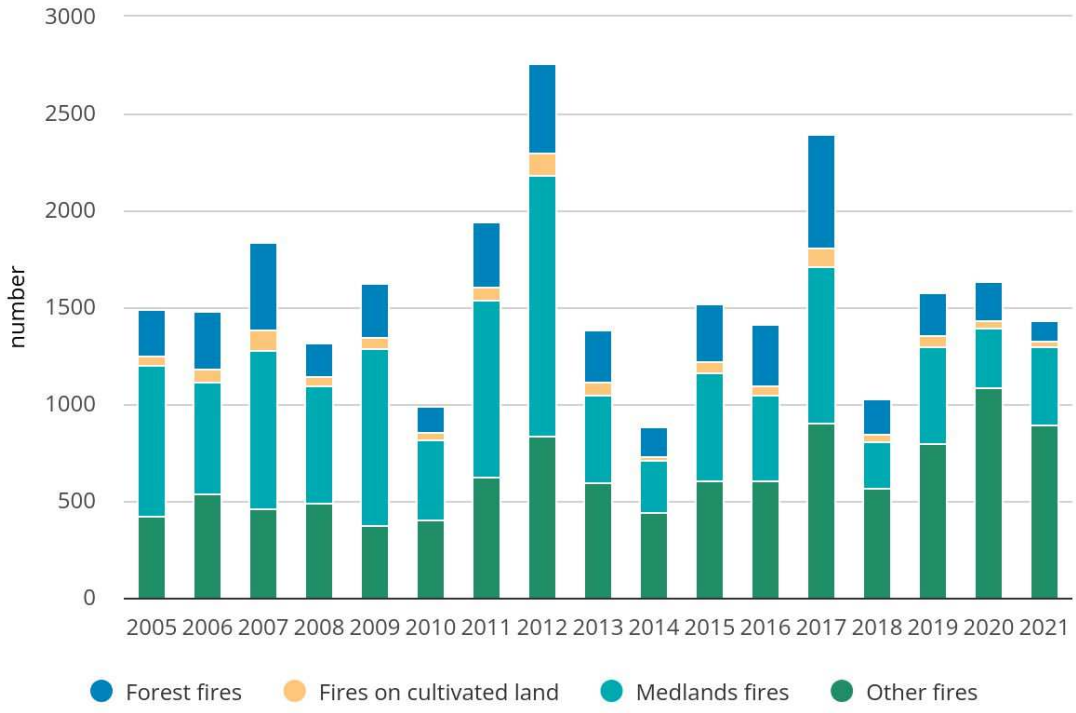

Figure 20. Annual number of fires in Slovenia from 2005-2021 (Source: ARSO).

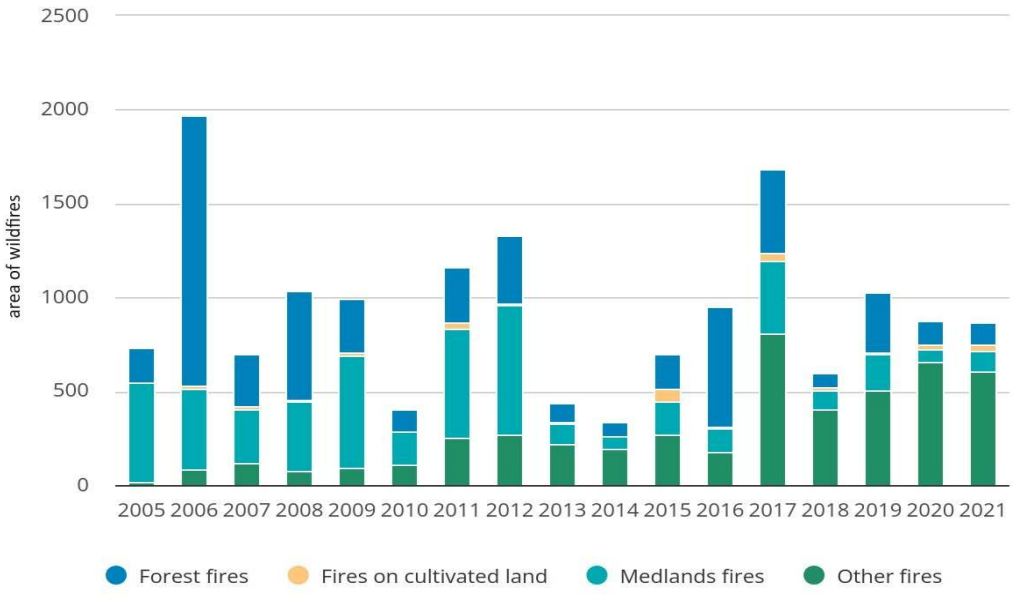

Figure 21. Annual burned area in Slovenia between 2005-2021 (Source: ARSO).

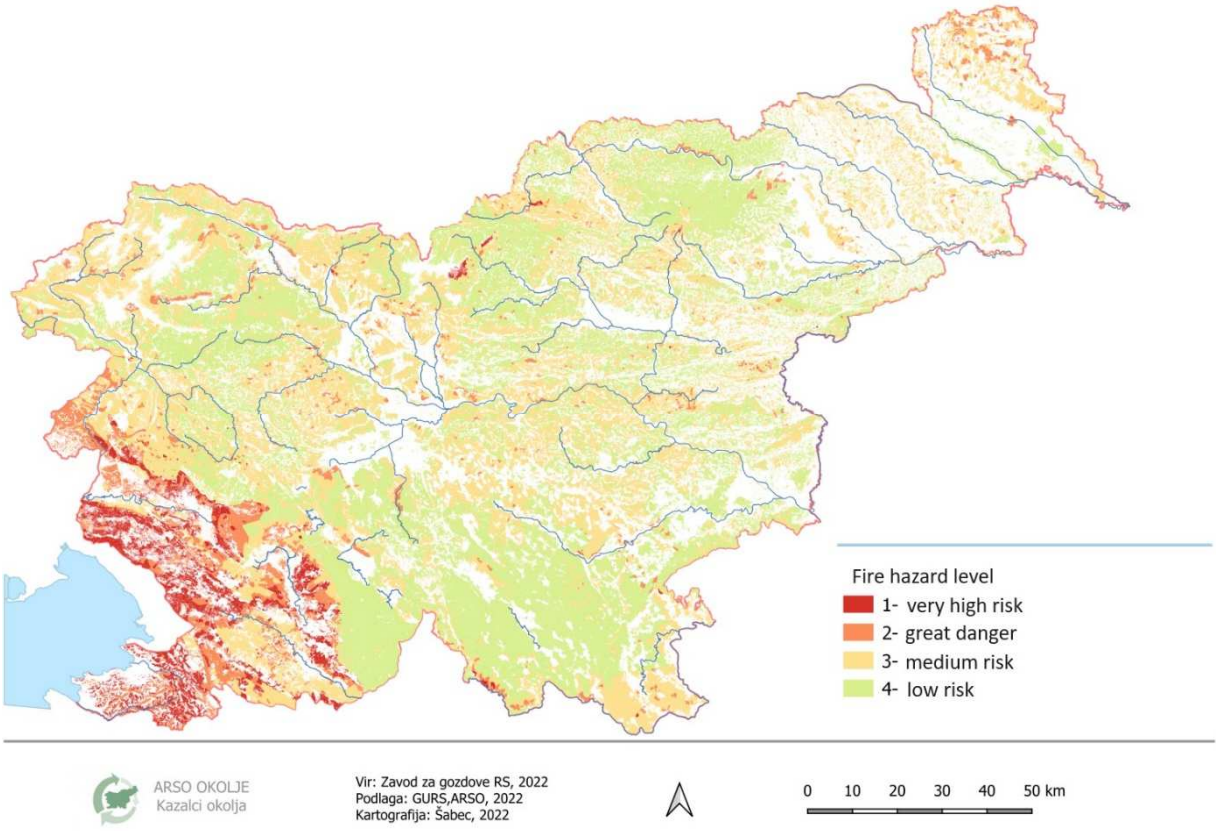

Figure 22. Levels of fire hazard in Slovenia (Source: ZGS).

The biggest fire in the history of independent Slovenia is the fire in the Karst, which started on July 15, 2022 and covered more than 3,000 hectares of the Italian and Slovenian part of the Karst plateau.

Most fires occur in the south-western, sub-Mediterranean part of the country, which can be seen on the fire risk map (Figure 22). In this predominantly sub-Mediterranean climate-vegetation area, in addition to the warm climate and uneven distribution of rainfall, the probability of fires is also increased by the carbonate rock base, which does not retain waters and frequent strong winds, especially gales. The natural factors are joined by the millennial influence of man, whose action is manifested mainly in the changed vegetation composition of forests, especially the presence of anthropogenic plantations of black and red pine. 150 years ago, the karst was a stony landscape that became green with a lot of work, patience and efforts. The economic losses of timber in forest fires are usually not great, but the indirect damage to ecosystems is great, so the danger of fires in this area must be taken very seriously.

3.2.1. Geographical Location and administration

The municipality of Komen is a karst municipality that extends over an area of 103 km², where it borders the municipality of Devin-Nabrežina, up to Braniška dolina on the northern edge of the karst, where the area continues into the Vipava valley and borders the municipalities of Miren-Kostanjevica, Nova Gorica, Ajdovščina and Vipava on the Slovenian side and Doberdob on the Italian side. On the southern side, it borders the municipality of Sežana and the Italian municipality of Zgonik. 20 village communities consist of 35 settlements and 3.556 inhabitants.

The municipality of Sežana, with its center in Sežana, is part of the Coastal Karst region and measures 217 km², which makes it one of the largest municipalities in Slovenia, with 13.702 inhabitants living in the municipality. The municipality is divided into 12 local communities. It borders the municipality of Komen in the north, Vipava in the northeast and Divača in the east, and in the south it also borders the municipality of Hrpelje - Kozina. The western border of the municipality of Sežana is also the state border between Slovenia and Italy.

The municipality of Divača covers an area of 145,8 km². The settlements are administratively divided into 6 local communities, with 4.371 inhabitants living in the municipality. The municipality is located in southwestern Slovenia and belongs to the Coastal-Karška region. It covers the Divaški Karst, the Senožeška region and the western part of Brkinov.

Hrpelje - Kozina municipality, the geographical area of the municipality extends over the area of Brkinov, Čičarije and Mali Karst. It borders Italy in the west and Croatia in the south. The border municipalities are Divača, Sežana, Koper and Ilirska Bistrica. The municipality comprises 39 settlements on an area of 195 km2 and has a population of 4.300 residents.

Figure 23. Area of operation of the Fire and Rescue Service Sežana.

3.2.2. Climatic conditions

Apart from the coastal area, Slovenia belongs to the warm zone. The southwestern part of Slovenia, which also includes the Karst, is classified as a moderately warm climate, more precisely continental humid with hot summers. The climate here can sometimes be very surprising, as it is influenced by many different climatic factors, so that strong winds and unusually high or low temperatures are quite common.

The climate of the Karst is typically Mediterranean with some peculiarities arising from the geographical and geomorphological characteristics of the area. Karst is a region in Slovenia known for its limestone base and characteristic karst landscape, which includes karst caves, sinkholes, and fields. At the same time the climate of the Karst is strongly influenced by the Mediterranean climate, which means mild winters and hot summers. Average winter temperatures rarely fall below freezing, while summer

temperatures often rise above 30°C. The karst receives moderate amounts of precipitation distributed throughout the year, with the most precipitation in autumn and spring. Annual rainfall is around 1.000 mm, but rainfall is often unevenly distributed, which can result in dry and wet periods. One of the most characteristic climatic features of the Karst is burja, a strong northeast wind that blows mainly in the winter months. A storm can reach high speeds and cause rapid cooling of the air, as well as carrying large amounts of dust and snow. Due to the limestone base, which quickly absorbs water, dry periods in the Karst are particularly pronounced. The vegetation on the Karst is adapted to dry periods, which is reflected in the predominance of hardy plant species such as oaks and pines .

The Karst landscape is exposed to large temperature fluctuations, especially between day and night. During the summer months, the days are very hot and the nights quite cold, which causes a marked daily temperature fluctuation.

Due to the karst subsoil, the availability of surface water resources is limited. Water quickly seeps through the limestone bedrock and collects in underground reservoirs, creating characteristic karst phenomena such as karst caves. These characteristics make the Karst a unique region with an interesting and complex climate that strongly influences the way of life, flora and fauna in the area.

Based on the Ombrothermic diagram for the period 1980-2022 (Figure 24), it appears that the summer average temperatures range from 19,49 °C to about 21,89 °C, with average precipitation between 95,1 mm and 138,42 mm. In winter, the average temperatures vary from 3,34 °C to 4,41 °C, and precipitation ranges from 87,9 mm to 127,48 mm. July is identified as the hottest month, averaging 21,89 °C, and January as the coldest, at 3,3 °C. October is the wettest month, with 180,88 mm of precipitation, while February is the driest, receiving 87,92 mm.

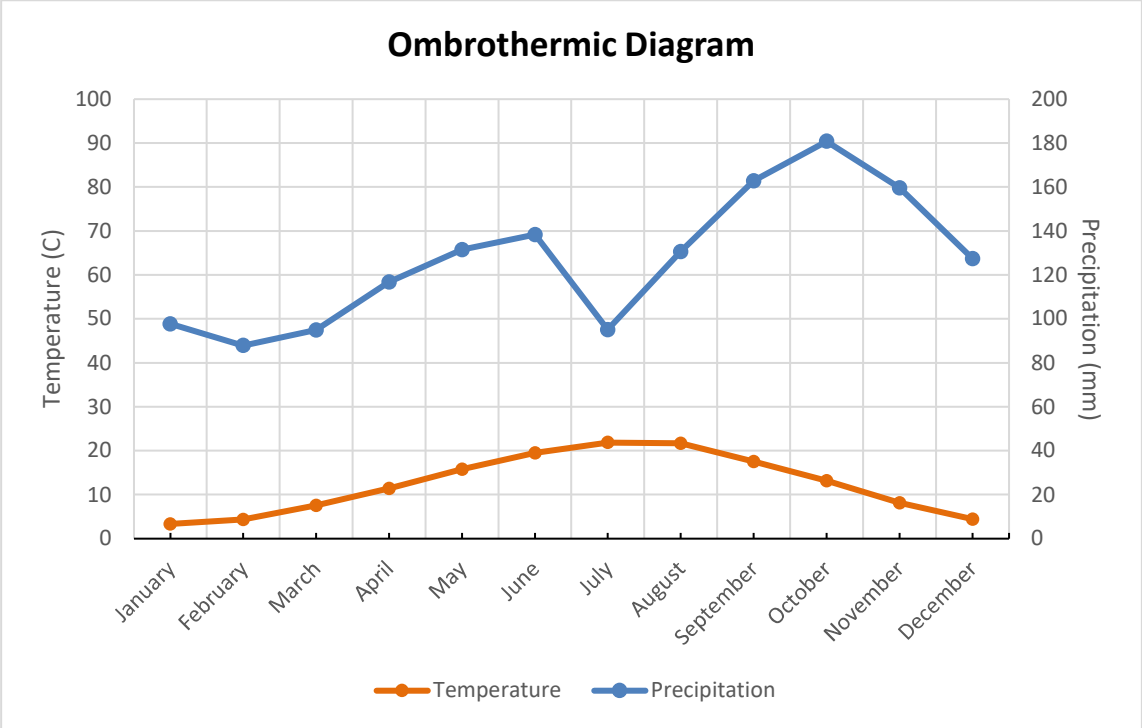

Figure 24. Ombrothermic Diagram of the Karst region in Slovenia for the years 1980-2022 based on the CRU TS dataset (Harris et al. 2020).

3.2.1. Land Uses

The Karst Plateau in Slovenia features a mix of land uses reflecting its unique geographical and cultural landscape. Forestry plays an essential role, with mixed woodlands of oak, pine, and beech contributing to local economies and biodiversity. Upon examining the chart generated using data from CORINE Land Cover (Figure 25), it becomes clear that Broad-leaved forests dominate the total area, covering a significant 39,2%. Traditionally, agriculture has been a significant activity, with vineyards, pastures, and small-scale farming prevalent in the region. Following up are transitional woodland-shrub areas, which cover 14,2% of the total area. Lastly the third most significant land use in the area is land principally occupied by agriculture with significant areas of natural vegetation, which take up to 10,16% of the total area. All the remaining land uses cover below 10% of the total area. In total it is clear that forested and agricultural areas are the two most significant land uses in the pilot area of Slovenia.

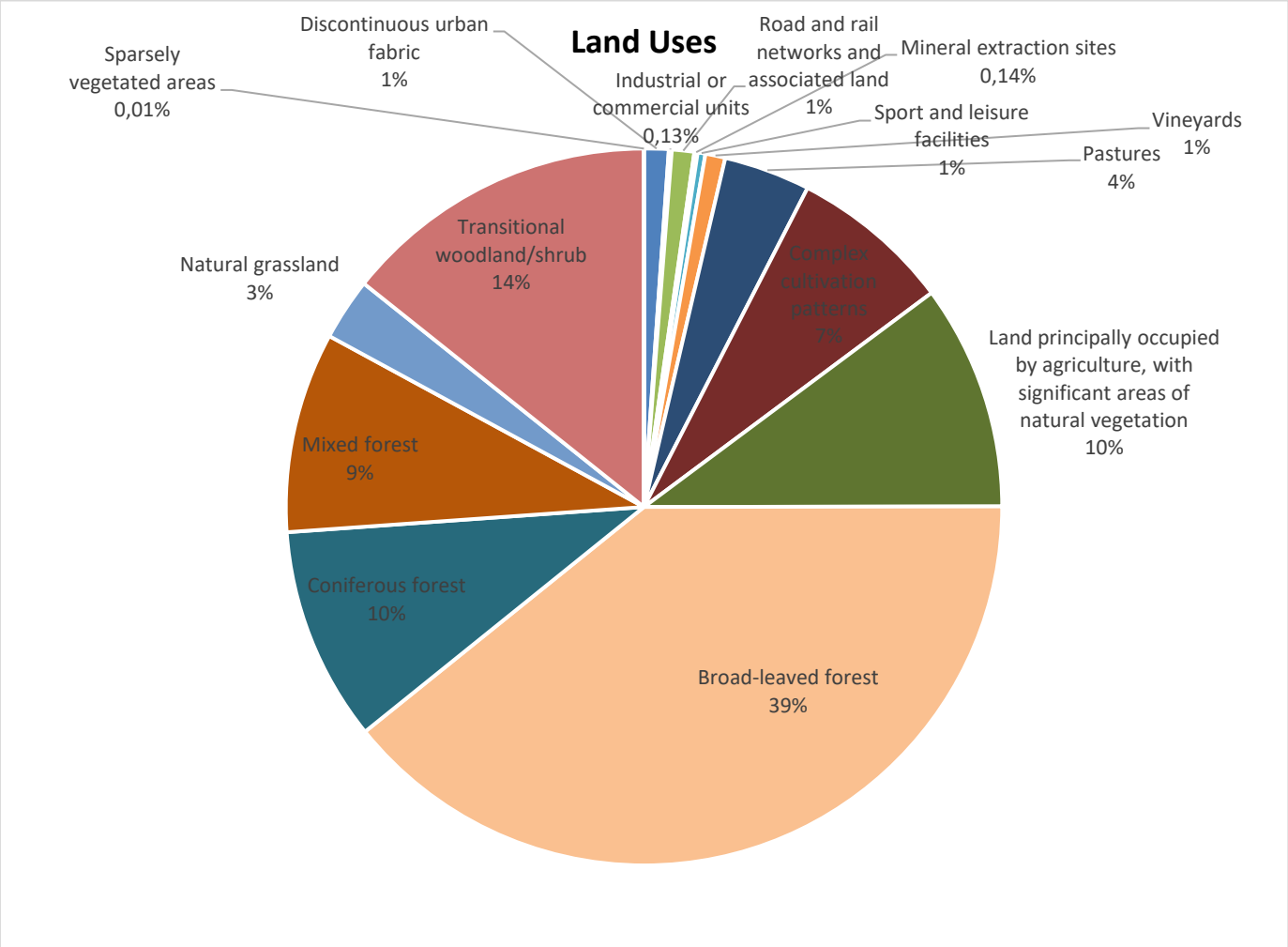

Figure 25. Percentage cover of different land use types that occupy the pilot area in Slovenia based on the CORINE land cover.

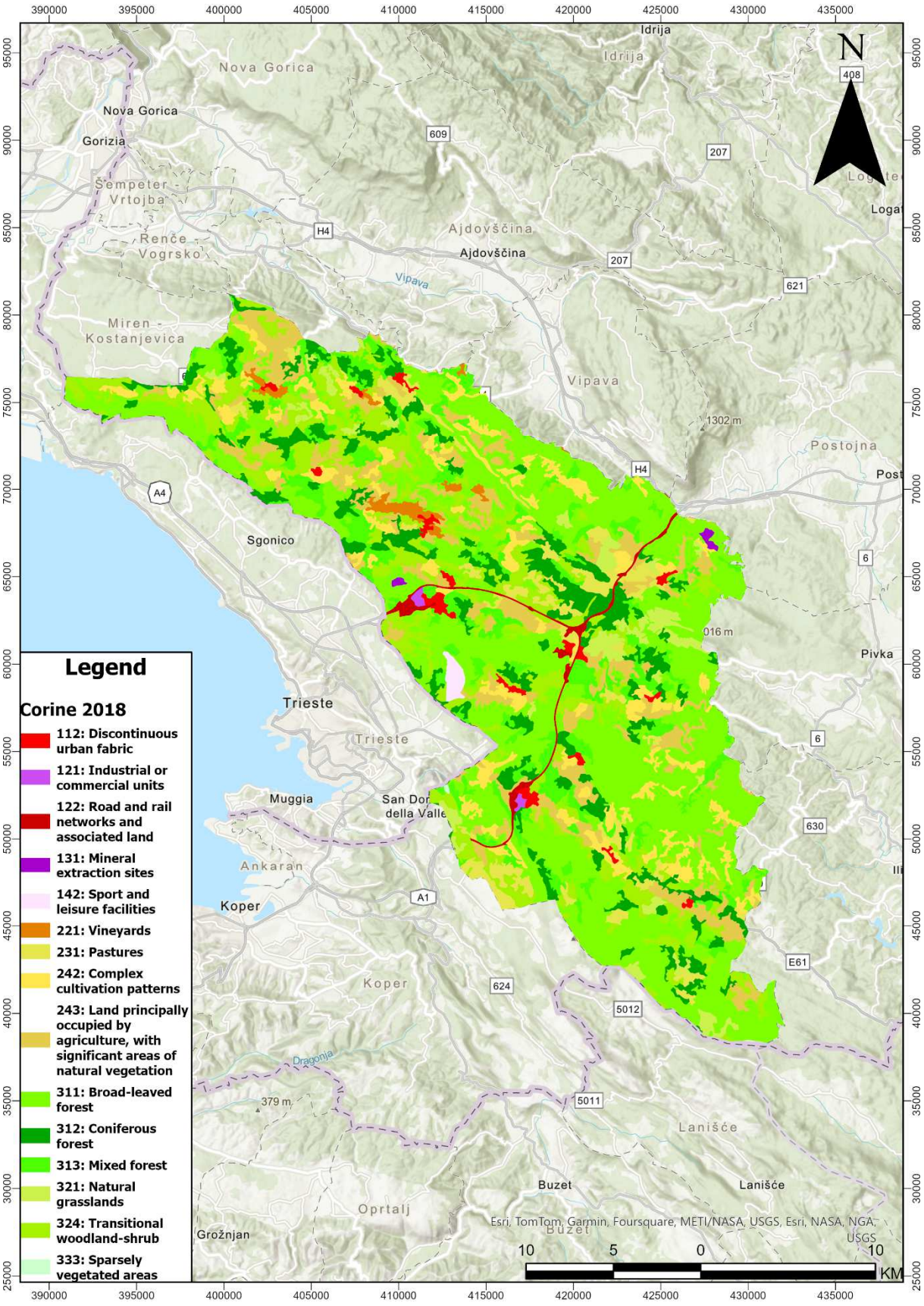

Figure 26. CORINE land cover map of the pilot area in Slovenia.

3.2.2. Flora and Vegetation

The remarkable biodiversity of the Karst is a result of its location on the periphery of the Mediterranean, which is the most species-rich region of Europe and one of the planet's biodiversity hotspots. These hotspots harbor the majority of endemic, original plant and animal species, representing the highest levels of natural diversity. The Mediterranean region's varied geological history and its role as a refuge for numerous species during the Ice Ages have driven rapid evolutionary processes. Situated at the intersection of western and eastern Mediterranean faunal regions, the Karst hosts species from both areas. Additionally, its position at the crossroads of Mediterranean and continental regions allows for a blend of inhabitants from both. Evidence of a historical connection with the Eastern European steppes is indicated by the presence of certain species. The intricate mosaic of grassland and forest ecosystems further enhances the Karst's diversity, supporting both grassland and forest species. The transitional phase, when grasslands are left to develop and eventually become overgrown, is particularly favorable for a wide variety of plants and animals.

For a long time, the Karst region was seen as an unwelcoming stone desert dominated by the bora wind. In the 19th century, the Austrians, who ruled the area, initiated afforestation efforts. The local population opposed this, as it encroached on their land and altered the climate, making it more humid and weakening the bora wind. Planting trees in the rocky terrain was challenging, but the Austrian Pine, not native to the Karst, proved most successful in taking root. Photographs over fifty years old still depict the barren stone landscape where forests now thrive. The Karst’s transformation accelerated after World War II when sheep and goat breeding was banned, allowing forests to grow naturally and continue to expand. Today, the region's wild forests predominantly feature European Hop-hornbeam, Downy Oak, and Manna Ash, with Beech trees more common at higher elevations.

To witness natural diversity in its full splendor, one should visit the stony grasslands and overgrown village commons. In this area, the food chains are based on a vast array of plant species. On rocky terrain with thin soil, different species thrive compared to those on deeper, more bush- and tree-covered ground. In March, yellow hues dominate the Karst, with Dogwood among the bushes and Cinquefoils on rocky pastures. Early bloomers include plants with bulbs, rhizomes, or tubers, which derive energy from their underground reserves to produce colorful flowers. These plants must complete their life cycle and seed production before the summer drought. The tiny blue flowers of the Common Grape Hyacinth bloom as early as March. Later, among the

dry grass, the modest Meadow Anemones, with their dark purple flowers protected by furry down, appear to bow toward the ground. In April, the village commons turn white with the blossoms of Mahaleb Cherries and Poet's Daffodils, creating the illusion of a snowy landscape, a rare winter sight in this region. The Illyrian Irises typically bloom around May Day, followed by the striking pink flowers of the Burning Bushes near the shrubs. The rare Slender Fritillary, a relative of the Snake's Head Fritillary, can be a fortunate find.

Figure 27. Sky blue flowers of the Trieste Gentian (Gentiana tergestina) bloom in the grass.

Another proof is that more than half of this territory is fully included in the Natura 2000 network, which protects habitats and species with the highest conservation value at the European level.

If we present it in numbers, Karst has:

• 16 habitats on the Slovenian side, of which 10 are recognized as priority;

• more than 200 bird species, of which 72 are included in Annex I of the European Birds Directive (2009/147/EC);

• 27 animal species of mammals, reptiles, amphibians, fish and invertebrates are protected by the Habitats Directive (92/43/EEC), among which four are priority;

• more than 500 species of butterflies;

• several endemic species of plants and animals.

Natura 2000 protects habitats such as: forests and shrubs, dry karst grasslands, calcareous thermophilic screes, cliffs, water bodies and underground environments.

Forests and shrubs

Long ago, the Karst was covered with oak forests, which were gradually destroyed after thousands of years of deforestation and grazing. The Karst scrubland is the most represented environment on the Karst Plateau. After the Second World War, with the abandonment of grazing, it grew rapidly. The thin preperine soil layer and the permeability of the bedrock are factors that favor the development of a sparse tree cover that is more shrubby than treelike.

Karst gmajna

Where the forest did not overgrow the ancient pastures, one of the most peculiar environments of this area was created: dry karst grasslands or Karst gmajna. They were created due to the pressure of grazing animals, mainly cattle, sheep and goats, which over thousands of years have selected a grass that is resistant to trampling and grazing.

Calcareous thermophilic screes

Prealpine calcareous thermophilic screes are very limited but extremely interesting. In this environment, colonization of plants is difficult due to the dryness and instability of the substrate and constant exposure to atmospheric factors. Therefore, a peculiar plant community develops in them, mostly limited to a low layer of herbaceous plants.

Water bodies

A special feature of the Karst is the almost complete absence of surface water, which is a result of the permeability of the strongly cracked bedrock. Water preferentially flows through underground tunnels, leaving the surface free of water environments. Kale, small depressions in the ground where rainwater was collected by adding clay, were used to water domestic animals and to supply water to the local population.

Underground environments

The wealth of the subterranean environment consists of systems of sinkholes, vertical chasms, caves and caverns, which are hidden beneath the ground and provide another type of habitat for living organisms. Vegetation inhabits it in such a way that it responds to the level of brightness and to changes in humidity and temperature.

Vegetation

Karst belongs to the sub-Mediterranean phytogeographical zone and is floristically very rich. Forest vegetation once dominated. Man has shrunk forest areas by cutting and burning. On deeper soil, farmers created

meadows and maintained them by regular mowing. They grazed on shallower and stony ground. Grazing, erosion processes and occasional fires turned pastures into bare stone surfaces, especially on the slopes. In the middle of the 19th century, they started reforesting the degraded karst soil. Several decades ago, due to reduced use, the overgrowth of pastures and meadows began.

The most widespread forest community is sub-Mediterranean heat-loving black hornbeam and small ash forests (Ostryo-Quercetum pubescentis), black hornbeam and autumn elm forests (Seslerio Autumnalis-Ostryetum group), and beech forests (Hacquetio-Fagetum) flourish in some places on the eastern slopes. A large part of the Karst is covered by secondary stands of black pine (Pinus nigra), which were used to reforest bare areas in the 19th century.

An important karst habitat are grasslands, especially communities of low sedge and rock sedge (Carici humilis- -Centaureetum rupestris). This is one of the most colorful and floristically richest grass communities in Europe.

The simultaneous presence of plants with such different ecological requirements is a great rarity in nature. Among the most iconic floristic elements of the Karst are some shrubs. In the autumn, the dry rocky karst landscape is covered in warm colors by common dogwood (Cotinus coggygria), red dogwood (Cornus sanguinea), yellow dogwood (Cornus mas) and blackthorn (Prunus spinosa).

3.2.3. Fauna

The karst also boasts an exceptional variety of animal groups, both on the surface and underground.

Many caves in the Karst are the habitat of a large number of animal species, which is why it is classified as one of the hotspots of cave fauna biodiversity. Underground organisms are at great risk, as the destruction or pollution of the habitat can mean the destruction of a species. The most important caves with a rich fauna, which are important from the point of view of preserving underground fauna in the Karst area, are Škocjanske jame, Dimnice, Dolenca, Belinca jama, Kačna jama.

One of the most recognizable representatives and a symbol of the natural heritage of the Dinaric karst is the proteus (Proteus anguinus), also known as the marsh wrasse or - because of its pale skin - the human fish, which is the only European amphibian that lives in the underground watercourses of the Dinaric karst. Its geographical area includes northeastern Italy, southern Slovenia, Croatia and Bosnia and Herzegovina.

More than twenty species of bats have been recorded in the Karst, and they have one of the largest habitats in the Škocjan Mountains caves, where they are most numerous and there are several thousand of them.

Another subterranean habitat on the Karst is epicras. It is the upper rock layer under the soil, through which water seeps from the surface. Research on the epicrastic fauna is relatively new, so it has not yet been widely studied.

In the area of the Karst, it has so far been investigated within the framework of the extensive Natura 2000 area on both sides of the border and due to the presence of previously protected natural areas. She was in the area in question fauna studied so far in the Škocjan Caves and in the Dimnice Cave.

Among the insects in the Karst, there are European endangered species of beetles that are designated as a Natura 2000 area.

Among the fauna of the Karst, butterflies stand out in terms of the number of species. The Karst area is extremely diverse, as over 500 species of diurnal and nocturnal butterflies are present here. Among the threatened species in Europe, four species in the Karst were included in the Natura 2000 network.

The Natura 2000 area has already been defined for many species of birds (e.g. mountain lark (Lullula arborea), grebe (Caprimulgus europaeus), skunk (Upupa epops), hornet (Pernis apivorus), great hornbill (Bubo bubo) and great hornbill (Otus scops), as a relatively high density of nesting sites of European importance was found in the Karst.

Dry karst grasslands are a very suitable habitat for a variety of reptiles. Among the snakes, there are the black snake (Hierophis viridiflavus carbonarius), common goad (Zamenis longissimus), while the cat's-eye snake (Telescopus fallax) and blue snake (Vipera ammodytes) are present in even drier environments than, for example, scree, scree or calcareous loam.

Lizards include the green lizard (Lacerta viridis), as well as the Dalmatian Wall Lizard (Podarcis melisellensis), the coastal lizard (P. sicula) and the black-spotted lizard (Algiroydes nigropunctatus).

Karst is also a habitat for animals. Wild cat (Felis silvestris), lynx (Lynx lynx), golden jackal (Canis aureus), wolf (Canis lupus) and brown bear (Ursus arctos) have been recorded.

Figure 28. The Dalmatian Wall Lizard (Podarcis melisellensis) basks in the autumn sun.

3.2.4. Spatial data

- **Aspect**

By examining the aspect map for the pilot area in Slovenia, we gain insight into the region's intricate and distinctive terrain, characterized by a diverse range of slope orientations. On average, the slopes predominantly face south-southwest, but there is also a significant proportion oriented towards north-northeast (Figure 29). This diversity in slope aspects highlights the varied landscape, which includes everything from urban areas and villages to mountainous regions and dense forests. This mixture of aspects provides a comprehensive representation of the region's topographical variations.

- **Slope**

The slope map for this pilot area reveals a pronounced contrast between flatter regions and those with steeper inclines. By analyzing Figure 30, it is clear that the northern part of the area, along with certain sections in the south, predominantly features flatter terrain. In contrast, the eastern side of the area is characterized by more pronounced, steeper slopes. This variation in topography is visually distinguishable on the map, where flatter areas are depicted in lighter brown tones and steeper areas in darker shades. This clear differentiation helps in understanding the diverse landscape features within the region.

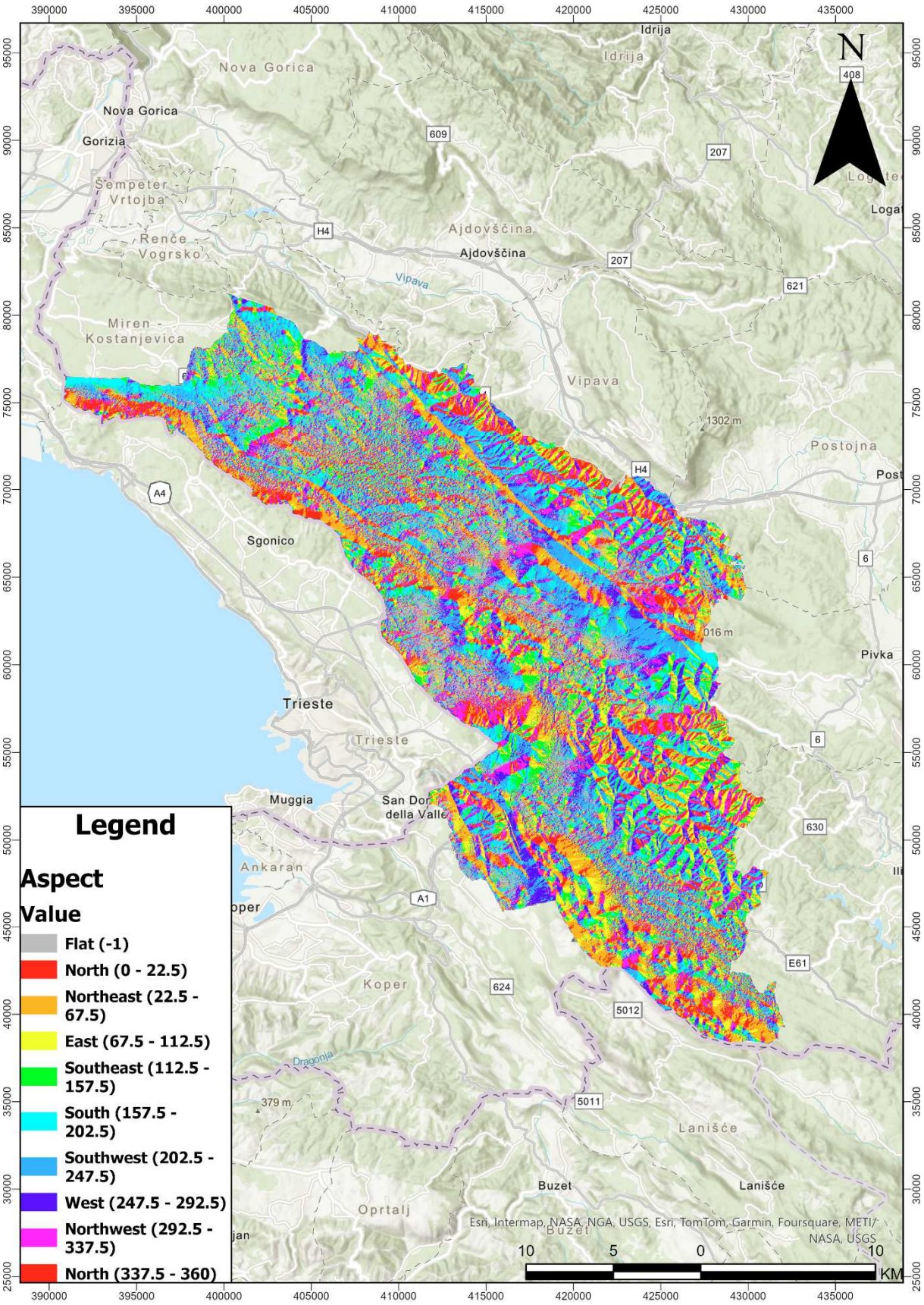

Figure 29. Aspect map of the pilot area in Slovenia.

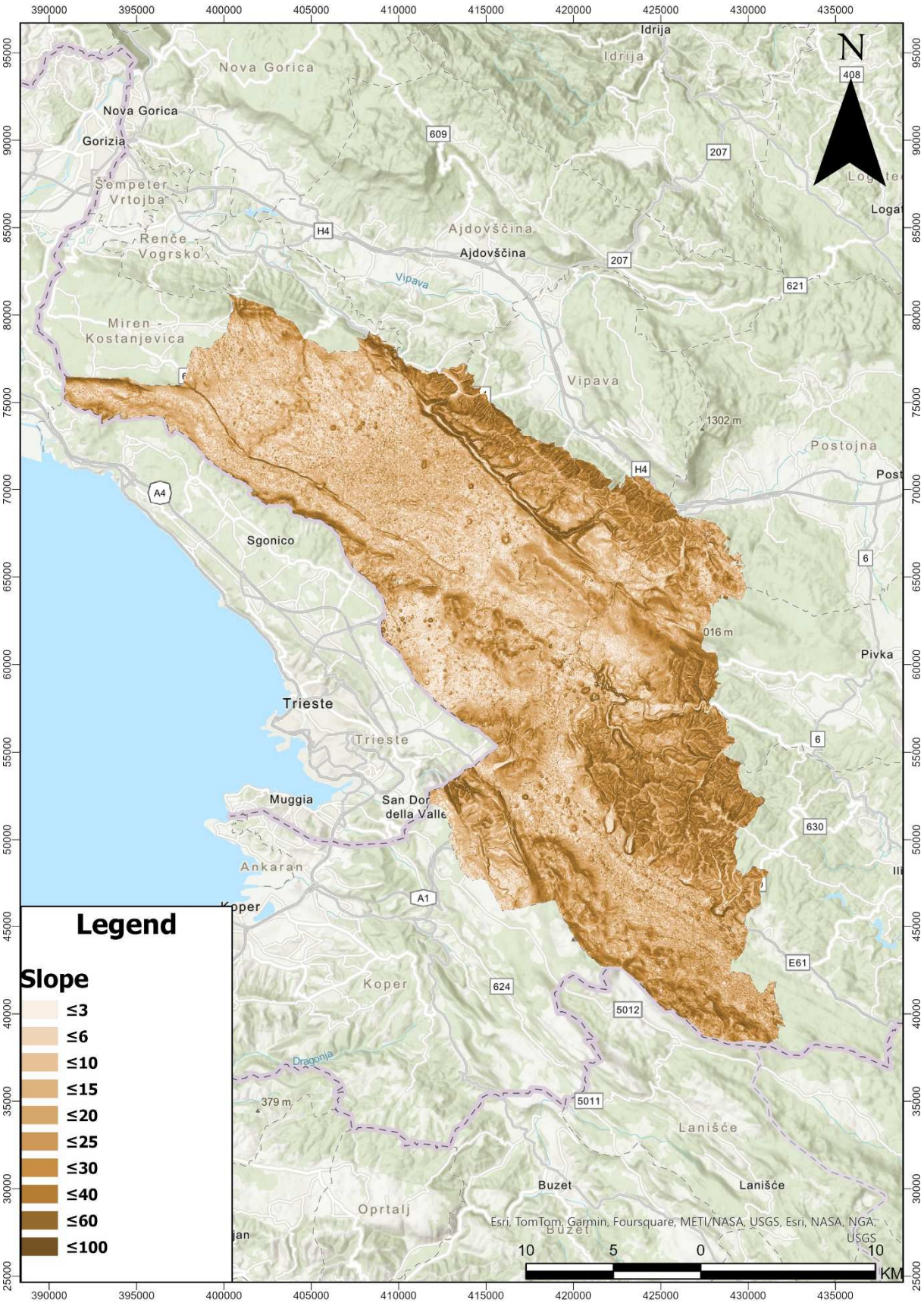

Figure 30. Slope map of the pilot area in Slovenia.

- **Geomorphology**

As previously noted, the geomorphology within this pilot area exhibits complexity, encompassing both mountainous terrain and flatter expanses. Upon closer inspection of the geomorphology map of this region (Figure 31), it becomes evident that the mountainous features are predominantly concentrated towards the eastern and southeastern sections of the map. On the other hand, the flatter areas, as indicated earlier in the slope analysis, appear to occupy the northern part of the map.

- **Canopy Height**

Upon examination of the Canopy Height Model (CHM) model for this pilot area, it becomes apparent that the majority of the forested areas are densely concentrated in the eastern and southeastern sectors, with some scattered patches of forest present in the western regions (Figure 32). This also fits with the geomorphology of the area as described above.

- **Tree cover density**

Additional confirmation of forested regions in the eastern, southeastern, and western sectors of the map comes from the tree cover density map. As depicted in Figure 33, it is apparent that the densest forested areas are situated in the eastern and southeastern portions, whereas sparse forests are found in the northern and western parts. Moreover, the central area of the region predominantly consists of non-forested areas with sparse vegetation, largely occupied by human infrastructure.

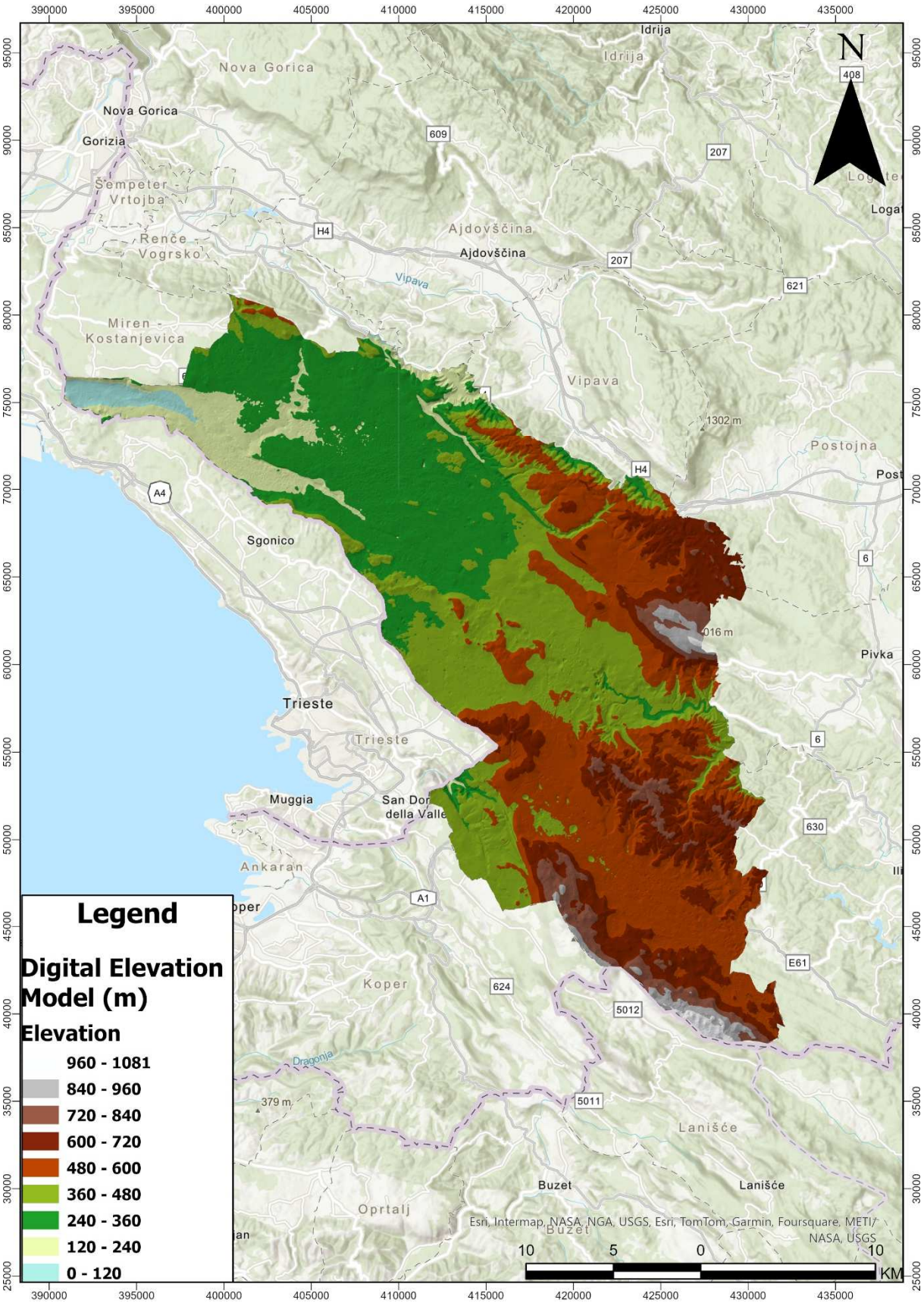

Figure 31. Geomorphology map of the pilot area in Slovenia.

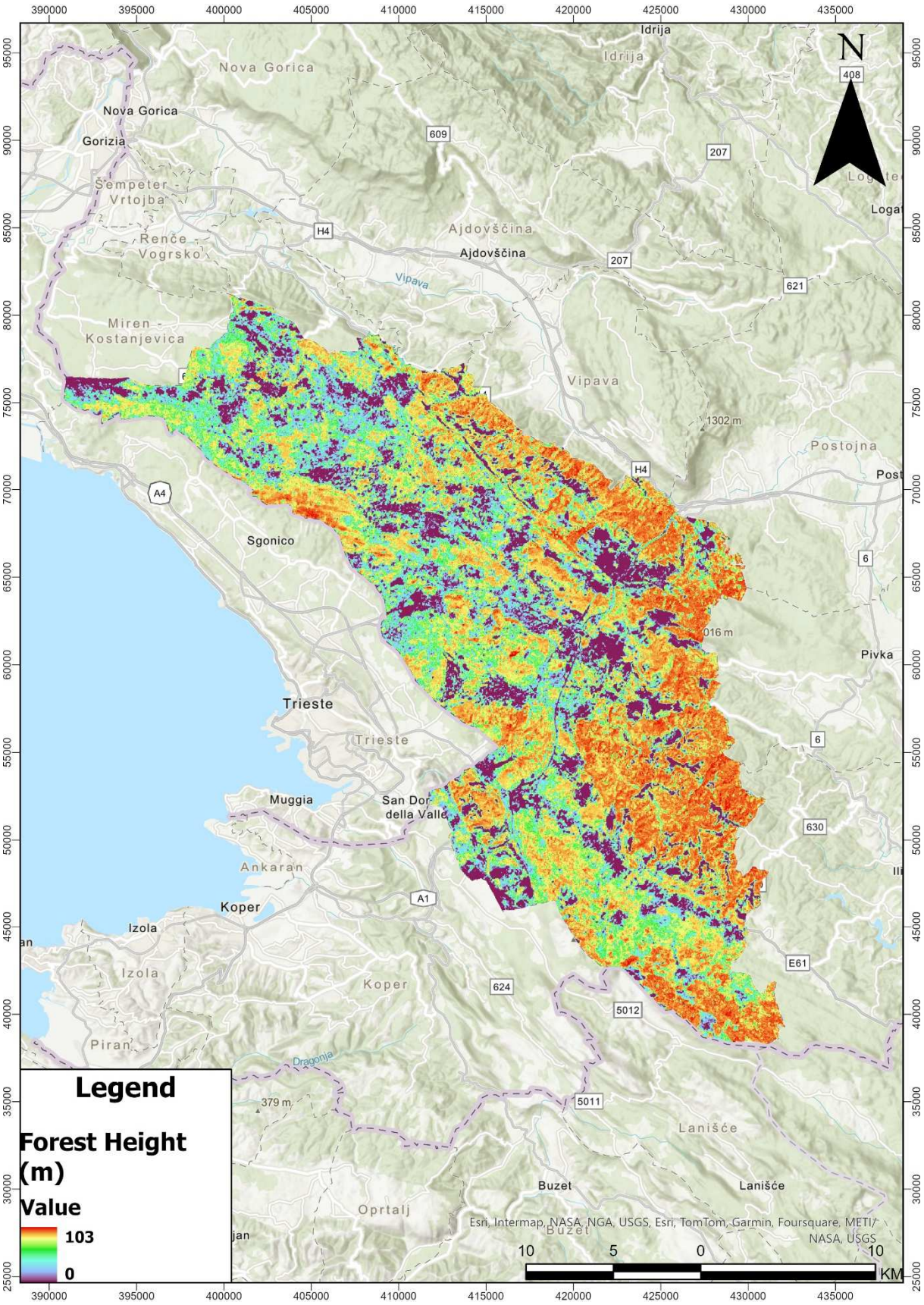

Figure 32. Canopy Height Model of the pilot area in Slovenia.

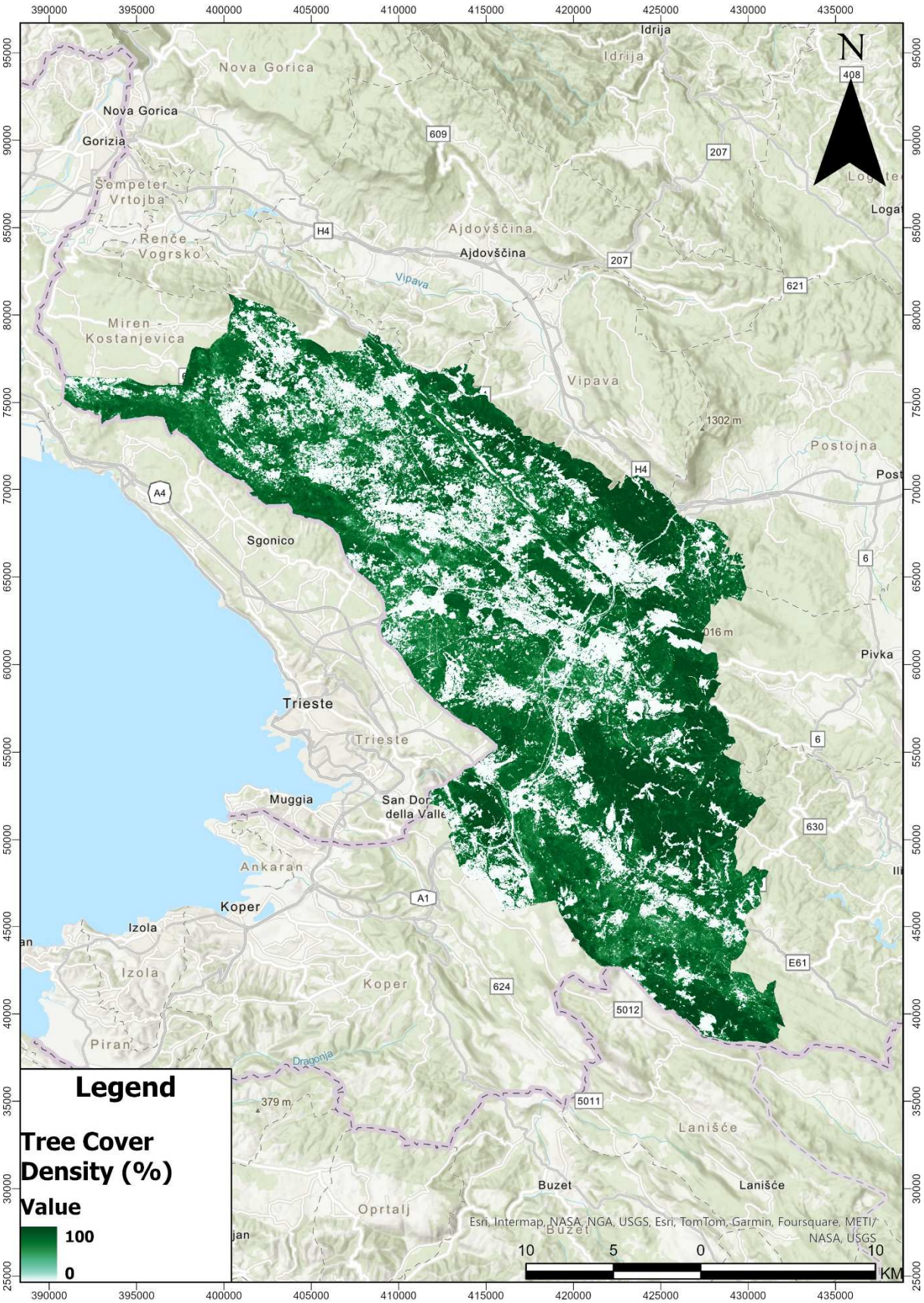

Figure 33. Tree cover density map of the pilot area in Slovenia.

- **Roads and buildings network**

Upon examination of the roads and buildings map of the pilot area in Slovenia (Figure 34), an extensive road network spanning across the region can be noted. A significant portion of this network traverses through forested and mountainous terrains, highlighting its importance in future planning efforts aimed at protecting these areas from wildfires. Some of these roads could potentially serve as designated emergency routes during fire incidents, ensuring crucial access for firefighting vehicles when rapid response is imperative. This designation plays a pivotal role in effectively managing and mitigating sudden wildfires, facilitating swift and coordinated emergency responses.

- **NDVI**

Upon closely examining the four NDVI (Normalized Difference Vegetation Index) maps, it becomes evident that the pilot area is heavily vegetated during the summer months, as shown in Figure 35. Although substantial vegetation remains during autumn, it is crucial to observe that a significant reduction in vegetation occurs during the winter, leaving much of the area barren. These seasonal variations in vegetation density are valuable for understanding and analyzing the patterns and impacts of past fires. Additionally, this information can be instrumental in developing comprehensive guidelines for the prevention of future ones.

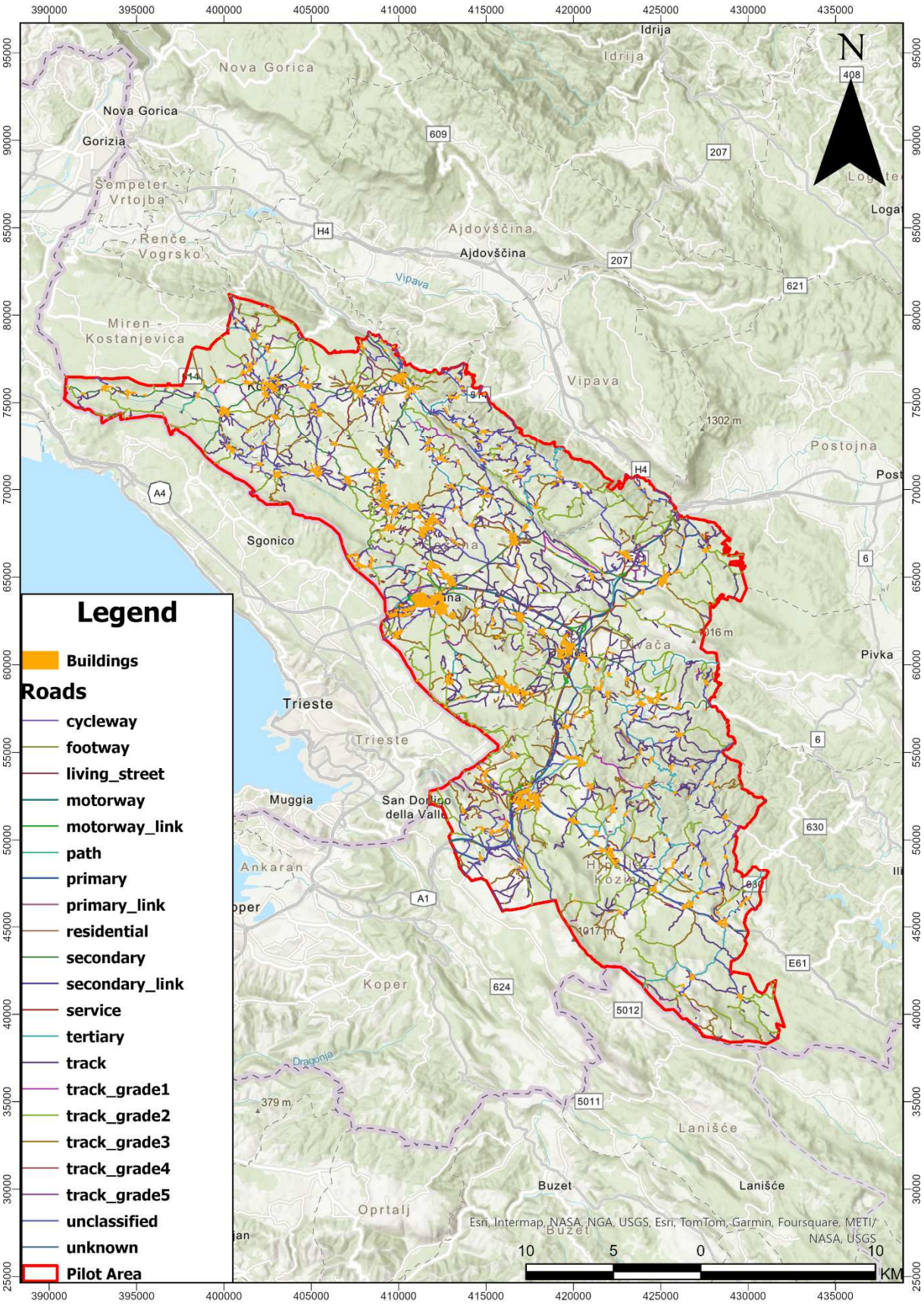

Figure 34. Roads and buildings map of the pilot area in Slovenia.

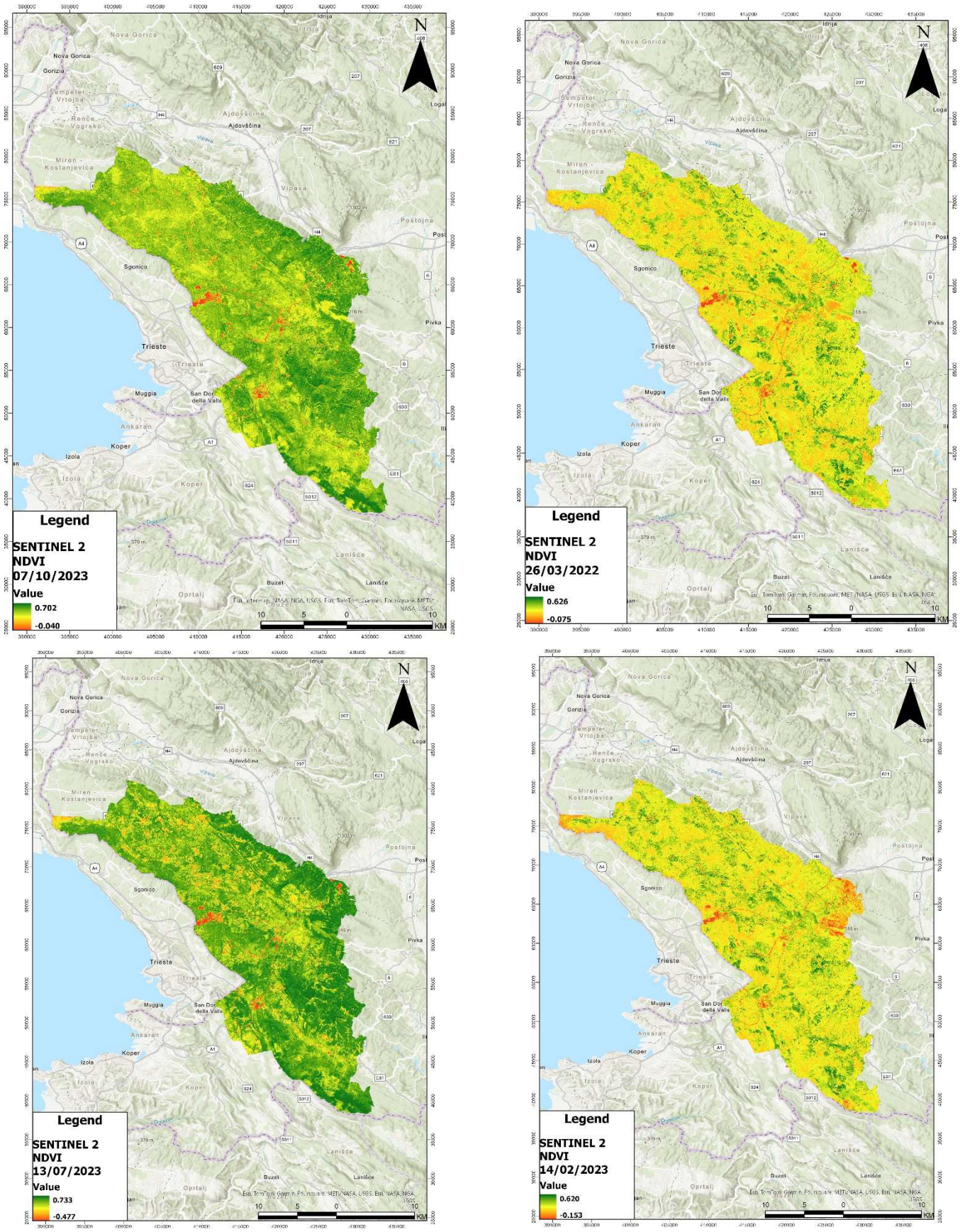

Figure 35. Figure 13. NDVI maps that cover all four seasons for the pilot area of Slovenia. The autumn NDVI map is displayed at the top left, the spring NDVI map at the top right, the summer NDVI map at the bottom left, and the winter NDVI map at the bottom right.

- **Sentinel 2 images**

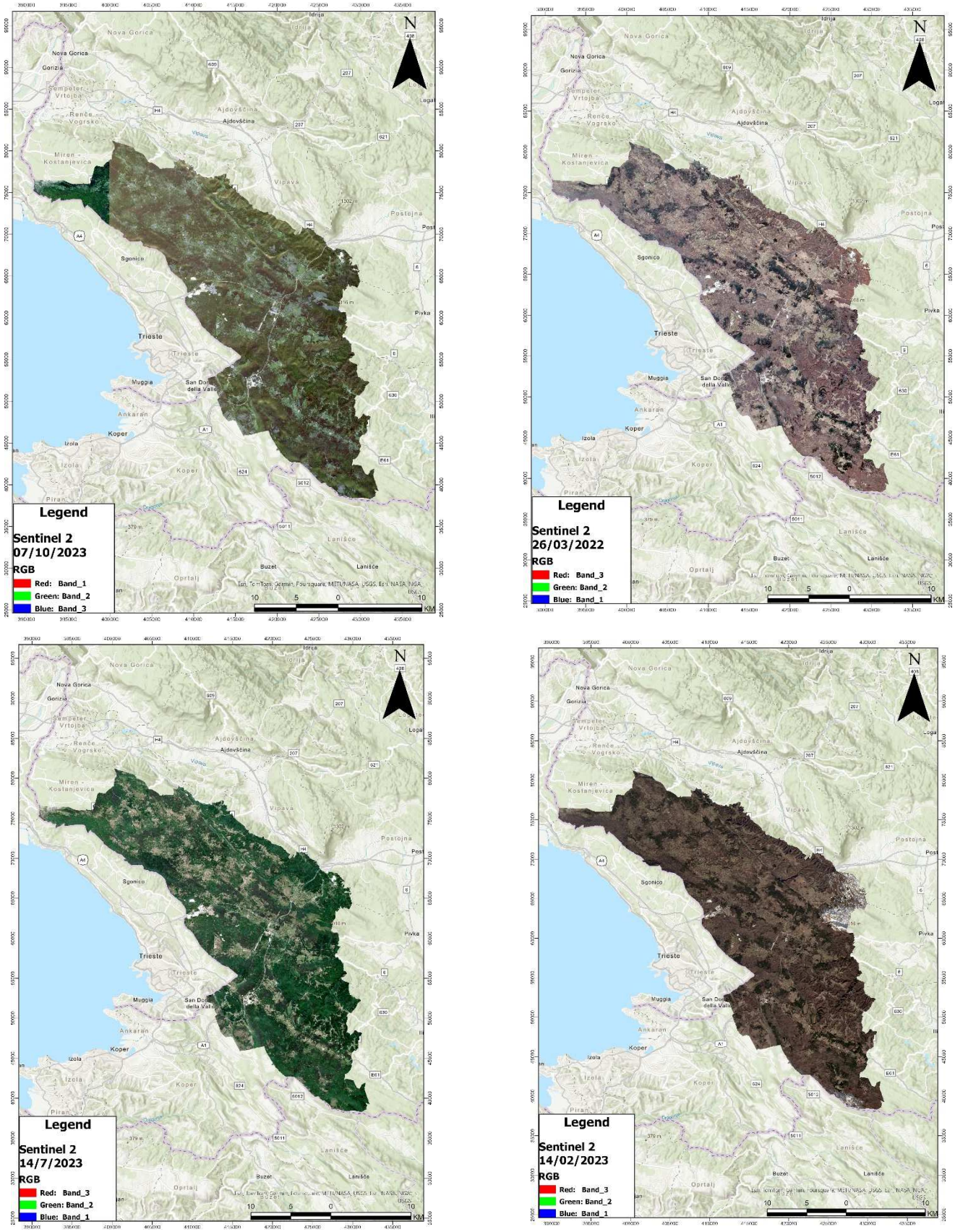

Figure 36. Sentinel 2 satellite images that cover all four seasons for the pilot area of Slovenia. The autumn Sentinel 2 image is displayed at the top left, the spring one at the top right, the summer one at the bottom left, and the winter one at the bottom right.

- **Planet image**

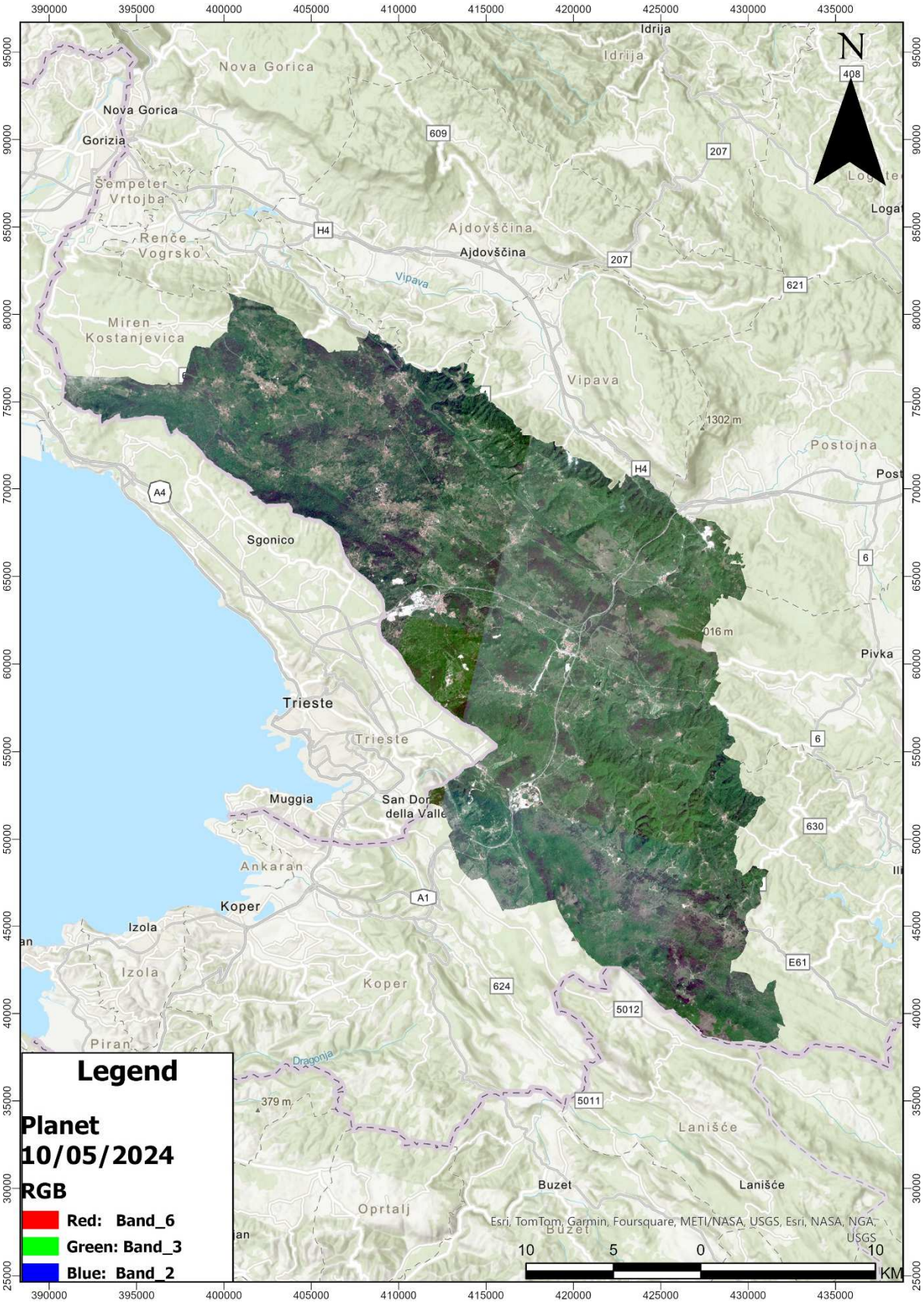

Figure 37. Planet image captured during spring for the pilot area of Slovenia.

3.3. Rocca di Cerere - Italy

Italy, situated in southern Europe, extends into the Mediterranean Sea, bordered by France, Switzerland, Austria, and Slovenia. Ecologically important, Italy is home to diverse ecosystems, including coastal areas, mountainous regions, and fertile plains. Its landscapes range from the rugged Alps in the north to the rolling hills of Tuscany and the volcanic features of Sicily. Italy boasts numerous protected areas, such as the Gran Paradiso and Stelvio National Parks, preserving its rich biodiversity and unique natural heritage. The country's commitment to environmental conservation is evident in its extensive network of parks and reserves, safeguarding flora, fauna, and crucial habitats. The pilot area of this project focuses on the province of Enna, which is located in the central part of the autonomous island region of Sicily (Figure 38). Enna is renowned for its striking landscape characterized by its elevated position on a plateau, earning it the nickname "Belvedere" or "panoramic viewpoint." At an altitude of around 931 m, Enna offers sweeping views of the surrounding countryside, dotted with rolling hills, fertile plains, and lush valleys.

Italy is prone to wildfires, particularly during the hot and dry summer months. The Mediterranean climate, characterized by high temperatures and limited rainfall in the summer, creates conditions that can easily lead to the ignition and spread of wildfires. Regions such as Sicily, Sardinia, and parts of southern Italy are especially vulnerable. According to the country's reports from National Fire Services (Gianfilippo et al. 2023), in 2022 the average fire danger in Italy during the fire season (July to September) exceeded the long-term average from 1988 to 2020, reaching 92% of the peak FWI recorded in 2007 (Figure 39). It's important to note that the FWI has not shown a significant trend over the analyzed period (red dotted line - Figure 39). A significant portion of the year-to-year variation in the total burnt area in Italy is attributed to changes in fire weather (Figure 40). The year-to-year shifts in FWI are correlated with changes in the burnt area, with 2022 exhibiting below-average changes in both FWI and burnt area.

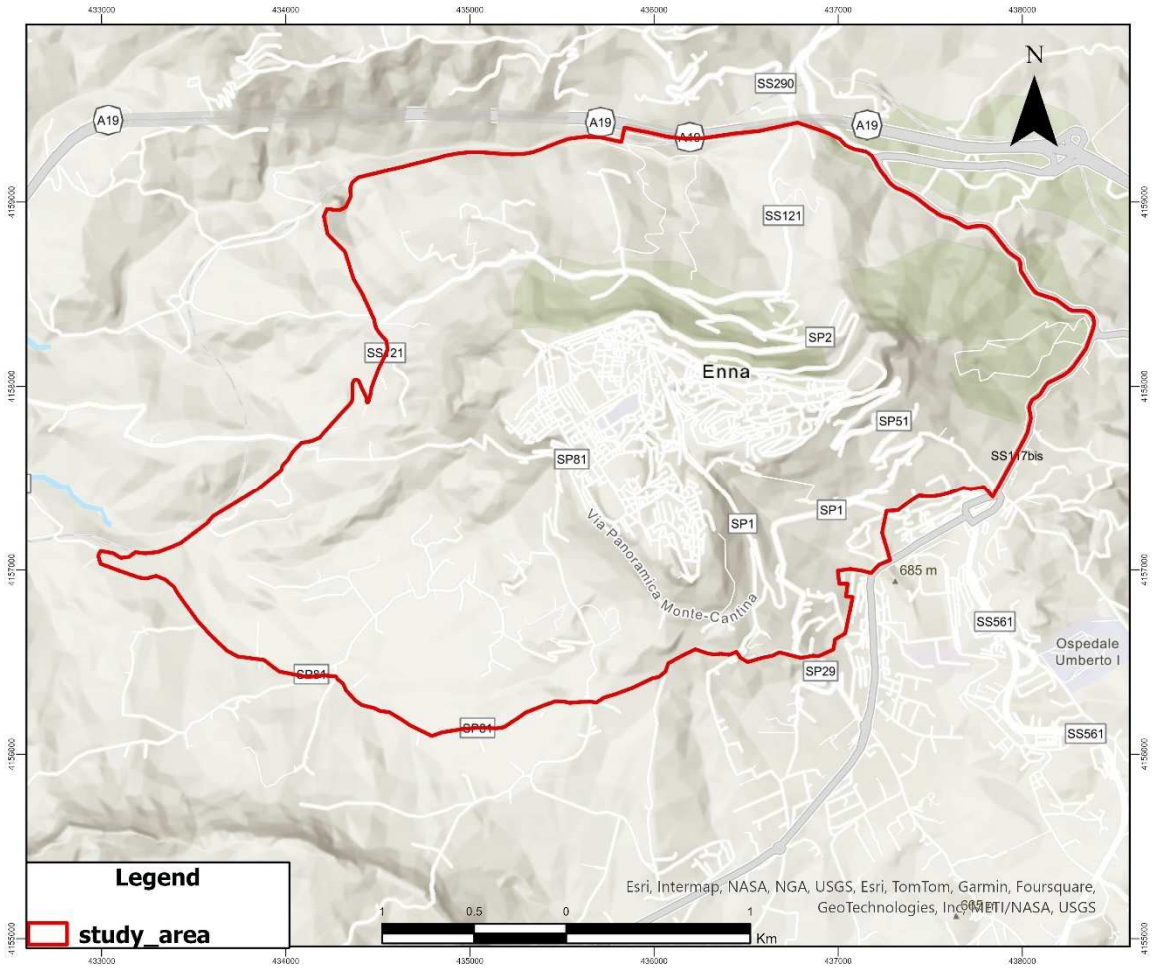

Figure 38. Pilot area of Italy.

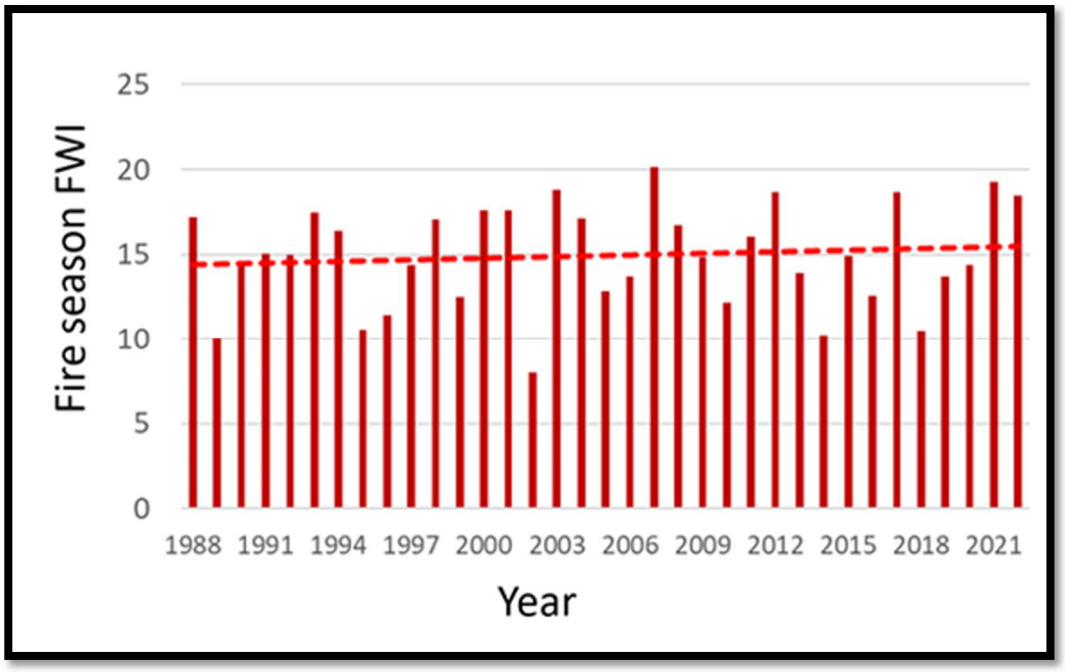

Figure 39. Mean daily fire weather in Italy during the fire season (July-September) from year 1988 to 2022. The red dotted line indicates the linear trend over the period of analysis (Gianfilippo et al. 2023).

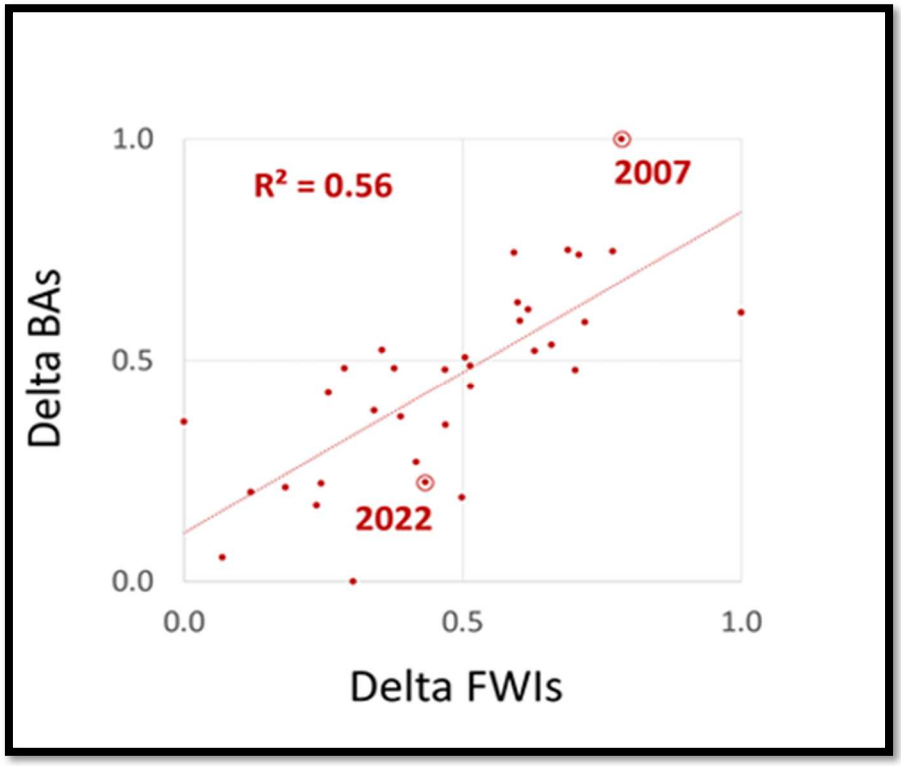

Figure 40. Total burnt area in Italy for years 1988-2022 as a function of mean daily fire weather during the fire season. Calculations used the delta approach to correct for autocorrelation: a change in burnt area (Delta BAs) from one year to the next is correlated with the corresponding delta in FWI. Changes are standardized from 0 to 1 (Gianfilippo et al. 2023).

Regarding fire occurrences and affected surfaces, in 2022 Italy was affected by a total of 6.529 forest fires, marking a 9,1% increase compared to the previous year. On the contrary, the burnt area showed a 52,82% reduction, from 151.964 ha in 2021 to 71.694 ha in 2022. Analyzing regional data reveals that this decrease is prevalent across nearly all southern and central regions. Sicily, Puglia, and Calabria remained the most affected, accounting for over 55% of the burnt area, followed by Lazio, Campania, and Tuscany. The average burnt area in Italy appears to fluctuate significantly over the years, however an estimate of the average burnt area seems to be around 100.000 ha (Figure 41). The average number of fires in Italy over the years seems to hover around 10.000 annually (Figure 42) and lastly the average annual fire size is around 15 ha (Figure 43).

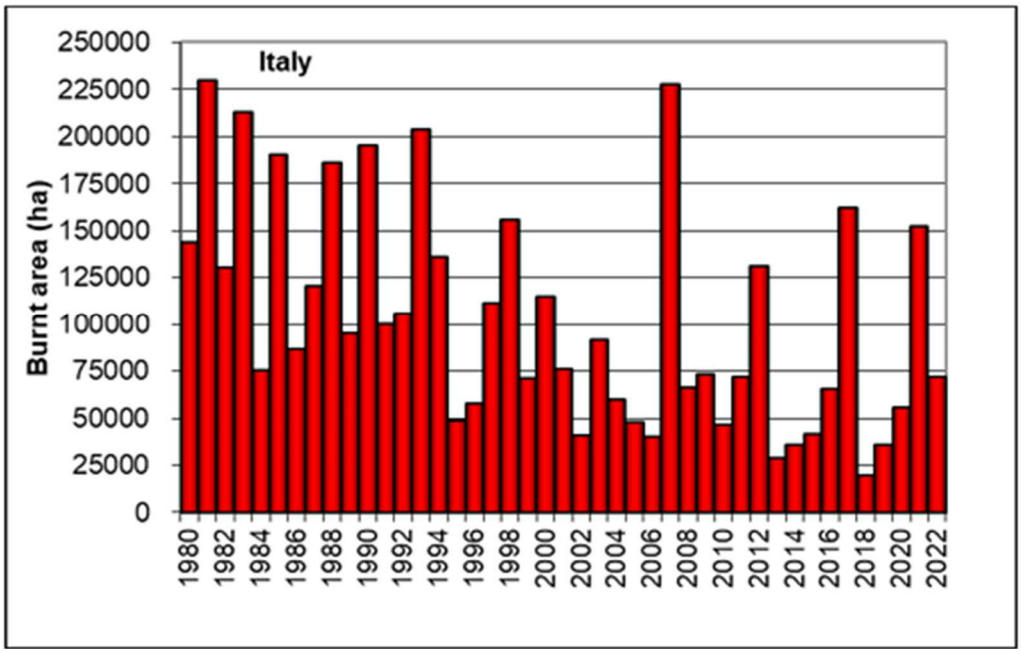

Figure 41. Annual burnt areas in Italy based on reports from the National Fire Services for the period 1980-2022 (Gianfilippo et al. 2023).

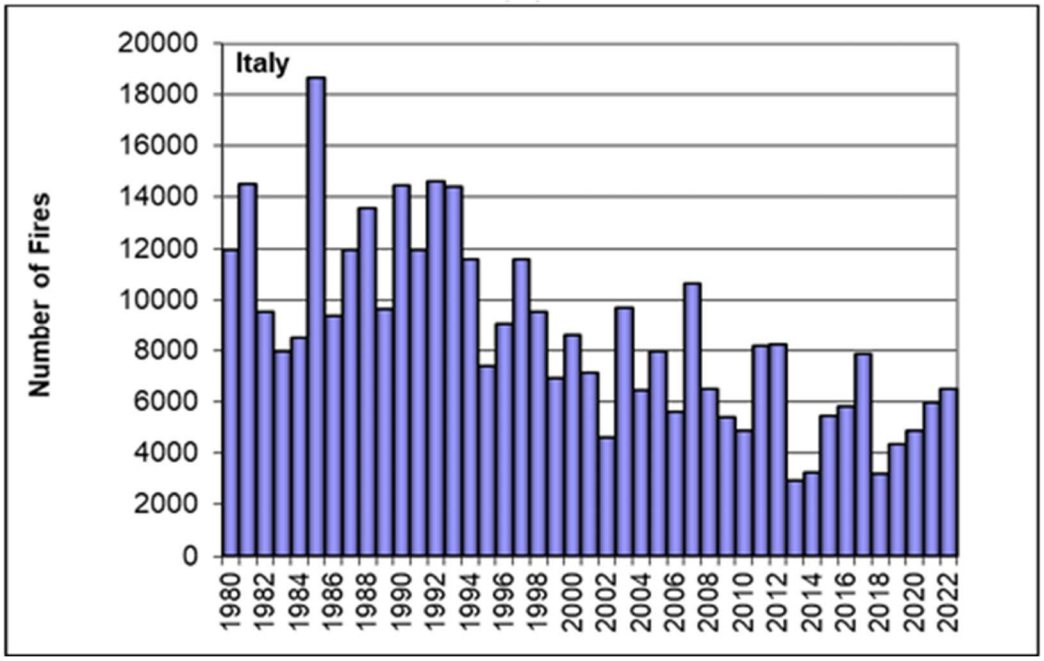

Figure 42. Annual fire occurrences in Italy based on reports from the National Fire Services for the period 1980-2022 (Gianfilippo et al. 2023).

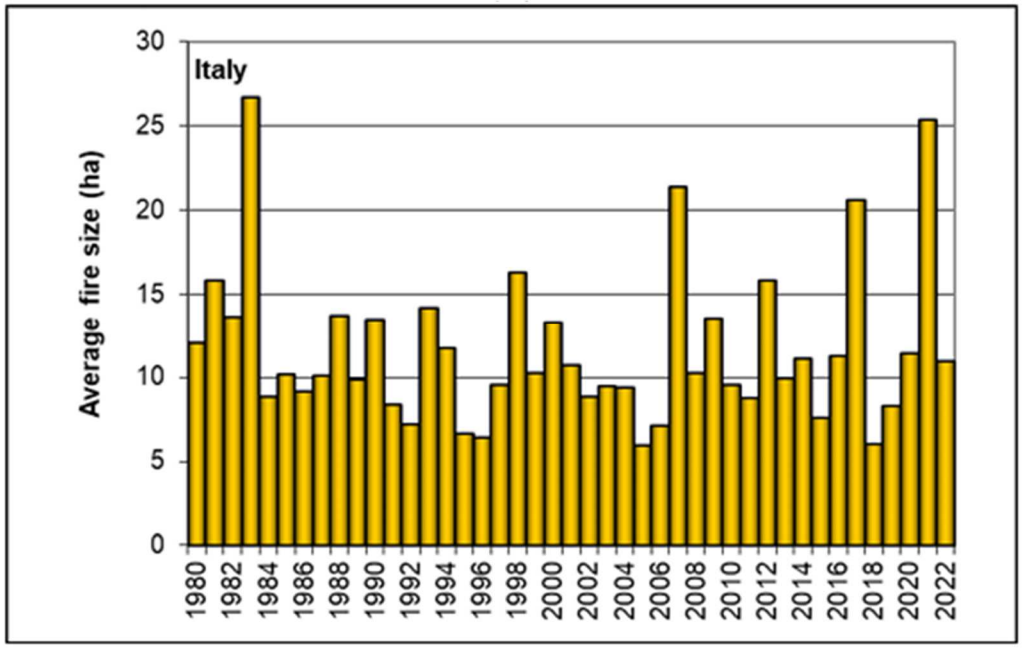

Figure 43. Annual average fire size in Italy based on reports from the National Fire Services for the period 1980-2022 (Gianfilippo et al. 2023).

3.3.1. Geographical Location and administration

The province of Enna covers an area of approximately 2.562 km^2. It is characterized by varying elevations, with the city of Enna itself positioned at one of the highest points on the island, at around 931 m above sea level. The province has a population of roughly 172.000 people, distributed across its 20 municipalities. The capital city of the province is Enna and the city serves as the administrative center. The province plays a significant role in Sicily's economy and culture, reflecting its strategic location and natural resources within the region.

3.3.2. Climatic conditions

Climatic conditions in Sicily are consistent with the Mediterranean semi-arid climate, with two rainfall seasons (Autumn, the minor one, and Spring, the major one) and two dry seasons (Winter and Summer).

The impact of climate change is statistically relevant in many areas of the Region, and it is visible both in temperatures and precipitation. The impact on precipitations is relevant to average rainfall and extreme events.

The next paragraphs present some of the outcomes of the most significant studies on the topic.

3.3.2.1. Trends in temperatures at the regional scale

In the Mediterranean region, Domonkos et al. (2003) investigated the variability of winter extreme low-temperature events and summer extreme high-temperature events analyzing the daily temperature series (1901-98) recorded in 11 sites of Central and Southern Europe; the study revealed several signs of a slight but general warming. Throughout the Eastern Mediterranean region, Kostopoulou and Jones (2005) detected statistically significant trends for both minimum and maximum temperatures.

In Italy, a number of studies have focused on the analysis of average temperatures (Ventura et al, 2002; Caloiero et al., 2015), while others have focused on extreme events (Bartolini et al. 2008; Boccolari and Malmusi, 2013). Brunetti et al. (2006) examined mean, maximum and minimum monthly temperature series recorded in Italy and found that, during the 1954-2003 period, the positive trend in maximum temperatures has been stronger than that for minimum temperatures. This result could seem in contradiction with the global increase of minimum temperatures higher than that of maximum temperature (Alexander et al., 2006; Donat et al., 2013). Nevertheless, Brunetti et al. (2006) also found that minimum temperature trend was higher than that of maximum temperature, if considering the 1865–2003 period. It has to be remarked that maximum and minimum temperature trends did not evenly occurred in space and in time, as demonstrated by the large number of regional studies, and the rate of increase highly depends on the location.

In a study carried out by Toreti and Desiato (2007), changes in temperature extremes across Italy during the period 1961-2004 were examined through the calculation and statistical analysis of 10 indices. Most of the indices showed a cooling trend until the end of the 1970s, followed by a more considerable warming trend in the last 25 years. The above-mentioned studies analysed extreme temperature series in Italy, but none of these studies focused on southern Italy, where, according to Brunetti et al. (2004), a stronger increase in annual mean temperatures compared to the rest of the peninsula occurred.

In Sicily, Viola et al. (2013) analysed temperature data from 80 spatially distributed stations for the period from 1924 to 2006 to investigate possible evidence of climate changes in the region. This analysis, which focused on mean temperature series, noted the occurrence of a general warming trend in Sicily during the analysed period. In this paragraph, a synthesis of the research carried out by Liuzzo et al. (2015) is reported.

In that study, annual, seasonal and monthly maximum and minimum temperature series from 84 measurement stations in Sicily were analysed for the 1924-2013 period in order to investigate the existence of trends in the region. First, the occurrence of abrupt change points in annual maximum, minimum and mean temperatures and temperature ranges - or change points - were investigated using spatially averaged values for the entire study area. These points were detected using cumulative sum (CUSUM) charts, and the confidence level for each point was determined through a bootstrap analysis. Afterwards, the non-parametric Mann-Kendall test was used to detect statistically significant trends in the above-mentioned series. The trend analysis was carried out at local and regional scale at the 90%, 95% and 99% confidence levels. Prior to the application of the Mann-Kendall test, the historical dataset was completed using geostatistical techniques and then processed in order to remove the influence of serial correlation on the results of the test. Once trends were detected, a spatial interpolation technique was used to verify whether trends are distributed throughout Sicily according to well-defined spatial patterns.

In the cited study, temperature data recorded in Sicily have been analysed. Sicily is an island of about 25.700 km^2 located in Southern Italy. The climate is Mediterranean, characterized by mild winters and hot, generally dry summer. The annual rainfall in the area varies from 400 mm/year (at lower elevations) to 1300 mm/year (at higher elevations). The mean annual temperature ranges between 11°C and 19.4°C. Namely, the highest temperatures (18.5-19.5 °C) are recorded along the coast, while the lowest temperatures (10.5-13.5 °C) are typical of the highest elevations.

Historical temperature series for the period 1924-2013 measured at 84 gauges across Sicily (Figure 44) were provided by the *Osservatorio delle Acque della Regione Sicilia.*

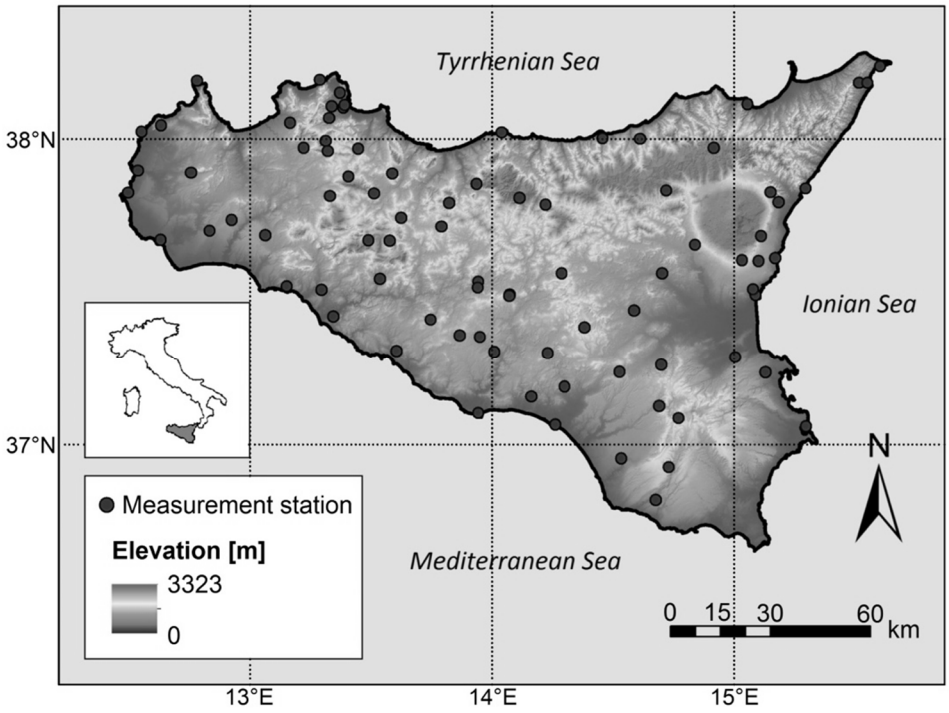

Figure 44. Location of measurement stations.

A preliminary examination of the monthly maximum and minimum temperature series recorded in the 84 gauges has been carried out, showing that about the 20% of the total number of data were missing. Since the investigation of trends in meteorological variables requires a complete and homogeneous series covering the entire period of analysis, only homogenous series were included in the analyzed dataset and a spatial interpolation technique was used in order to have a complete dataset. Once a complete dataset of monthly temperature was obtained, data were aggregated at the annual and seasonal scale. Seasonal data were obtained as follows: autumn data are the average of September, October and November temperatures; winter data are the average of December, January and February temperatures; spring data are the average of March, April and May temperatures; summer data are the average of June, July and August temperatures. The complete series of maximum and minimum temperatures, $T_{\max}$ and $T_{\min}$, were used to calculate mean temperature T_{mean} and the diurnal temperature range DTR series for each time period. Trends in these variables were analysed as well.

In Figure 2 the spatial distribution of average annual $T_{\max}$, $T_{\min}$, T_{mean} and *DTR* (°C) over the 1924-2013 period is displayed. Average annual $T_{\max}$ approximately ranged from 15°C to 24°C, with the highest values occurring

in the south-eastern part of the island and the lowest values occurring at the highest elevations. Average annual T_{min} varied from 7.2°C to 15.7°C; the lowest values occurred across a wide central area and in the highest mountains. The spatial patterns of average annual T_{mean} clearly reflect the distribution of T_{max} and T_{min}. In terms of average annual *DTR*, the values varied from 6°C to 11.5°C. The difference between T_{max} and T_{min} was more marked in the south-east, where *DTR* varied from 9.3°C to 11.5°C. The northern coast had the lowest *DTR* values (6°C - 9.2°C).

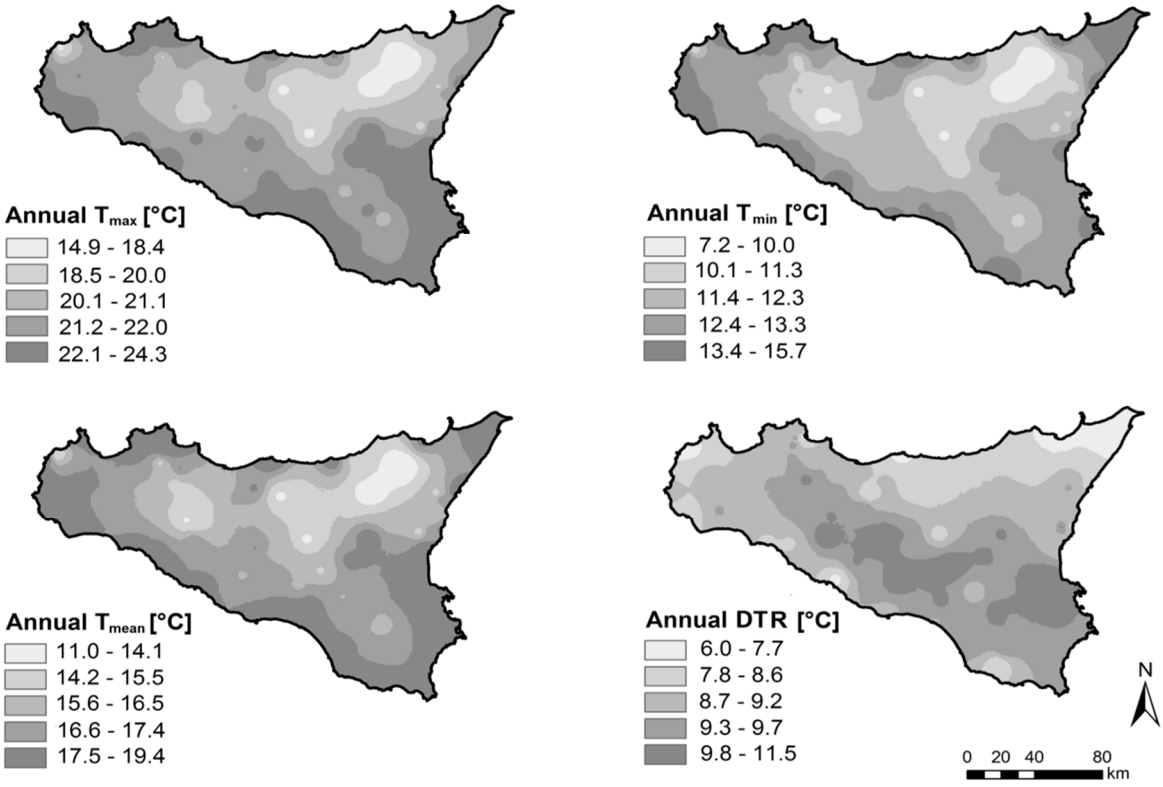

Figure 45. Spatial distribution of average annual T_{max}, T_{min}, T_{mean} and DTR (°C).

Figure 46 shows the mean monthly T_{max}, T_{min}, T_{mean} and *DTR* for the spatially averaged series and for three stations located in northern, central and southern Sicily, namely Palermo (Istituto Castelnuovo), Caltanissetta and Ragusa. The spatially averaged series are quite representative of the Sicilian climate, being the mean monthly values comparable with those measured in three different locations.

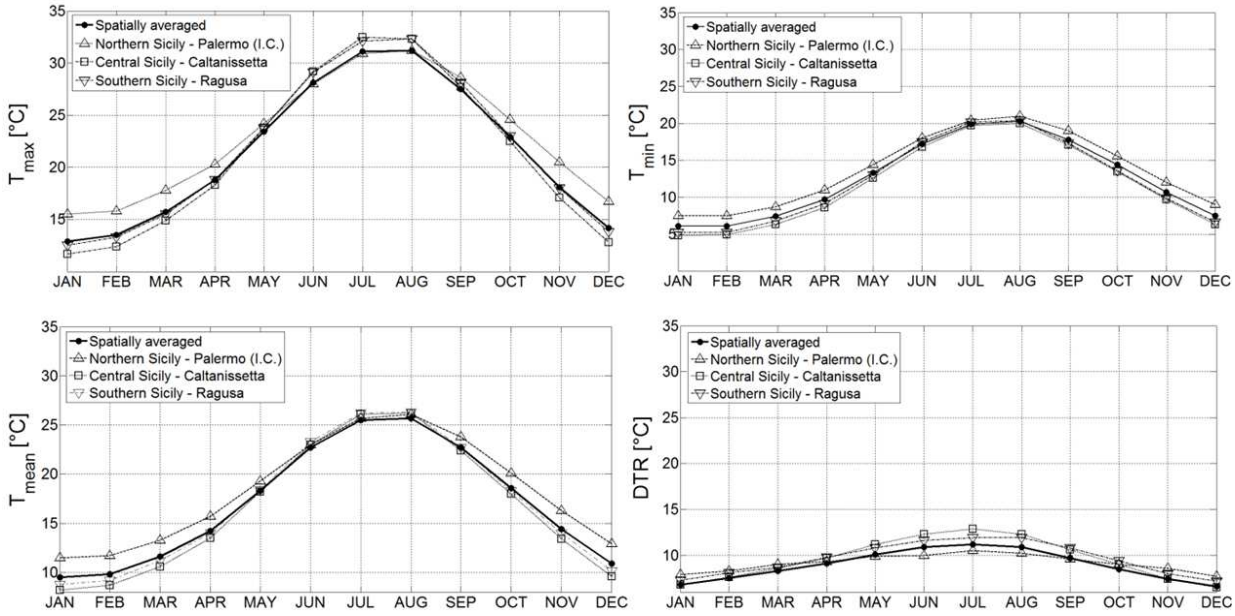

Figure 46. Mean monthly T_{max}, T_{min}, T_{mean} and *DTR*

The cumulative sum (CUSUM) is a statistical technique that permits the rapid identification of abrupt change in a series of data. In the study, CUSUM charts were developed following the procedure suggested by Taylor (2000).

The section of the CUSUM charts with an ascending trend indicated a period in which the values were above the overall average. Similarly, the section with a descending trend indicated a period of time in which the values were below the overall average.

In this study, the analysis of CUSUM charts was carried out on temperature values that were spatially averaged over the entire study area. A bootstrap analysis provided the confidence level. Table 3 summarizes the results for each analysed variable.

Table 3. Significant changes in annual average T_{max}, T_{min}, T_{mean} and DTR (°C).

	Year	Confidence interval	Confidence level	From [°C]	To [°C]	Level
T_{max}	1985	1983-1986	100%	21.08	22.43	1
	2004	1996-2006	98%	22.43	21.73	2
T_{min}	1933	1929-1950	99%	12.74	12.24	2
	1987	1985-1987	100%	12.24	13.27	1
	2004	2002-2204	100%	13.27	12.61	2
T_{mean}	1985	1983-1986	100%	16.69	17.82	1
	2004	1999-2005	100%	17.82	17.17	2
DTR	1943	1933-1948	100%	8.50	9.05	3
	1963	1944-1967	94%	9.05	8.70	4
	1981	1977-1985	100%	8.70	9.08	2
	1998	1997-1998	98%	9.08	9.67	3
	2003	2003-2004	98%	9.67	9.10	4

Figure 47 reports the CUSUM charts; the change points are indicated with a grey background. Each change is associated with a level. Level 1 change is the first change detected by the process; on a second pass through the data, level 2 changes were detected. The number of levels equals the number of changes found.

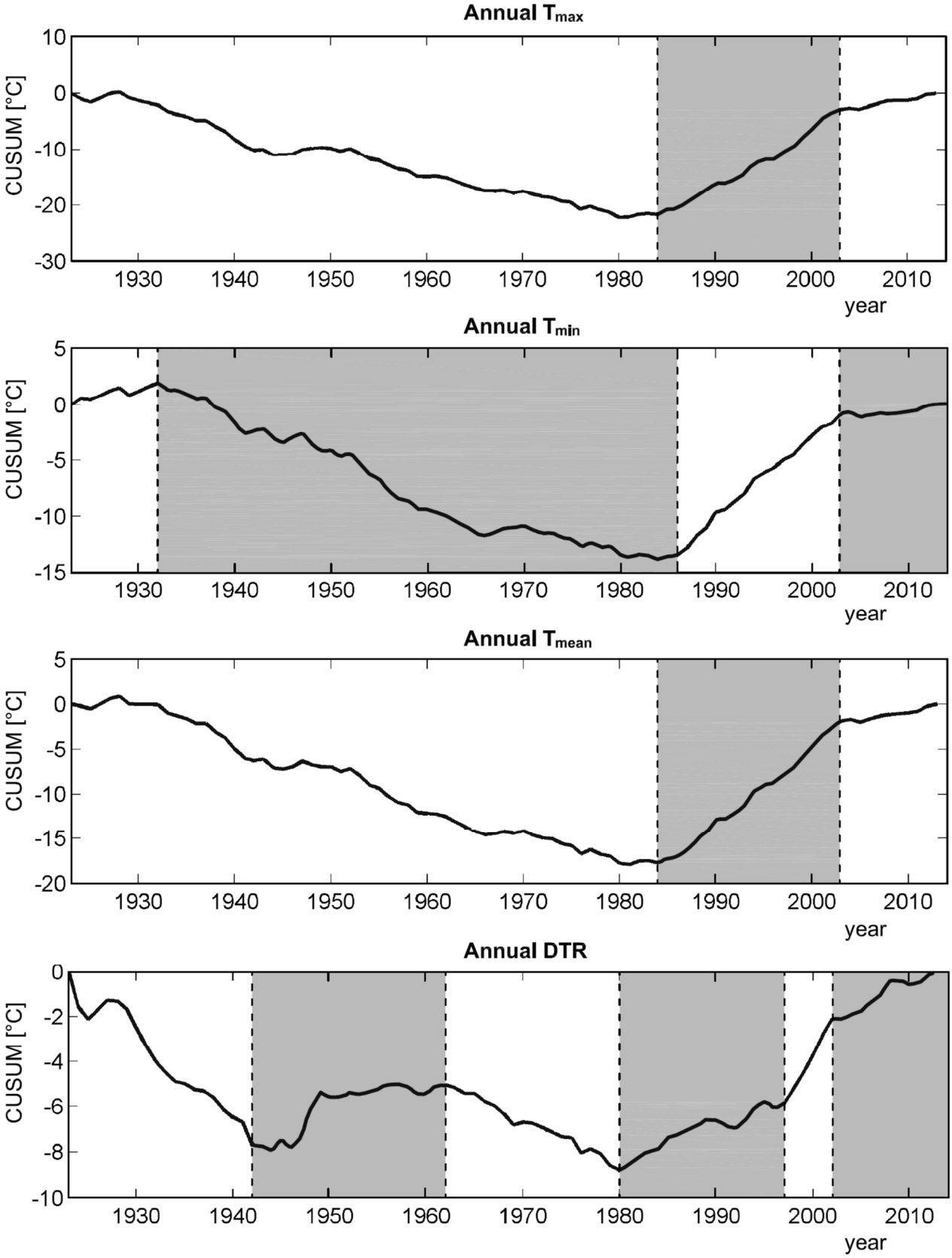

Figure 47. CUSUM charts for average annual T_{max}, T_{min}, T_{mean} and DTR (°C).

The analysis highlighted that the average annual T_{max} underwent a significant level 1 change in 1985 (confidence interval 1983-1986) at a confidence level of 100%. Prior to the 1985 change, the average annual T_{max} was 21.08°C, while after the change it became 22.43°C. The magnitude of change was 1.35°C. At level 2, a significant change occurred in 2004 (confidence interval 1996-2006) with a confidence level of 98%. According to the CUSUM chart, a decreasing trend occurred until 1985; after this year, T_{max} showed an increasing trend until 2004.

A significant level 1 change in average annual T_{min} was detected in 1987 (confidence interval 1985-1987). Prior to this change, the average annual T_{min} was 12.24°C, whereas after the change it became 13.27°C. The magnitude of change was 1.03°C. Two changes occurred at level 2, one in 1933 and 2004. The CUSUM charts indicate that T_{max} and T_{min} experienced similar trends over the examined period. These trends also affected the average annual T_{mean}, for which a significant level 1 change occurred in 1985 (confidence interval 1983-1986), with a confidence level of 100%. Prior to the level 1 change, the average annual T_{mean} was 16.69°C, whereas after the change it became 17.82°C. In this case, the amount of change was 1.13°C. A level 2 change occurred in 2004.

Over the entire period of analysis, average annual *DTR* forward and backward changes were found (at levels 2, 3 and 4) in 1943, 1963, 1981, 1998 and 2003. A second level change has been detected in 1981, approximately in correspondence of the first level change points found for T_{max} and T_{min} (in 1985 and in 1987 respectively). From the 1940s to the 1960s, the average annual *DTR* has been subject to a smooth increase followed by a decrease up to the 1980. During this period the change in slope is not pronounced and the range, that is the difference between the highest and lowest value, is small. After the 1980, a moderate increase occurred up to the 1998. Thus, these trends resulted in a second level change point for *DTR*. The analysis of CUSUM charts clearly demonstrates similarities between T_{max}, T_{min}, T_{mean} and *DTR*. Indeed, all of the series showed a change point approximately within the same range of years, in particular T_{max}, T_{min} and T_{mean} showed increasing trends starting from 1985. As regards to T_{mean}, these results are in agreement with the findings of previous studies. Annual, monthly and seasonal series were analysed for each variable. The first main result was that in most of the cases, all variables exhibited statistically significant trends. For annual temperatures (Table 4), T_{max}, T_{min}, and T_{mean} were frequently affected by positive trends. In particular, T_{max} increased at most of the measurement stations, while decreasing trends occurred occasionally, affecting only 3 series at a 90% confidence level. The magnitude of positive trends ranged

from +0.05°C/decade to +0.5°C/decade. Several positive trends were detected for annual T_{min} as well, but in that case, negative trends were statistically significant in almost 20% of series (95% confidence level).

Table 4. Percentage of statistically significant trends of average annual Tmax, Tmin, Tmean and DTR (°C) at 90%, 95% and 99% level of confidence.

	Confidence level	T_{max}	T_{min}	T_{mean}	DTR
No trend	*90%*	7	10	6	7
	95%	8	13	8	8
	99%	11	16	15	12
Positive trend	*90%*	74	58	73	46
	95%	74	55	72	46
	99%	72	53	66	44
Negative trend	*90%*	3	16	5	31
	95%	2	16	4	30
	99%	1	15	3	28

Positive trends had magnitudes that varied between +0.01°C/decade and +0.3°C/decade, while the range of magnitude of negative trends was -0.5°C/decade — -0.04°C/decade. The number of positive trends in annual T_{mean} series was similar to that of T_{max}, probably because the increase in T_{max} was more rapid than the decrease in T_{min}. In that case, the magnitude of the positive trend ranged from +0.02°C/decade and +0.2°C/decade. This result agrees with the magnitude of the temperature trend reported in the latest IPCC report (2013), according to which an increase of about 1°C occurred during the 1901-2012 period over the study area. Moreover, a study carried out by Viola et al. (2013) pointed out the presence of a statistically significant trend in annual T_{mean} in the 1924-2006 period.

As regards annual *DTR*, both positive and negative trends were observed. At 90% confidence level, 54.8% of the series were affected by a positive trend, while 36.9% showed a negative trend. Both annual T_{max} and T_{min} positive trends were affected primarily by positive trends. Still, where the magnitude of annual T_{min} positive trends was greater than that of T_{max} positive trends, the combined effect of these trends caused the occurrence of negative trends in annual *DTR* series. The range of magnitudes of increasing trends was +0.03°C/decade — +0.8°C/decade, while decreasing trends varied from -0.3°C/decade to -0.02°C/decade.

The results of the monthly temperatures trend analysis are summarized in Figure 48. Percentage of statistically significant trends of average monthly Tmax, Tmin, Tmean and DTR (°C) at 90%, 95% and 99% level of confidence., where the x-axis represents the absolute number of stations. The number of trends is reported for each month and each confidence level. Positive trends are predominant in most of the cases. As observed for the annual series, some negative trends occurred for T_{min} and *DTR*. The highest number of T_{max} positive trends was observed in January (89.3% of series at 90% level confidence). Increasing trends were frequent also in May and August. Monthly positive variations ranged between +0.06°C/decade and +0.6°C/decade. Few negative trends in T_{max} were founded in September, November and December. As observed for T_{max}, positive trends of monthly T_{min} were frequent in May, January and August. The increases varied between +0.03°C/decade and +0.4°C/decade. Negative trends occurred in every month. The magnitude of these trends ranged between -0.4°C/decade and -0.1°C/decade. At the monthly scale, variations in T_{mean} were similar to those of T_{max}, even though, in this case, a small number of negative trends were detected. Significant positive trends showed a magnitude within the range +0.04°C/decade - +0.4°C/decade. Monthly *DTR* series were affected by both positive and negative trends, as observed for the annual *DTR* series. Increasing trends occurred in every month, but were distinctive in January, February and March, while negative trends were observed in summer months and were distinctive in June. Magnitudes ranged between +1°C/decade — +0.02°C/decade and -0.04°C/decade — -0.5°C/decade for positive and negative trends, respectively.

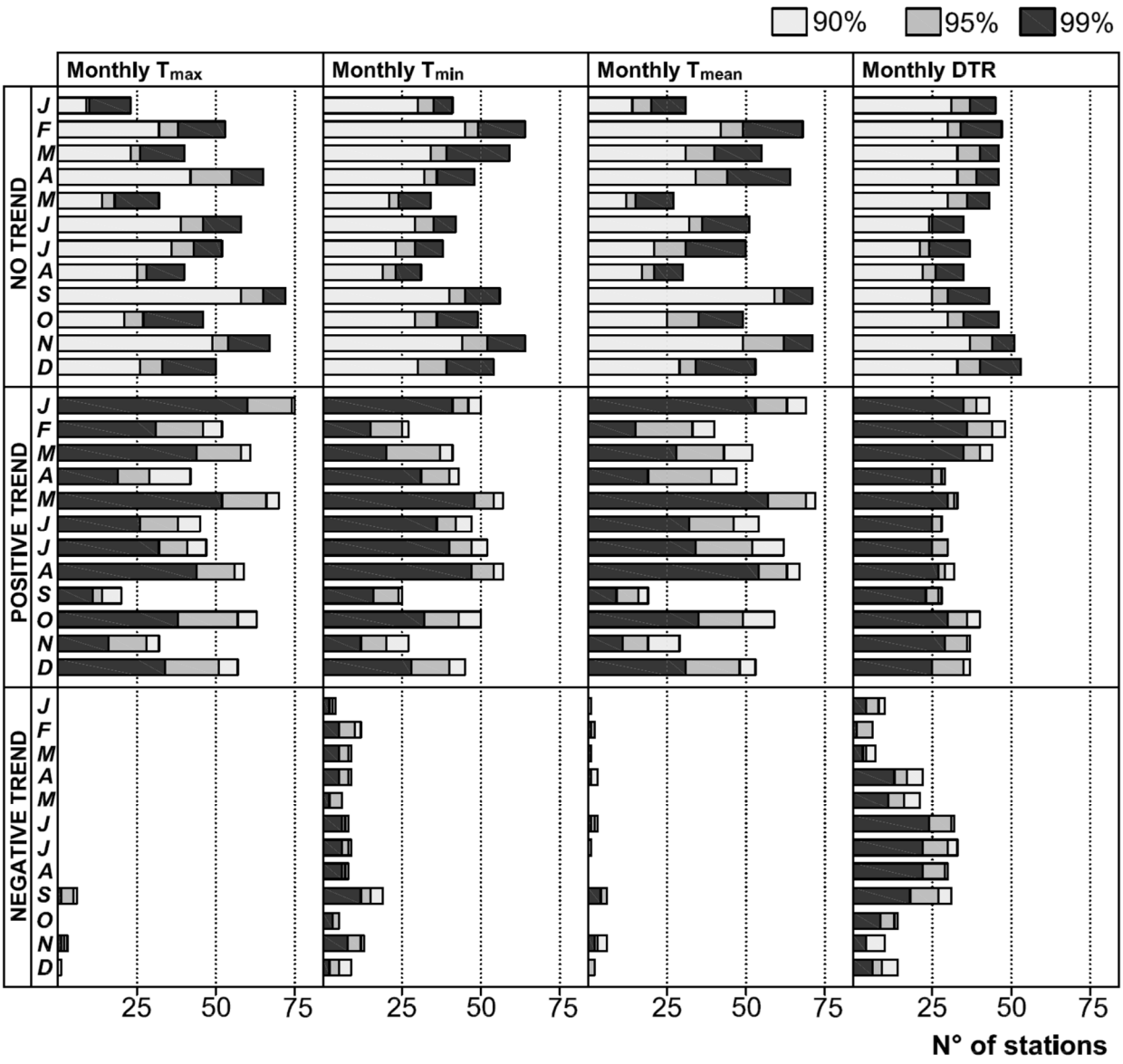

Figure 48. Percentage of statistically significant trends of average monthly Tmax, Tmin, Tmean and DTR (°C) at 90%, 95% and 99% level of confidence.

Figure 49 shows the results for seasonal series. Positive trends are prevalent for all variables, with prevailing trends in T_{max} and *DTR* during the winter, trends in T_{min} during the summer and in T_{mean} during the spring. In the winter, 74 series (88% of the considered stations) showed a positive trend of T_{max} at 90% confidence level, basically the same number of series that exhibited an increasing trend at the annual scale. The magnitude of T_{max} increases is similar for all the seasons, ranging from +0.05°C/decade to +0.5°C/decade. Decreasing trends were observed mainly for T_{min} and *DTR*. Some negative trends occurred in every season for T_{min}, with the greatest number in

autumn. Variations in T_{min} were similar for all seasons and ranged between +0.06°C/decade and +0.3°C/decade in the case of positive trends, and between -0.1°C/decade and -0.6°C/decade for negative trends. As already observed for annual and monthly series, seasonal variations in T_{mean} were similar to those observed for T_{max}. Significant downward variations in *DTR* were more frequent in the summer (about 37% of series at a 90% confidence level), probably due to the presence of negative trends in T_{min} for series where a positive trend in T_{max} had not occurred.

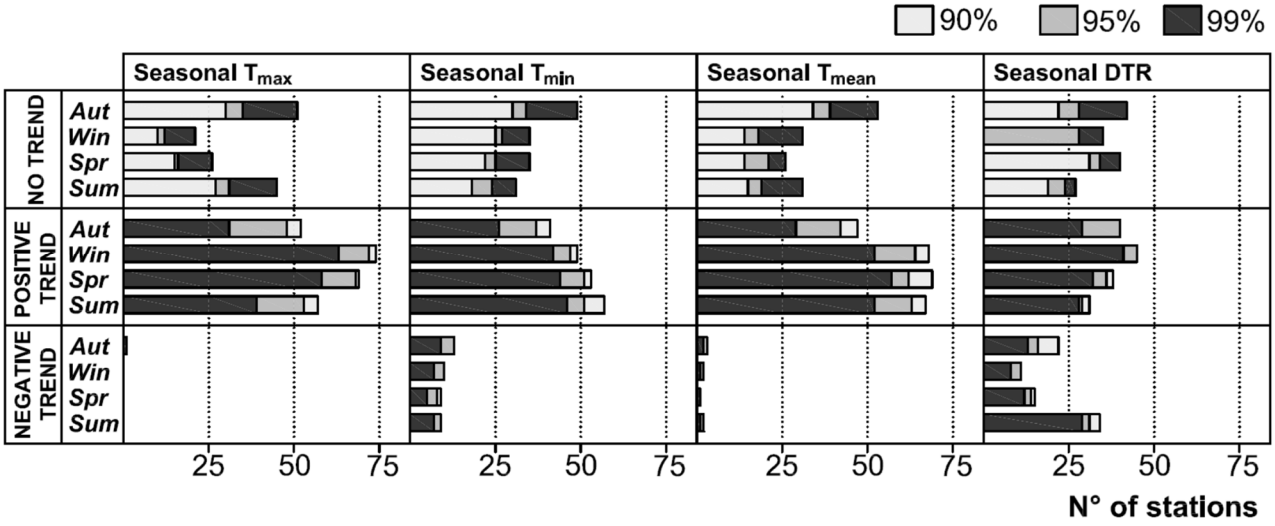

Figure 49. Percentage of statistically significant trends of average seasonal T_{max}, T_{min}, T_{mean} and DTR (°C) at 90%, 95% and 99% level of confidence.

The analysis of monthly and seasonal data showed that the greatest contributions to annual trends came from statistically significant variations that occurred in the winter and summer months. The detected trends were generally higher for T_{max} than for T_{min} at the annual and seasonal scale. These results are in accordance with previous studies that revealed the presence of a positive temperature trend across the Mediterranean region (Domonkos et al., 2003; Kostopoulou and Jones, 2005; Brunetti et al., 2006; Fioravanti et al., 2016).

Most of the stations included in this analysis are located in small towns, far from largely urbanized areas where the recording of temperature data could be frequently affected by the presence of increased anthropogenic activities and where temperature trends could be mistaken with human-induced warming effects (due to heating and cooling systems). Because most stations in this study were located away from these influences, the

temperature variations detected in this analysis are likely to be attributed to climate change.

It has to be remarked that, in general, historical temperature datasets can be affected by other uncertainty sources that can produce discontinuities or abrupt changes. These sources may include the replacement of measurement instruments, the relocation of the stations or the possible use of different procedures for collecting and validating the raw temperature data. For this reason, before performing a trend analysis, a preliminary investigation of data should be carried out in order to verify if possible variations are related to non-climatic factors.

3.3.2.2. Trends in annual and seasonal precipitation at the regional scale

Historical rainfall series for the period 1921-2012 measured in 245 raingauges across Sicily (Figure 50) have been provided by Osservatorio delle Acque - Agenzia Regionale per i Rifiuti e le Acque (OA-ARRA) of Sicily.

A preliminary examination of the monthly rainfall series showed that missing data are about the 20% of the total number of monthly values. Since the investigation on rainfall trends requires homogeneous and complete series covering the period of analysis, a method of spatial interpolation, hereinafter described, has been used to create a complete dataset.

Once a complete dataset of monthly rainfall has been achieved, data have been aggregated at annual and seasonal scale. Seasons have been defined as follows: autumn included September, October and November, winter included December, January and February, spring included March, April and May, and summer included June, July and August.

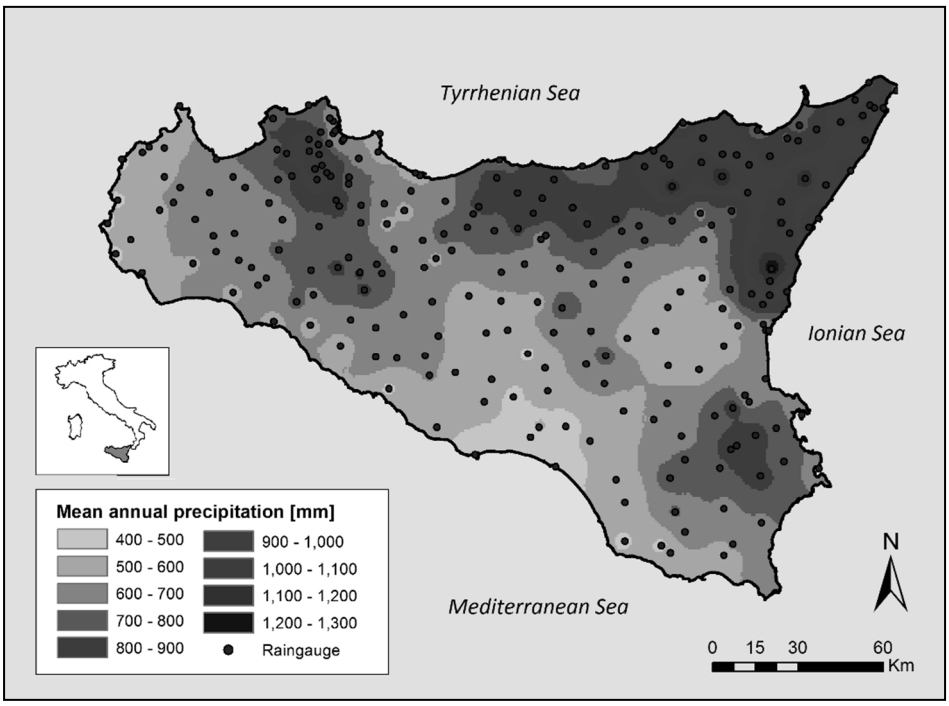

Figure 50. Location of raingauges and mean total annual precipitation over the period 1921-2012.

The results of the Mann-Kendall trend test revealed that the total annual precipitation series were affected mainly by negative trends during the period 1921-2012. Figure 51 illustrates these results. Annual rainfall measured in the 57.1% (140), the 49.8% (122) and the 35.5% (87) of raingauges showed a statistically significant decrease with 90%, 95% and 99% confidence level respectively. Positive trends have been detected in a small number of series, The 3.7% of series (9) experienced an increase with 90% confidence level. With the same confidence level, no significant trends were found in the 39.2% of raingauges (96). The magnitudes β of negative trends range from to -5.3 mm/year to -0.5 mm/year. Positive trends have magnitudes that vary in the range 0.7÷3.4 mm/year. Figure 52 shows the total annual rainfall and the relative trends for the raingauges in which the positive and negative trends with the highest values of β have been detected (Linguaglossa and Buccheri, with β equal to 3.4 mm/year and -5.3 mm/year respectively).

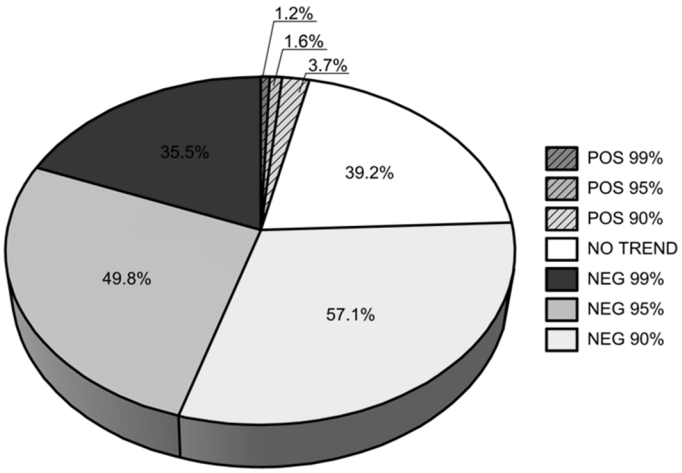

Figure 51. Percentage of stations with statistically significant trends in total annual precipitation at 90%, 95% and 99% level of confidence.

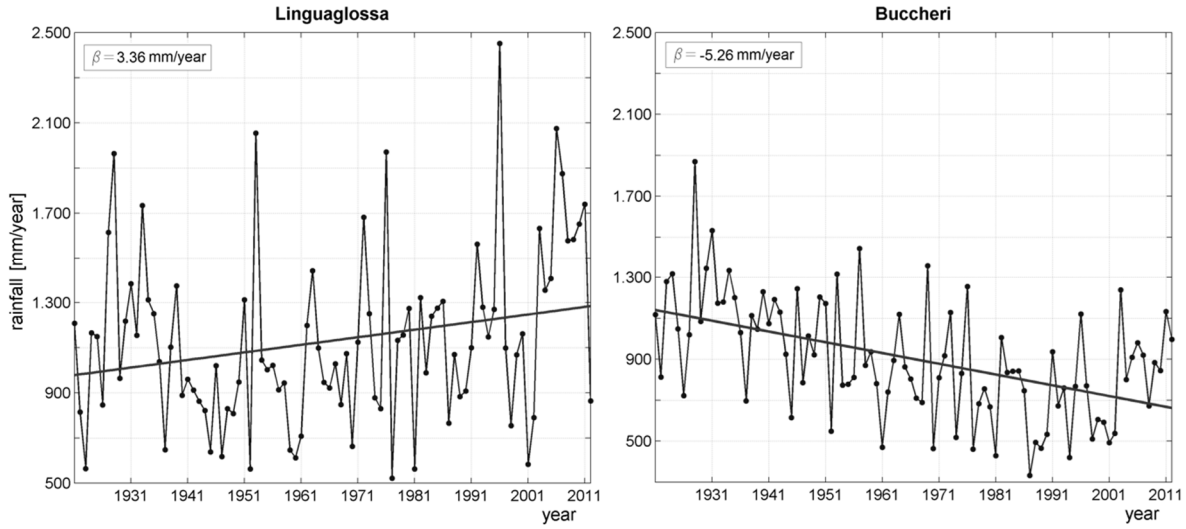

Figure 52. Total annual rainfall and relative trends for the raingauges in which the positive and negative trends with the highest magnitudes β (mm/year) have been detected (Linguaglossa and Buccheri respectively).

As regards to seasonal rainfall, Figure 53 shows that positive and negative precipitation trends, at all confidence levels, exist for each season. The histograms show that negative trends are more frequent in autumn and winter, specifically in 91 and 137 out of 245 raingauges respectively for 90% confidence level. Therefore, the annual rainfall decrease should be mainly attributed to the negative trends occurring in winter and autumn. Some positive trends have been found in autumn and summer. In winter only one positive trend has been detected in the raingauge of Erice. Spring is the season with the lowest number of trends, both positive and negative.

The monthly rainfall analysis allowed to identify which months are most responsible for the detected seasonal trends. The histograms in Figure 54 illustrates results obtained in the monthly rainfall analysis. December is the month that shows the highest number of negative trends (97, 65 and 12 series for 90%, 95% and 99% confidence level respectively). Since in January and February a few trends have been found, negative trends of December provide the main contribution to the winter rainfall decrease. August and October are the months which show the highest number of trends in both positive and negative directions. October is the month mainly responsible for the autumn positive and negative trends. Summer negative trends can be attributed to the decrease of rainfall during all summer months, in particular June and August. The increase of rainfall in April does not produce a seasonal tendency, since the number of positive trends in spring is very low (10 trends with 90% confidence level). The lowest number of positive trends occurs in January and November. September does not show any negative trend.

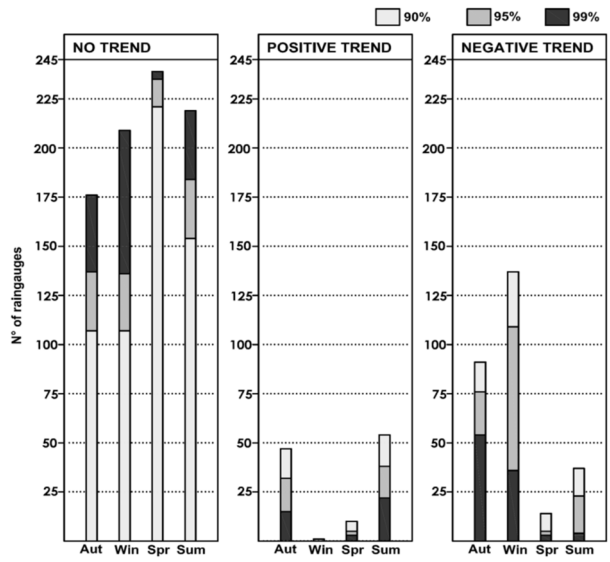

Figure 53. Number of statistically significant trends in total seasonal rainfall for 90%, 95% and 99% level of confidence.

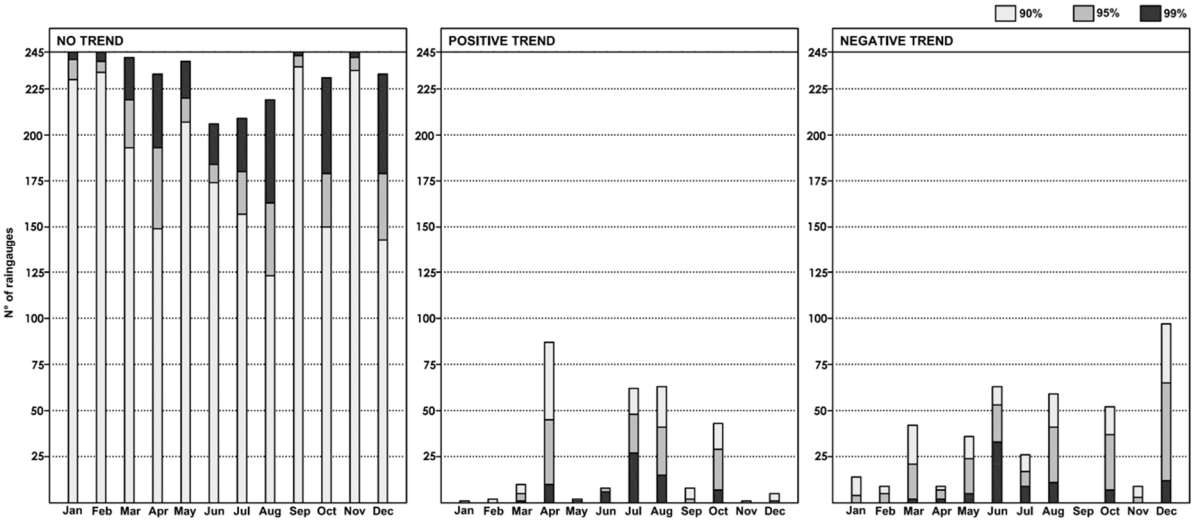

Figure 54. Number of statistically significant trends in total monthly rainfall for 90%, 95% and 99% level of confidence.

In order to evaluate trends at regional scale, the regional Mann-Kendall test and the bootstrap procedure have been used and compared. With regard to annual data, the application of the Mann-Kendall test at the regional scale indicated the existence of a negative trend for each considered confidence level (S_m = -547.76). The test revealed also the existence of a trend for all the considered temporal scale, from annual to monthly, with the only exception of spring rainfall, that has not been affected by a regional trend at 95% confidence level. These results have to be attributed to the fact that a spatial interpolation method has been used to obtain a complete dataset. This procedure introduced a spatial correlation in data, that affects the test results. The use of the bootstrap technique allowed to remove this effect from results. The spatial representation of the detected rainfall trends enables a better understanding of rainfall variations in Sicily over the period 1921-2012. The observed trends were spatially interpolated by applying the *Inverse Distance Weighted* (IDW) interpolation method. By the use of IDW raster surfaces have been created.

Figure 55 shows the spatial distribution of the annual rainfall trends in Sicily with their confidence level and the relative magnitudes of these trends in mm/year (at 90% confidence level). Most of the area of study is dominated by decreasing trends, with a few small zones presenting positive trends. A wide area affected by negative trends (with confidence level up to 99%) is located in the southeastern part of the island, in which reduction occurred with the highest magnitudes (from -5.2 mm/year to -1.5 mm/year). Another wide negative trends area, not completely connected, is located at North-West. However, it can be concluded that the detected trends are not

spatially distributed according a well-defined pattern. The spatial interpolation of seasonal results revealed the absence of clear patterns in this case as well (Figure 56). In autumn small areas affected by positive trends are located along the Tyrrhenian coast and in the northwestern part of the island. The rest of the region is interested by negative trends, concentrated along the Mediterranean coast and in the northwestern part of the region. Winter rainfall experienced a decrease in most of the island, although some areas in the map are not interested by statistically significant trends. The spatial patterns of negative trends in winter is similar to the one of annual negative trends.

The interpolation of spring rainfall trends provided some scattered areas, distributed without any particular spatial pattern. Otherwise spring is the season with the lowest number of significant positive and negative trends.

As regards to summer rainfall, two wide areas are characterized by increasing trends, one in the eastern part of the island and one in the South along the Mediterranean coast. Some scattered areas, in which negative trends occurred, can be observed as well.

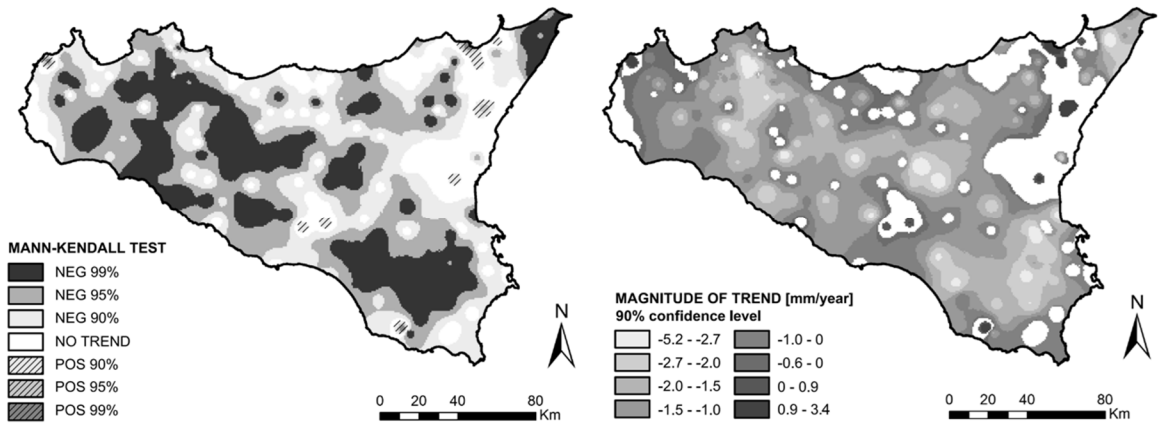

Figure 55. Spatial distribution of Mann-Kendall test results and trend magnitudes (mm/year) for total annual rainfall (1921-2012).

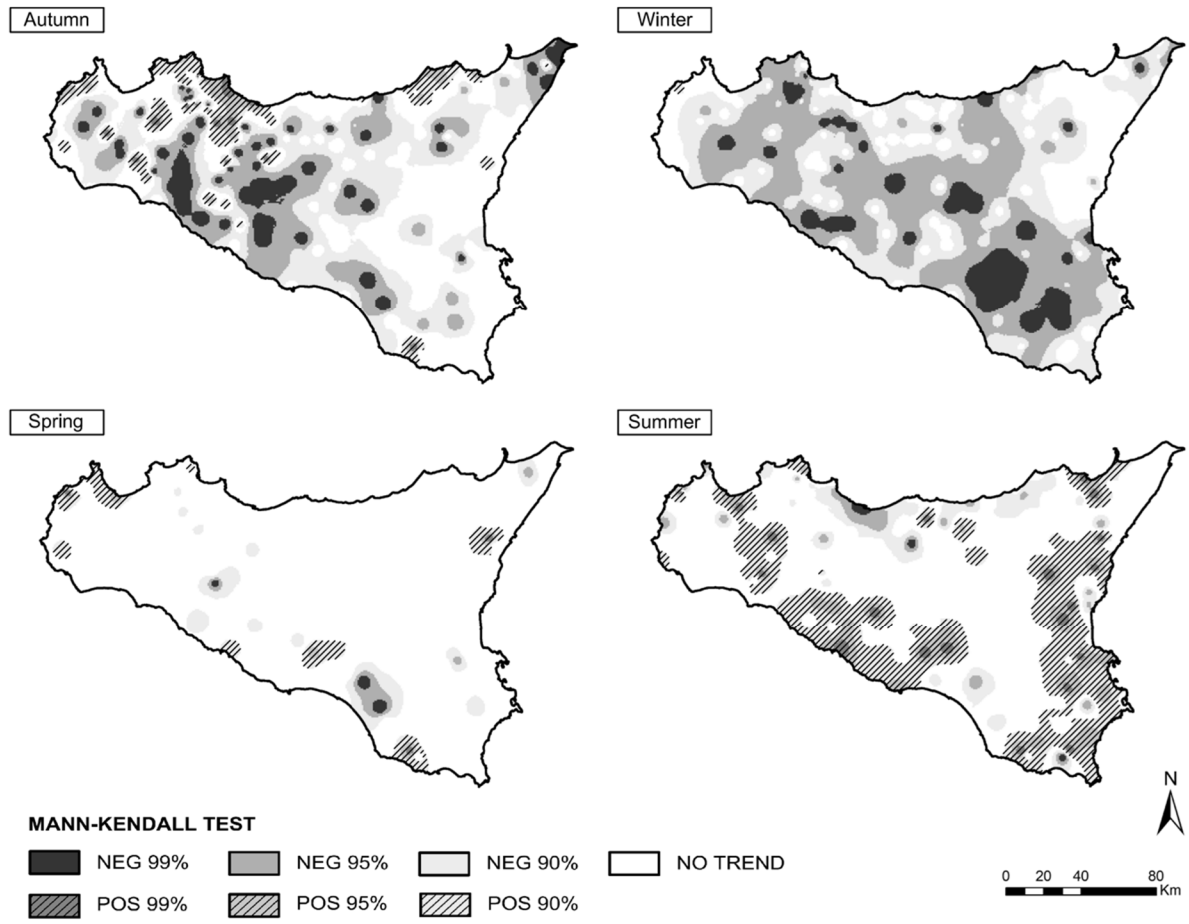

Figure 56. Spatial distribution of Mann-Kendall test results for total seasonal rainfall (1921-2012).

According to the latest report IPCC, the number of heavy precipitation events over land has increased in more regions than it has decreased, since about 1950. In Europe there have been likely increases in either the frequency or intensity of heavy precipitation with some seasonal and/or regional variation. Indeed, a number of devastating rainfall extremes occurred in Europe during the last decade. Germany, England and Italy have been the most affected country, mainly during the summer months.

The increased occurrence of extreme events suggests the possibility that in the Mediterranean area also total annual rainfall could increase, undergoing to a possible change of trend direction. The concentration of extreme events during summer, together with the reduction of total winter rainfall, could indicate a recent partial “tropicalization” of climate in the Mediterranean area, that would bring to a redefinition of seasonal precipitation patterns.

In this context, it could be useful to investigate on short-term rainfall trends, in order to detect possible change of trend direction. For this reason, the trend analysis has been repeated focusing on the latest 30-years of data, i.e. the period 1981-2012. A recent period of at least 30 years has been selected, as recommended by the *World Meteorological Organization* (WMO, 1992) for climate analysis.

Firstly, the mean total annual rainfall calculated for the periods 1921-1980 and 1981-2012 have been compared. Figure 57 shows the percentage variations between these values. In the latest 30-years mean annual rainfall experienced a reduction in most of the island. The entity of this reduction is very strong in the central part of the Sicily, in which mean annual rainfall decreased of a percentage up to -32.5%. Mean rainfall reduction in the period 1981-2012 shows a spatial pattern similar to the one observed for the negative trend over the period 1921-2012. Some increases occurred in small scattered areas.

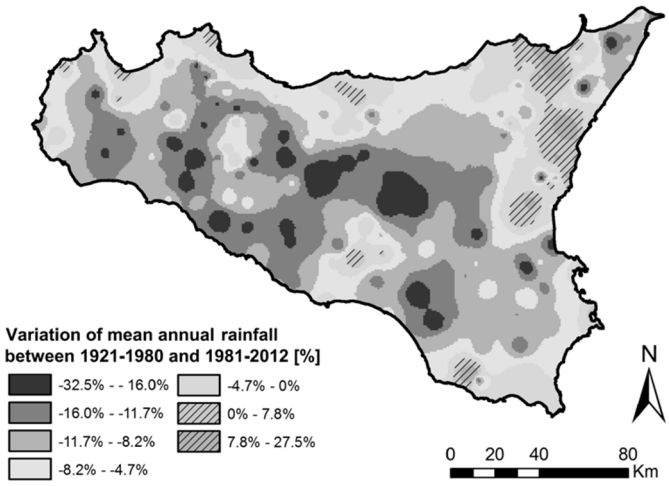

Figure 57. Variation of mean total annual precipitation between the period 1921-1980 and the period 1981-2012.

The spatial interpolation of the detected trends highlight the presence of a wide area characterized by an increase of total annual precipitation over the last 30-years in the eastern part of Sicily (Figure 58). The magnitudes of trend range between 2.8 mm/year and 19.6 mm/year, while the mean increase is about 8 mm/year.

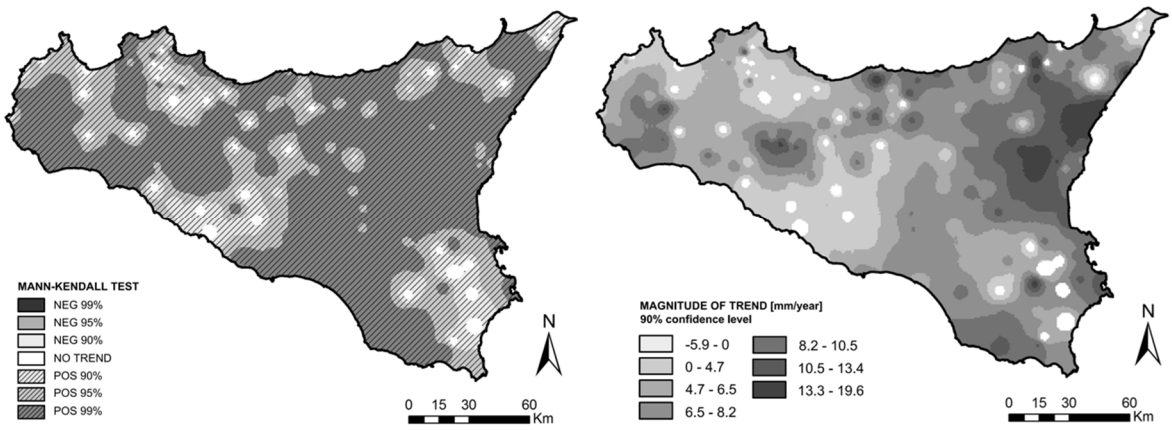

Figure 58. Spatial distribution of Mann-Kendall test results and trend magnitudes (mm/year) for total annual rainfall (1981-2012).

Combining these results with the ones reported in Figure 57, it can be concluded that the total annual rainfall did experienced a decrease in the latest 30-years, if compared with the previous period 1921-1980, however the total amount of rainfall has been affected by a general positive trend in the short-term. The reason of these change of trend direction need to be deepened, in order to verify, if the recent positive trends could be attributed to possible trends in extreme rainfall. In Italy many authors (e.g. De Michele et al., 1998; Pagliara et al., 1998; Brath et al., 1999) have claimed the presence of a valuable increasing tendency in high intensity rainfall in urban areas. Moreover, investigating where the change point of trend direction occurred is another critical issue that requires further analysis.

In order to investigate on possible temporal and spatial variations of PCI, the index was calculated, on an annual scale, for each series for the period 1921-2012 and the sub-period 1981-2012. Figure 59 shows that the PCI ranges from 12.7 to 20.3 in both periods and spatially increases from North-West to South-East. Spatial patterns are slightly different, since, in the map of the period 1981-2012, a wider area is characterized by lower values of the index (ranging from 12.7 to 14.7), if compared with the same area in the map of the period 1921-2012. In both periods the highest values (from 18.0 to 20.3) of PCI are concentrated in the southeastern part of the island, along the Ionian coast.

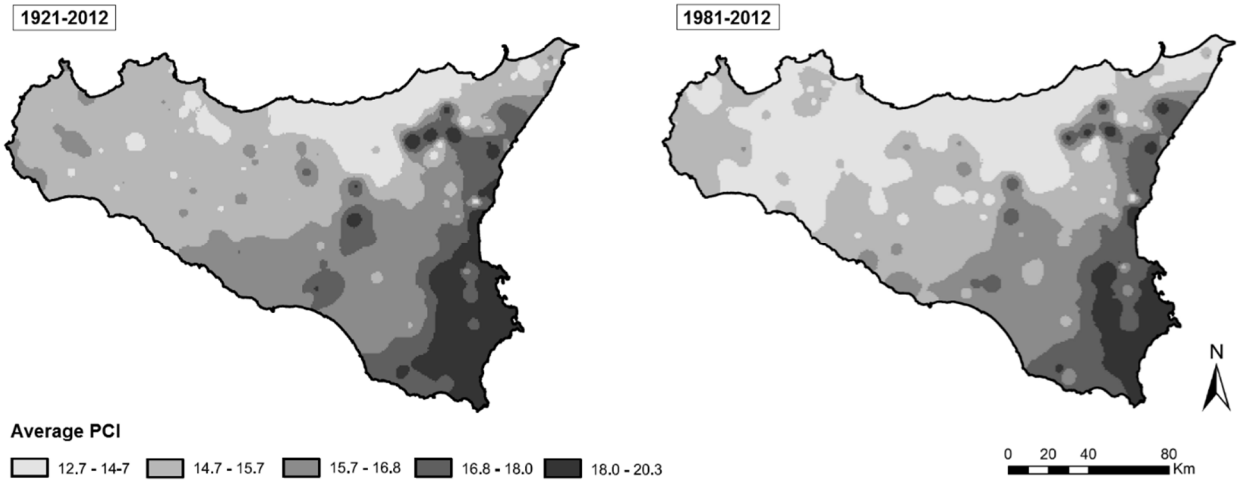

Figure 59. Average Precipitation Concentration Index (PCI) for the period 1921-2012 and the period 1981-2012.

A decrease in PCI values has been detected in the period 1921-2012 is some small areas (Figure 60), for which the magnitude of trend ranges from -0.008 to -0.05. For these areas the presence of a negative trend implies that the rainfall distribution during the year is becoming more uniform.

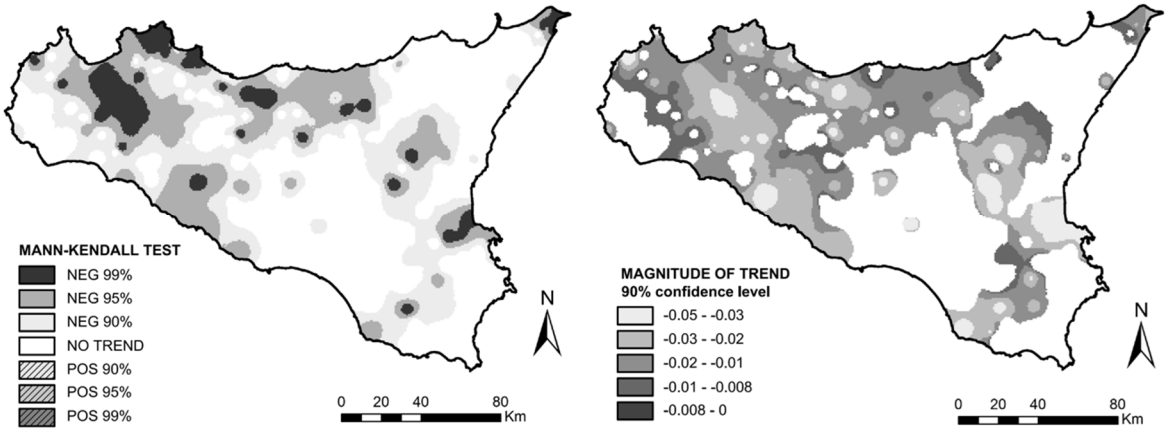

Figure 60. Spatial distribution of Mann-Kendall test results and trend magnitudes (mm/year) for PCI (1921-2012).

Analyzing the period 1981-2012, a lower number of trends has been detected, but with higher magnitudes (from -0.24 to -0.06). Figure 61 shows the spatial distribution of trends and their magnitude. Two small areas located at North-West and at South-East are characterized by negative trends. Only one positive trend has been detected in the North-East (β = 0.07).

The presence of few negative trends in the PCI values during the period 1981-2012 strengthens the hypothesis that the increase of total annual amount of rainfall should be attributed to a possible increase of extreme rainfall depths. Indeed, the small number of trend in the PCI series over the latest 30-years indicates that the distribution of rainfall during the year have not be subjected to remarkable variations. Therefore, an increased occurrence and entity of extreme events could provide an explanation for the short-term positive rainfall trends.

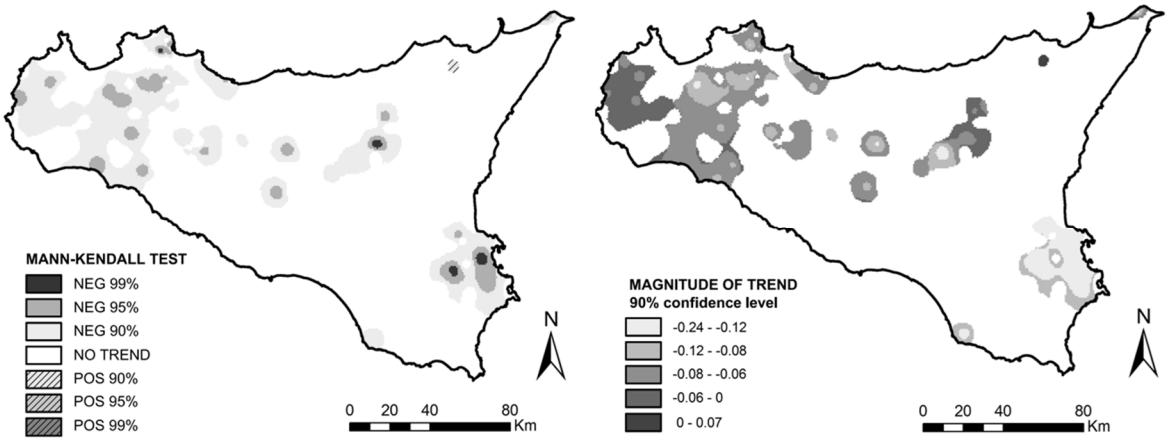

Figure 61. Spatial distribution of Mann-Kendall test results and trend magnitudes (mm/year) for PCI (1981-2012).

3.3.2.3. Impacts of climate change on extreme rainall

Historical extreme rainfall series for the period 1950-2008 measured in 65 rain gauges across Sicily (Figure 62) have been provided by Osservatorio delle Acque – Regione Siciliana (OA-RS). Data have been recorded in rain gauges equipped with pluviographs and refer to five different durations: 1, 3, 6, 12 and 24 hours. From the analysis of the empirical cumulative distribution functions, the ranges of variation and the medians of extreme rainfall can be determined, with the latter being 25.6 mm, 35.0 mm, 42.7 mm, 51.6 mm and 61.6 mm for 1, 3, 6, 12 and 24 hours, respectively.

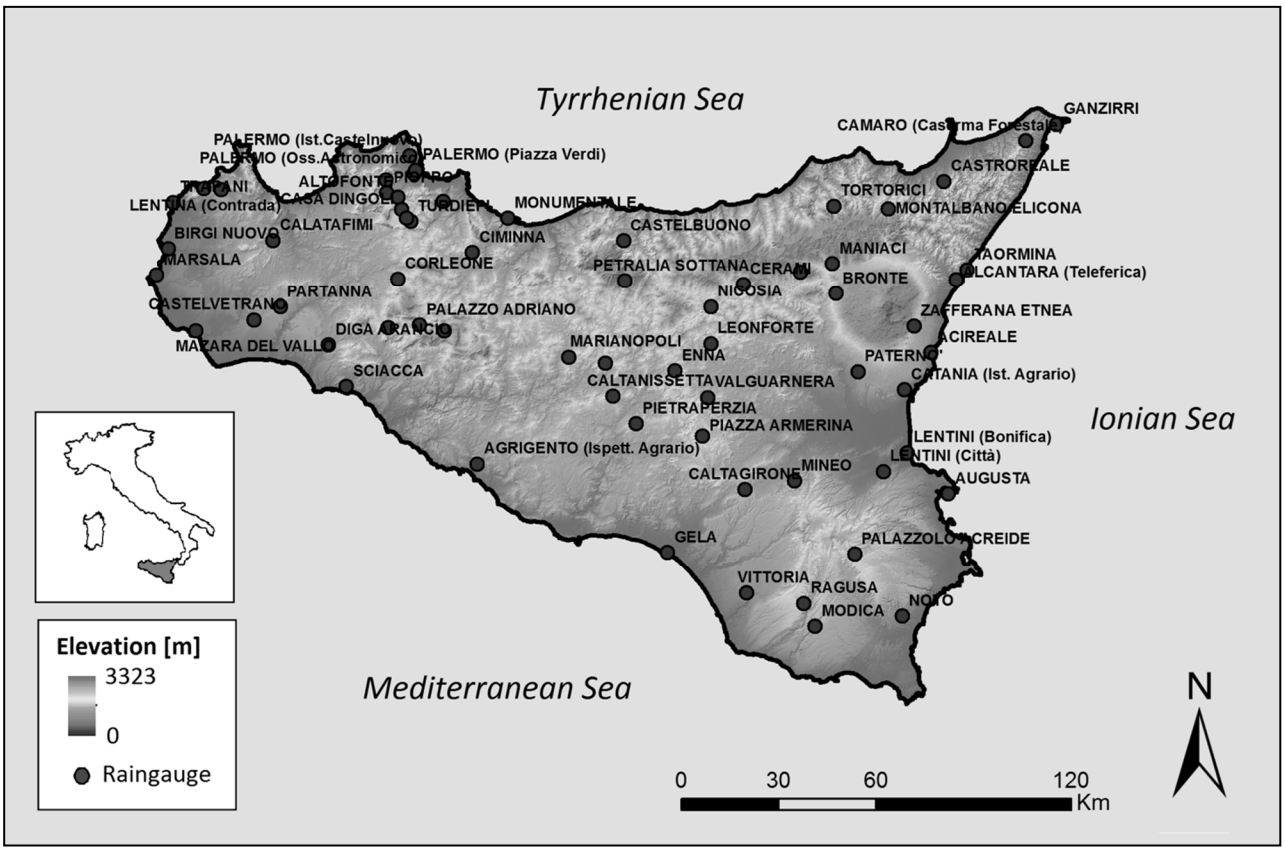

Figure 62. Rain gauges location for the extreme events trend analysis.

The trend analysis has been carried out using the Mann–Kendall non-parametric test, and the magnitude of significant trends has been estimated using Equation (5). Confidence levels of 90%, 95% and 99% have been chosen as thresholds to classify positive and negative trends. Trends with confidence level below the 90% have been excluded.

The results obtained from the analysis of the extreme rainfall data are summarized in Table 5, where the number of trends (total, positive and negative) and their confidence levels have been reported for each station. In Table 6, the mean value, the mean ranges of variation of magnitude β (mm/year), and the p-values have been reported.

Table 5. Number of stations with significant trends at the 90%, 95% and 99% confidence level. The symbol "+" indicates positive trend, while the symbol "-" indicates negative trend.

Duration	Confidence level											
	90%				95%				99%			
	No trend	Trend			No trend	Trend			No trend	Trend		
		Total	+	-		Total	+	-		Total	+	-
1 hr	31	34	22	12	38	27	18	9	46	19	13	6
3 hr	33	32	14	18	41	14	12	12	53	12	3	9
6 hr	35	30	14	16	46	19	10	9	56	9	3	6
12 hr	39	26	14	12	41	24	13	11	50	15	6	9
24 hr	41	24	13	11	44	21	10	11	48	17	8	9

Table 6. Mean value (mm/year) and range of variation of magnitude β (mm/year), and p-value for positive and negative trends.

			Duration				
			1 hr	3 hr	6 hr	12 hr	24 hr
POSITIVE TRENDS	β [mm/year]	range	0.08 ÷ 0.40	0.08 ÷ 0.41	0.09 ÷ 0.48	0.04 ÷ 0.56	0.26 ÷ 0.85
		mean	0.17	0.19	0.22	0.29	0.46
	p-value	range	$1.21 \cdot 10^{-7}$ ÷ 0.09	$3.17 \cdot 10^{-8}$ ÷ 0.07	$5.19 \cdot 10^{-8}$ ÷ 0.08	$1.98 \cdot 10^{-6}$ ÷ 0.06	$7.00 \cdot 10^{-6}$ ÷ 0.10
		mean	0.02	0.03	0.04	0.02	0.02
NEGATIVE TRENDS	β [mm/year]	range	-0.27 ÷ -0.06	-0.55 ÷ -0.02	-0.66 ÷ -0.02	-0.62 ÷ -0.06	-0.78 ÷ -0.15
		mean	-0.14	-0.22	-0.29	-0.38	-0.47
	p-value	range	$3.29 \cdot 10^{-5}$ ÷ 0.08	$8.89 \cdot 10^{-7}$ ÷ 0.10	$2.55 \cdot 10^{-7}$ ÷ 0.09	$1.24 \cdot 10^{-6}$ ÷ 0.09	$8.44 \cdot 10^{-8}$ ÷ 0.03
		mean	0.03	0.03	0.04	0.01	$4.71 \cdot 10^{-3}$

Regarding a duration of 1 hour, 52.3%, 41.5%, and 29.3% of the rain gauges showed trends with a confidence level of 90%, 95%, and 99%, respectively. These trends were more frequently positive, ranging from +0.08 mm/year to +0.40 mm/year, and the statistically significant negative trends ranged from -0.27 mm/year to -0.06 mm/year.

Considering *d*=3 hr, significant trends have been detected in 49.2%, 36.9% and 18.5% of the rain gauges for confidence levels of 90%, 95% and 99%, respectively. In this case, the number of negative trends is slightly higher than number of positive ones. Ranges of magnitude of positive and negative trends are similar to the ones for d=1 hr. The analysis of the extreme rainfall with *d*=6 hr showed a positive trend in 46.1%, 29.2% and 13.8% of the rain

gauges, for a confidence level of 90%, 95% and 99%, respectively. Focusing on the 90% confidence level, the percentage of positive and negative trends was slightly reduced if compared with d=1 hr and d=3 hr. This reduction persists in the percentage of trends in extreme rainfall series with *d*=12 hr. In this case, a trend has been detected in 40%, 32.3% and 23.1% of the cases at 90%, 95% and 99% confidence levels, respectively. The range of variation of positive trends is +0.04 ÷ +0.56 mm/year, and the magnitudes of the negative trends vary between -0.62 and -0.06 mm/year.

For *d*= 24 hr, the extreme rainfall series of 36.9%, 32.3% and 26.2% of the rain gauges showed a trend at 90%, 95% and 99% confidence levels, respectively. For each duration, decreasing trends showed higher magnitudes. This result could be related to the generalized reduction of rainfall occurring in Sicily over the latest decades (Cannarozzo et al., 2005). In Figure 63, the precipitation series with the highest increases and decreases are shown for each duration. The series recorded by the rain gauge at Palermo (Ist. Castelnuovo), placed on the northwest coast of the island, showed the highest increases for the durations of 1, 3, 6 and 12 hours. For the series recorded in this rain gauge, the percentage of missing data is 15%. The positive trend with the greatest magnitude for 24 hours has been observed at the Montalbano Elicona rain gauge, placed on a hilly area in the northeast part of the island. The highest decreases were observed in the Vittoria, Catania (Ist. Agrario), Marsala, Marianopoli and Pioppo rain gauges for the durations of 1, 3, 6, 12 and 24 hours, respectively. These rain gauges are distributed throughout the region; three of them are in the inland and only two are on the coast. For these rain gauges, the percentage of missing data is about 15%.

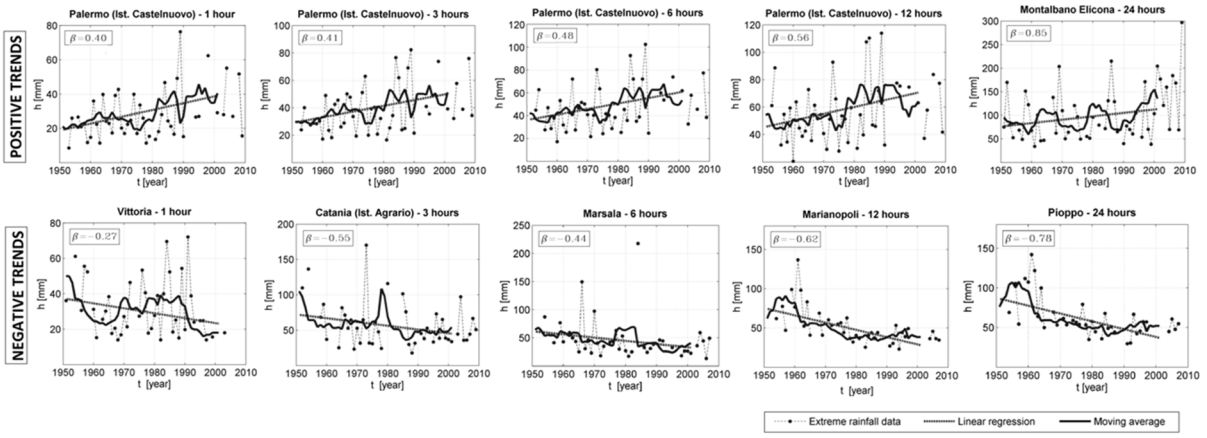

Figure 63. Positive and negative trends for the raingauges that showed the highest increases and decrease in terms of magnitude β (mm/year).

Results indicate that both positive and negative trends are present in the region for each duration. At a 90% confidence level, positive trends are more frequent for the *d*=1 hr extreme rainfall series. The analysis of magnitudes of positive and negative trends revealed that the ranges of variation are comparable for the durations of 1, 3, 6 and 12 hours and that the magnitudes of increases and decreases are slightly higher for 24 hours of extreme rainfall.

To investigate the existence of spatial patterns of the detected trends, the confidence levels of the trend test and the magnitude of the trend have been spatially interpolated using the *Inverse Distance Weighted* (IDW) interpolation method, which provided raster surfaces as output. In the IDW method, each rain gauge has a local influence that decreases with distance by means of the use of a power parameter. For the case of study, the IDW method can be considered an appropriate interpolation method, since rainfall data are moderately correlated to elevation. Specifically, the linear correlation coefficient is equal to 0.42 for total annual rainfall, and ranges from -0.3 to 0.05 for maximum annual rainfall (from 1 hr to 24 hr). Figure 64 and Figure 65 show the interpolated trends and the magnitude of significant trends for each duration. In these figures, for a 90% significance level, the no-trend areas have been masked. As regards to *d*=1 hr (Figure 64, *a)* and *b)*) positive trends are mainly localized in the western areas, which exhibit the highest increase (about +0.39 mm/year). Small, unconnected areas of negative trends are located at to the east and the south (Figure 64, *c)* and *d)* show trends and relative magnitudes for *d*=3 hr. Negative trends are located mainly in the southern part of the island, and some positive trends are concentrated in the northeast area, with the maximum magnitude equal to +0.4 mm/year. For *d*=6 hr (Figure 64 *e)* and *f)*), two different areas of decreasing trends can be identified in the central and southern areas. In the northeast area, a concentration of positive trends can be observed in this case as well. The spatial patterns for *d*=12 hr and *d*=24 hr are similar (Figure 65 *a)* and *c)*). There is a large area characterized by increasing trend in the northeast, where positive trends have been detected for *d*=3 hr and *d*=6 hr, but the northwest part of the island is characterized by negative trends.

The analysis provides a complex picture of the possible impact of climate change on design rainfall. The areas characterized by positive trends can probably face an increase of urban drainage surcharge frequency due to the increase of rainfall intensities for the design return period. If the climate change is coupled with an increase of drained impervious area, the process may greatly increase flooding risk. At the opposite, negative trends may

require additional combined sewer maintenance due to the reduction of wet weather flows flushing capacity (OFWAT, 2008).

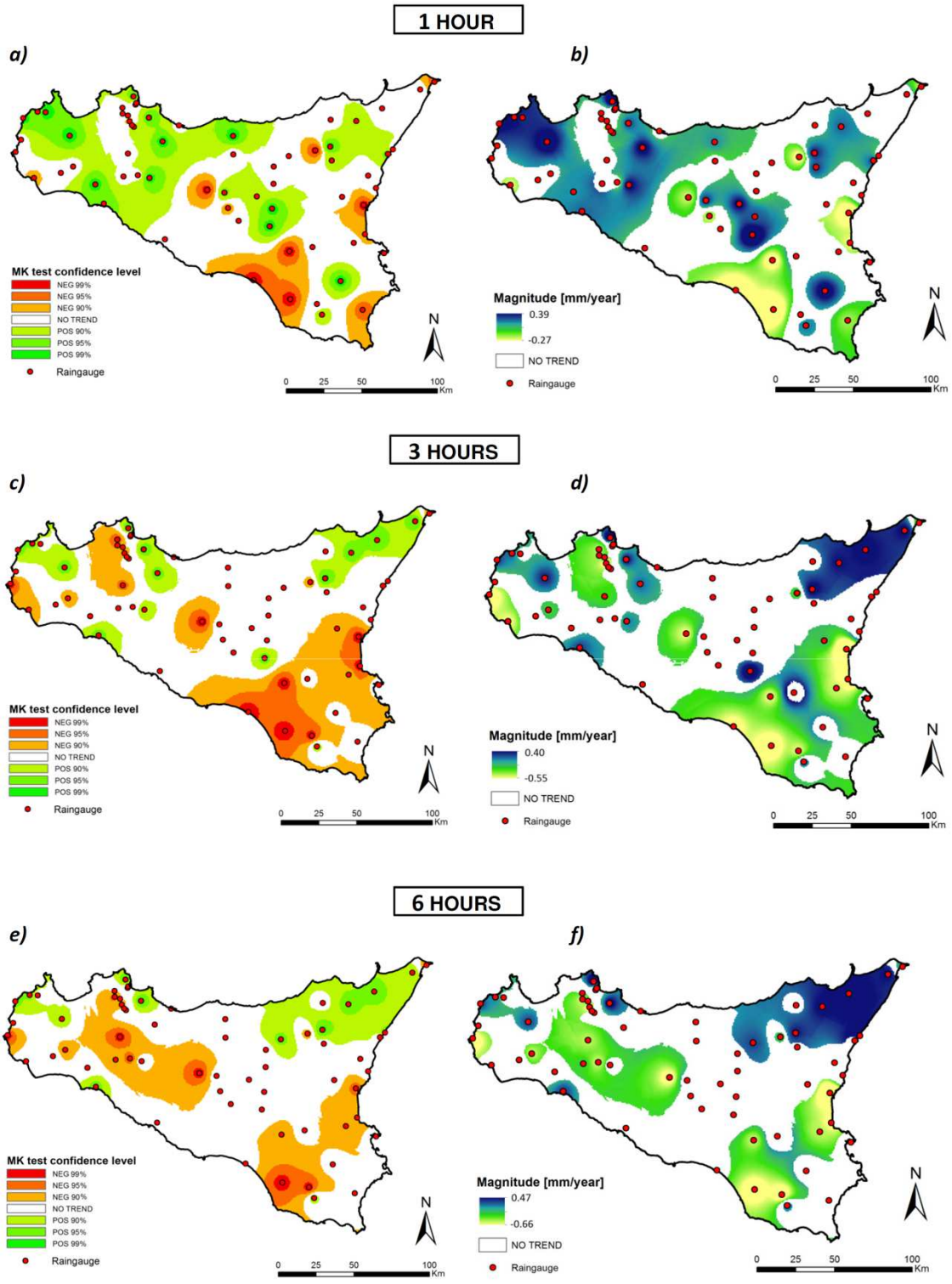

Figure 64. Spatial distribution of statistically significant trends and their magnitude (at 90% confidence level) for 1, 3, and 6 hours durations.

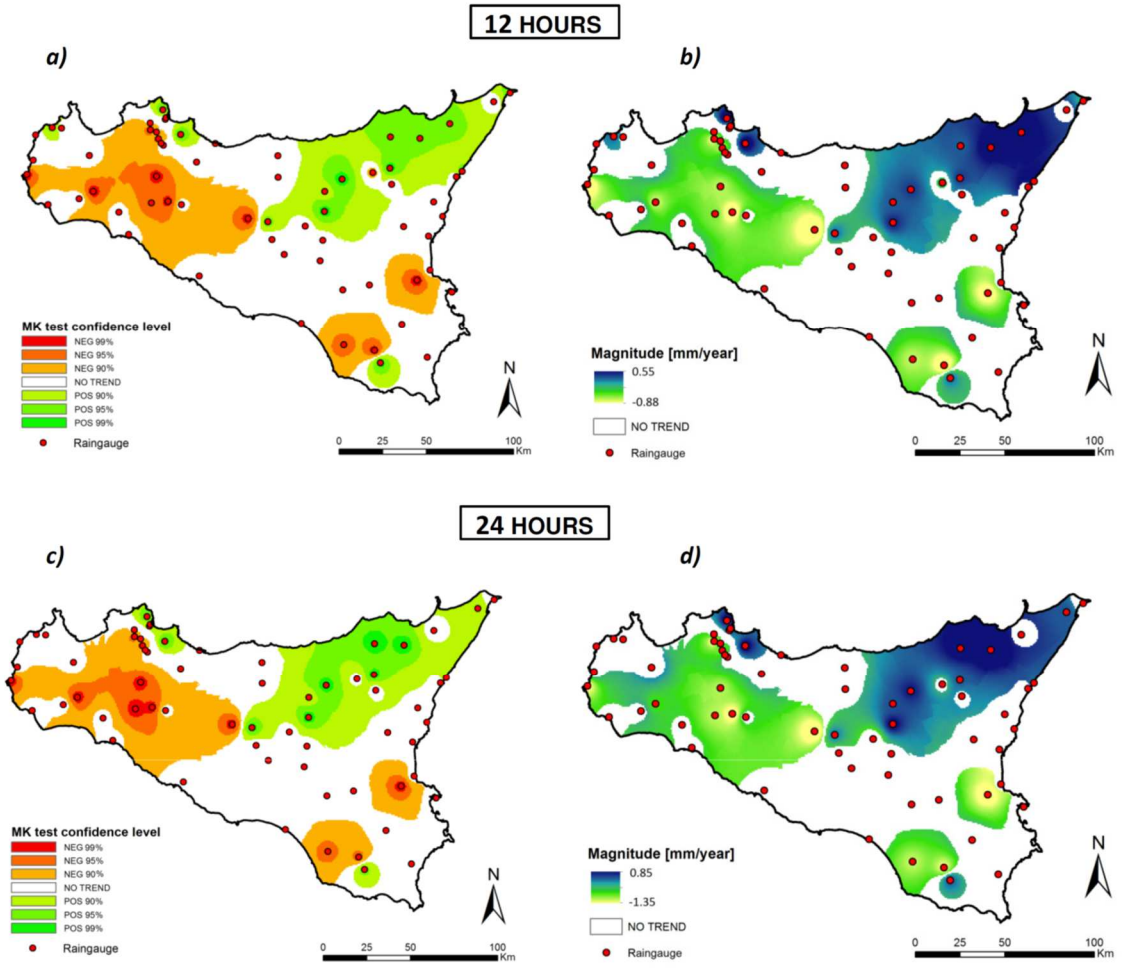

Figure 65. Spatial distribution of statistically significant trends and their magnitude (at 90% confidence level) for 12 and 24 hours durations.

Based on the Ombrothermic diagram for the period 1980-2022 (Figure 66Figure 87), the average summer temperatures in the area range from 20,90 °C to about 24,16 °C, with average precipitation varying between approximately 6,97 mm and 16,89 mm. During winter, average temperatures range from 7,21 °C to 9 °C, and average precipitation ranges from 44,84 mm to 71,69 mm. August is identified as the hottest month with an average temperature of 24,16 °C, while February is the coldest with an average temperature of 67,21 °C. November is the wettest month, receiving 73,94 mm of precipitation, and July is the driest, with just 6,97 mm of rainfall. A dry period is also observed from mid-May to mid-September.

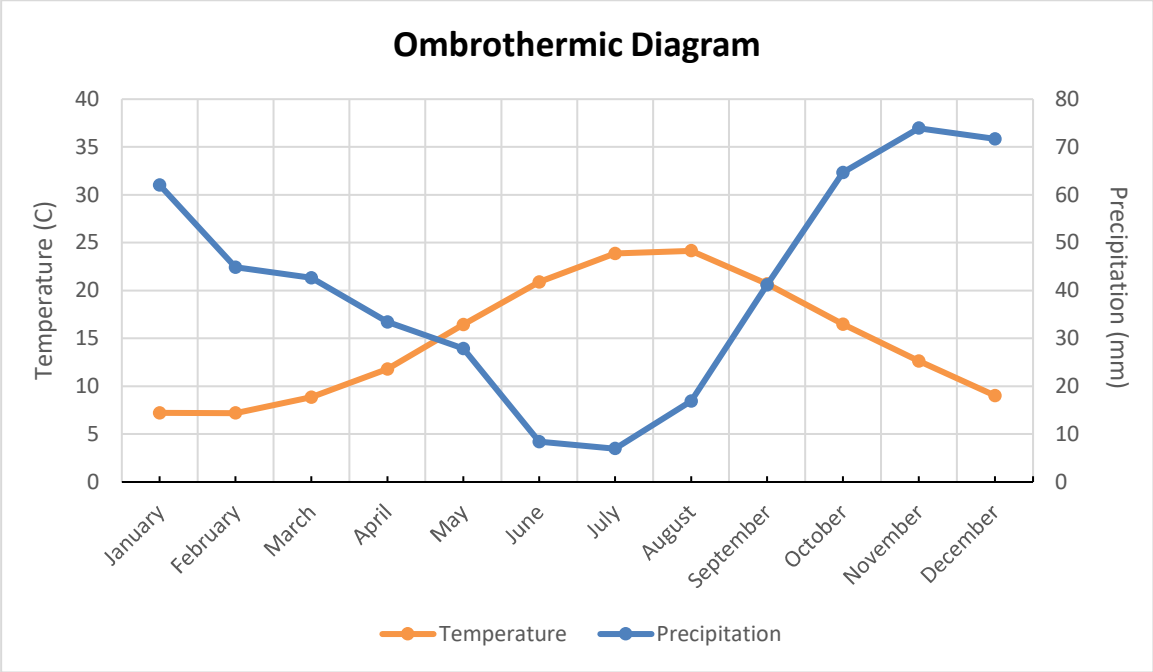

Figure 66. Ombrothermic Diagram of Rocca di Cerere for the years 1980-2022 based on the CRU TS dataset (Harris et al. 2020).

3.3.3. Land Uses

The pilot area of Italy, although one of the smallest, exhibits a clear division of land use into three primary types: urban, agricultural, and forested areas, each with distinct subcategories. Figure 67 reveals that the most significant land use is land principally occupied by agriculture, with significant areas of natural vegetation, which takes up to 33% of the total area. In total agricultural areas occupy most of the region, encompassing 64,6% of the total region and following are forested areas, comprising 19,4% of the region. The remaining parts of the area are predominantly covered by urban areas.

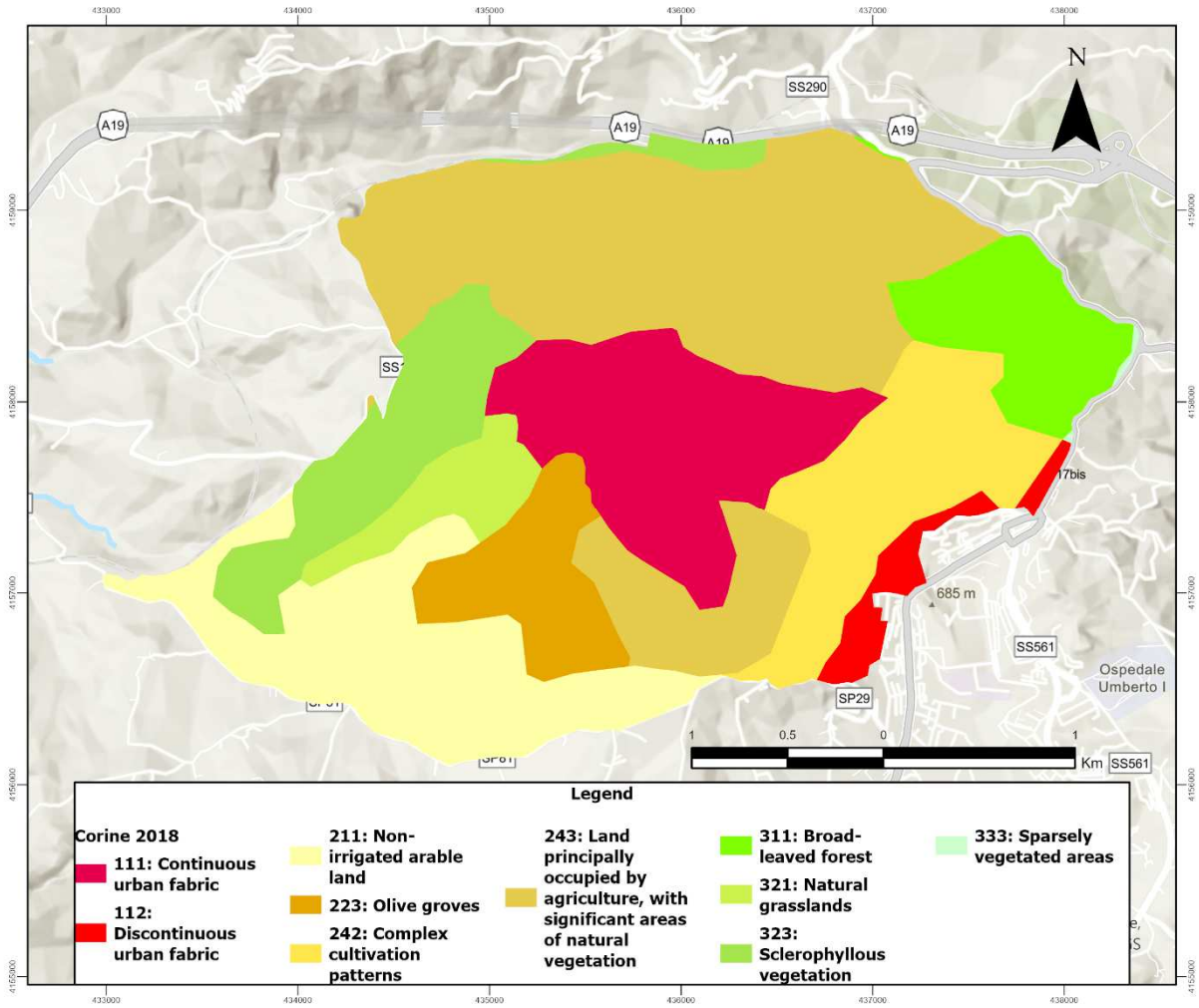

Figure 67. CORINE land cover map of the pilot area in Italy.

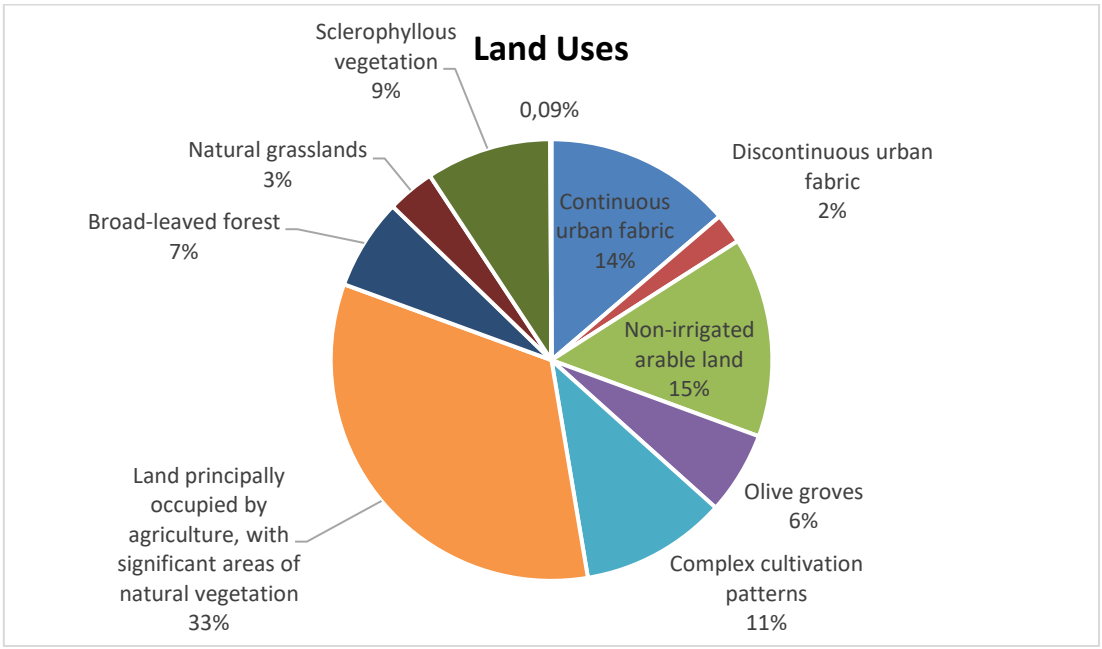

Figure 68. Percentage cover of different land use types that occupy the pilot area in Italy based on the CORINE land cover.

3.3.4. Flora and Vegetation

The territory of the Geopark extends in the central area of Sicily , on the Erei Mountains , in the territories of the municipalities of Enna , Aidone , Assoro , Calascibetta , Nissoria , Leonforte , Piazza Armerina , Valguarnera and Villarosa .

The name " Rocca di Cerere " was chosen due to the ancient dedication of this territory to the Kthonic deities . Already the indigenous peoples of ancient Sicily, Sicani and Siculi, worshiped figures connected with the Earth and the subsoil. These cults can be summarized in the Latin name of Ceres , the Greek Démeter, tutelary deity of agriculture, venerated on the highest peak of the city of Henna, the Rock of Ceres.

The name, therefore, reflects the close relationship, established over time, between Mother Earth and man.

Geologically the area covers the central part of the Sicilian Foredeep between the Apennine-Magrebis chain and the Iblean Foreland and is characterized by a wide geological diversity.

To the north the area has both trassic and flimsy deposits with quartzarene formations , while to the south the presence of the chalky-sulphurous plateau created by the Messinian crisis 5,96-5,33 million years ago prevails . This crisis occurred due to a sudden drying up of the Mediterranean with the consequent cyclical deposition of powerful levels of evaporites. The crisis ended with the return of the sea in the Zanclean period .

Figure 69. Natural endemic vegetation in the area.

The conformation of the territory is typically hilly-mountainous , with over 10% of the surface located above 700 m, the maximum elevation of which (1,192 m above sea level) is reached at the top of Mount Altesina .

Therefore enclosed by a sort of mountainous perimeter , the district offers the gaze a decidedly evocative landscape, dotted with valleys , rivers , streams and lakes (including Lake Pergusa , the only natural Sicilian lake and place of the myth of Proserpina), ancient perched centers and hills that slope down towards the extensive eastern plains which, over the centuries, have been the scene of intense human activity and whose testimonies, today, define the historical-cultural heritage of the Geopark . Just think of the presence of two of the major classical archaeological areas of the entire Mediterranean, such as the Roman Imperial Villa of Casale and the Greek Polis of Morgantina , as well as other 150 archaeological sites including the Byzantine village of Canalotto and the Necropolis of Malpasso and Realmese dating back to the Copper and Bronze Ages. The territory also boasts the only Archaeological and Mining Park on the island: Floristella-Grottacalda , numerous other deposits of industrial archeology and 4 protected areas of notable historical-naturalistic value (RNS Lago di Pergusa , RNO Monte Altesina , RNO Rossomanno- Grottascura-Bellia and RNO Monte Capodarso and southern Imera Valley).

Reducing the very different forms of Nature into categories has always been a desire of the man of science, but any categorization must be obtained with a necessary reduction of the multiplicity of aspects. To try to give an easy reading of the ecosystemic aspects present in the vast territory of the Geopark, we wanted to group into categories those natural environments that are most frequently encountered while walking in these areas.

The altitude of the Geopark area ranges from the Dittaino and southern Imera valleys , which run towards the sea a few hundred meters above sea level to the top of Altesina , the ancient Mons Aereus , located at 1192 m above sea level .

This altitude means that the landscape includes different vegetation bands ranging from the thermo-Mediterranean one to that of the deciduous broad-leaved forest .

Starting from the lowest and most sunny lands , in the valley areas of the territory, between the fields and the gully areas , we can still find signs of the original vegetation of the Thermo-Mediterranean belt . This vegetation was characterized in these areas by sclerophyllous species accustomed to the scorching heat of the long Sicilian summer. The dominant ones must have been the carob tree (Ceratonia siliqua) and the wild olive tree (Olea oleaster),

mixed with other arboreal and above all shrubby species such as the mastic tree (Pistacia lentiscus) and the terebinth tree (Pistacia terebinthus), which today are less frequent but typical of this formation. also the strawberry tree (Arbutus unedo), the phillyrea (Phillirea latifolia and P. angustifolia), but also the dwarf palm (Chamaerops humilis), the only native palm in Sicily.

Once upon a time the Mediterranean strip characterized by the presence of a forest cover dominated by holm oak (Quercus ilex) and in association with other broad-leaved essences must have represented the most widespread feature of the landscape of the area, but starting from the classical age and in particular from In the Roman age , the need for cereal production, as demonstrated both by Cicero's writings and by the countless wheat cisterns found in all ancient urban areas, had to trigger a centuries-old process of deforestation and isolation of tree vegetation in the steepest and most inaccessible areas. On the other hand, the frequency of grazing and the abundance of flocks and herds contributed to preventing the natural innovation of the shrub and tree cover to the point of eliminating its potential in much of the valley and hilly territory.

Today the landscape in vast areas is dominated by the extensive presence of wheat fields or rotational crops closely linked to the same cereal, almost as if the mythical choice of the mother of the cereal, Ceres - Demeter , had monopolized the production capacity of these lands.

Figure 70. Wheat fields.

The fundamental climax of the Italian Mediterranean vegetation is therefore that of the holm oak forest (Quercus ilex) in whose undergrowth sclerophyllous shrubs and various species of climbing herbaceous plants and lianas such as the sarsaparilla (Smilax aspera) or the flamewort (Clematis flammula) predominate.

In the warmer parts, the holm oak can give way to the cork tree (Quercus suber), another evergreen oak characterized by a notable development of the suberal part of the bark.

The procession sees various species mix with the holm oak, especially in areas where the cover is less dense, among these both the almond pear (Pyrus amygdaliformis) and the peraster (Pyrus piraster) are frequent, which in spring are among the first rosaceae to earn their flowery mantle.

The lower-growing herbaceous plants are rarer when the vegetation is in climatic conditions, as the lack of lighting on the ground prevents their development, but precisely due to the great degradation that the forest formation has had to endure in the last two thousand five hundred years, not rarely have arboreal essences given way to herbaceous-shrub ones and today it is easier to find a scrub formation characterized by a tangle of vegetation that is often impenetrable which the locals indicate with the name of sciara from the Arabic Sha'ra = bush .

Among the vegetation of the scrub you will find brambles (Rubus spp.), roses and sarsaparilla , the rare Calabrian pygamo (Thalictrum calabricum), and the cistus with various species.

Higher up, to close the vegetation bands present in the Geopark area, we find the most thermophilic part of the deciduous broad-leaved forest here dominated by the downy oak (Quercus pubescens sensu latu).

In association with it, both the two species of Pyrus mentioned above, as well as the coronilla (Coronilla emerus), the sessile-leaved cytisus (Cytisus sessifolius), the blackthorn (Prunus spinosa), the evergreen rose (Rosa sempervirens) and the canina (Rosa canina). Rarer is the buckthorn (Rhamnus alaternus).

In this case, the herbaceous layer concentrates its maximum vegetation during the early spring, when the oaks have not yet put out new leaves and the sun allows the development of the smaller species. In this period in the oak forest it will be possible to find blooms of anemone (Anemone hortensis) and cyclamen (Cyclamen repandum). The aqualine fern(Pteridiumaquilinum) will then grow between the rocks and near the cists and in the more humid areas the Venus navel (Umbilicus rupestris).

3.3.5. Fauna

The Italian fauna is made up of approximately 57.422 species of which 52.168 invertebrates and 1.254 vertebrates, represented by a great variety of endemisms . Sicily includes a notable contingent of the species that make up the Italian fauna, above all due to the geographical position of the island and the smaller islands that make up the archipelago.

3.3.5.1. The paleofauna of Sicily

Sicily has undergone and suffers those conditions that isolation activates towards the different taxa. Speciation, which occurs at a greater speed due to the lack of gene flow between populations, has made its effects felt in the past with the appearance of very interesting species. Among these, some of those belonging to a warm period of past times must certainly be mentioned, such as in the " Milazzian ". In this period, in Sicily lived the Falconeri dwarf elephant (Elephas melitensis or Elephas falconeri), a pachyderm, demonstrating the phenomenon of reduction in size, to the point of presenting individuals only 40 centimeters tall at the withers , a giant dormouse (Leithia melitensis) much larger than today's forest dweller known by the Sicilians as " surci giacalun i", but also hippos , crocodiles and various species of ungulates whose remains have sometimes remained in the deposits of the natural caves in the Geopark territory.

3.3.5.2. Current fauna

Since the end of the last glaciation, the fauna of Sicily has stabilized in today's general conditions with both boreal and palearctic , as well as Mediterranean and micro-Asian elements , characterized above all in the herpetofauna. Fundamentally, the Sicilian fauna, in its larger species, maintains a certain belonging to the paleoarctic area. The mammal species , for example, are almost all European, dominated (ab antiquo) by the presence of the wolf (Canis lupus) which later became extinct, and including ungulates such as the deer (Cervus elaphus hippelaphus) and the roe deer (Capreolus capreolus) also they extinct. Perhaps only one rodent, the porcupine (Hitrix cristata), represents the most African and oriental origin although widespread within the Mediterranean basin.

The situation found in minor species is different: in fact, it is not uncommon to recognize both extremely specific endemisms and African origins, not only among insects and arthropods in general, but also among reptiles which, having survived the glaciations, have managed to maintain a colonization of the island and its archipelago as evidence of past eras.

The complexity of the territory and the presence of different environments not only due to the different edaphoclimatic conditions but also due to the historical use of the territories, mean that in this portion of Sicily it is extremely difficult to describe the faunal presence.

Certainly some general characteristics of the animal presence must be considered such as, for example, the positioning of the island and in particular of this part of it on the main Palearctic migratory route , as well as, here and also in the rest of the island, the proximity to the world of Northern Africa on the one hand and Europe on the other, has allowed over time the stabilization of typical populations of the fauna of the two continental areas or even a speciation of some of the species once coming from one of the two areas.

On the other hand, the enormous weight that man has exerted on the populations themselves has been such that today the fauna appears deprived of some fundamental presences from the point of view of the organic nature of the different ecosystems. The lack of the wolf , extinct at human hands between 1930 and 1960 , or the large ungulates, definitively eliminated during the 19th century, are nothing more than the tip of the iceberg of the degradation that man has triggered towards natural communities.

The weakest populations probably disappeared in such distant times that their scientific registration was not possible. We do not know, for example, whether urodele amphibians (amphibians with tails such as the salamander and the newt) were present in nature in Sicily, we know for sure that they have never been scientifically recorded, but their presence, even in the territory of the Geopark, of different districts with toponyms such as Tino del Drago along the Salso Cimarosa river , but also Gorgo del Drago or similar, suggests that once upon a time the pools created by the Sicilian rivers must have hosted these cute beings so fragile with respect to water pollution.

Figure 71. Emys Trinacris.

3.3.6. Spatial data

- **Aspect**

The aspect map for the pilot area in Italy reveals a diverse topography with slopes oriented in various directions (Figure 72). While there appears to be a predominance of south, southwest, and west-facing slopes, there are also numerous slopes facing north and northeast.

- **Slope**

The slope map for the region of Enna clearly illustrates the hilltop topography of the city (Figure 73). It is evident that Enna is situated at the top of a hill, with the surrounding areas displaying a gradient that transitions from steep slopes near the hill to flatter terrain further out.

- **Geomorphology**

The geomorphology map for this area provides a valuable dataset for visualizing the hilltop topography (Figure 74). This model clearly demonstrates that the elevation decreases gradually from the hill's peak, which stands at 987 meters and is the location of the city of Enna, down to the lower surrounding altitudes.

- **Canopy Height**

The Canopy Height Model (CHM) distinctly shows a sparse distribution of trees in the region (Figure 75). This is evident not only because the maximum canopy height is relatively low, but also because the deforested areas outnumber the forested ones. The CHM highlights a landscape where tree cover is limited and fragmented, underscoring the predominance of open or non-forested land over regions with significant tree presence.

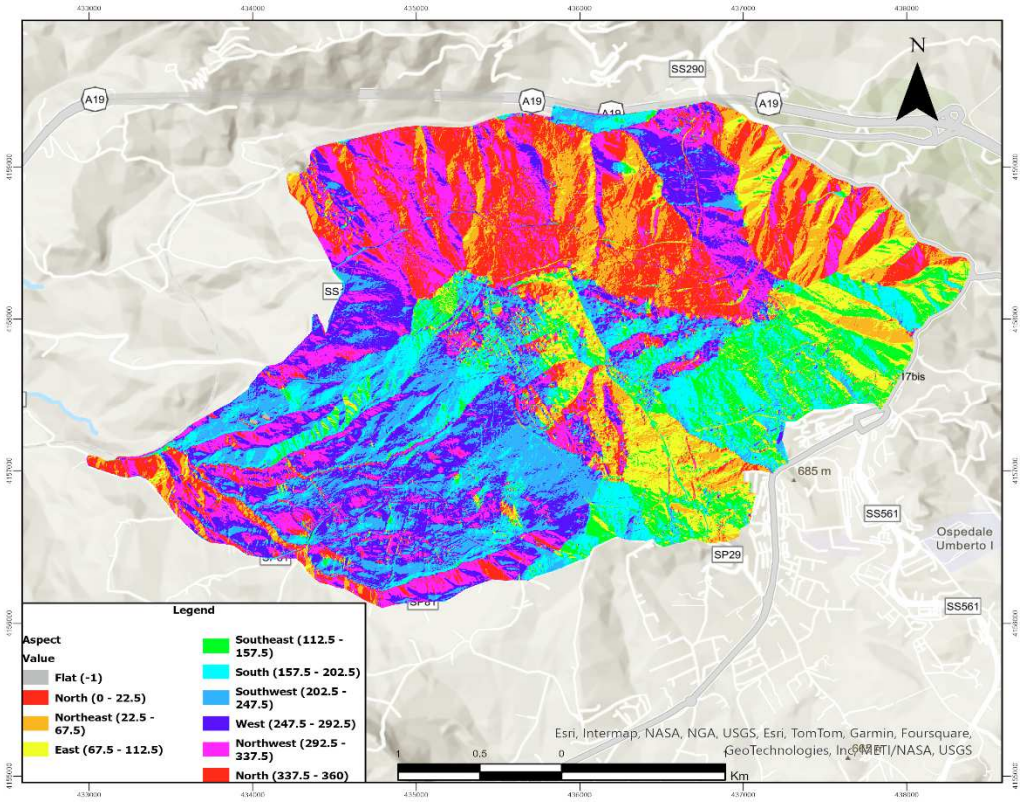

Figure 72. Aspect map of the pilot area in Italy.

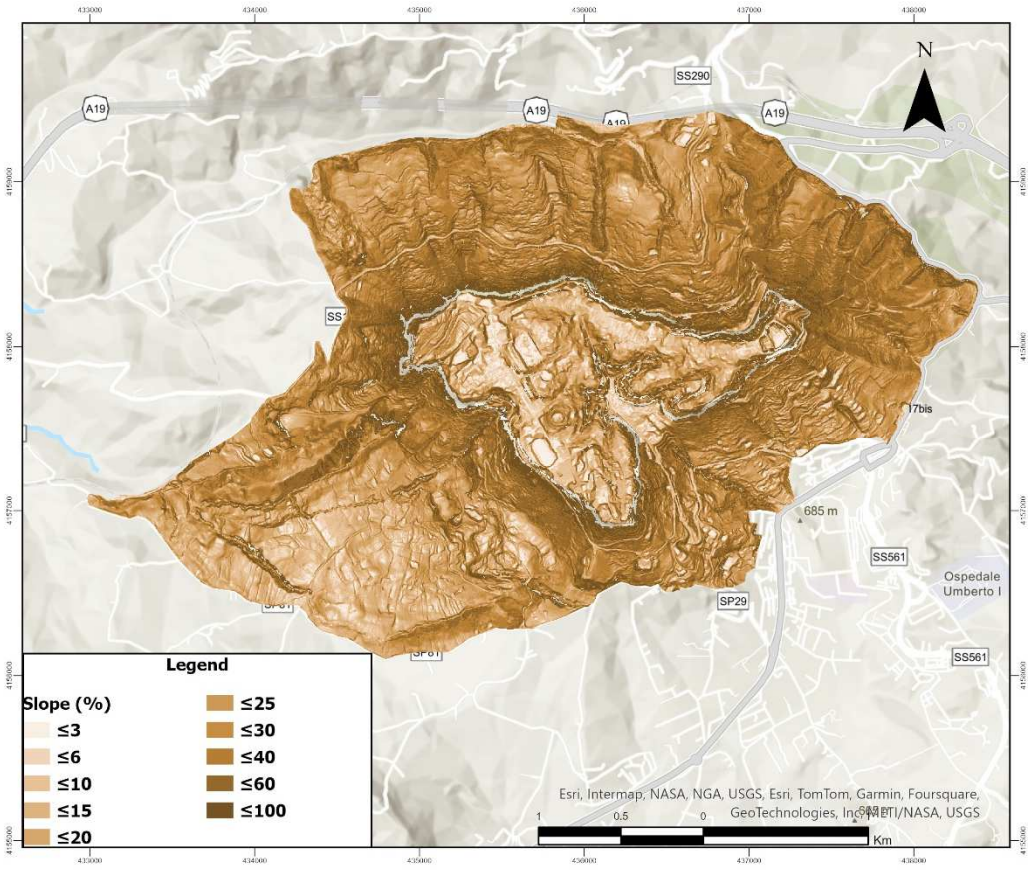

Figure 73. Slope map of the pilot area in Italy.

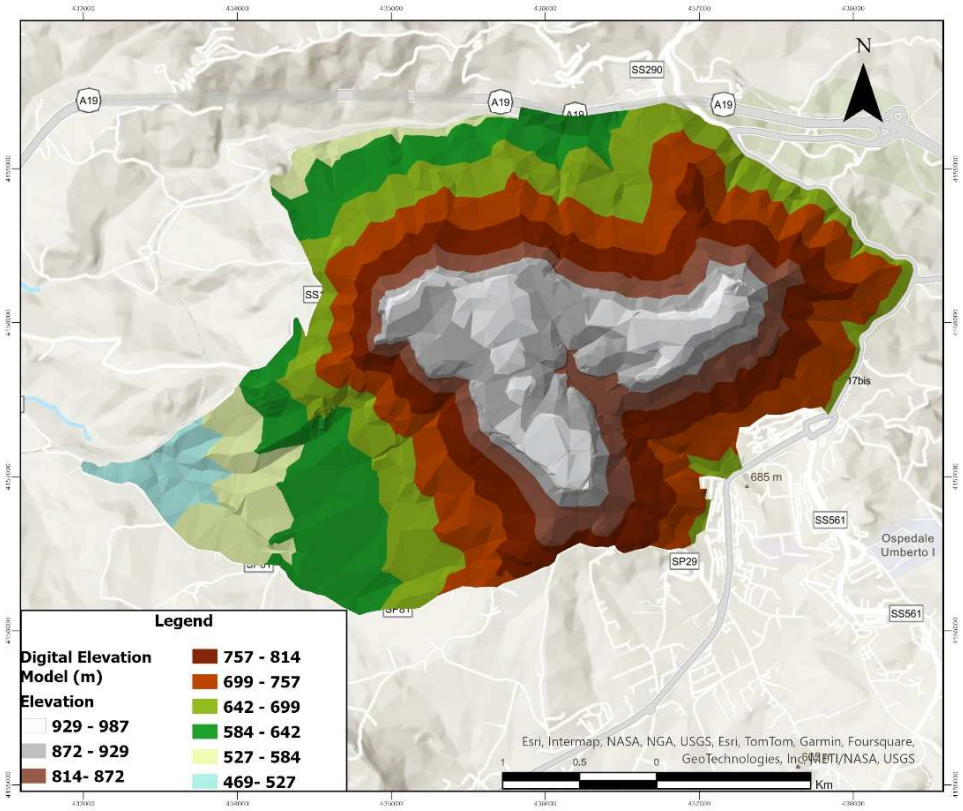

Figure 74. Geomorphology map of the pilot area in Italy.

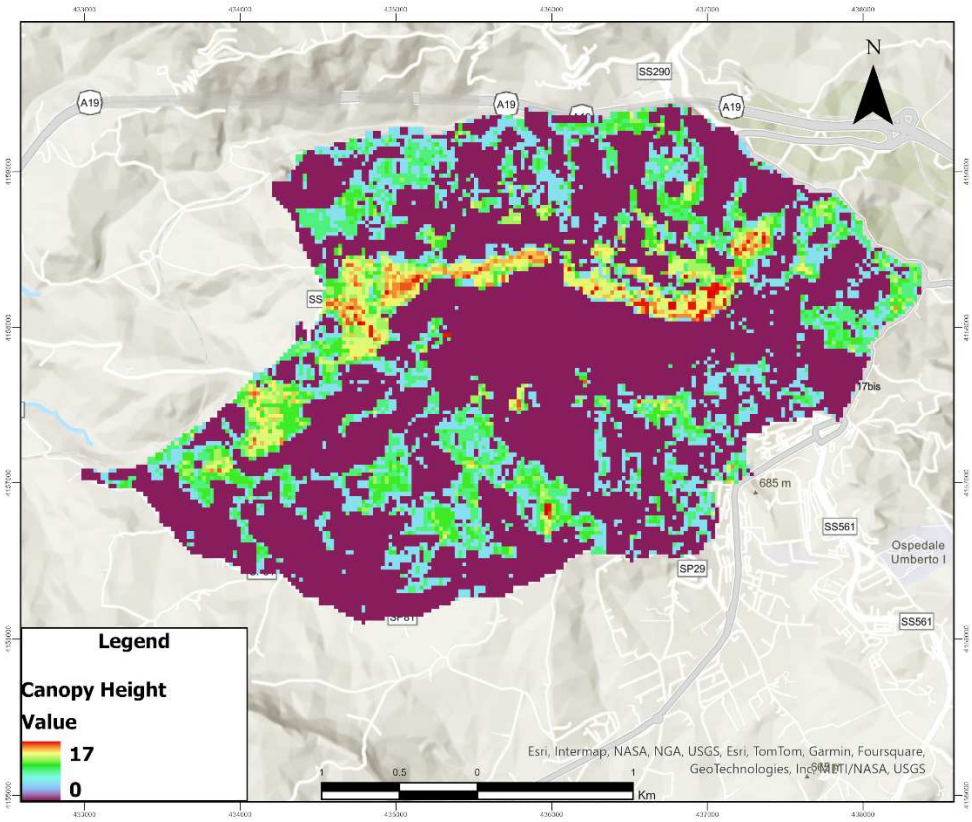

Figure 75. Canopy Height Model of the pilot area in Italy.

- **Tree cover density**

Similar to the Canopy Height Model (CHM), the tree cover density map clearly illustrates the lack of trees in the region. When examining Figure 76, it becomes apparent that tree density at the hilltop, where the city of Enna is situated, is nonexistent or extremely low. In contrast, the areas surrounding the city display a higher density of tree cover. The northern part of the region has the highest concentration of trees, highlighting a significant disparity in tree distribution between the city hilltop and its surrounding areas.

- **Roads and buildings network**

After examining the roads and buildings network of the pilot area (Figure 77), it becomes evident that there is a plethora of roads traversing through the city of Enna. It is also notable that many of the roads are spread throughout the rest of the area, giving immediate access to firetrucks that may need to use them in the future, in order to prevent the spread of wildfires.

- **NDVI**

Analyzing the NDVI models for the region can offer valuable insights into the distribution of vegetation and its seasonal variations. As previously noted, the vegetation in the city of Enna is sparse, which is evident when observing the NDVI values for this area across different seasons Figure 78. It is also apparent that during the summer, the majority of the pilot area exhibits very low NDVI values. This suggests that the bulk of the region's vegetation is primarily derived from agricultural land, with only a small amount of permanent vegetation present. The low NDVI values during the summer months clearly reveal that, apart from the cultivated crops, there is minimal lasting vegetation in the area, with most of it being observed on the northern side of the city.

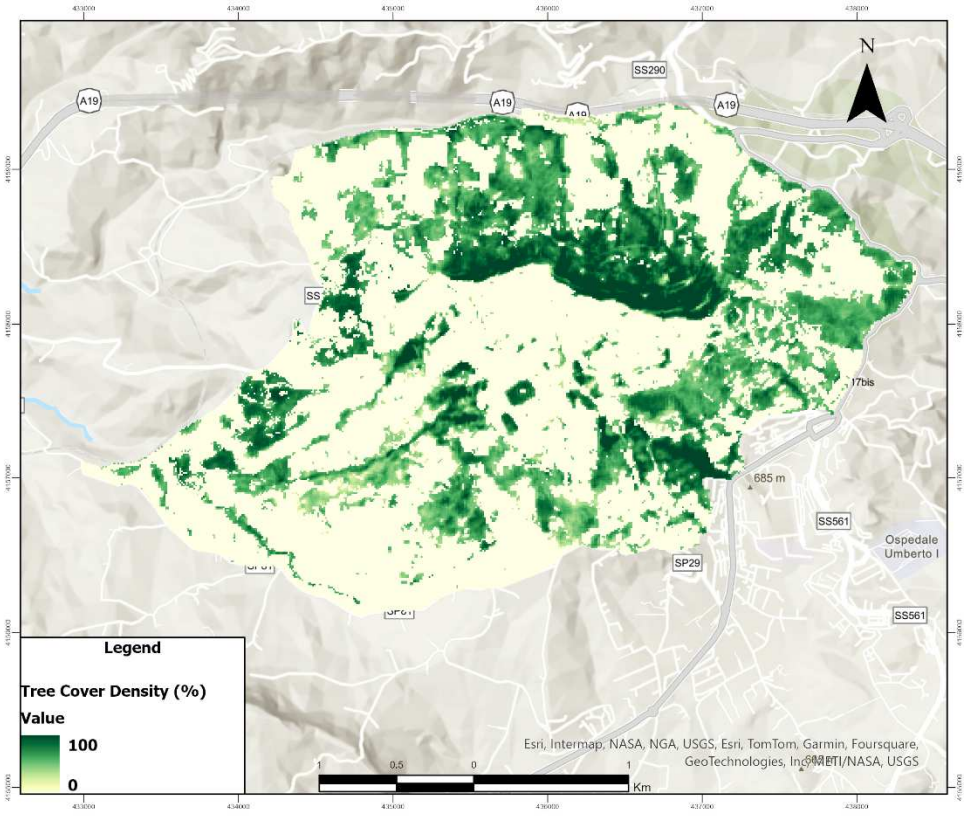

Figure 76. Tree cover density map of the pilot area in Italy.

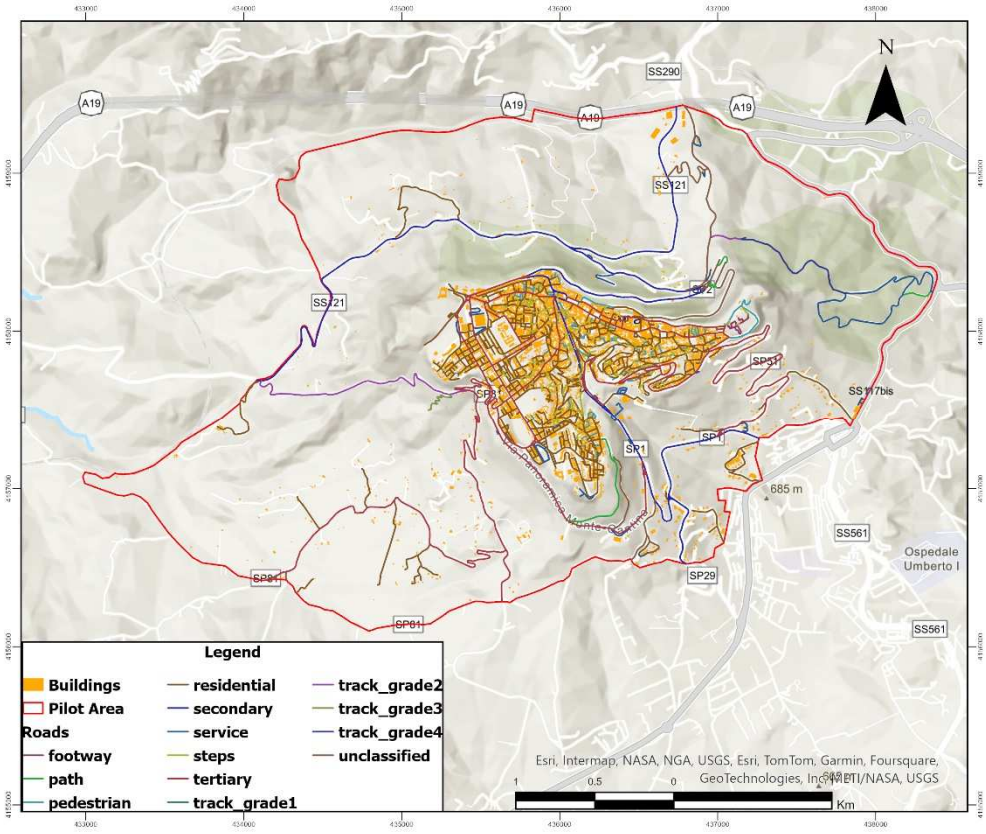

Figure 77. Roads and buildings map of the pilot area in Italy.

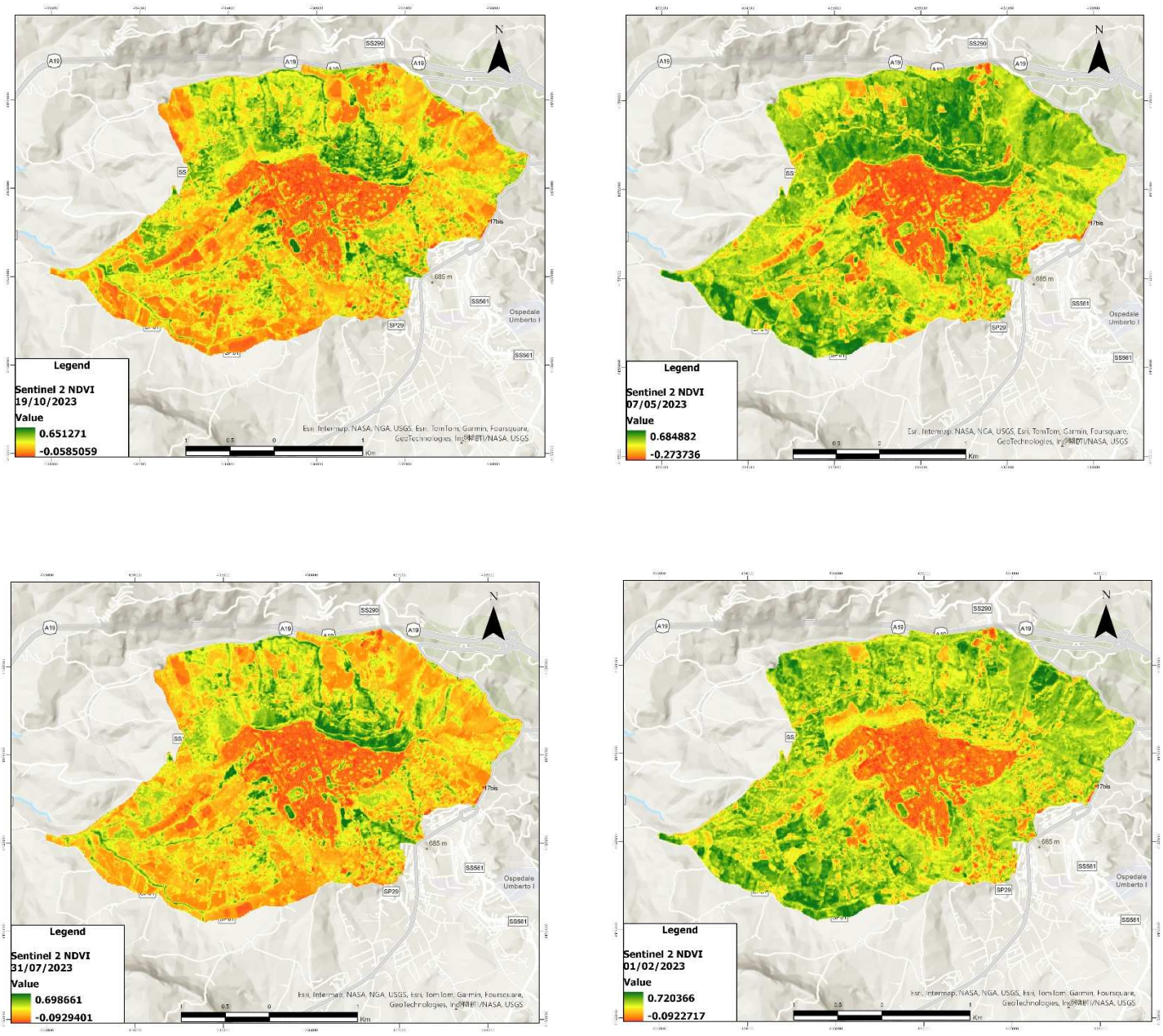

Figure 78. NDVI maps that cover all four seasons for the pilot area of Italy. The autumn NDVI map is displayed at the top left, the spring NDVI map at the top right, the summer NDVI map at the bottom left, and the winter NDVI map at the bottom right.

- **Sentinel 2 images**

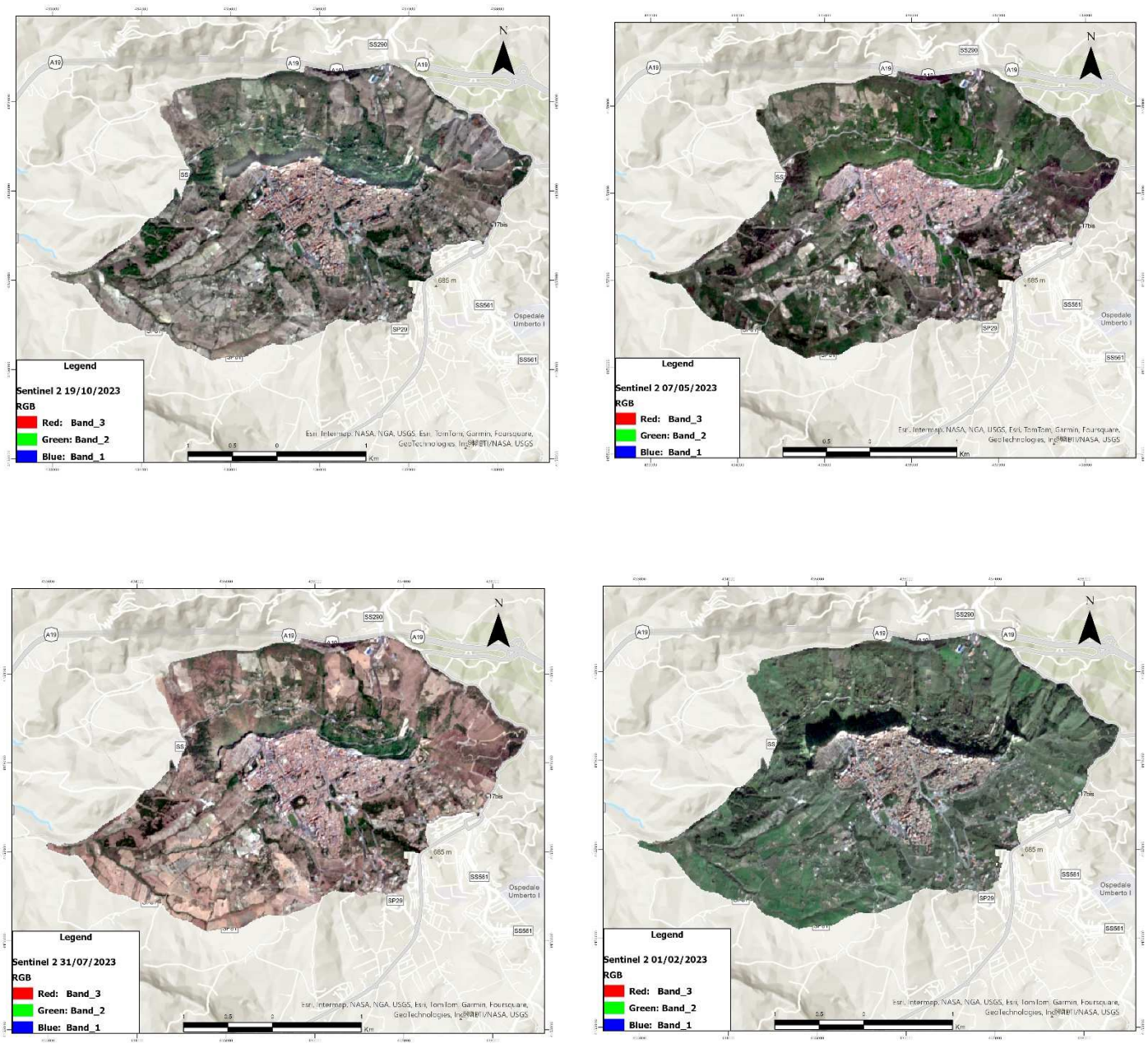

Figure 79. Sentinel 2 satellite images that cover all four seasons for the pilot area of Italy. The autumn Sentinel 2 image is displayed at the top left, the spring one at the top right, the summer one at the bottom left, and the winter one at the bottom right.

- **Planet image**

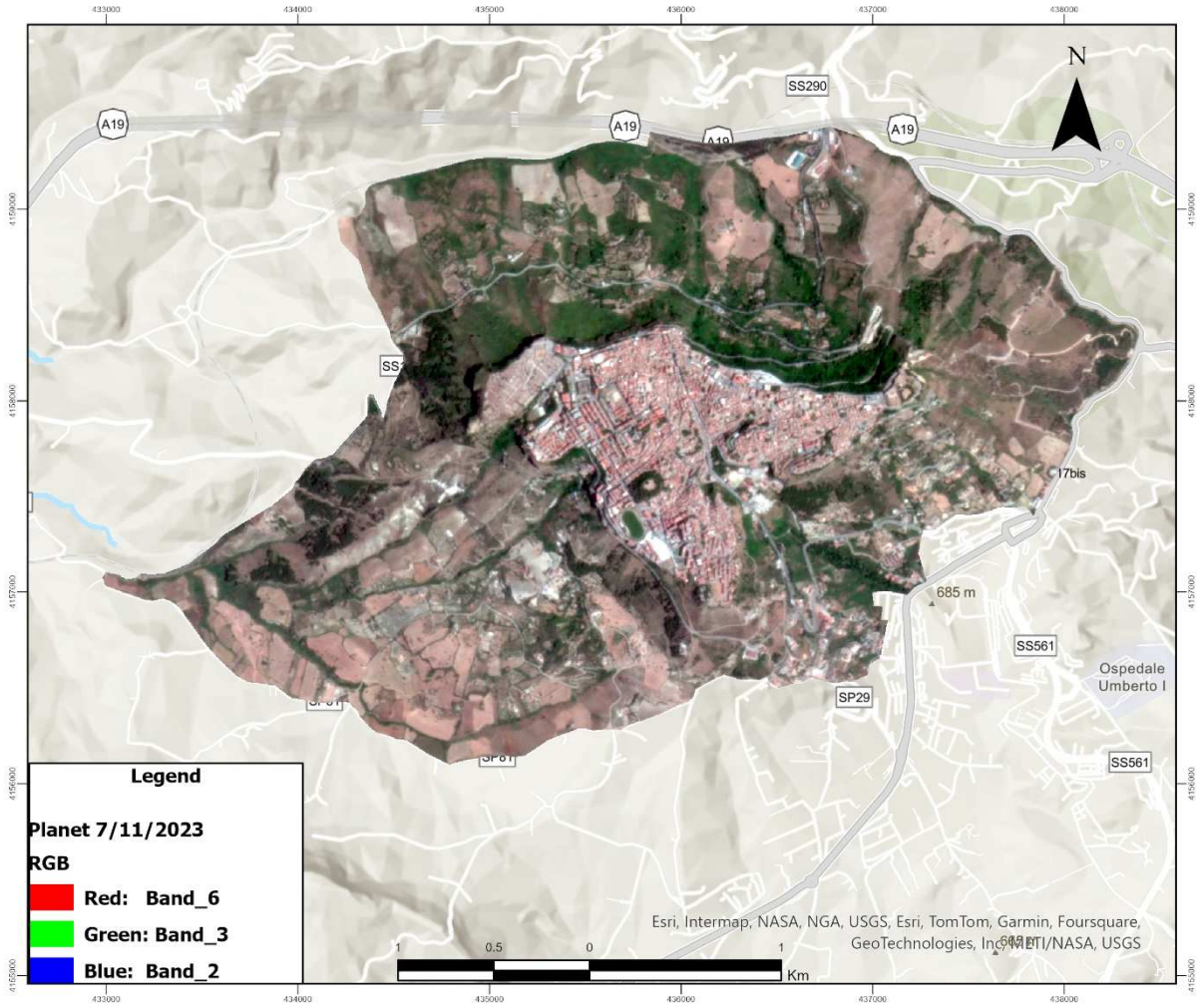

Figure 80. Planet image captured during autumn for the pilot area of Italy.

3.4. Baixo Alentejo - Portugal

Portugal, located on the Iberian Peninsula in southwestern Europe, is a country renowned for its rich history, diverse culture, and stunning landscapes. It hosts a variety of ecosystems, from the lush forests of the north to the sun-soaked beaches of the Algarve. Portugal is ecologically significant due to its unique biodiversity and varied habitats, which are protected in several national parks and natural reserves. Notable among these are Peneda-Gerês National Park, the only national park in Portugal, which is located in the northwest corner of the territory and it is known for the mountainous terrain and endemic species. The Ria Formosa Natural Park, a coastal lagoon system vital for bird migration, is also a significant ecosystem in Portugal. The Madeira and Azores archipelagos also hold important ecological reserves, preserving unique flora and fauna. Portugal's commitment to conservation is evident in its extensive network of protected areas, which play a vital role in maintaining regional biodiversity and offering opportunities for ecotourism and scientific research. The province which this project focuses on is Baixo Alentejo (Figure 81). More specifically it concentrates on four municipalities within the region of this province and specifically Ourique, Santana da Serra, Almodóvar, and São Barnabé.

Portugal has experienced a significant number of wildfires, particularly during the summer months. These fires often occur in forested and rural areas, intensified by factors such as high temperatures, drought conditions, and strong winds. The country's extensive eucalyptus and pine plantations are especially susceptible to fire. Wildfires in Portugal have had devastating effects on communities, the environment, and the economy. The deadly fires of 2017, which resulted in numerous fatalities and a widespread destruction of around 539.000 ha, highlighted the urgent need for improved fire management and prevention strategies. The country's national parks and protected areas are also focal points for conservation efforts to preserve biodiversity and restore fire-damaged landscapes.

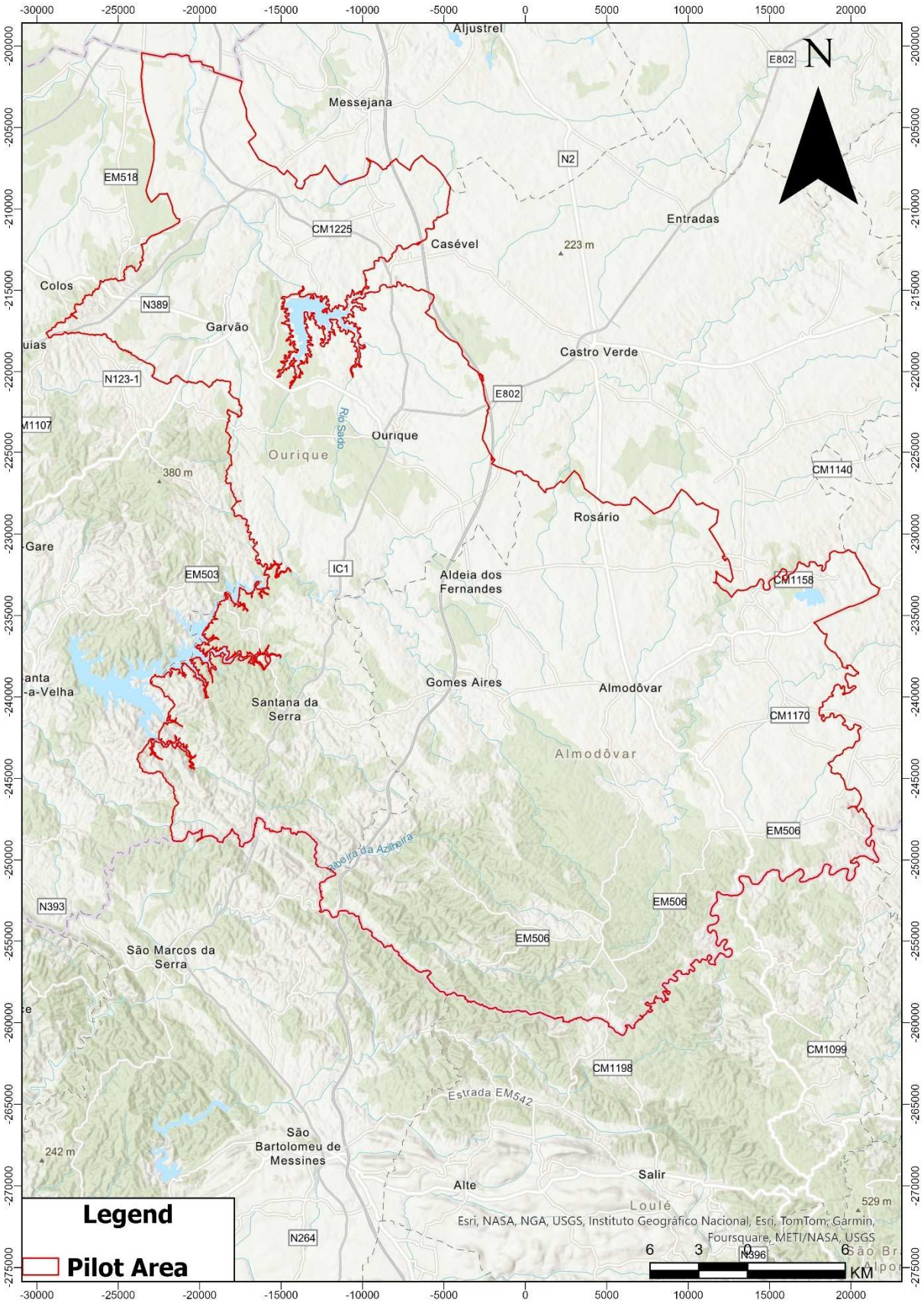

Figure 81. Pilot area of Portugal.

According to the country's reports from National Fire Services (João et al. 2023), in 2022 the burnt area on the Portuguese mainland was 110.097 ha (Figure 82). This represents a 13% decrease compared to the average burnt area of 125.831 ha over the previous decade. The largest wildfire of 2022 took place in the Serra da Estrela Natural Park in the Centre region, burning 24.300 ha. The average burnt area in Portugal, is around 120.000 ha (Figure 82). Based on the Figure 83, the average number of fires per year in Portugal seems to fluctuate but generally falls between 15,000 and 25,000 fires annually. There are notable peaks, such as in the early 2000s, where the number of fires exceeded 35,000. The trend shows a decrease in the number of fires in recent years compared to the high activity period from the late 1990s to the early 2000s. Lastly the average annual fire size is around 8 ha (Figure 84).

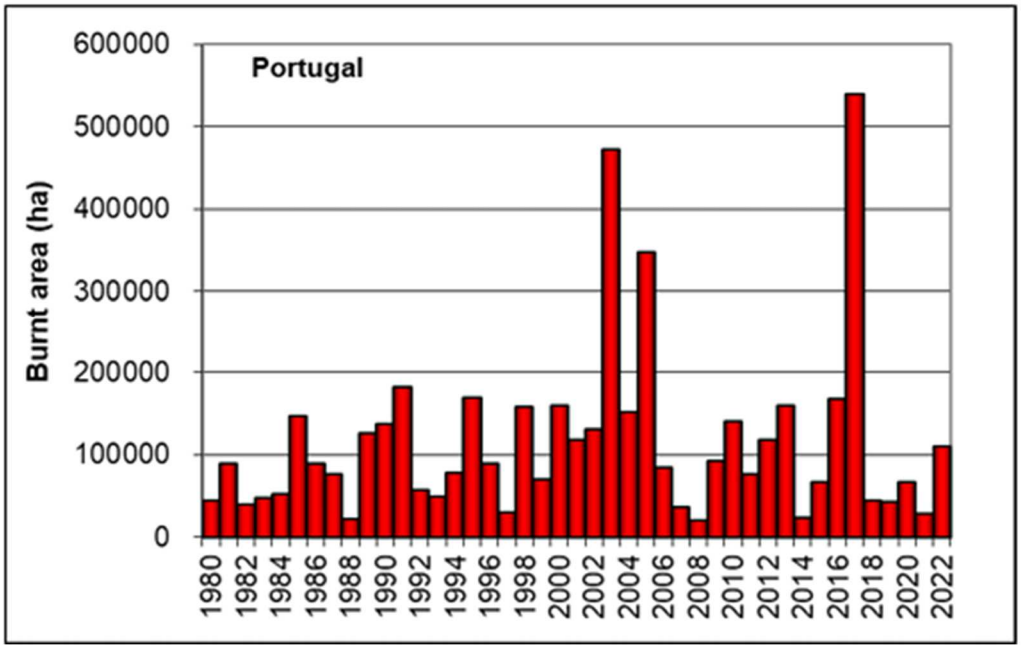

Figure 82. Annual burnt areas in Portugal based on reports from the National Fire Services for the period 1980-2022 (João et al. 2023).

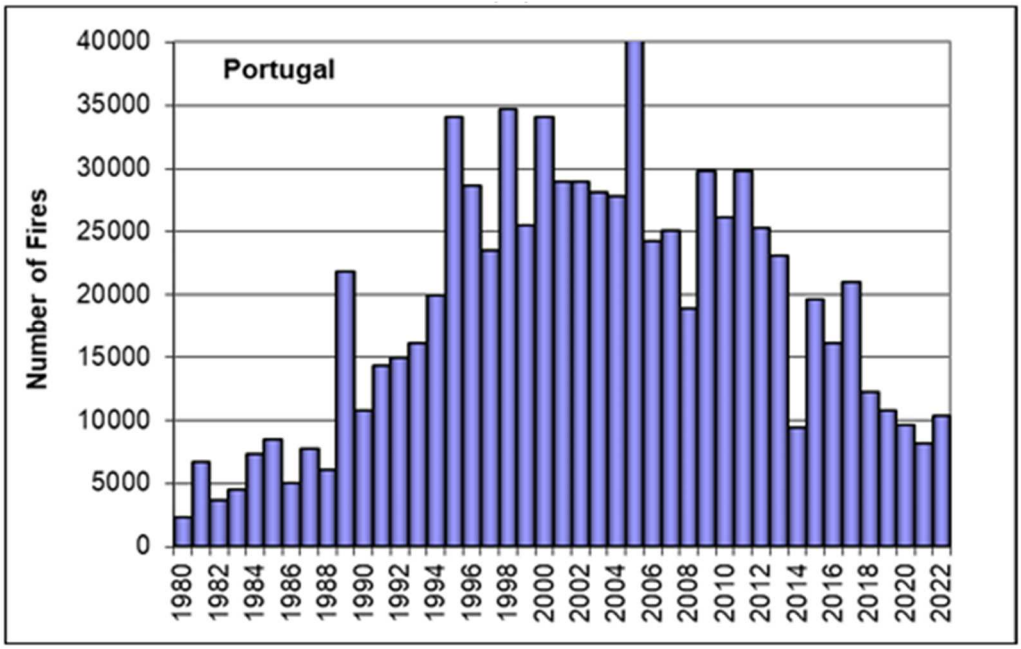

Figure 83. Annual fire occurrences in Portugal based on reports from the National Fire Services for the period 1980-2022 (João et al. 2023).

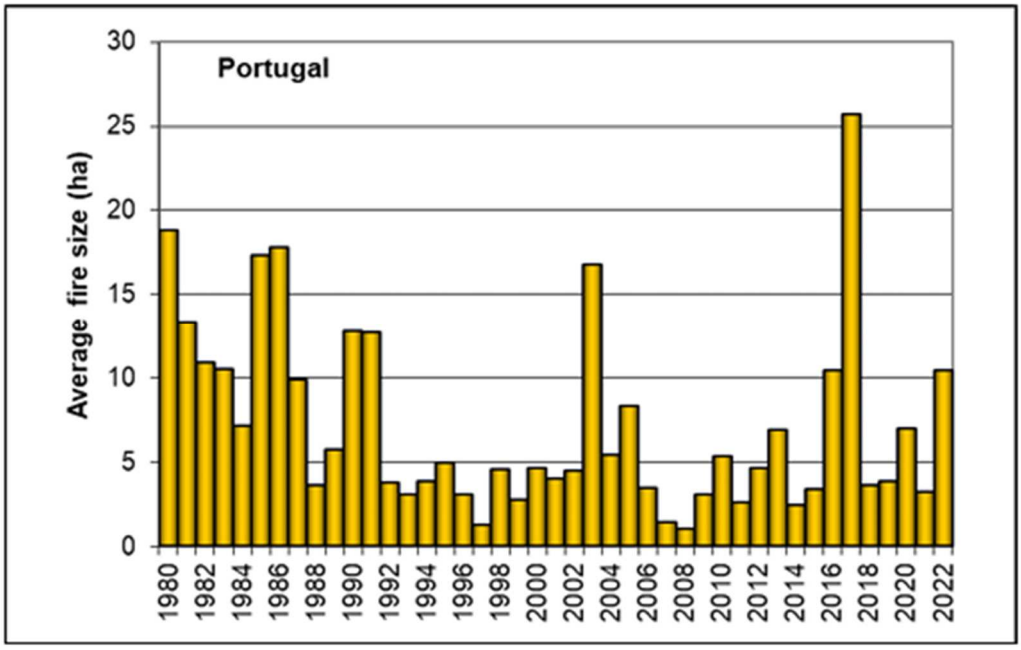

Figure 84. Annual average fire size in Portugal based on reports from the National Fire Services for the period 1980-2022 (João et al. 2023).

3.4.1. Geographical Location and administration

Baixo Alentejo occupies an area of 8.542,72 km², corresponding to 9,26% of the national territory, bordered to the north by Central Alentejo, to the south by the Algarve Region, to the west by Alentejo Litoral and to the east by Spain. The Baixo Alentejo territory is marked by peneplain, reaching relatively low altitudes, generally less than 250 metres. The territory is punctuated by low, gently sloping hills and irrigated by generally small watercourses, many of which almost dry up (or even dry up) in summer.

Hydrographically, Baixo Alentejo is marked by the presence of the Guadiana River valley, which crosses its eastern part from north to south, separating the main plain from a territory between the river and the Spanish border. In the northern part of the territory, the Alqueva reservoir stands out, the largest artificial lake in Europe, which extends over an area of 250 Km². Baixo Alentejo is also home to the Mira and Sado river basins. The Mira River rises in Serra do Caldeirão, at an altitude of 470 metres, running southeast-northwest for around 100 Km to Vila Nova de Milfontes. Sado river rises in Serra da Vigia (Ourique) at an altitude of 230 metres and flows south-north to Setúbal, covering around 180 Km.

As far as the mountain ranges are concerned, the main notable elements are already outside the Baixo Alentejo territory, forming its boundaries. Within the Baixo Alentejo, the highest altitudes are reached in the Serra da Adiça, which covers Moura and Serpa municipalities and reaches 522 m, in the Serra do Mendro, in Vidigueira municipality, with 412 m and in the Serra da Alcaria Ruiva, near Mértola municipality, which reaches 370 me.[1]

3.4.2. Climatic conditions

Baixo Alentejo is a Mediterranean climate region, being characterized by a high average annual temperature that oscillates between 15° and 17.5°[2]. According to the Iberian Climate Atlas, the Baixo Alentejo territory falls within the "CSA" variation of the Köppen classification, i.e., a temperate climate with a hot, dry summer. As a type C climate, it has an average temperature of the coldest month of between 0 °C and 18 °C, with a markedly dry period in summer (CS) and an average temperature of the hottest month of over 22 °C (A). There is also a small region of the Baixo Alentejo, in the district of Beja, with an Arid Climate - Type B, Subtype BS (steppe climate), variety BSk (cold steppe climate of medium latitude).

[1] Source: PIAACBA - Baixo Alentejo Intermunicipal Climate Change Adaptation Plan
[2] Caraterização do Baixo Alentejo (cimbal.pt)

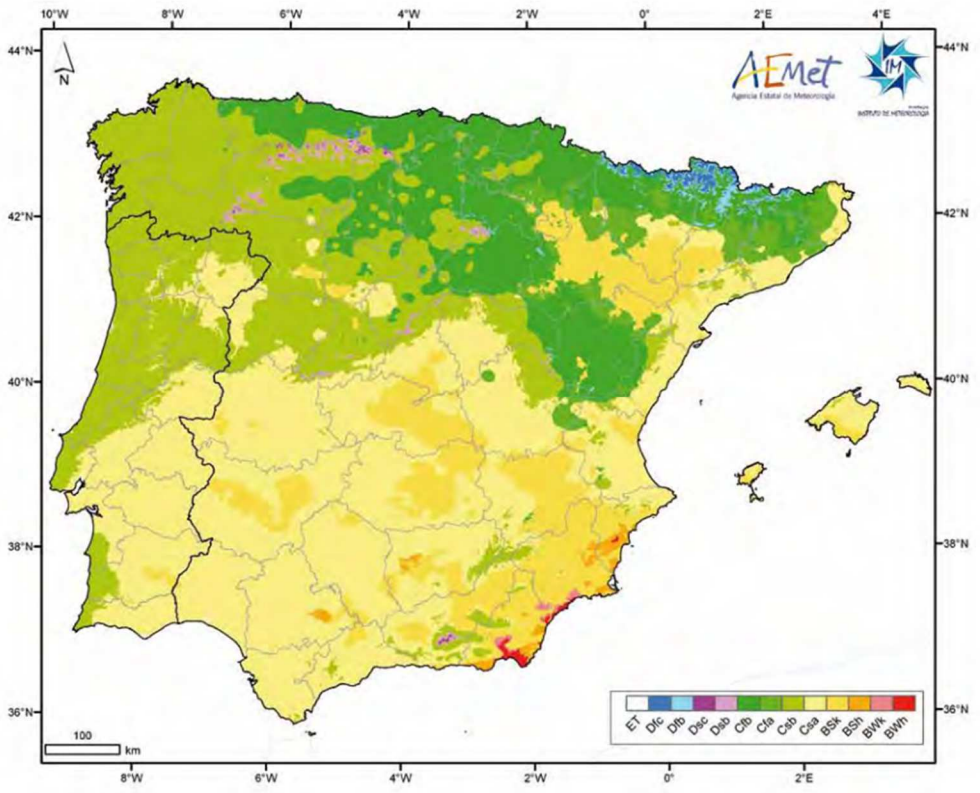

Figure 85. Köppen-Geiger Climate Classification for the Iberian Peninsula and the Balearic Islands.

Source: Iberian Climate Atlas

Using the Climate Normals from the Portuguese Institute for Sea and Atmosphere (IPMA) between 1981-2010, the following characteristics emerge[3]:

- The average minimum temperature in the coldest months (December to February) is around 6 °C; by way of comparison, in Lisbon temperatures are around 8 to 9 °C in the same months;
- Average maximum temperatures in the hottest months (July and August) reach 33 °C; by comparison, in Lisbon temperatures are around 28 °C in the same months;
- There are frequent extremes of maximum air temperature, with values of around 45 °C being recorded in June, July and August.

In terms of rainfall, the average annual value within the region ranges between 400 and 600 mm. Generally, annual rainfall is poorly distributed, with an excess of water in autumn and winter and a marked shortage in summer.

[3] For reasons of proximity, data come from the Beja Meteorological Station, as there is no specific data for all the municipalities in the CIMBAL.

Despite these characteristics, Baixo Alentejo is undergoing important changes due to the climate change, which are mostly evident, among others, in the municipalities of Almodovar and Ourique.

The Baixo Alentejo Intermunicipal Climate Change Adaptation Plan (PIAAC BA) assessed the region's climate change over the course of the current century[4].

Forecasts point to increases in temperature and decreases in precipitation (Figure 86).

From the middle of the century onwards the projections point to greater climatic dissimilarity for the municipalities of Ourique and Barrancos, territories associated, respectively, with reductions in annual precipitation and more significant average increases in temperature. Towards the end of the century, the dissimilarity increases for the municipalities of Almodôvar and Castro Verde, which are also associated with more pronounced reductions in annual precipitation.

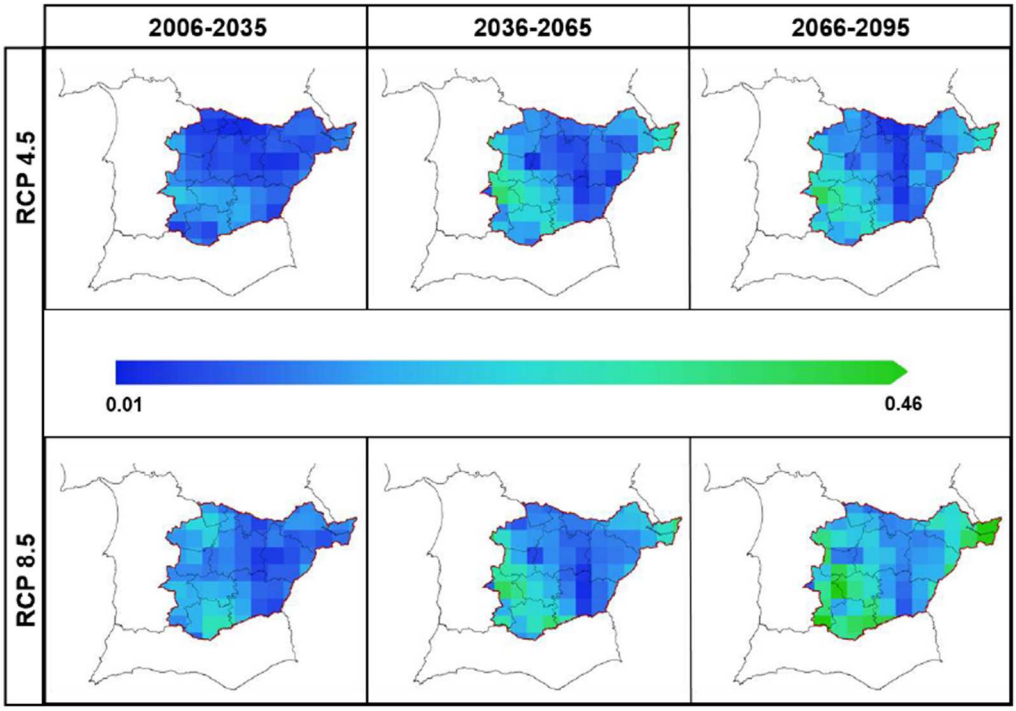

Figure 86. Projection and evolution of the emergence of new climates until the end of the 21st Century, based on the similarity of the future climate in relation to the reference period, according to RCP 4.5 and RCP 8.5.

Source: PIAAC BA

[4] The study includes past climate data (historical or reference) and future projections from the IPCC AR5, namely those generated from simulations carried out under the CORDEX project for the European domain (Euro-CORDEX11). These data are the result of regional climate models (RCM) determined from the forcing of global climate models (GCM).

Based on the Ombrothermic diagram for the period 1980-2022 (Figure 87), the average summer temperatures in the area range from 21,39 °C to about 23,86 °C, with average precipitation varying between approximately 1,76 mm and 10,89 mm. During winter, average temperatures range from 11,02 °C to 12,03 °C, and average precipitation ranges from 55,98 mm to 92,95 mm. August is identified as the hottest month with an average temperature of 23,86 °C, while January is the coldest with an average temperature of 11,02 °C. December is the wettest month, receiving 92,95 mm of precipitation, and July is the driest, with just 1,76 mm of rainfall. A dry period is also observed from mid-May to the end of September.

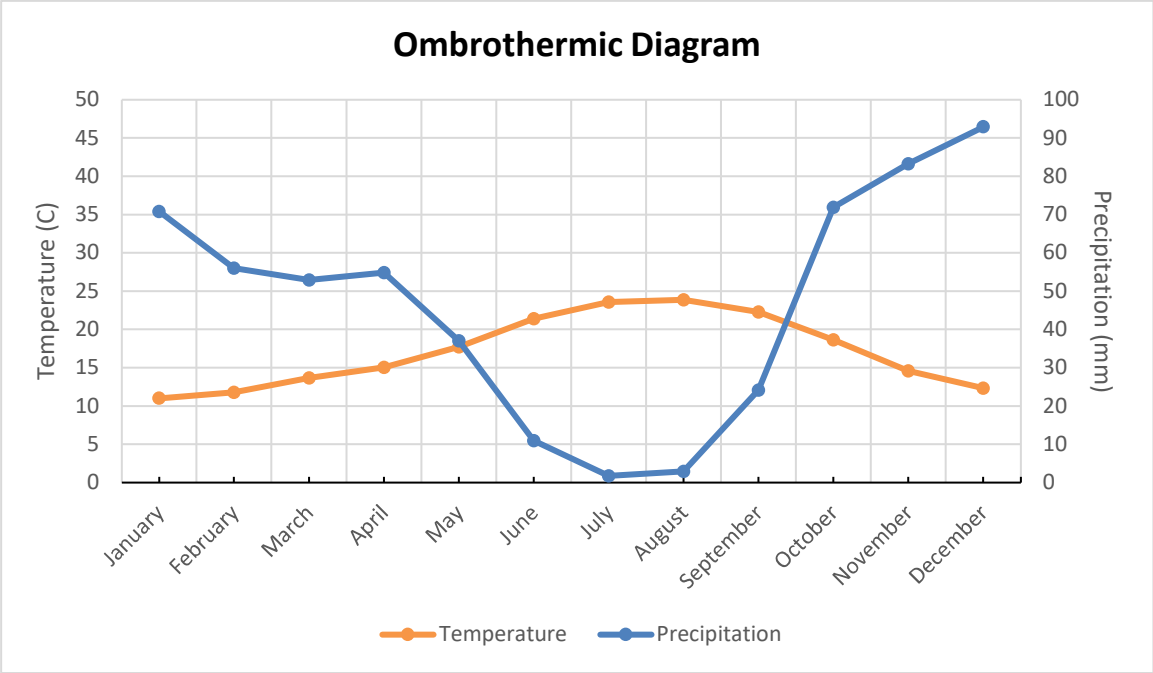

Figure 87. Ombrothermic Diagram of Baixo Alentejo for the years 1980-2022 based on the CRU TS dataset (Harris et al. 2020).

3.4.3. Land Uses

The pilot area in Portugal consists primarily of agro-forestry and forested zones. According to the chart (Figure 88), which is created based on the CORINE Land Cover, the predominant land uses include agro-forestry areas covering 26.1% of the total area, and transitional woodland/shrub areas covering 23%. Broad-leaved forests and non-irrigated arable land follow, covering 14.18% and 13.9% of the total area, respectively.

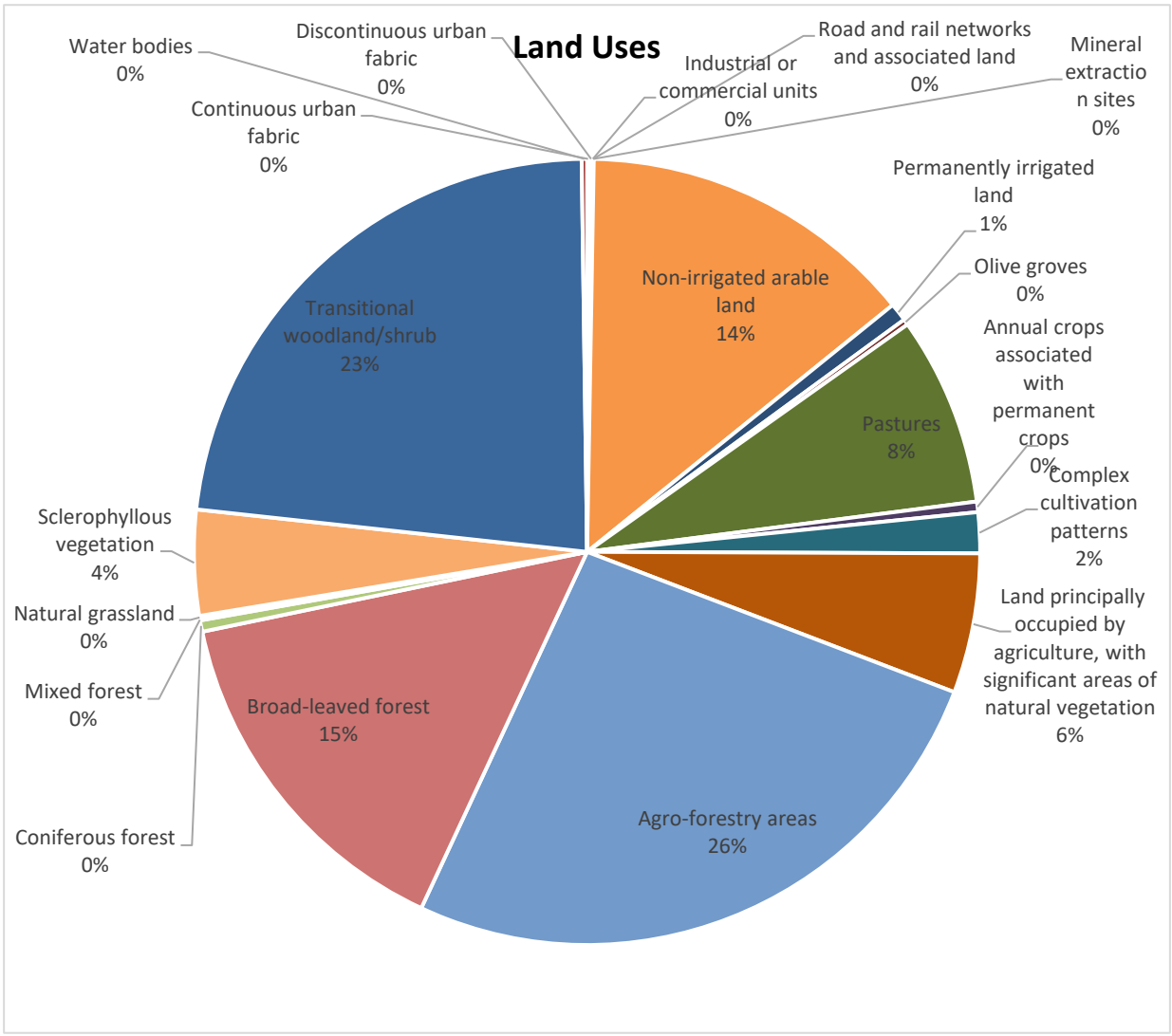

Figure 88. Percentage cover of different land use types that occupy the pilot area in Portugal based on the CORINE land.

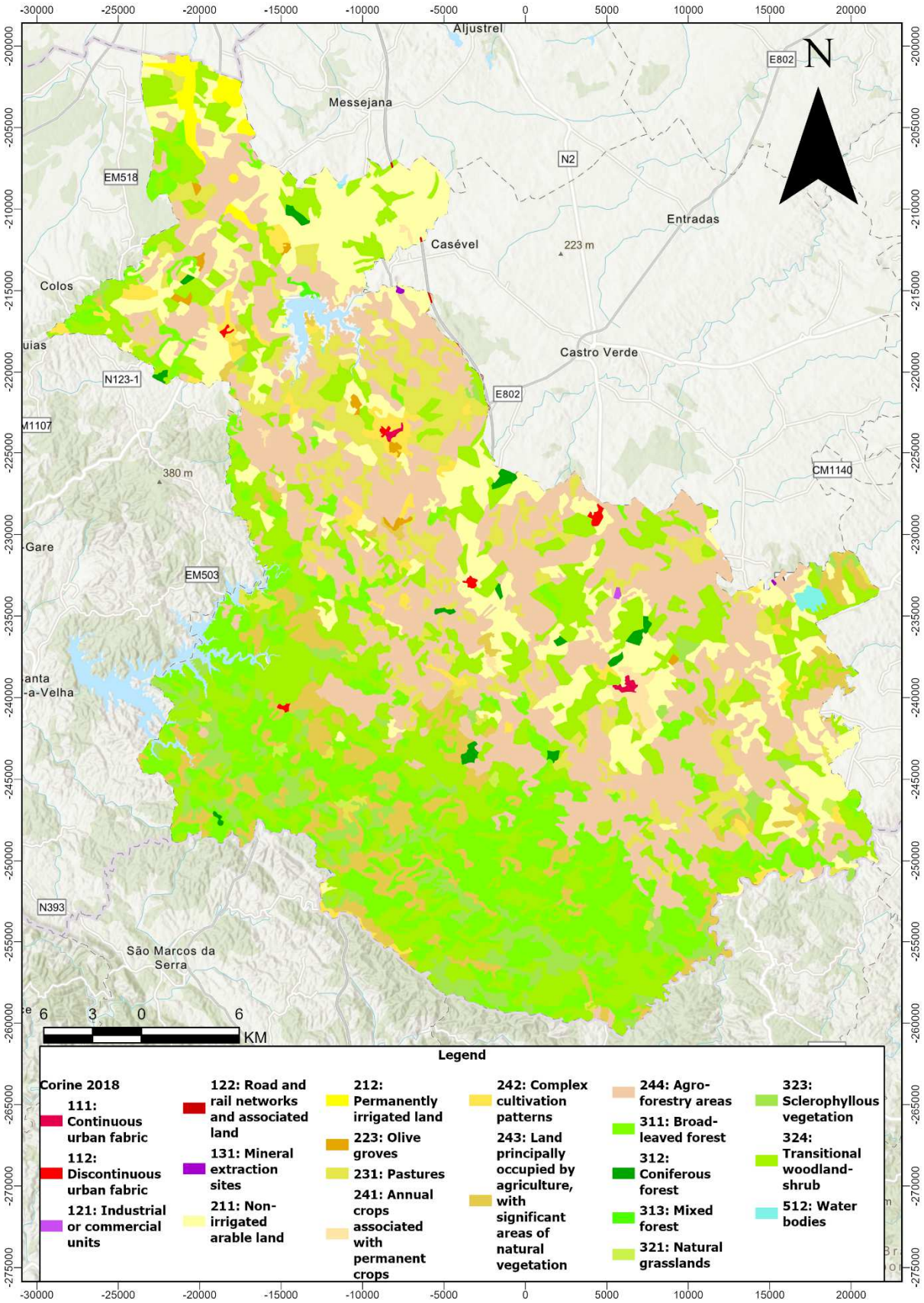

Figure 89. CORINE land cover map of the pilot area in Portugal.

3.4.4. Flora and Vegetation

The Alentejo Region is an area of Portugal where both the flora and fauna are rich and varied. It has 45% of forest cover, 42% agriculture land and the remaining 13% for other land uses. Therefore, it is a very rural area where forests play a very important role, with more than a half of them being dedicated to the production of cork and stone pine. The main forest tree species in the region are: cork oak (45%); holm oak (27%); eucalyptus (16%) and stone pine (6%). Very typical of the Alentejo plains are olive trees and cistus as well.

The most characteristic landscape of Baixo Alentejo is undoubtedly the montado, an agrosilvopastoral system characterized by low density trees combined with agriculture or pastoral activities. The main tree species encountered in the Montado are cork oak (Quercus suber L) and/or holm oak (Quercus rotundifolia L). Mixed stands with a combination of these species are also common.

The enormous biodiversity of the Montado system turns this area into a buffer zone against the advance of the ongoing global process of desertification, a very relevant problem for the region. According to a recent study[5], NUTS Baixo Alentejo, which comprises 13 municipalities - including Beja, Mértola and Serpa, has 38% of its territory with critical susceptibility to desertification, 35% very high and 21% high (and only 5% moderate and 1% low). On the left bank of the Guadiana, the values rise almost to 100%, with 96% of the area susceptible to desertification (32% critical, 37% very high and 27% high).

Figure 90. A Montado agrosilvopastoral system characterized by low density trees combined with agriculture or pastoral activities.

[5] Baixo Alentejo with 94% susceptibility to desertification – REA Alentejo (rea-alentejo.pt)

In ecological terms, the Guadiana Valley Natural Park, part of the National Network of Protected Areas, and several areas classified as Special Protection Areas (SPA) or Sites of Community Importance (SCI), part of the Natura 2000 Network, should be highlighted: SPA Moura/ Mourão/ Barrancos and SIC Moura/ Barrancos, SPA and SIC Vale do Guadiana, SPA Cuba and SIC Alvito/ Cuba, SPA Piçarras, SPA Castro Verde, SPA and SIC Caldeirão (mostly in the Algarve, but covering part of the municipality of Almodôvar) and SPA and SIC Monchique (mostly in the Algarve region, but covering part of the municipality of Ourique).

3.4.5. Fauna

The variety of species that can be found in Alentejo stems from the unique characteristics that this region offers. The low population density, extensive cultivation with little human intervention (such as vineyards, cork oak forests or the cereal steppe), sustainable agricultural practices, as well as the rivers, streams and reservoirs, are all hallmarks of the Alentejo.

In the more open areas, there is the presence of the Hunting Eagle (Circus pygargus), the Black Kite (Milvus migrans), the Round-winged Eagle (Buteo buteo), the Partridge (Alectoris rufa), the Quail (Cotornix cotornix) and the Thrush (Emberiza calandra). In the olive groves, the blackbird (Turdus merula) and the thrushes (Turdus iliacus and Turdus philomelos) make their presence felt. Among the mammals, it is possible to find the Genet (Genetta genetta), the Wildcat (Felis sylvestris), the Weasel (Mustela nivalis), the Bullfinch (Mustela putorius), the Fox (Vulpes vulpes), the Wild Boar (Sus scrofa) and the Badger (Meles meles). As for reptiles, on the hottest days you can easily spot the Sardão (Lacerta lepida) on the side paths.

The Western Swamphen and the Black Stork are two of the most beautiful and exotic birds to be seen in the Alentejo landscape. Another species that finds its perfect habitat in the Alentejo is the otter, mainly due to the abundance of unpolluted freshwater systems. The bee, whose role is fundamental in pollination and maintaining the biodiversity of the flora, is also a characteristic species of the Alentejo region: feeding on the pollen of cistus, sargassum, rosemary or viper's-bugloss, this species is responsible for producing the renowned Alentejo honey, a product with Protected Designation of Origin (PDO).

Figure 91. The white stork (Ciconia Ciconia) standing on top of its nest.

3.4.6. Spatial data

- **Aspect**

In the pilot area of Portugal, various aspects are distributed throughout the region, highlighting the complexity and diversity of the landscape (Figure 92). While it appears that there are many south and southwest-facing aspects, east and northeast-facing aspects are also prevalent. This indicates a varied topography with a mix of different orientations across the area.

- **Slope**

When examining the slope map of this pilot area (Figure 93), it becomes evident that the majority of the region is characterized by gentle slopes. However, steeper slopes are predominantly located in the southern and southwestern parts of the area, with some steeper slopes also present in the northern sections. This distribution highlights a variation in the terrain, where most of the landscape is relatively smooth, scattered with areas of more significant elevation changes in specific parts of the region.

- **Geomorphology**

Upon examining the geomorphology map for the area (Figure 94), the structure of the landscape becomes clearer. There is a definite transition in the landscape when traversing from the north to the south and it is evident that the elevation of the landscape slowly increases from one end to the other. The highest elevation in the area is observed in the southern region, reaching 576 meters and while this is the peak altitude for the region, it is relatively modest in height.

- **Canopy Height Model**

Concerning the forested areas within the region (Figure 95), an analysis of the canopy height model (CHM) reveals that the majority of these forested zones are situated in the southern and southwestern parts of the map. While there are some forested patches scattered throughout the central and northern areas, these are relatively sparse. The remaining parts of the region, however, appear to be predominantly empty of forest cover, highlighting a significant contrast between the heavily forested south and southwest and the largely unforested rest of the area.

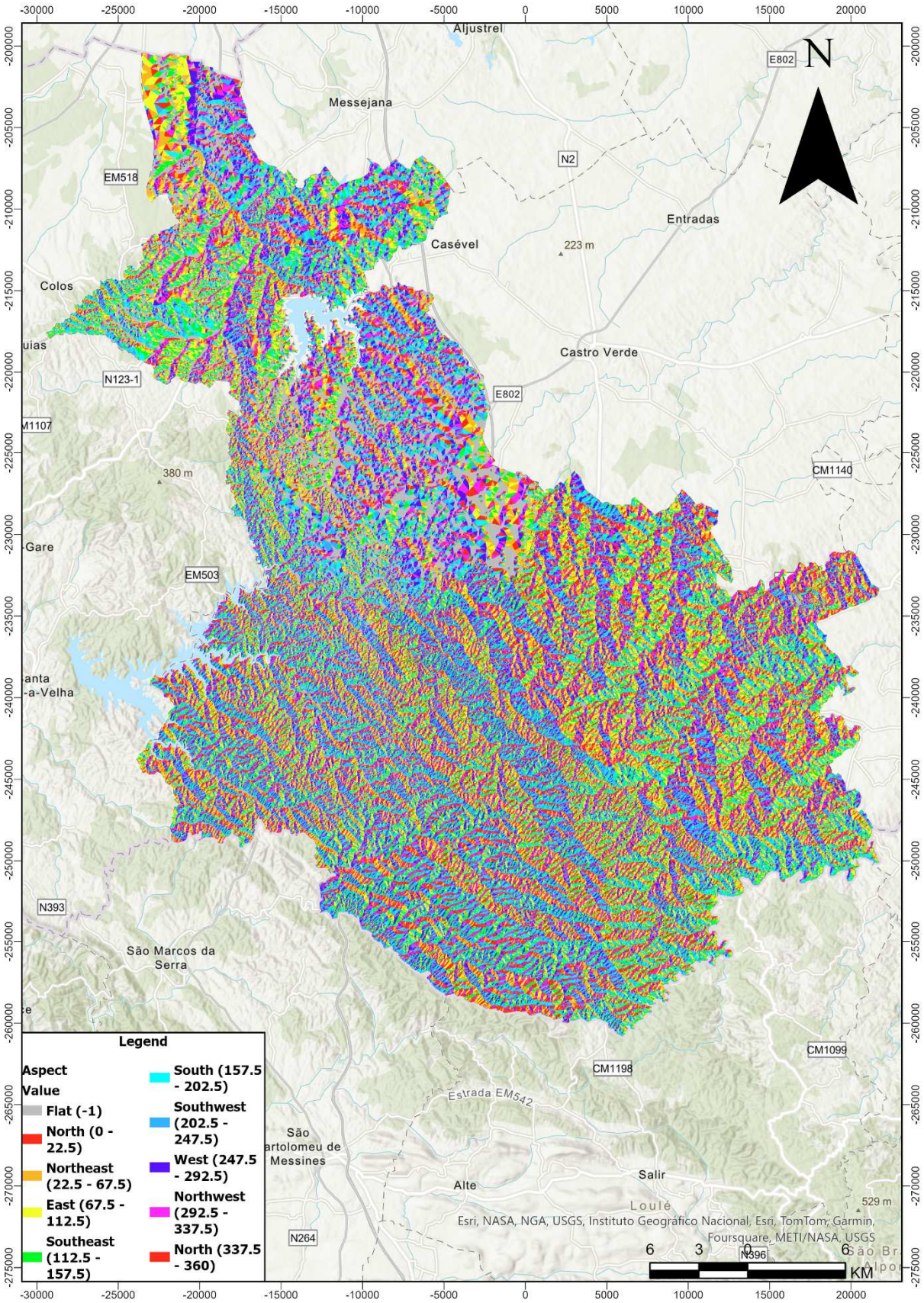

Figure 92. Aspect map of the pilot area in Portugal.

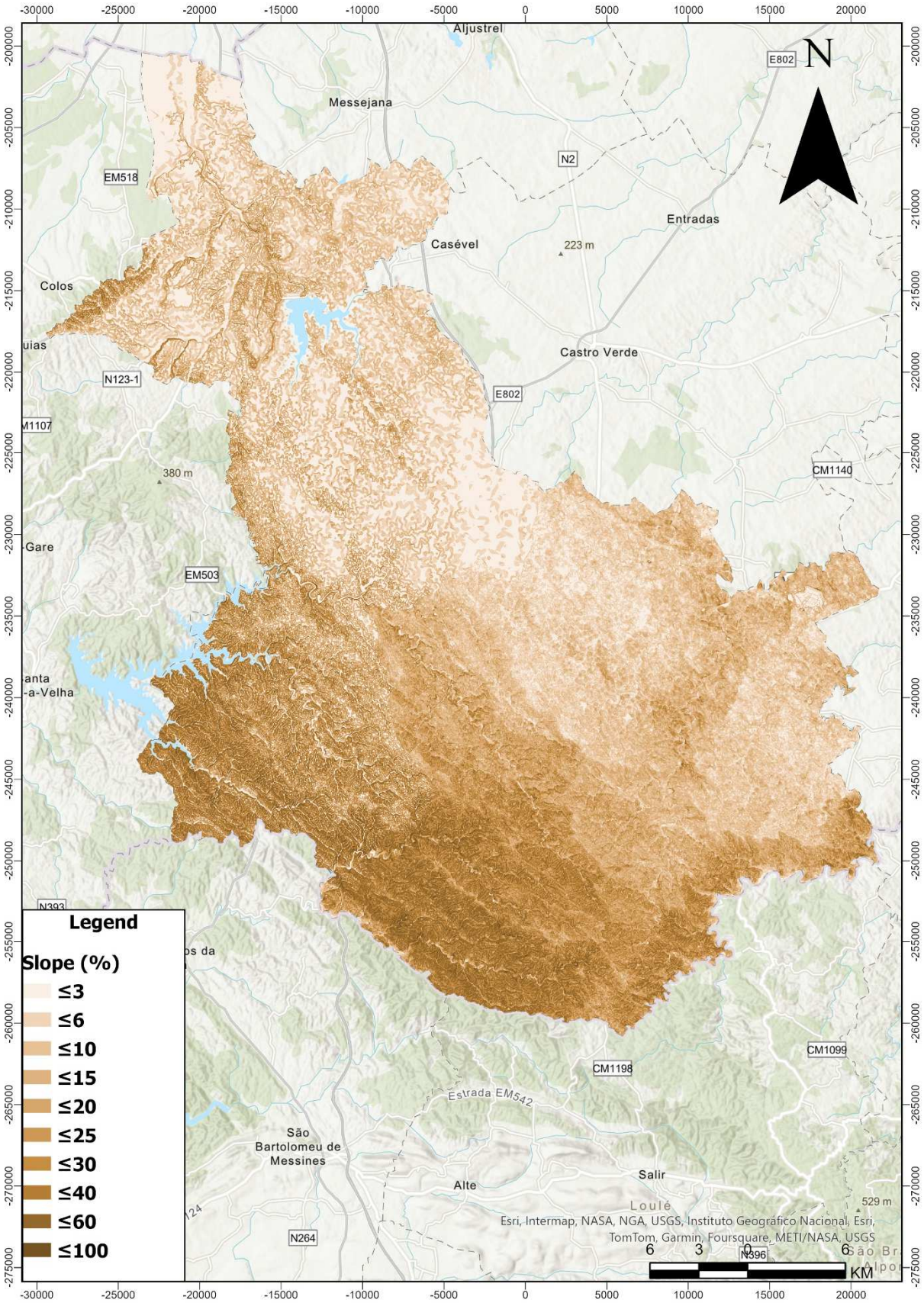

Figure 93. Slope map of the pilot area in Portugal.

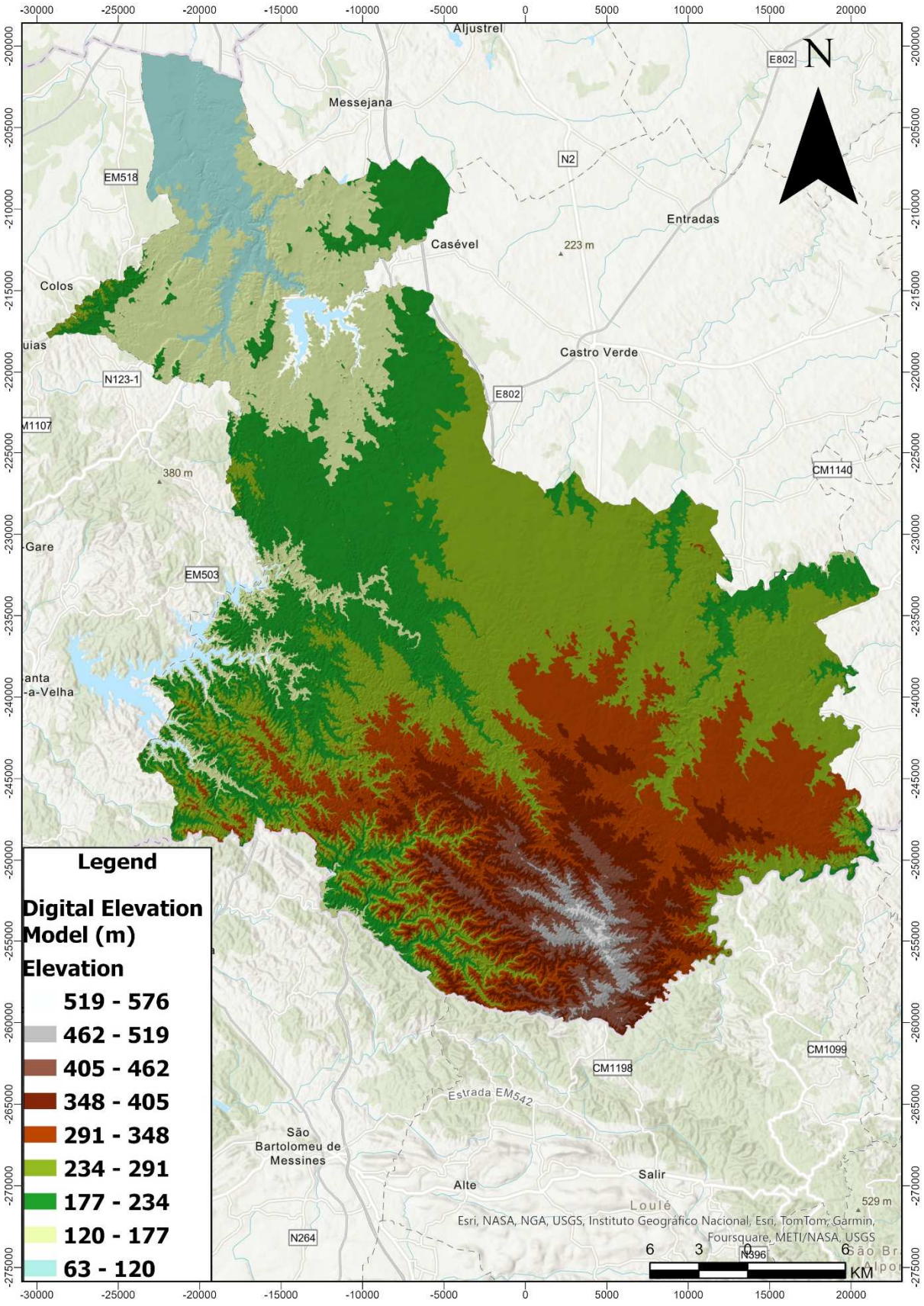

Figure 94. Geomorphology map of the pilot area in Portugal.

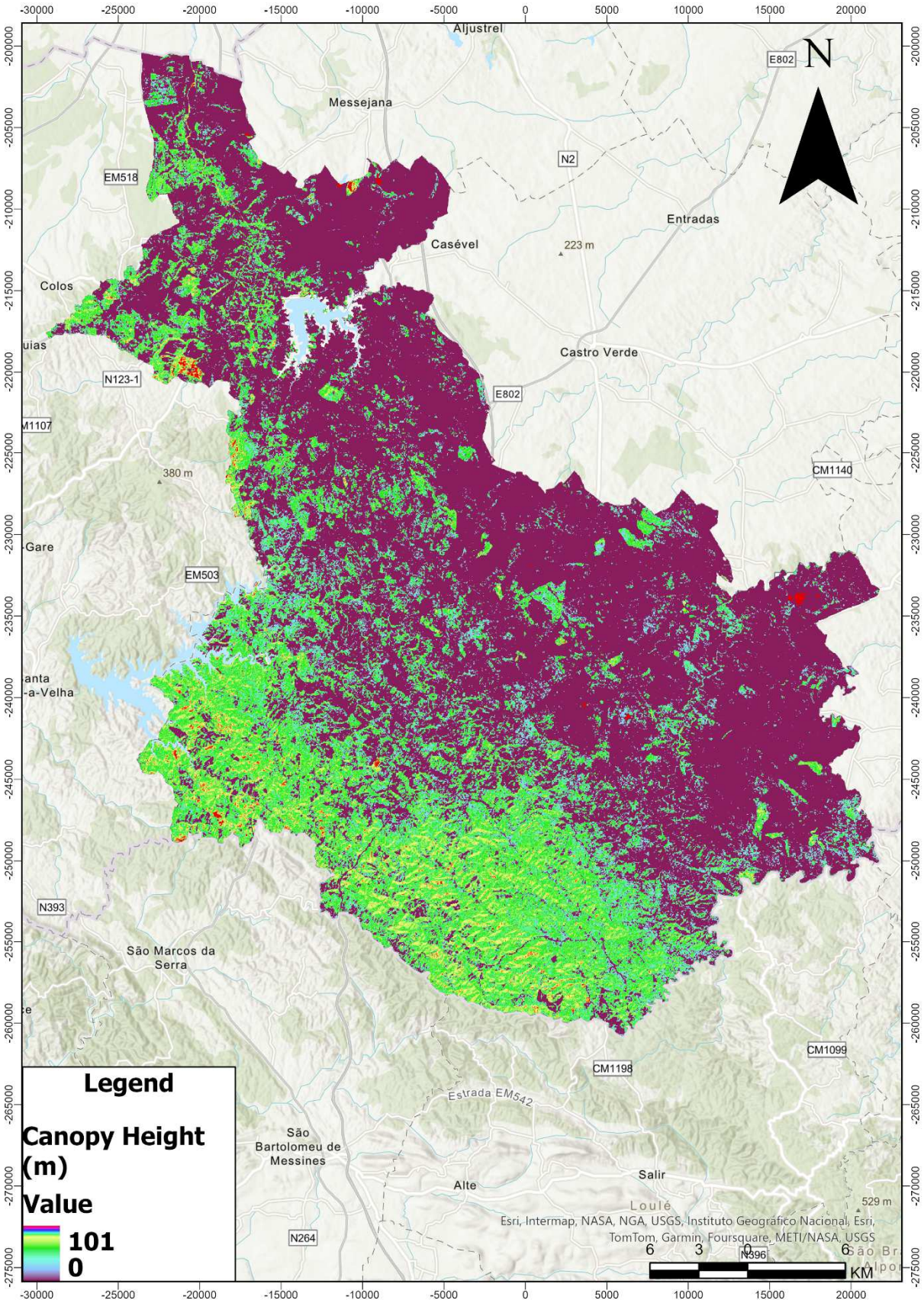

Figure 95. Canopy Height Model of the pilot area in Portugal.

- **Tree cover density**

Alongside the Canopy Height Model (CHM), the tree cover density map reveals the primary locations of tree concentrations (Figure 96). As previously observed, the majority of the forests are found in the northern and southern parts of the region, with additional scattered patches in the eastern areas.

- **Roads and buildings network**

The road network within the pilot area in Portugal covers an extensive region, seamlessly connecting urban environments with natural landscapes. It is evident that this network extends into mountainous areas, where the presence of roads is particularly significant. These roads play a vital role in facilitating future conservation initiatives and in the prevention and management of wildfires, ensuring both the protection of natural habitats and the safety of surrounding communities.

- **NDVI**

Examining the NDVI maps for this pilot area reveals a fascinating insight into the region's vegetation structure (Figure 98). The southern parts of the region consistently exhibit high NDVI values year-round, except in December when the trees shed their leaves. Interestingly, the northern and eastern sections, which are utilized for agroforestry, display elevated NDVI values primarily during the winter. These NDVI patterns highlight a noteworthy aspect of the area's agriculture.

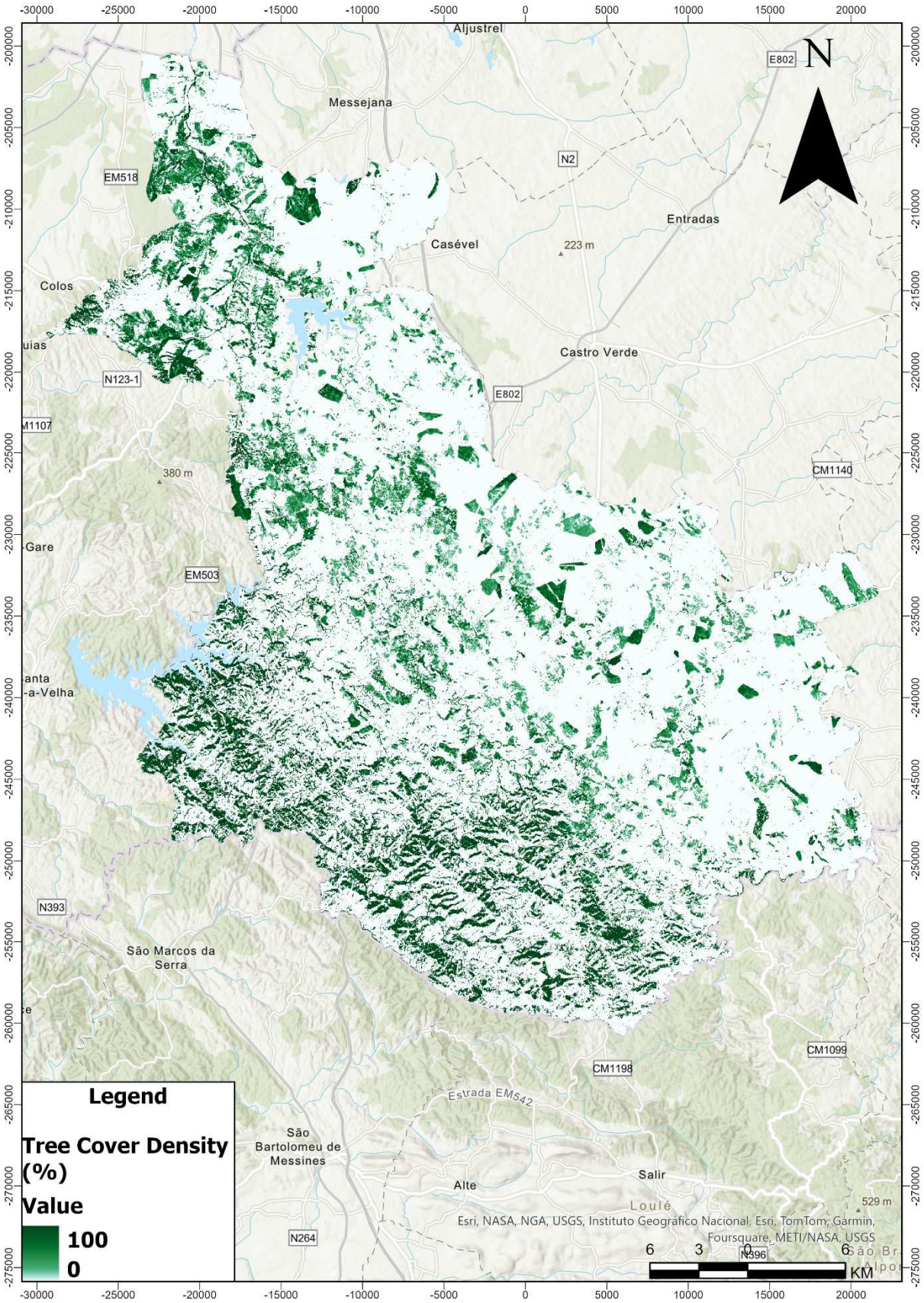

Figure 96. Tree cover density map of the pilot area in Portugal.

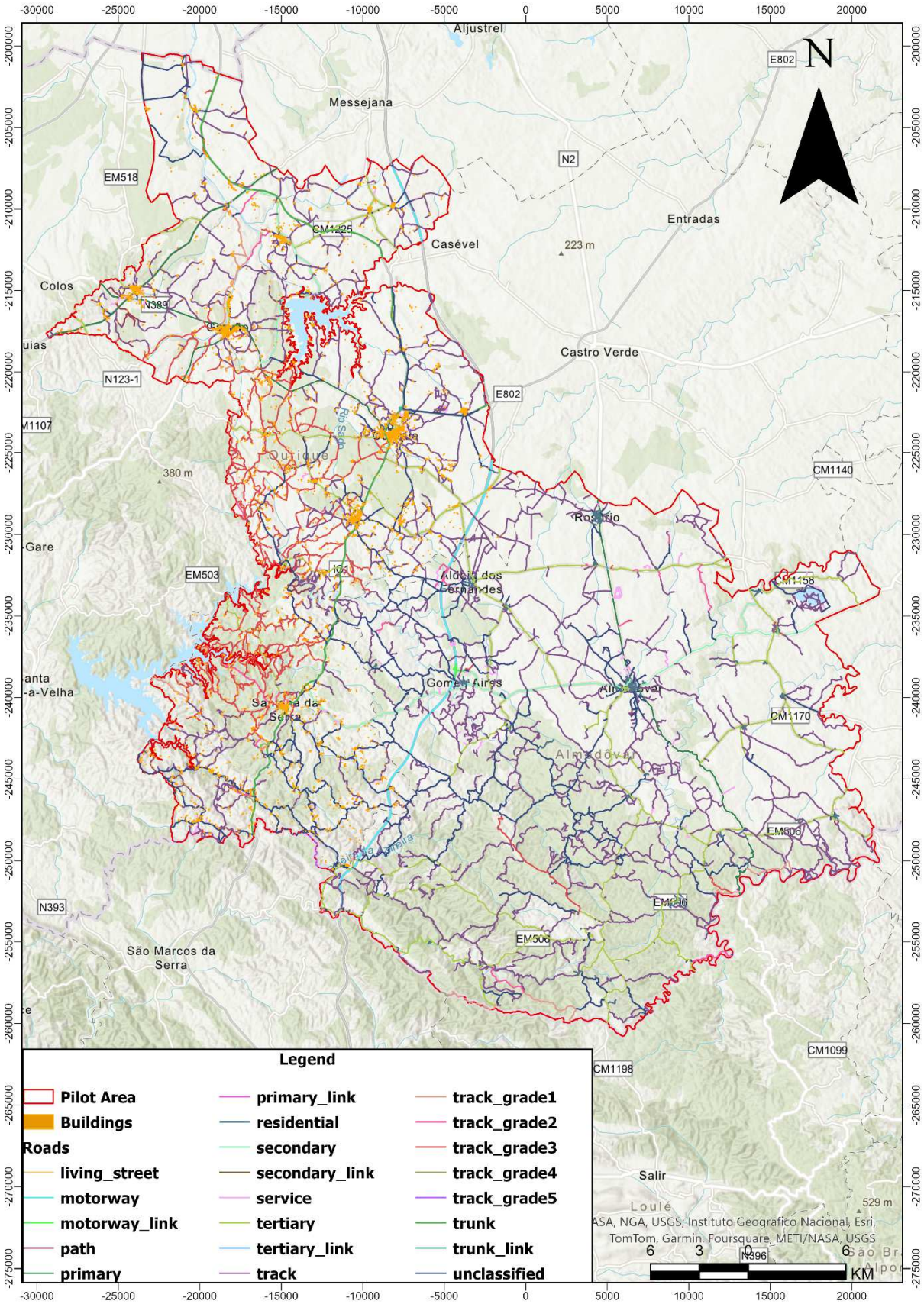

Figure 97. Roads and buildings map of the pilot area in Portugal.

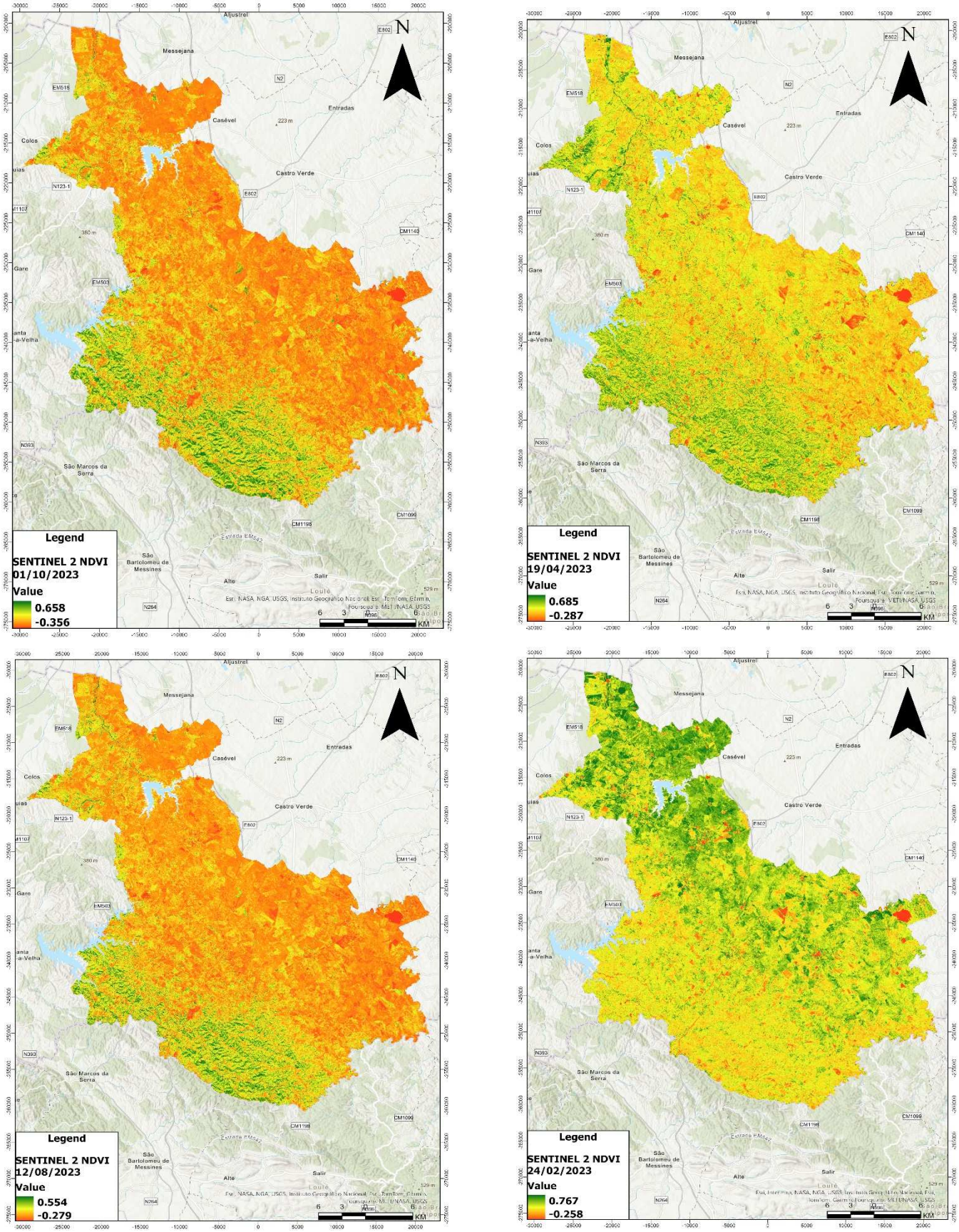

Figure 98. Figure 99. NDVI maps that cover all four seasons for the pilot area of Portugal. The autumn NDVI map is displayed at the top left, the spring NDVI map at the top right, the summer NDVI map at the bottom left, and the winter NDVI map at the bottom right.

- **Sentinel 2 images**

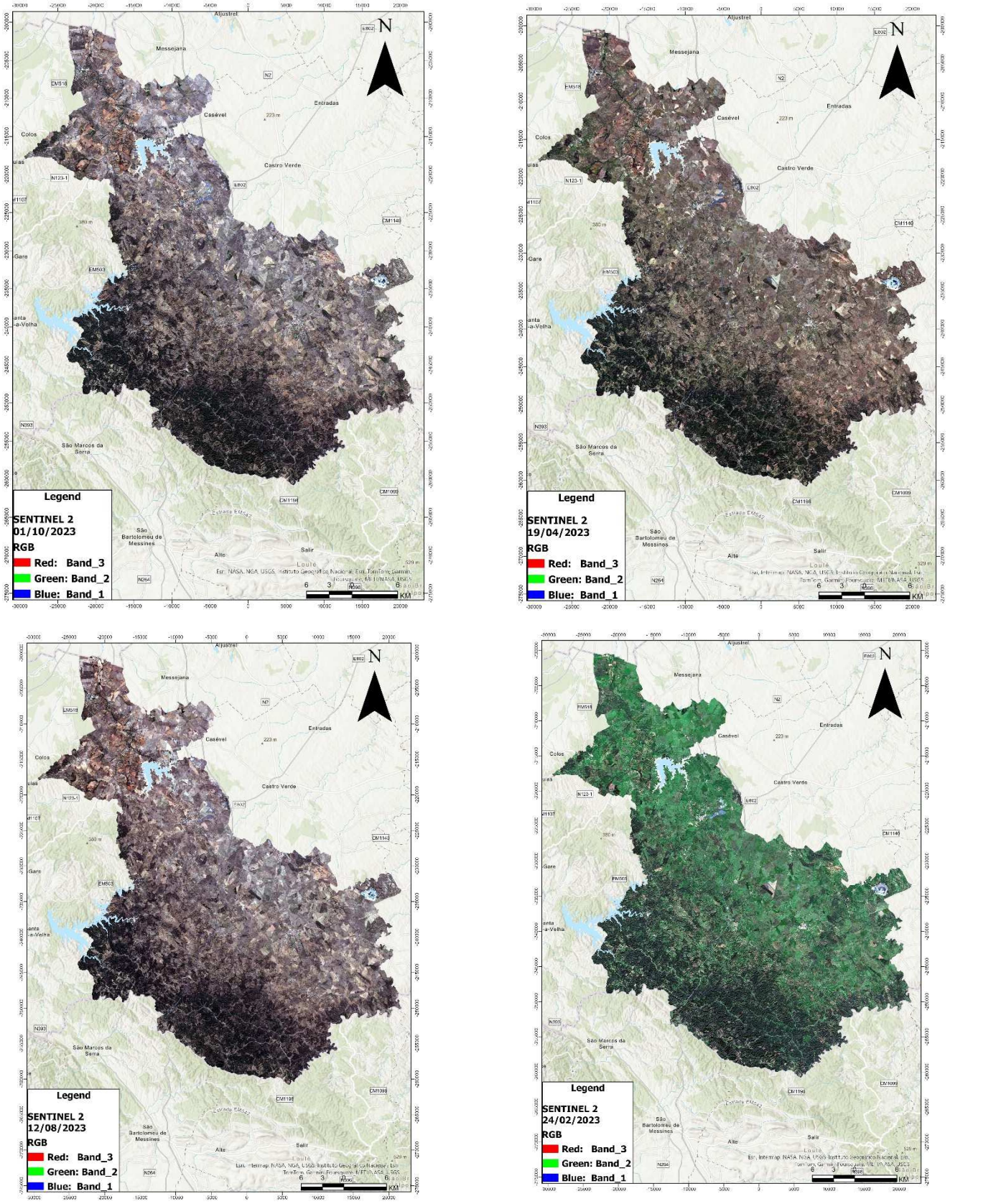

Figure 100. Sentinel 2 satellite images (true color combination) that cover all four seasons for the pilot area of Portugal. The autumn Sentinel 2 image is displayed at the top left, the spring one at the top right, the summer one at the bottom left, and the winter one at the bottom right.

- **Planet image**

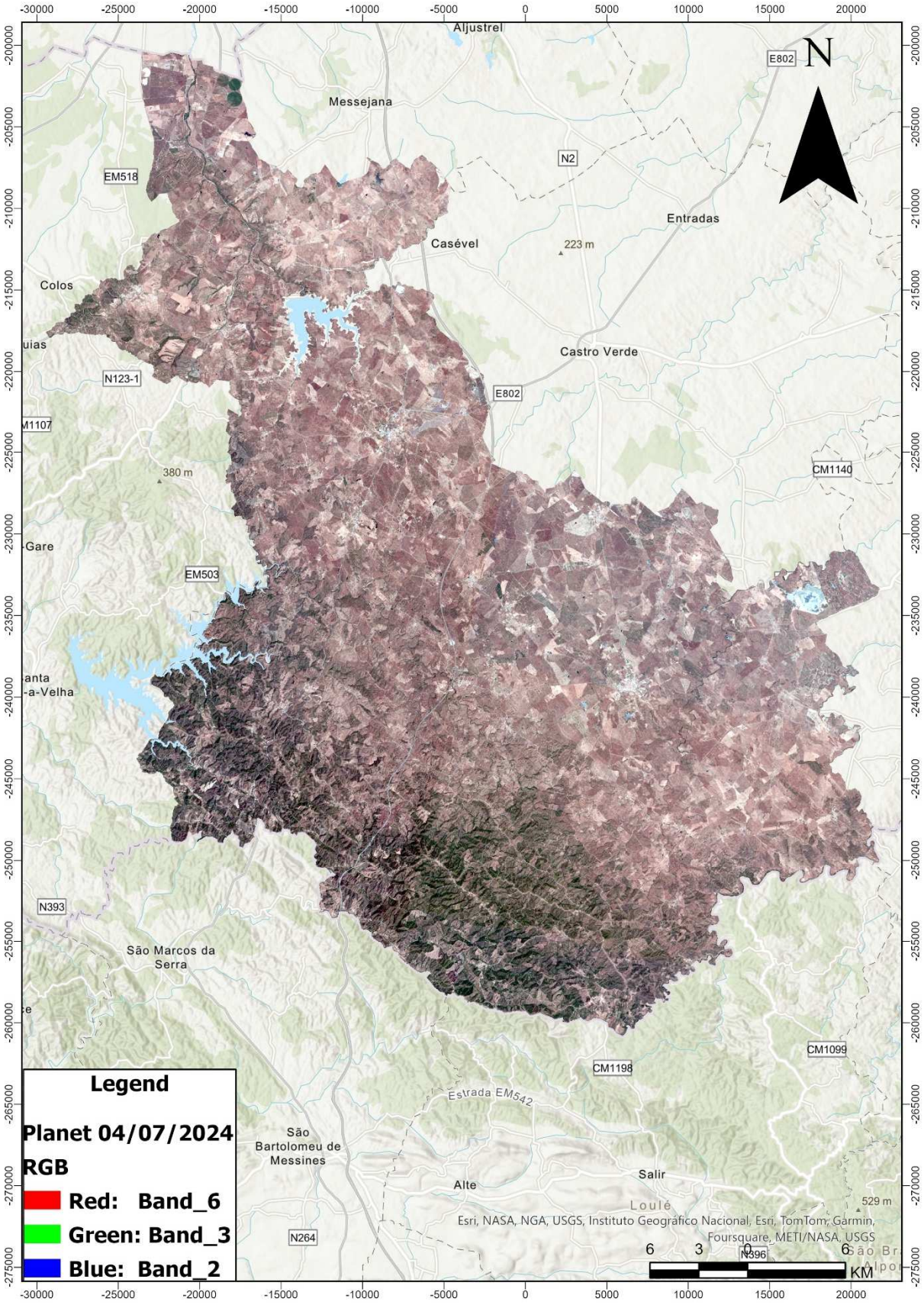

Figure 101. Planet image captured during summer for the pilot area of Portugal.

3.5. Municipality of Ulcinj - Montenegro

Montenegro, located in Southeast Europe on the Adriatic Sea, is known for its diverse landscapes that range from rugged mountains to stunning coastal areas. The country boasts five national parks, each offering unique ecological significance and natural beauty. Durmitor National Park, a UNESCO World Heritage Site, features dramatic peaks, glacial lakes, and dense forests, while Biogradska Gora National Park houses one of the last three remaining virgin forests in Europe. The Bay of Kotor, a UNESCO World Heritage Site, is renowned for its fjord-like scenery and medieval towns. Montenegro's biodiversity includes rare and endemic species, making its conservation efforts crucial. The designated pilot area for the country of Montenegro, is the municipality of Ulcinj (Figure 102).

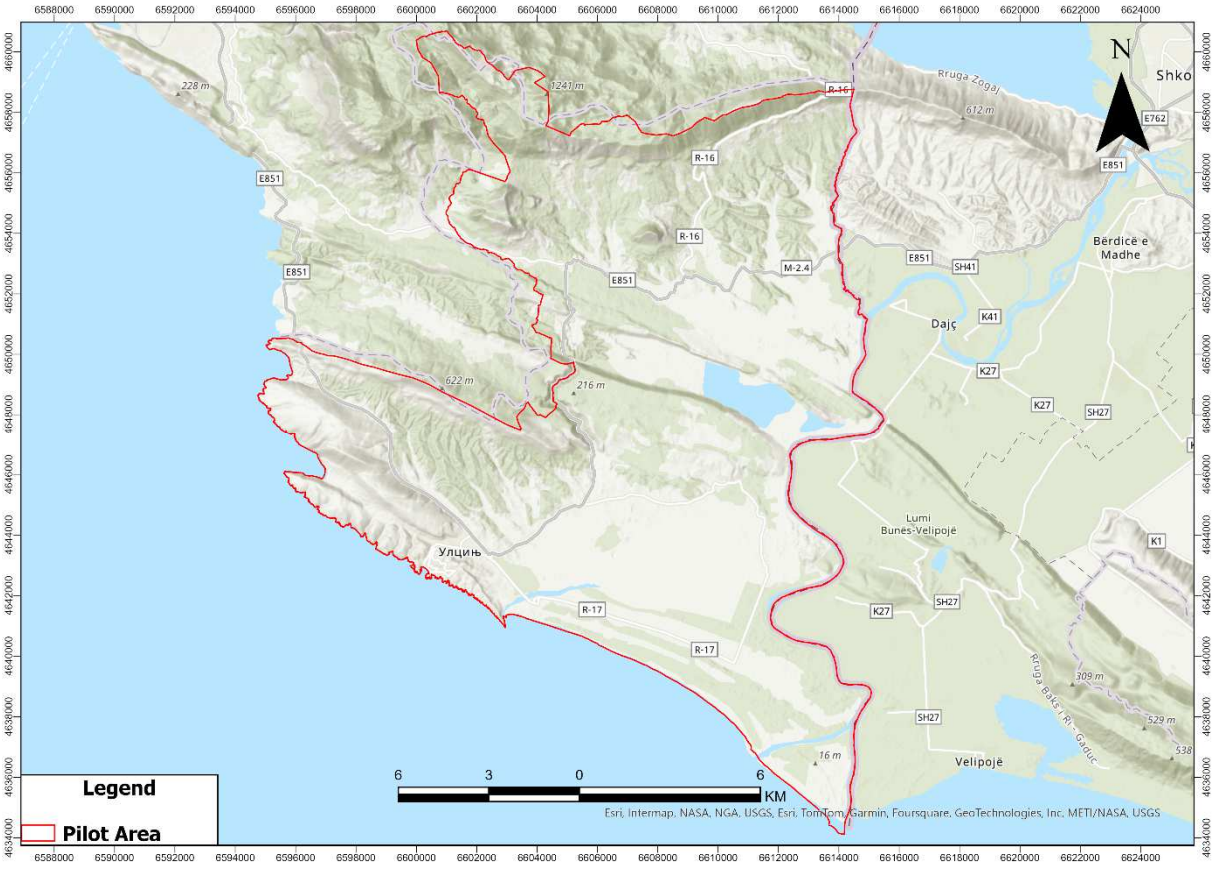

Figure 102. Pilot area of Montenegro

3.5.1. Geographical Location and administration

Ulcinj municipality is situated in the southernmost part of Montenegro, along the Adriatic coast. It borders Albania to the south and Bar municipality to the north. Administratively, Ulcinj is part of the Ulcinj municipality and is governed by a local council and mayor. The municipality covers an area of approximately 255 km^2 and has a population of around 20.000 residents. Known for its historical significance and cultural diversity, Ulcinj attracts visitors with its sandy beaches, ancient architecture, and vibrant local traditions, making it a key destination in Montenegro's coastal tourism industry.

Montenegro, like the rest of the countries which are included in this project, is a country prone to wildfires and especially during the dry summer months. The country's Mediterranean climate creates conditions favorable for the ignition and spread of wildfires. According to the rapid damage assessment of the European Forest Fire Information System (EFFIS) (San-Miguel-Ayanz et al. 2023), the fire season during 2022 in Montenegro was less severe compared to the preceding two years. A total of 26,332 hectares were affected by 260 fires. Similar to other countries, March was the most problematic month, responsible for two-thirds of the annual total (Figure 103). Four fires burned more than 1,000 hectares each, with an additional 11 fires surpassing 500 hectares. The annual average of burnt areas is around 21.000 ha (Figure 104).

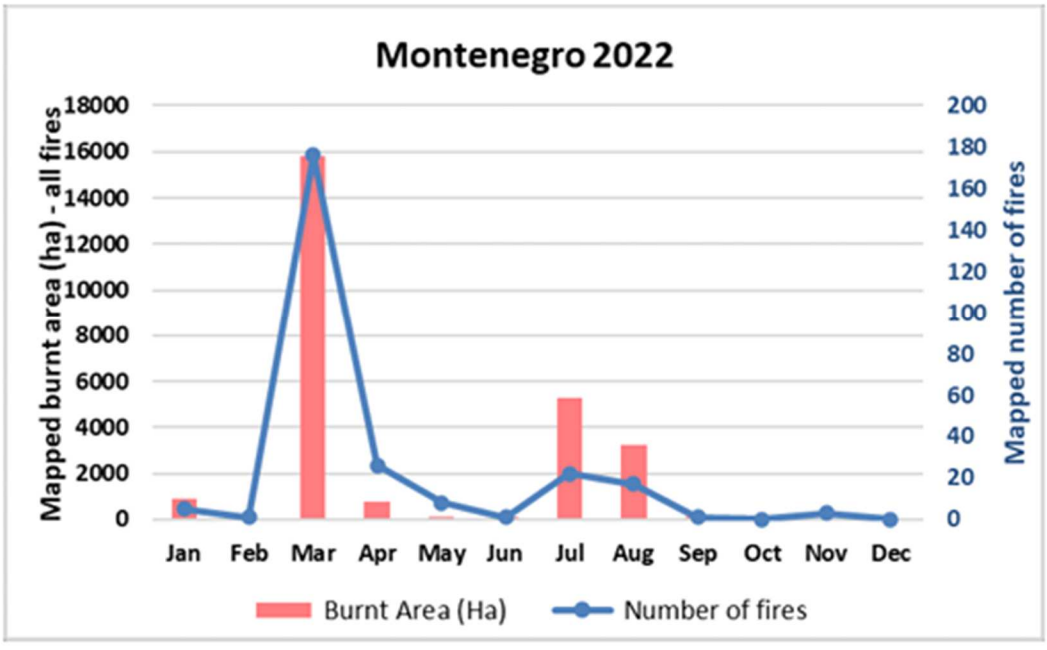

Figure 103. Monthly burnt areas in Montenegro for the year 2022 (San-Miguel-Ayanz et al. 2023).

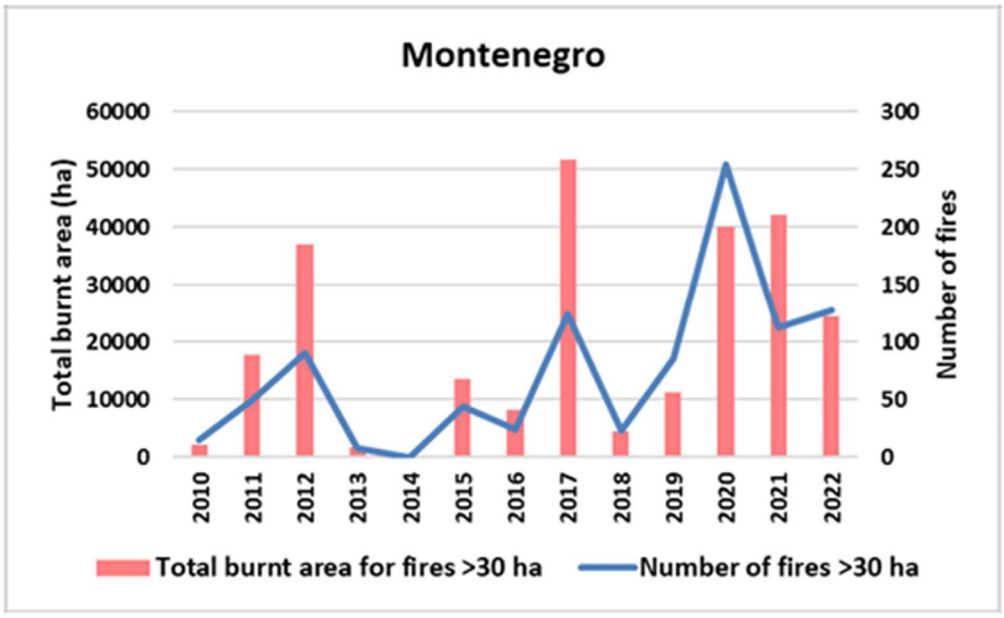

Figure 104. Annual burnt areas in Montenegro for the period 2010-2022 (San-Miguel-Ayanz et al. 2023).

3.5.2. Climatic conditions

Ulcinj municipality, experiences a Mediterranean climate characterized by hot, dry summers and mild, wet winters. According to the Ombrothermic diagram for the period 1980-2022 (Figure 105), the summer average temperatures on the area range from 22,73 °C to approximately 6,37 °C, with average precipitation between 32,5 mm and 60 mm. In winter, average temperatures vary from 5.85°C to 8,13°C, and average precipitation ranges from 45,48 mm to 59,78 mm. The data indicates that August is the hottest month, with a temperature of 26,24 °C, while January is the coldest month, with a temperature of 6,37 °C. Regarding rainfall, November appears to be the wettest month, with 210,82 mm of precipitation, and July the driest, with 3 mm of precipitation. It's also worth noting that the area experiences a dry period from July to late mid-August.

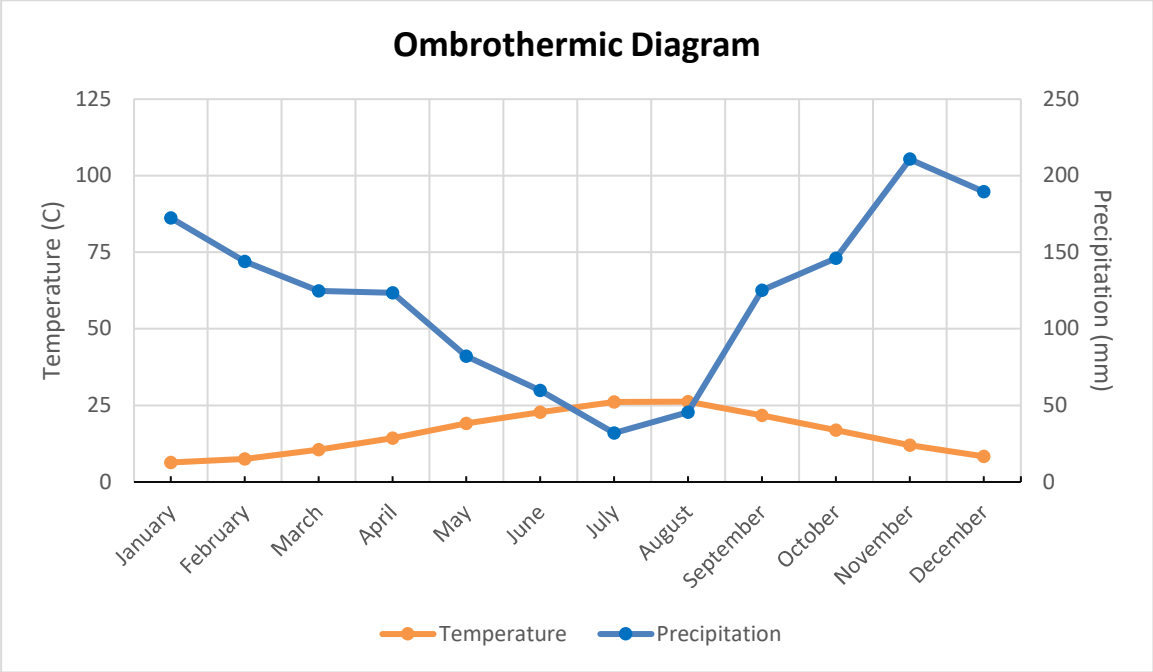

Figure 105. Ombrothermic Diagram of the Ulcinj municipality for the years 1980-2022 based on the CRU TS dataset (Harris et al. 2020).

3.5.3. Land Uses

In this region of Montenegro, there appears to be a diverse array of land uses. Among these various land use categories, six occupy more than a thousand hectares each (Figure 106). Beginning with the most extensive category, broad-leaved forests dominate by covering approximately 27.50% of the total area. Following closely are lands with complex cultivation patterns, which take up to 19.42% of the area. Transitional woodland-shrub areas also make up a significant portion, covering 12.76% of the land. The remaining three land use categories include regions principally occupied by agriculture with significant areas of natural vegetation, sclerophyllous vegetation areas, and saline regions. These last three categories are relatively similar in the amount of land they cover, accounting for 7,9%, 6,15%, and 5,65% of the total area, respectively.

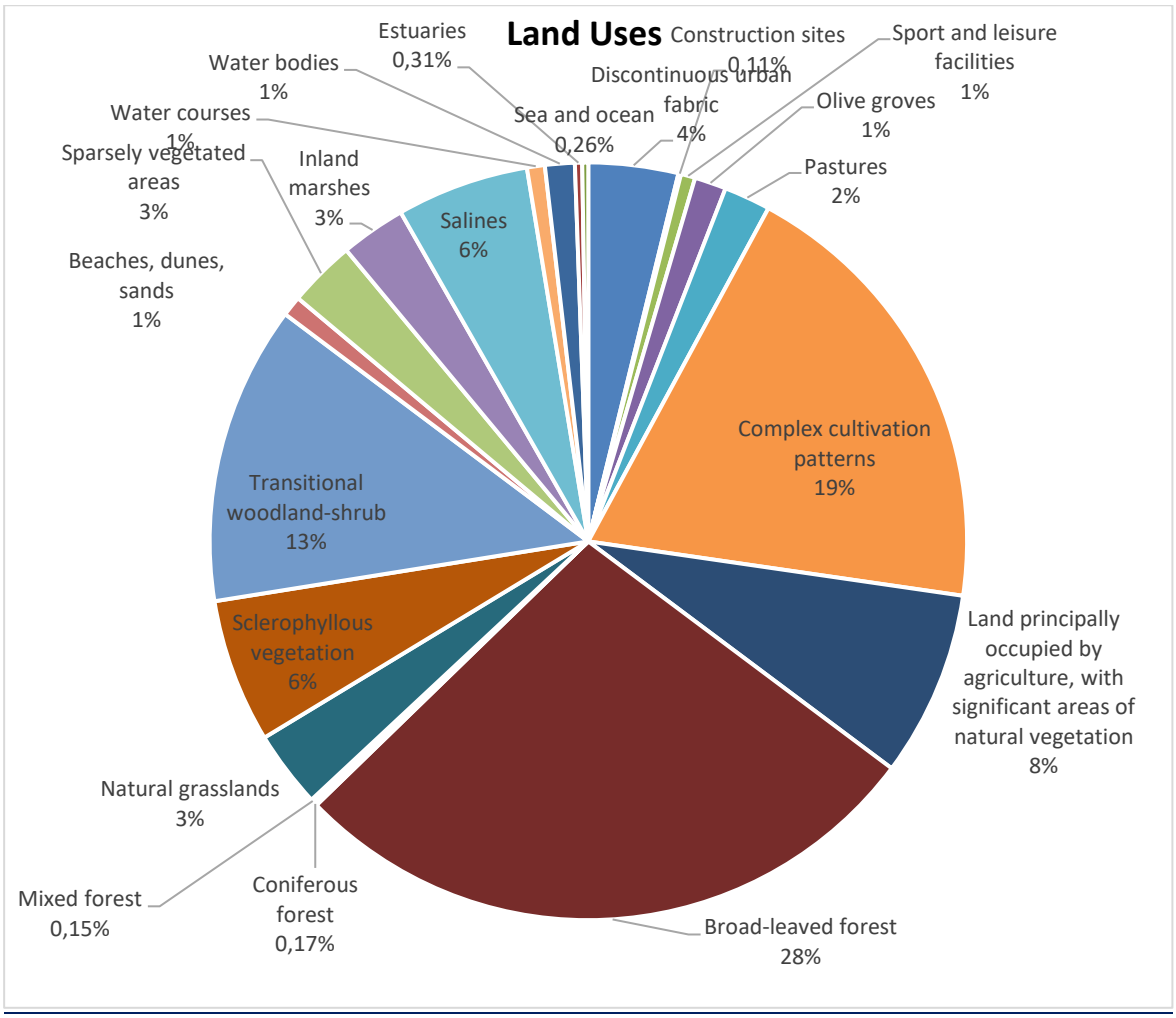

Figure 106. Percentage cover of different land use types that occupy the pilot area in Montenegro based on the CORINE land cover.

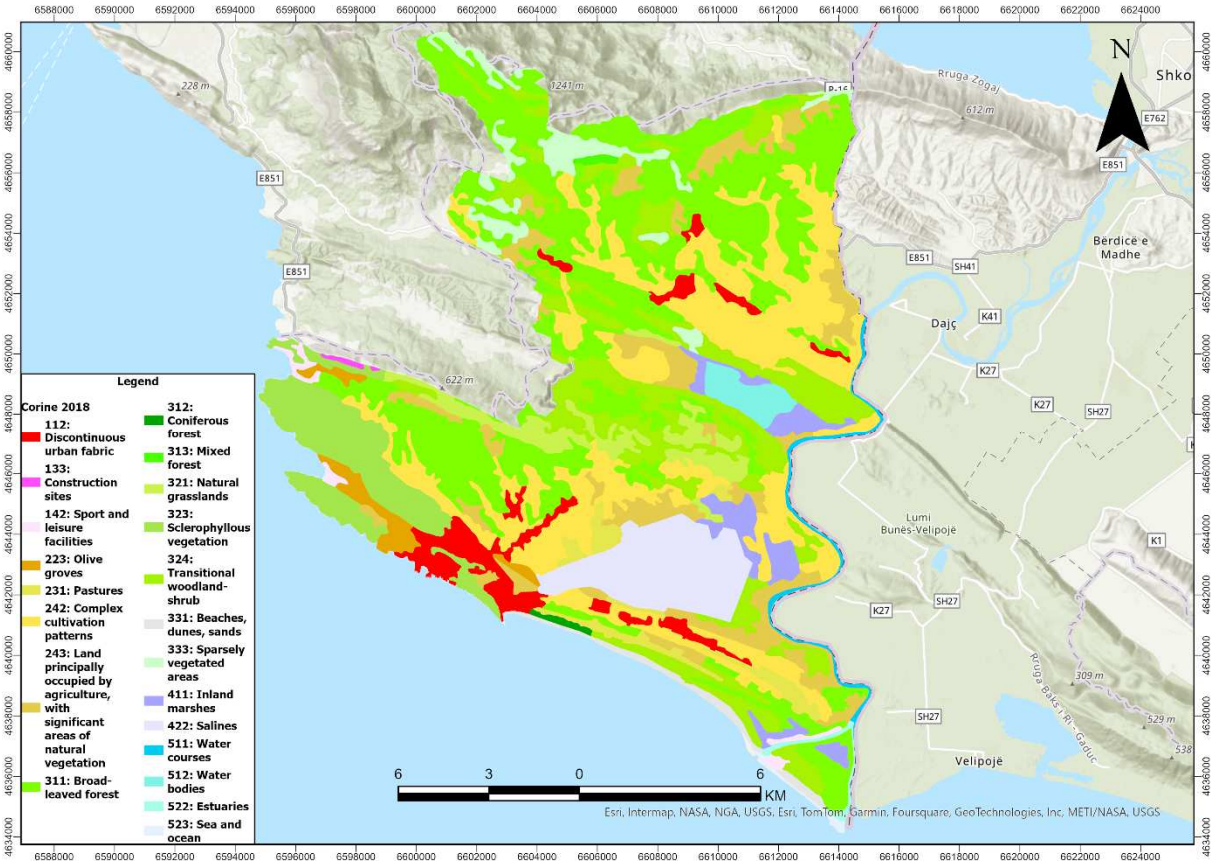

Figure 107. CORINE land cover map of the pilot area in Montenegro.

3.5.4. Flora and Vegetation

The municipality of Ulcinj hosts a highly significant area for biodiversity known as Ulcinj Salina. Situated in the southernmost part of Montenegro, it is the largest saltpan in the Adriatic, located just 1 km from both Ulcinj city and the Albanian border. Covering slightly under 14,5 km², the salina was established in the 1930s and ceased salt production in 2013. It consists of various sections that played distinct roles in the salt production process, such as crystallization and evaporation. Today, the majority of the saltpan is covered by grassland, halophyte vegetation, and reeds. According to reports, Ulcinj Salina is globally recognized as a biodiversity hotspot, fulfilling 6 out of 9 Ramsar criteria. It supports at least 11 bird species and encompasses four habitat types eligible for inclusion in the Natura 2000 network of protected sites.

Three habitat types based on the composition of various halophyte species are listed in Annex I of the EU Habitats Directive, making them significant at the EU level. The Coastal lagoons habitat type, characterized by the presence of Ruppietea maritimae, is designated as a priority habitat in Annex I of the EU Habitats Directive. This habitat type is widespread in many basins,

especially in Jezero 1 and Jezero 2, where water is present year-round. During the period of salt production, the Crystallization area lacked vegetation, however today about one-third of it is covered with vegetation.

3.5.5. Fauna

Approximately 250 bird species have been recorded in the Ulcinj Salina, representing about half of the regularly occurring bird species in the EU. Among these, 60 species are numerous and/or frequent, 69 are rare and/or infrequent but still significant for the area, and the remainder are occasional and less important visitors or breeders. The Greater flamingo stands out as a flagship species requiring the highest conservation attention. Regular and numerous breeders include the Black-winged stilt, Stone curlew, Collared pratincole, Kentish plover, Little tern, and Common tern. For some of these species, the salina is the most crucial breeding ground in the region. The Little egret, Spoonbill, Pygmy cormorant, Redshank, and Spotted redshank are important due to their numerous presence year-round, although they either do not breed or breed only in small numbers and irregularly. Ulcinj Salina is also vital for migratory birds, particularly waders and ducks, with over 100.000 waterbirds estimated to stop during spring and autumn migrations for feeding and resting. Up to 15.000 birds are present daily during the winter.

Apart from birds, the significance of other vertebrates in the area is moderate. The lack of hiding and reproduction spots likely limits mammal populations, while the relatively small area of permanently dry land constrains reptiles, and the absence of fresh water affects amphibians. Fish can be numerous, with their taxonomic composition likely influenced by influxes from the sea and nearby rivers.

The waters of Ulcinj Salina harbor two predominant crab species, one belonging to the Amphipoda group and the other to the Isopoda group. They are abundant to the extent that they are considered key species in this ecosystem. Conversely, the population of brine shrimps has either disappeared or their numbers have declined significantly, likely due to inadequate management of the water regime. Amphipod and Isopod crabs are capable of surviving and reproducing in waters with varying salinity levels, but their abundance decreases when the basins dry out, negatively impacting the presence of all other animals in the ecosystem.

3.5.6. Spatial data

- **Aspect**

Upon reviewing the aspect map for the pilot area of Montenegro, an intriguing observation about the landscape emerges (Figure 108). A significant portion of the area is flat, primarily located in the central and southern regions. The rest of the terrain, which consists mostly of slopes, predominantly faces south and southwest.

- **Slope**

The slope map gives a better representation of the landscape for the area of Montenegro (Figure 109). Through the examination of the map, It becomes clear that the central and southern regions of the pilot area are flatter in comparison to the western and northern regions. The steeper slopes appear to be at the north part, where the mountainous regions start emerging into the landscape, creating a diverse relief with slopes that mostly exceed 40%.

- **Geomorphology**

The geomorphology map further confirms the area's flatness. As shown in Figure 110, the majority of the landscape is flat with low elevation values. The highest point reaches 1.416 meters and the most notable elevation changes are observed in the northern and western parts of the area.

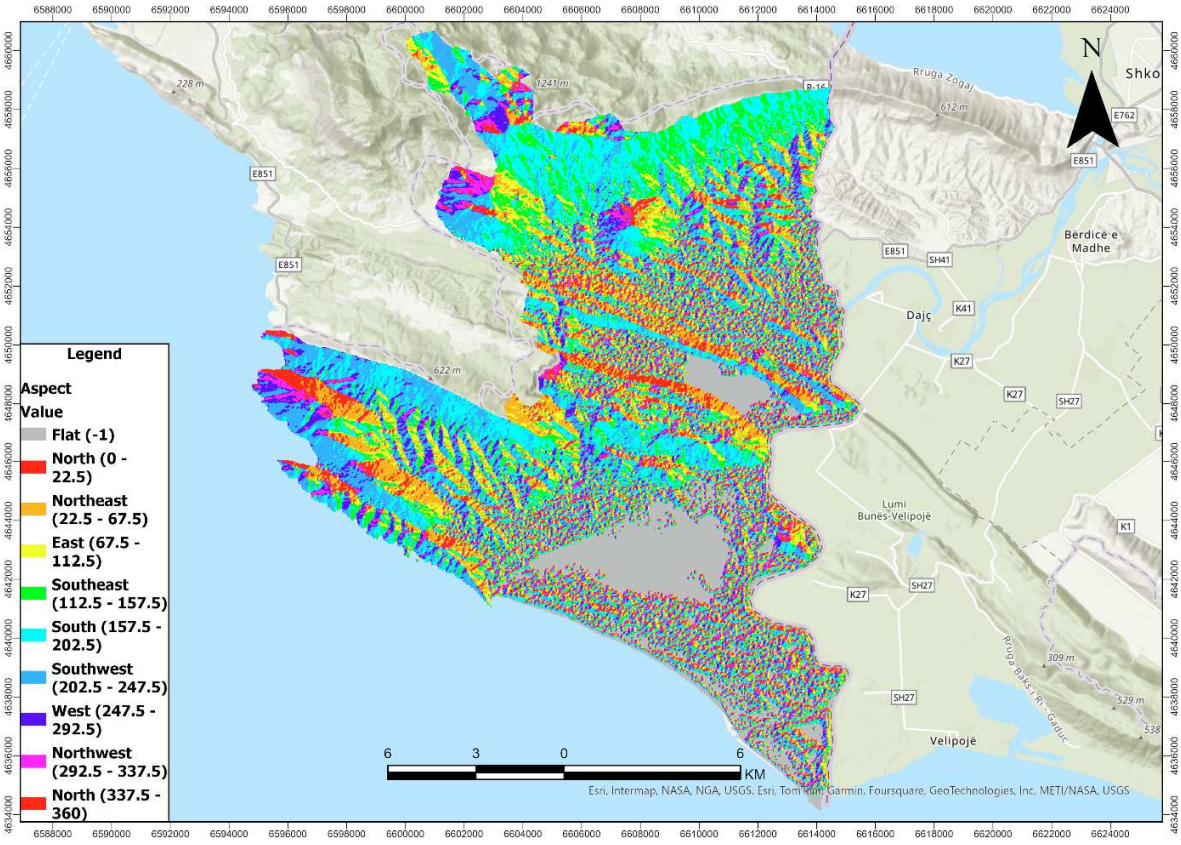

Figure 108. Aspect map of the pilot area in Montenegro.

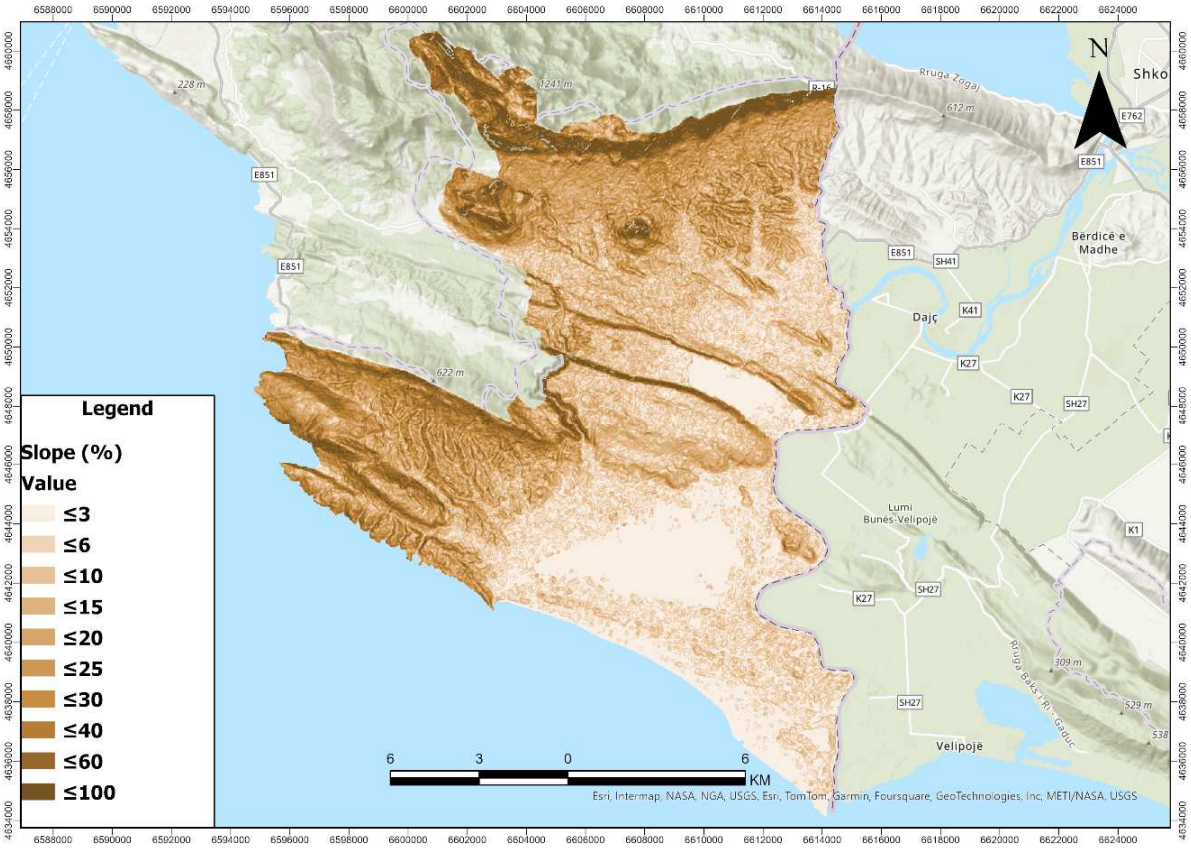

Figure 109. Slope map of the pilot area in Montenegro.

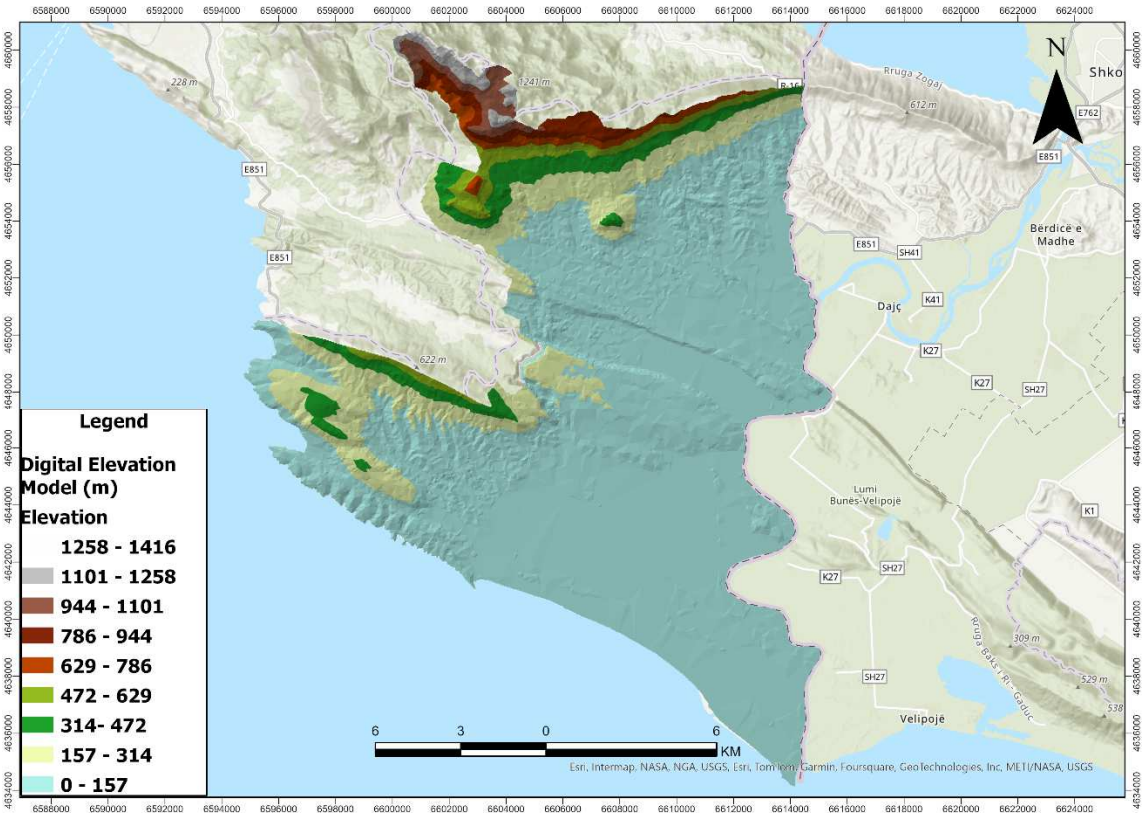

Figure 110. Geomorphology map of the pilot area in Montenegro.

- **Canopy Height**

By examining the Canopy Height Model (CHM) for the pilot area of Montenegro, the locations covered by forests are easily identified (Figure 111). The forested areas of the region are primarily situated in the central, northern, and southwestern parts with some also appearing in the southeast.

- **Tree cover density**

In combination with the CHM, the tree cover density provides additional information about the location of the forested areas (Figure 112). Specifically, it is clear that the same regions as mentioned above are areas which are densely covered by forests.

- **Roads and buildings network**

Like the other pilot areas, Montenegro features extensive road networks that link urban environments with forested and agricultural lands (Figure 113). The connectivity provided by these not only facilitates efficient transportation and access but also presents a valuable infrastructure for managing and mitigating wildfire risks.

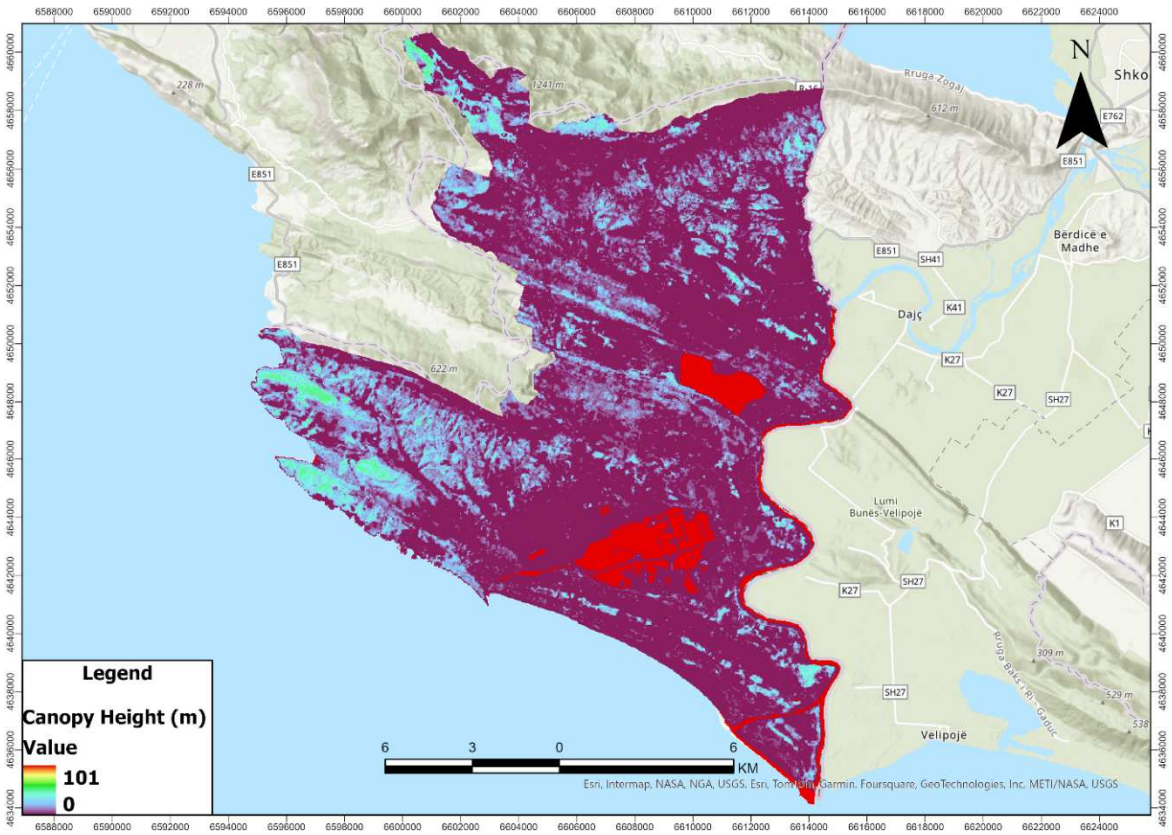

Figure 111. Canopy Height Model of the pilot area in Montenegro.

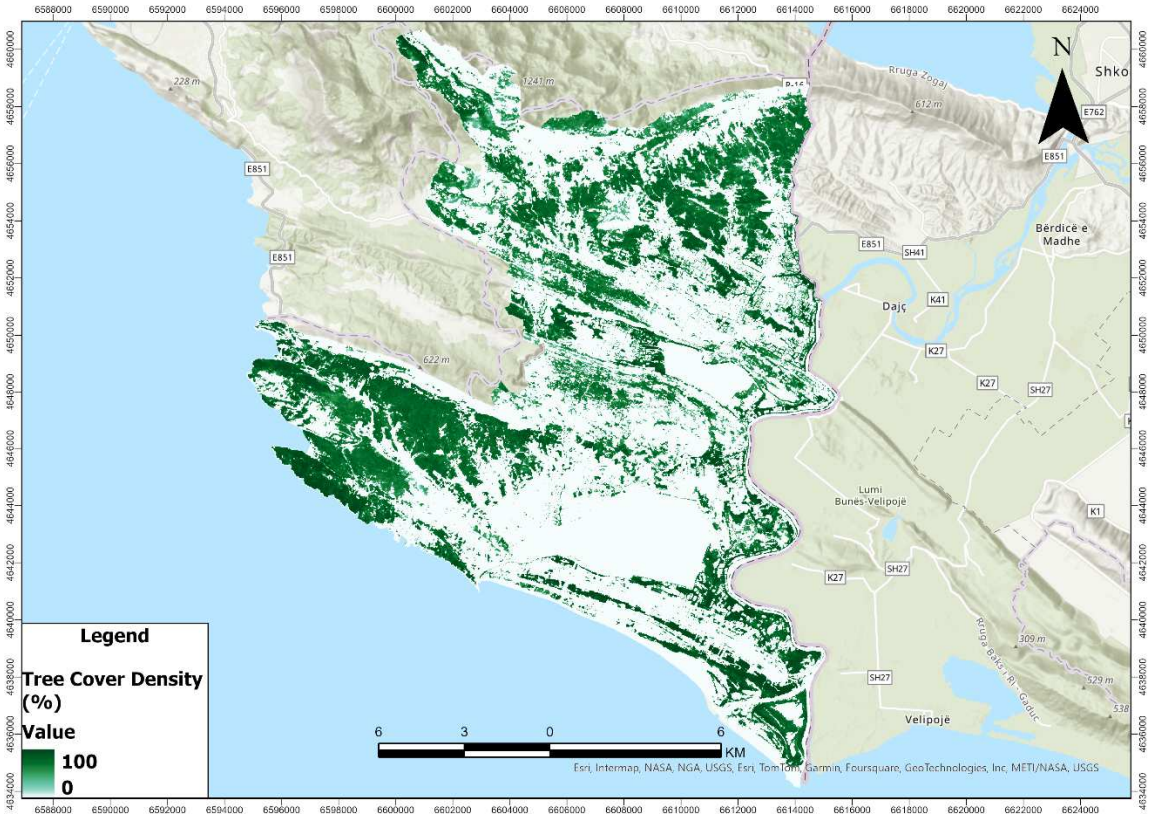

Figure 112. Tree cover density map of the pilot area in Montenegro.

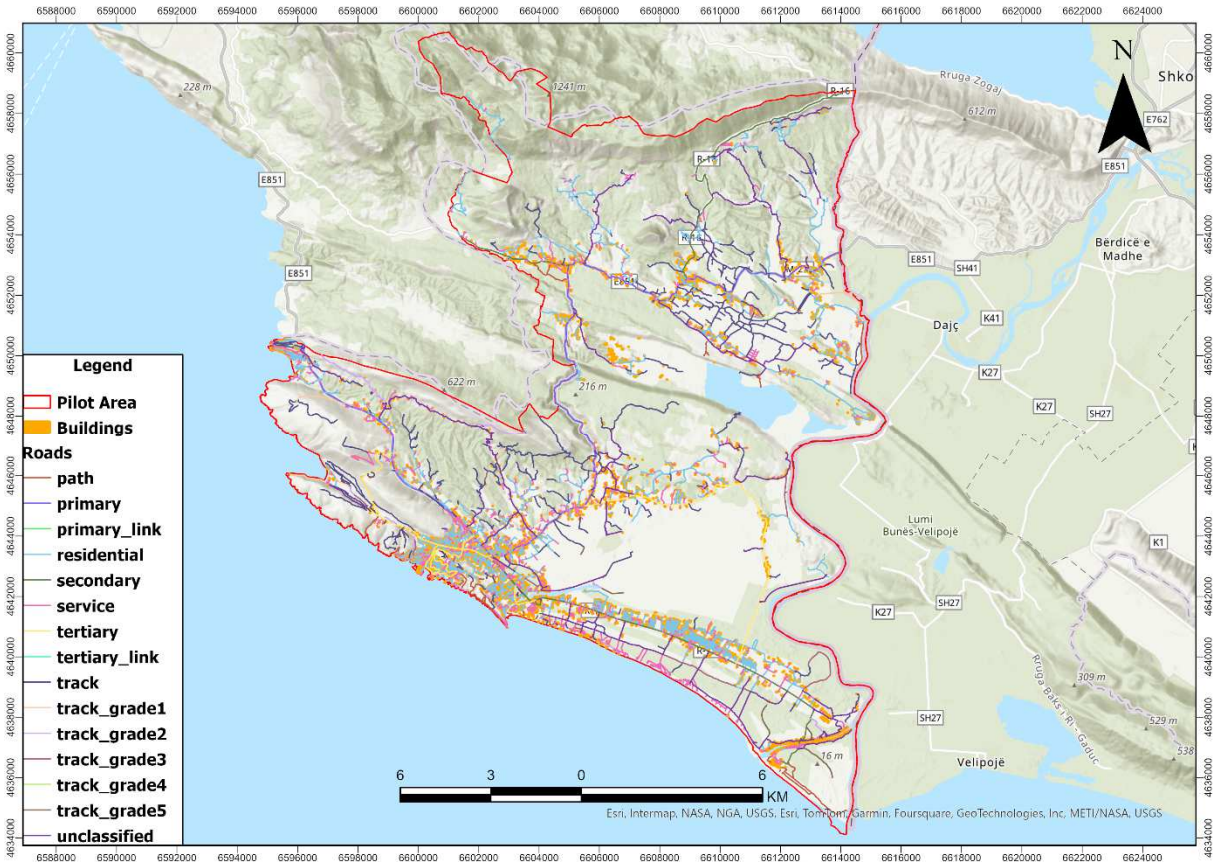

Figure 113. Roads and buildings map of the pilot area in Montenegro

- **NDVI**

The vegetation in the area exhibits a distinctive pattern, evident from the analysis of NDVI models throughout all four seasons, revealing intriguing findings (Figure 114). It is apparent that the northern and some western regions are predominantly forested, a distinction highlighted by seasonal variations between summer and winter. Additionally, a significant portion of the remaining area is characterized by agricultural lands. In winter, the highest NDVI values are observed in these agricultural areas.

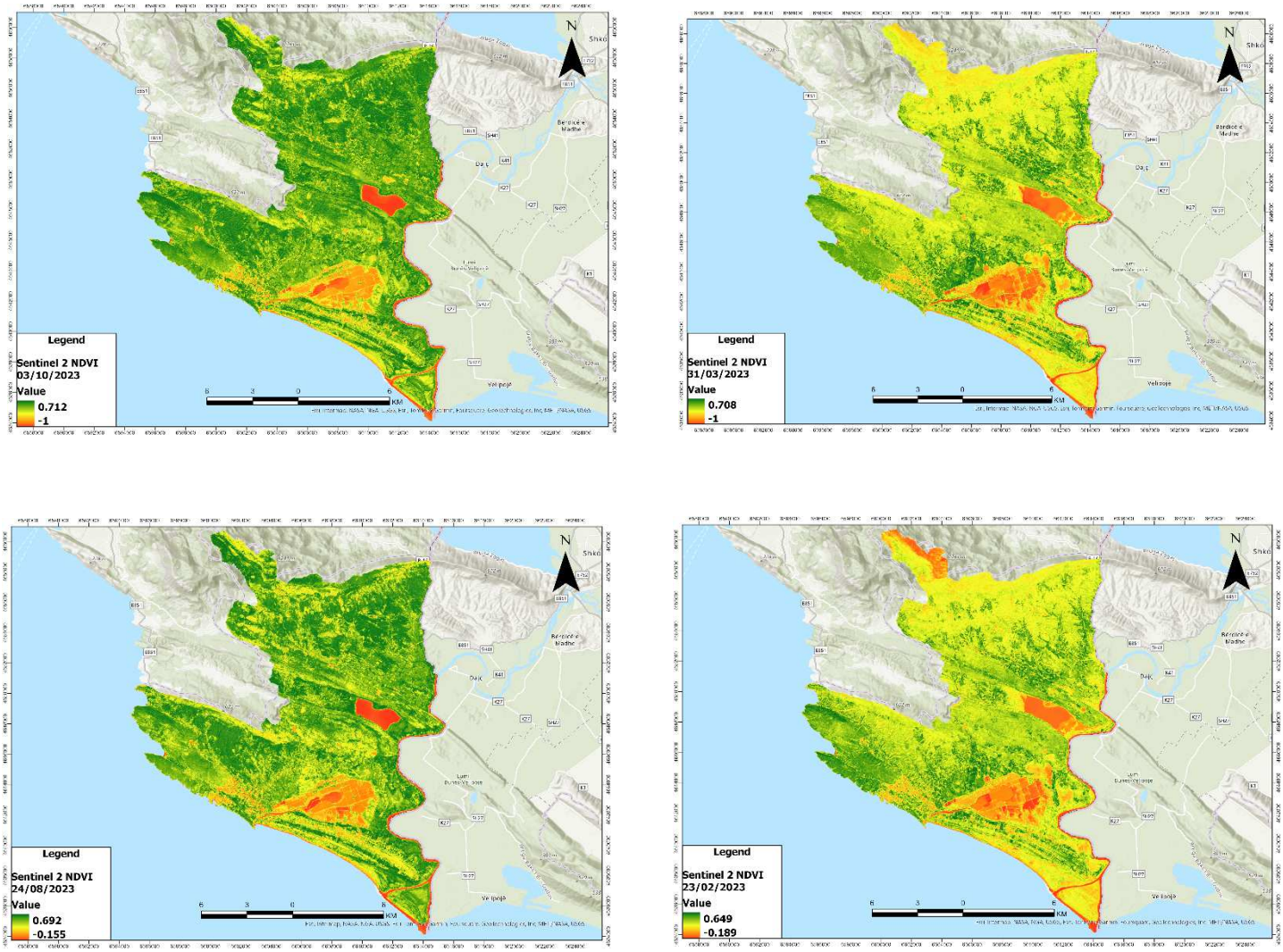

Figure 114. NDVI maps that cover all four seasons for the pilot area of Montenegro. The autumn NDVI map is displayed at the top left, the spring NDVI map at the top right, the summer NDVI map at the bottom left, and the winter NDVI map at the bottom right.

- **Sentinel 2 images**

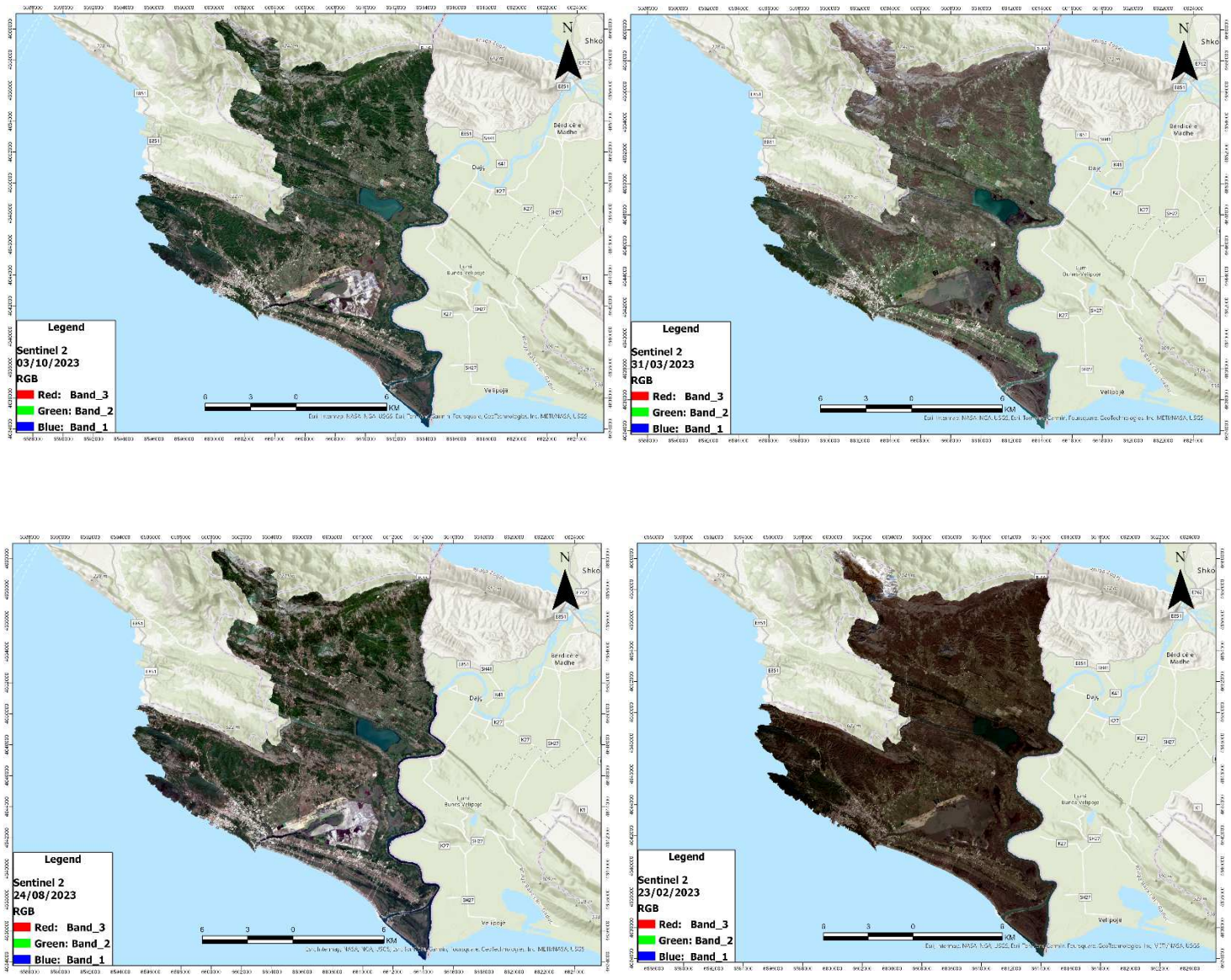

Figure 115. Sentinel 2 satellite images that cover all four seasons for the pilot area of Montenegro. The autumn Sentinel 2 image is displayed at the top left, the spring one at the top right, the summer one at the bottom left, and the winter one at the bottom right.

- **Planet image**

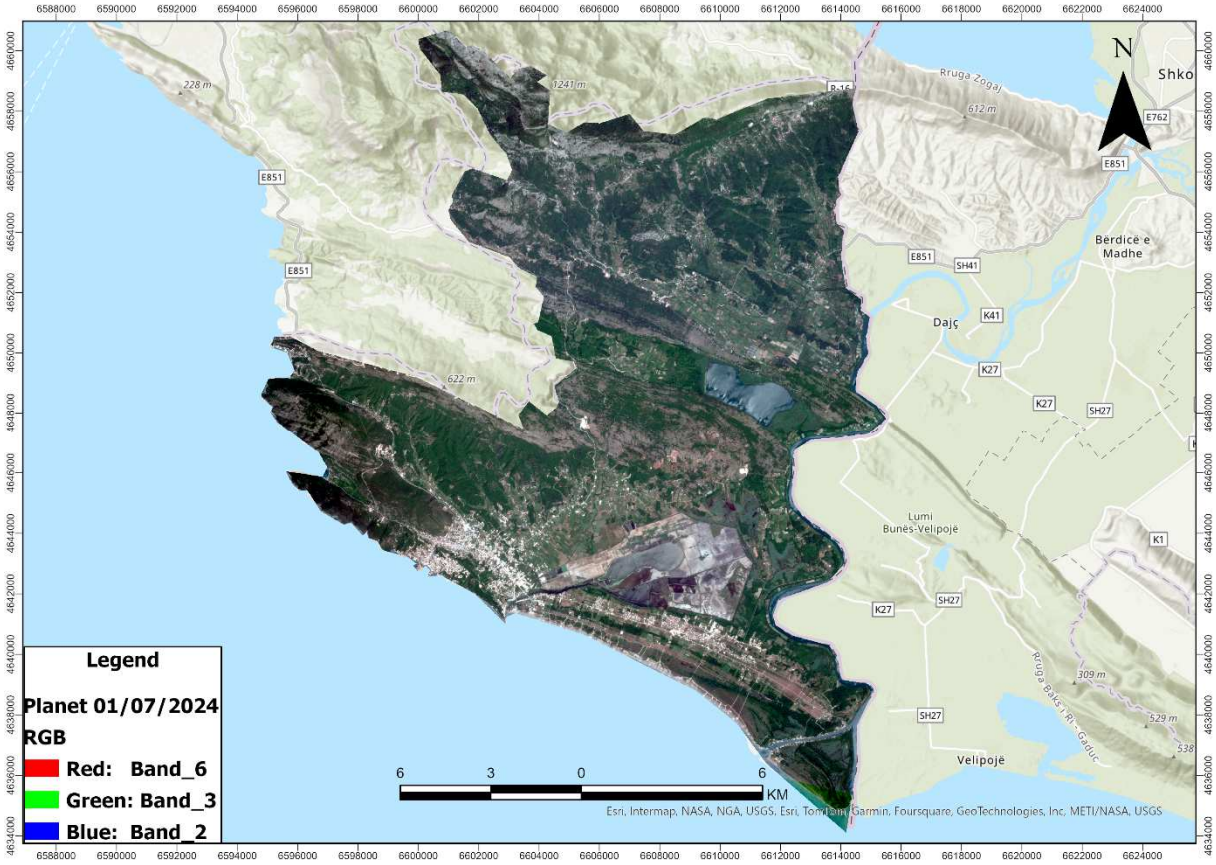

Figure 116. Planet image captured during summer for the pilot area of Montenegro.

3.6. National Park Una - Bosnia and Herzegovina

Bosnia and Herzegovina is located in Southeastern Europe on the Balkan Peninsula, bordered by Croatia to the north and west, Serbia to the east, and Montenegro to the southeast. The country spans an area of approximately 51,200 square kilometers and has a diverse geography that includes mountainous regions, rivers, and forests, contributing to its rich biodiversity. Bosnia and Herzegovina is home to a variety of plant and animal species, many of which are protected within its national parks. The population of Bosnia and Herzegovina is around 3.3 million people. The country boasts several national parks, including Una National Park, Sutjeska National Park, Kozara National Park, and Drina National Park, which protect its unique natural landscapes and wildlife. The region which this project places its focus is the Una National Park ().

Wildfires pose a significant threat in Bosnia and Herzegovina due to its diverse landscapes and climate conditions. Like most of the mediterranean countries, Bosnia and Herzegovina experiences hot and dry summers, which increase the risk of wildfires, particularly in forested areas. Human activities such as agricultural burning, forestry practices, and accidental ignitions contribute to fire occurrences. The impacts of wildfires in Bosnia and Herzegovina include environmental degradation, loss of biodiversity, damage to infrastructure, and threats to human health and safety. Efforts to mitigate wildfire risks involve fire prevention strategies, early detection systems, coordinated firefighting efforts involving local authorities and firefighting agencies, as well as public awareness campaigns to promote responsible behavior in fire-prone areas.

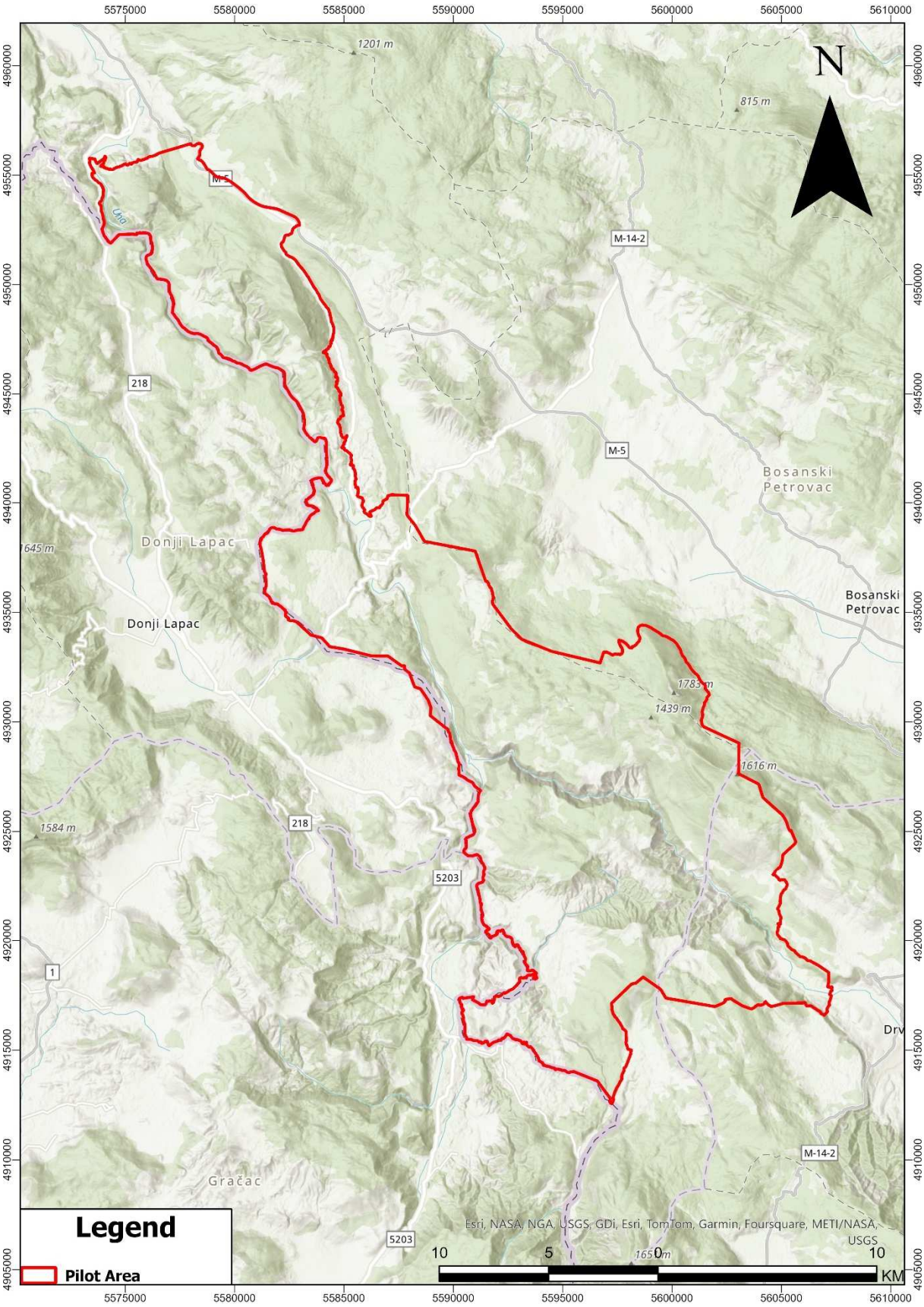

Figure 117. Pilot area of Bosnia and Herzegovina.

According to the rapid damage assessment of the European Forest Fire Information System (EFFIS) (San-Miguel-Ayanz et al. 2023), the fire season in Bosnia and Herzegovina in 2022 mirrored that of 2021 in terms of the overall burned area. However, unlike 2021, which saw two distinct peaks in spring and summer, the majority of the damage in 2022 occurred in March (Figure 119). A total of 578 fires were identified, encompassing 76,473 hectares. The country's largest fires each exceeded 2,000 hectares, with an additional ten fires exceeding 1,000 hectares and eleven others exceeding 500 hectares. Fires affected various types of land cover, with Broadleaf Forest being the most impacted, accounting for one-third of the total burned area.

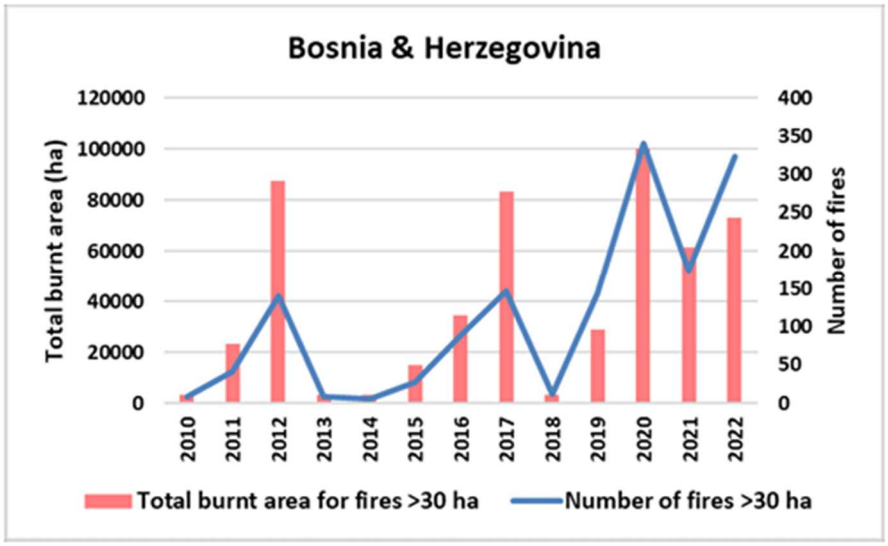

Figure 118. Annual mapped burnt area of fires >=30ha in Bosnia and Herzegovina for the years 2010-2022 (San-Miguel-Ayanz et al. 2023).

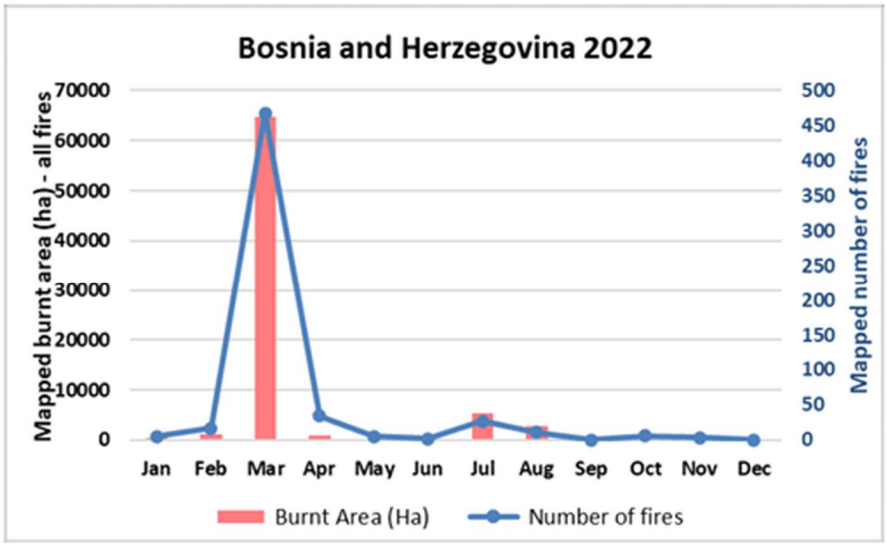

Figure 119. Monthly mapped burnt area and number of fires in Bosnia and Herzegovina in 2022 (San-Miguel-Ayanz et al. 2023).

3.6.1. Climatic conditions

Una National Park, located in the northwestern part of Bosnia and Herzegovina, features a continental climate with some Mediterranean influences. Based on the Ombrothermic diagram for the period 1980-2022 (Figure 120), it appears that the summer temperatures average from 17,5 °C to about 19,71 °C, with average precipitation between 80,87 mm and 103,50 mm. In winter, the average temperatures vary from -0,6 °C to 5,4 °C, and precipitation ranges from 88,19 mm to 133,44 mm. July is identified as the hottest month, averaging 19,71 °C, and January as the coldest, at -0,6 °C. The wettest month is November with an average of 147,36 mm of precipitation, while July is the driest, receiving 80,87 mm.

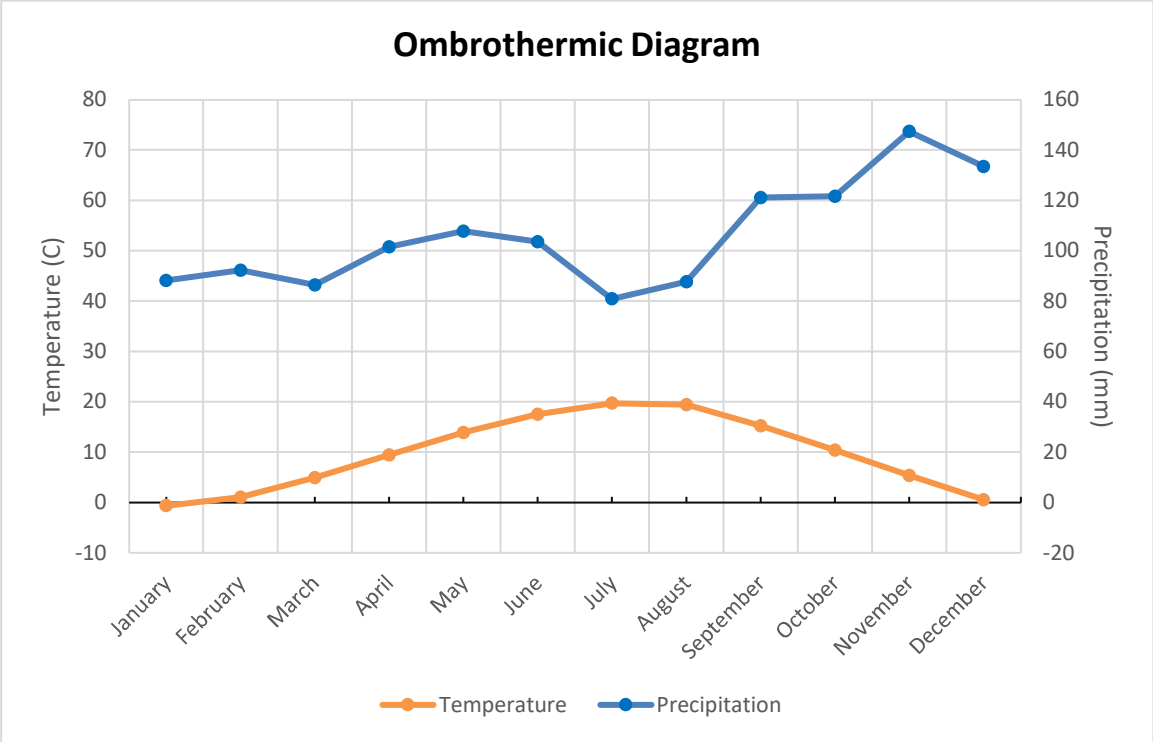

Figure 120. Ombrothermic Diagram of the Una National Park for the years 1980-2022 based on the CRU TS dataset (Harris et al. 2020).

3.6.2. Land Uses

The terrestrial habitats within Una National Park encompass meadows, pastures, and forests, with forests covering the majority of the park's surface. These forests vary in type, ranging from climazonal and extrazonal to azonal. Grasslands in the park are primarily anthropogenic and require continuous human intervention through grazing or mowing to maintain their ecological integrity. Water habitats include the Una and Unac rivers, where aquatic macrophytic vegetation is sparse except for sporadic occurrences in small, tranquil lagoons. Wet habitats in the area consist of marshy grasslands, tall reeds, and wetlands. The travertine waterfalls in the park represent a unique biotope with distinct ecological conditions compared to other freshwater habitats. Based on the CORINE land cover, a significant portion of the park consists of broad-leaved forests, which occupy approximately 58.5% of the total area and are the most abundant land use type of the area.

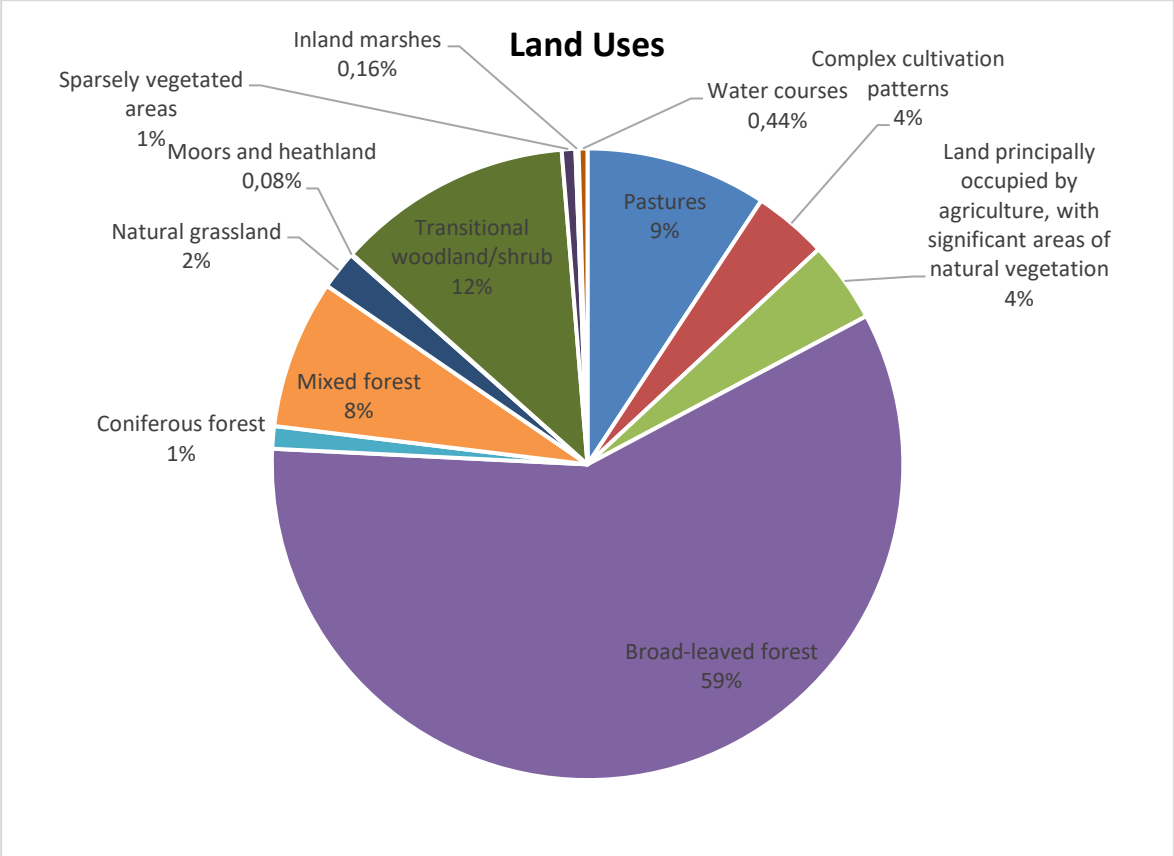

Figure 121. Percentage cover of different land use types that occupy the pilot area in Bosnia and Herzegovina based on the CORINE land cover.

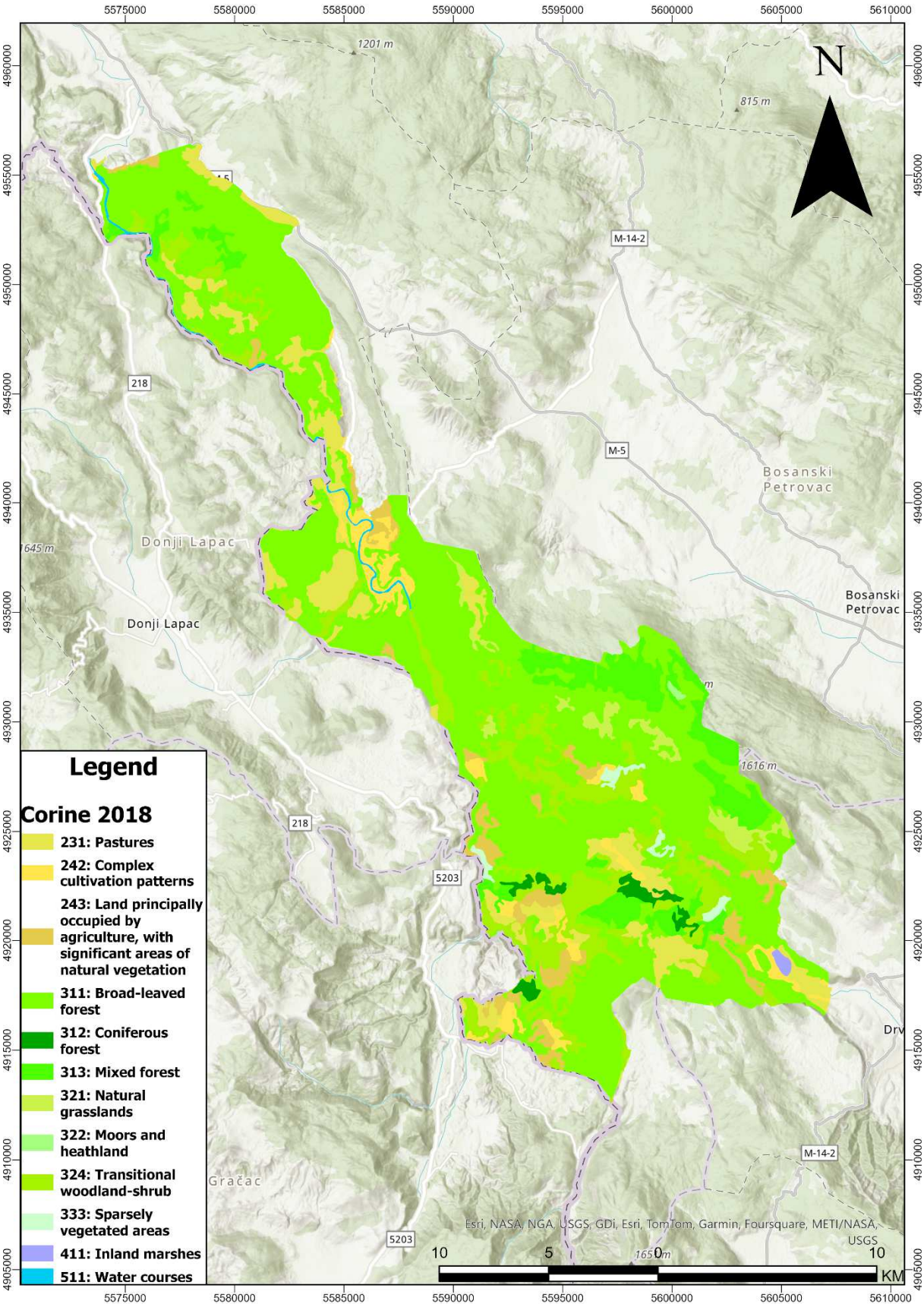

Figure 122. CORINE land cover map of the pilot area in Bosnia and Herzegovina.

3.6.3. Flora and Vegetation

The flora and fauna of Una National Park, designated for its protected natural treasures, thrive with a wide array of plant and animal species. The park's terrain configuration, soil geomorphology, varying altitudes, and diverse flora collectively foster a vibrant microcosm that, alongside other life forms, enhances the park's biodiversity richness. In this region, there are numerous rare and endemic species, including lincura (Gentiana lutea), spotted lincura (Gentiana punctata), eelgrass (Leontopodium alpinum Cass), and juniper pine (Pinus mugo). The Una bellflower (Campanula unensis) is an endemic species named after the Una River, while the Bosnian iris (Iris reichenbachii Heuffel var. Bosniaca) thrives in dry meadows and pastures on carbonate and serpentine rocks with shallow soil. The Bosnian iris is exclusive to the central and southeastern Dinarides. The ecological conditions in the area have also fostered the development of diverse plant communities of significant value, boasting over 1.900 plant species, which constitute 52,19% of all species found in Bosnia and Herzegovina. Among them, 177 species are officially recognized, and 105 species have potential medicinal, edible, vitamin-rich, or aromatic properties.

The National Park area is mostly composed of limestone rocks hosting distinct vegetation adapted to the unique conditions of such habitats, including chasmophytic plants thriving within fissures. Below the larger rocky outcrops, local depressions are formed where parts of the rock slope are influenced by hydrological and atmospheric factors. Weedy and ruderal vegetation is prevalent around all settlements in the region. The communities of Bidentetea, Artemisete, and Chenopodiete classes thrive due to traditional rural practices, extensive agriculture, and widespread livestock grazing.

The diverse habitats within the National Park support a wide array of species and communities. While the exact number of taxa and communities in the park cannot be precisely determined, we can draw a comparison with Austria, which hosts around 2.000 species. Despite the National Park's relatively small size, it is estimated to harbor more than 1.000 species. Moreover, the park is home to numerous endemic species and relict-refugial communities, which are not only significant locally but also contribute to the overall biological diversity of Europe. Therefore, it is anticipated that a substantial portion of the park will be included in the Natura 2000 ecological network.

3.6.4. Fauna

The fauna of Una National Park stands out as one of the most diverse in this region of Europe across all its aspects. Numerous animals have made the park their habitat, enriching it with increasing diversity each day. This includes a wide array of mammals, birds, reptiles, fish, amphibians, and butterflies.

According to the Law on Nature Protection and the Ordinance on the Protection of Certain Mammal Species (N.N. 31/95), 33 mammal species in the Una area and National Park receive protection, with an additional 8 species protected under the Wild Animals Ordinance. Among the protected mammals are numerous endangered and sensitive species of bats, alongside three prominent large carnivores: the wolf, lynx, and bear, which are among Europe's largest predators. Other significant species include the otter, badger, weasel, and marten. Seventeen mammal species from this group are listed on the IUCN Red List of Threatened Species for Europe under various threat categories. Moreover, the area's biodiversity is safeguarded under the Bern Convention, which protects 50 species of wild fauna and their habitats within the National Park.

Based on the data of observation and study of birds in the wider area of the park, more than 120 species of birds have been recorded, based on literature data and data on the ornitofauna of the wider area, we can expect the number of bird species to exceed 160 species. It is interesting to mention the great grouse, which is quite endangered due to excessive hunting, the black grouse, which is a rather rare and secretive species (often seen in the Doljan area). In the wider area of the park there are 12 species of reptiles from two orders, namely turtles (Chelonia) and scales (Squamata), the following species are also present: the scaly scaly lizard (Algyroides nigropunctatus), the Velebit lizard (Lacerta horvathi) and the mountain yellow circle (Vipera macrops). According to the Convention on the Protection of European Wild Species and Natural Habitats, 11 species of reptiles are strictly protected. Among the 15 species of fish that are present in the river Una in the area of the park and its tributaries, the most important are brown trout (Salmo trutta) and grayling (Thymallus thymallus). Among the rare species here, we can find a species called pesh (Cottus gobio) as well as the two-striped uklia, a rare and relatively endangered species. Amphibians that live in the calm waters of the plains, overgrown with aquatic plants, relatively deep lakes in hilly and mountain areas are the big green frog (Rana ridibunda) and the salamander (Salamandra salamandra). One of the best indicators of a healthy and balanced ecosystem is the abundance of various types of

butterflies. So far 75 species of butterflies have been identified in the park, and the assumption is that this number is over a hundred.

3.6.5. Spatial data

- **Aspect**

Upon examining the aspect map for the pilot area of Bosnia and Herzegovina (Figure 123), it becomes evident that there are mainly south, southwest and west facing slopes. These comprise most of the area with the remaining slopes facing mostly east.

- **Slope**

The landscape of Una National Park is varied, featuring numerous slopes of differing gradients. As illustrated in Figure 124, the region comprises multiple mountain ranges that result in steeper slopes compared to the flatter areas. It is evident that the majority of these steep slopes are situated at the boundaries of the mountain ranges, where the flat terrain transitions into mountainous areas. Although there is a balanced distribution of gentle and steep slopes throughout the park, it appears that the southeastern part of the pilot area predominantly contains the steeper slopes.

- **Geomorphology**

To gain a more comprehensive understanding of the landscape in this region, one can examine the geomorphology map (Figure 125). This map clearly reveals the presence of various mountain ranges, which are distinctly identifiable from the flatter regions. The elevation across the area spans from 218 meters to 1783 meters. The highest elevation point is found in the southwest part of the area. Additionally, there are two more significant mountain peaks, one located in the southern part and the other in the northern part of the region.

- **Canopy Height**

Forested regions are the predominant feature in the pilot area of Bosnia and Herzegovina. As depicted in Figure 126, the Canopy Height Model (CHM) for this region clearly illustrates the extensive coverage of forests within the national park. The CHM provides a detailed visual representation, making it easy to observe the vast expanse and dominance of forested areas throughout the Una National Park.

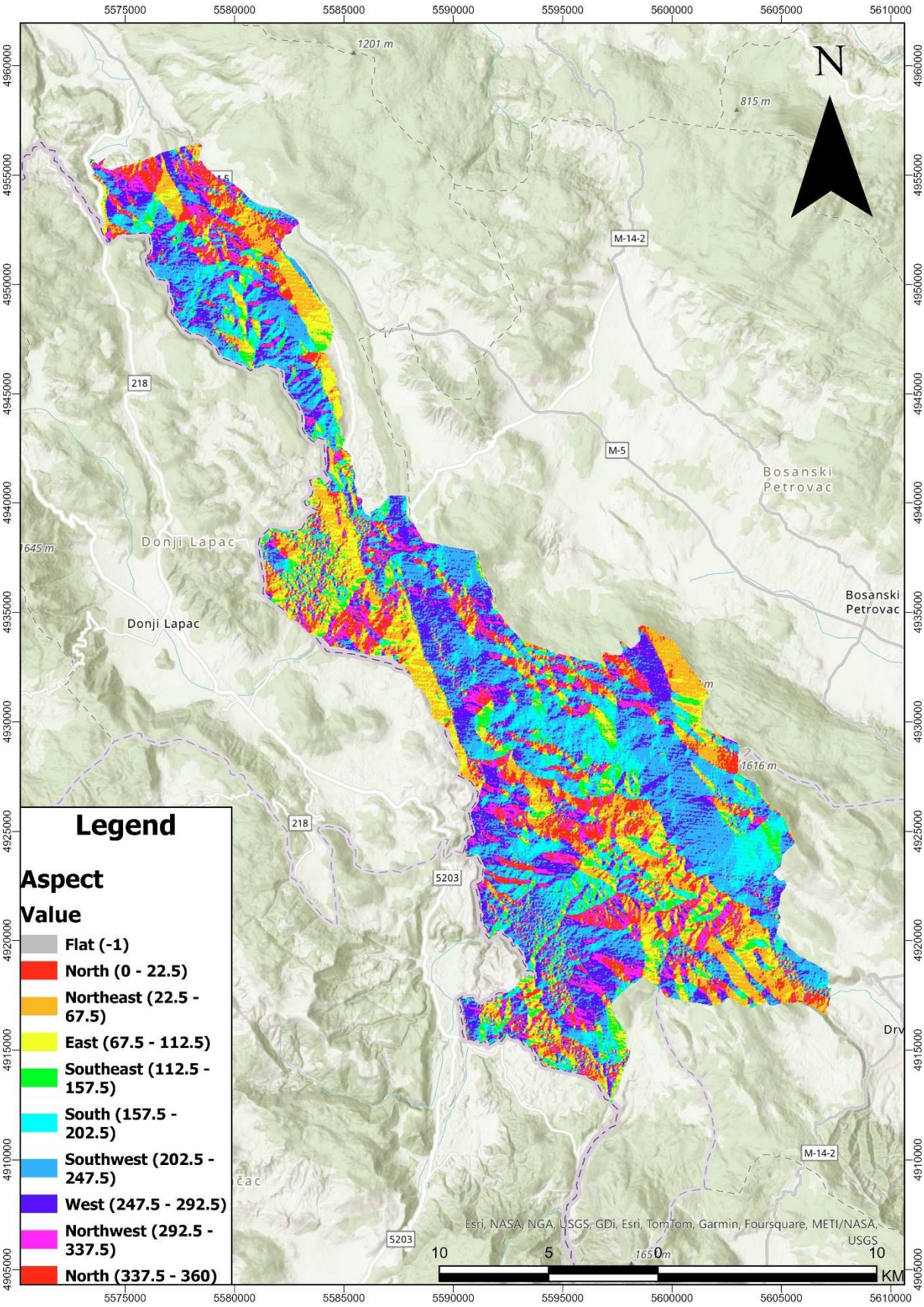

Figure 123. Aspect map of the pilot area in Bosnia and Herzegovina.

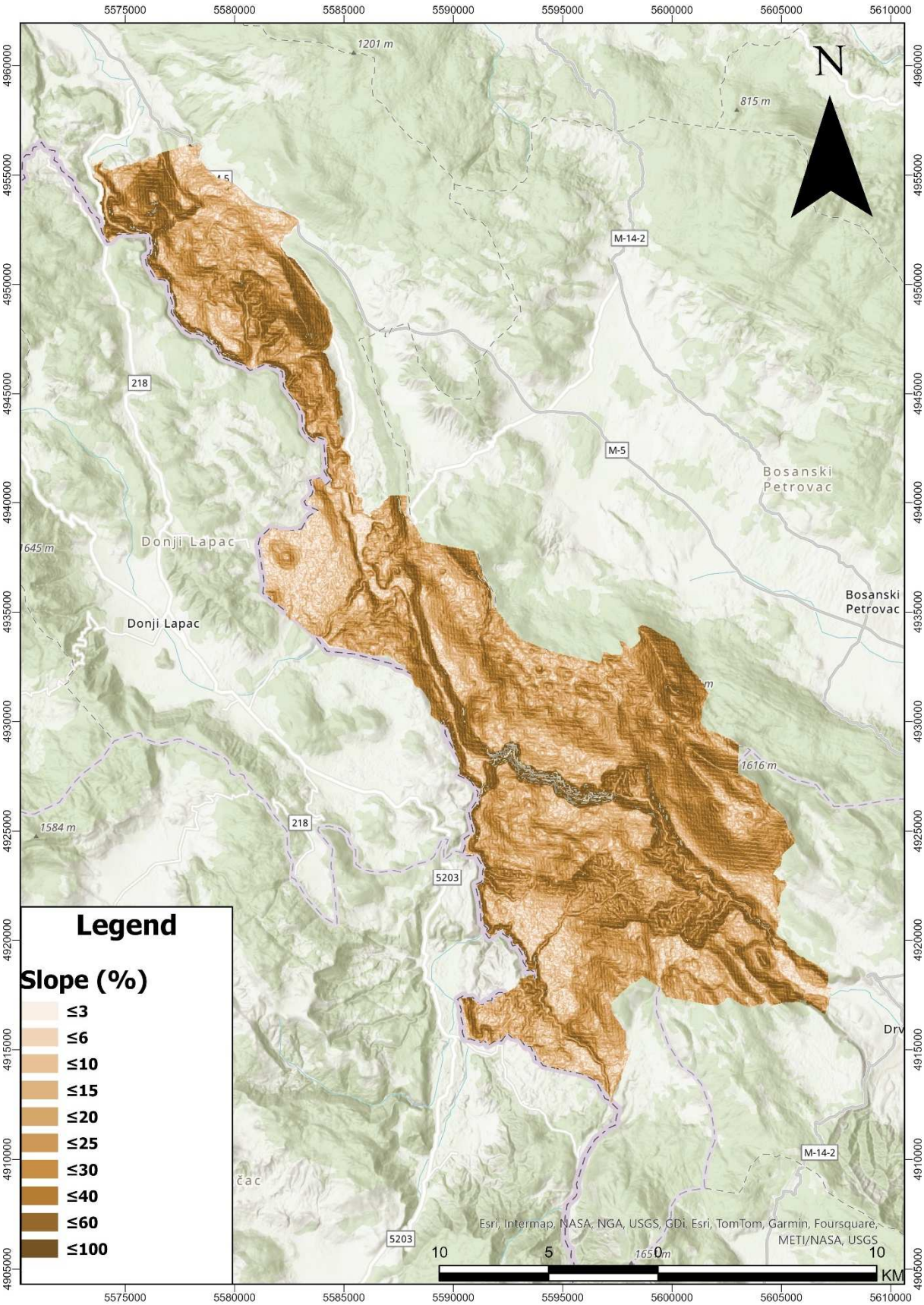

Figure 124. Slope map of the pilot area in Bosnia and Herzegovina.

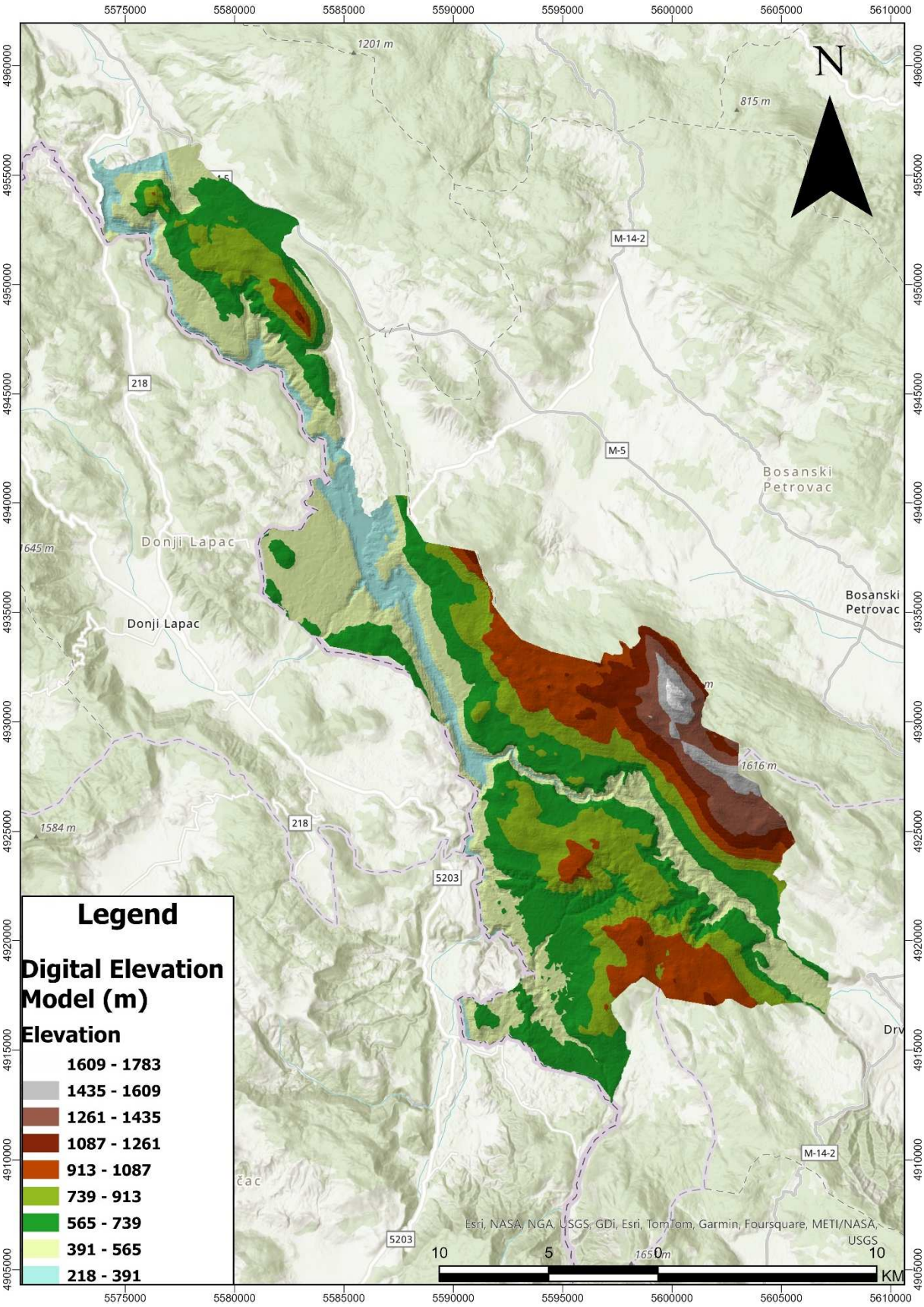

Figure 125. Geomorphology map of the pilot area in Bosnia and Herzegovina.

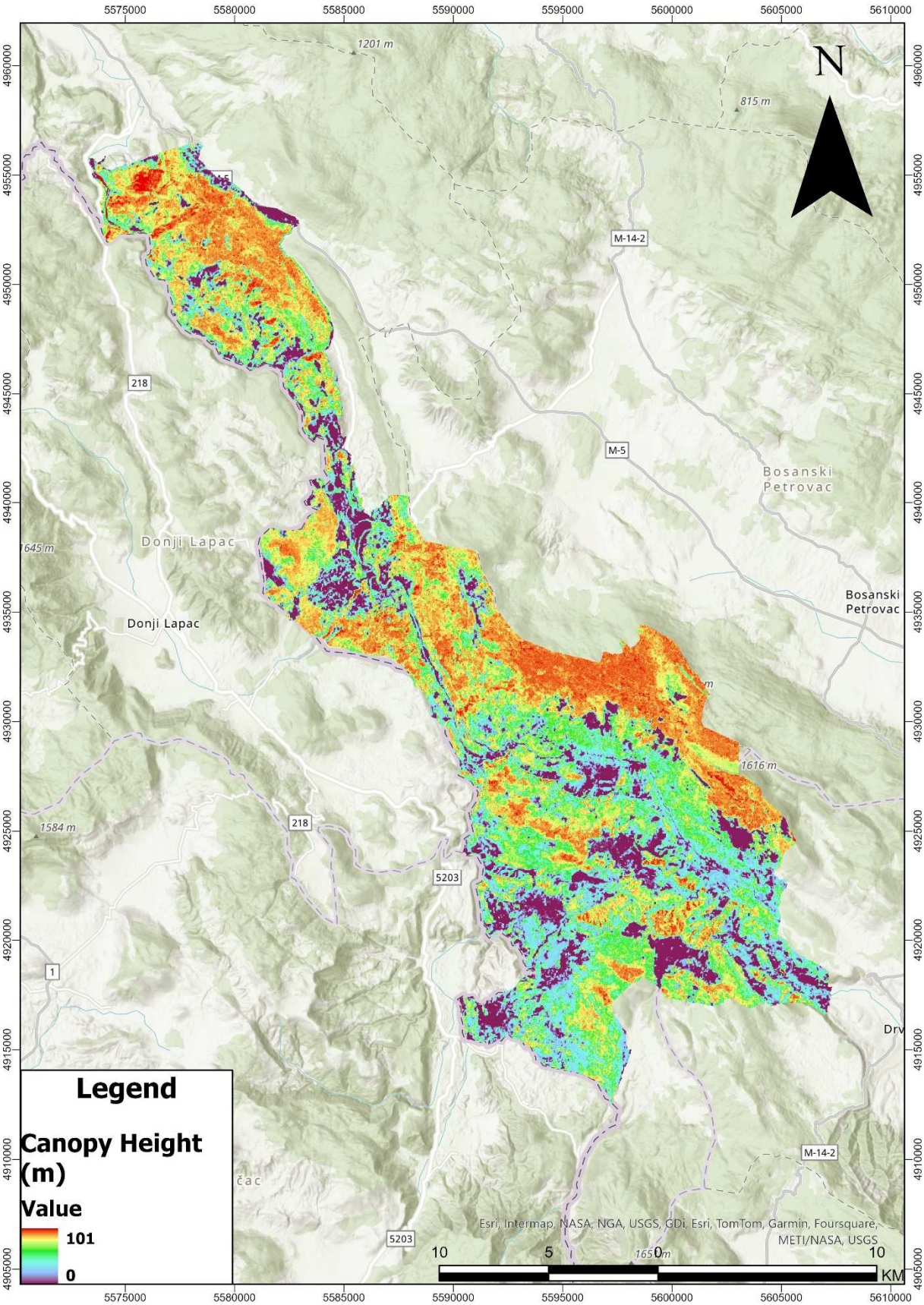

Figure 126. Canopy Height Model of the pilot area in Bosnia and Herzegovina.

- **Tree cover density**

As previously observed from the Canopy Height Model (CHM) map, a significant portion of the area is densely forested. This observation is further supported by the tree cover density map (Figure 127), which shows that apart from the flat areas and urban regions, the remainder of the pilot area is extensively covered by a network of trees. This extensive tree coverage is an important factor to consider, as it could greatly influence the forthcoming analysis of wildfires. Trees are one of the most crucial fuel sources for wildfires, playing a key role in their spread and intensity.

- **Roads and buildings network**

The national park boasts a road network that extends throughout all of the mountainous regions (Figure 128). These roads, which span the entire park, are crucial elements to consider when devising effective strategies for preventing future wildfires. The connectivity provided by this road network is vital for both accessing different parts of the park and implementing preventive measures against wildfires. Understanding the layout and reach of these roads will be instrumental in developing accurate and efficient wildfire prevention methods.

- **NDVI**

The NDVI index vividly illustrates the extensive forest coverage throughout Una National Park. By analyzing Figure 129 and particularly by comparing images from the summer and winter seasons, it becomes evident that the entire region is densely forested, exhibiting high NDVI values in the summer. During the winter, these values decrease significantly across most of the area as trees lose their leaves. This substantial tree cover underscores the park's importance as a biodiversity hotspot, highlighting the need for robust protection measures to ensure its protection from future wildfires.

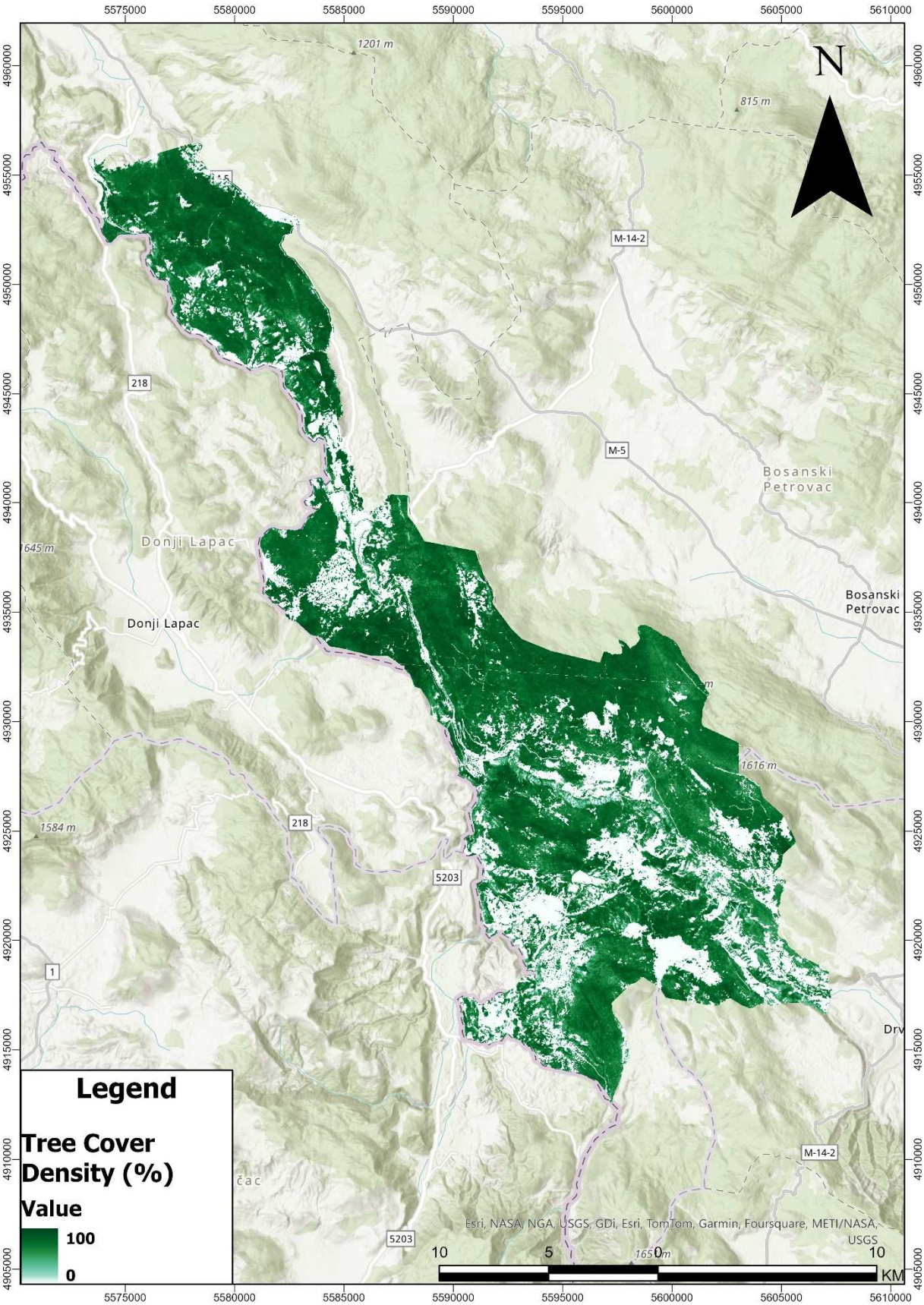

Figure 127. Tree cover density map of the pilot area in Bosnia and Herzegovina.

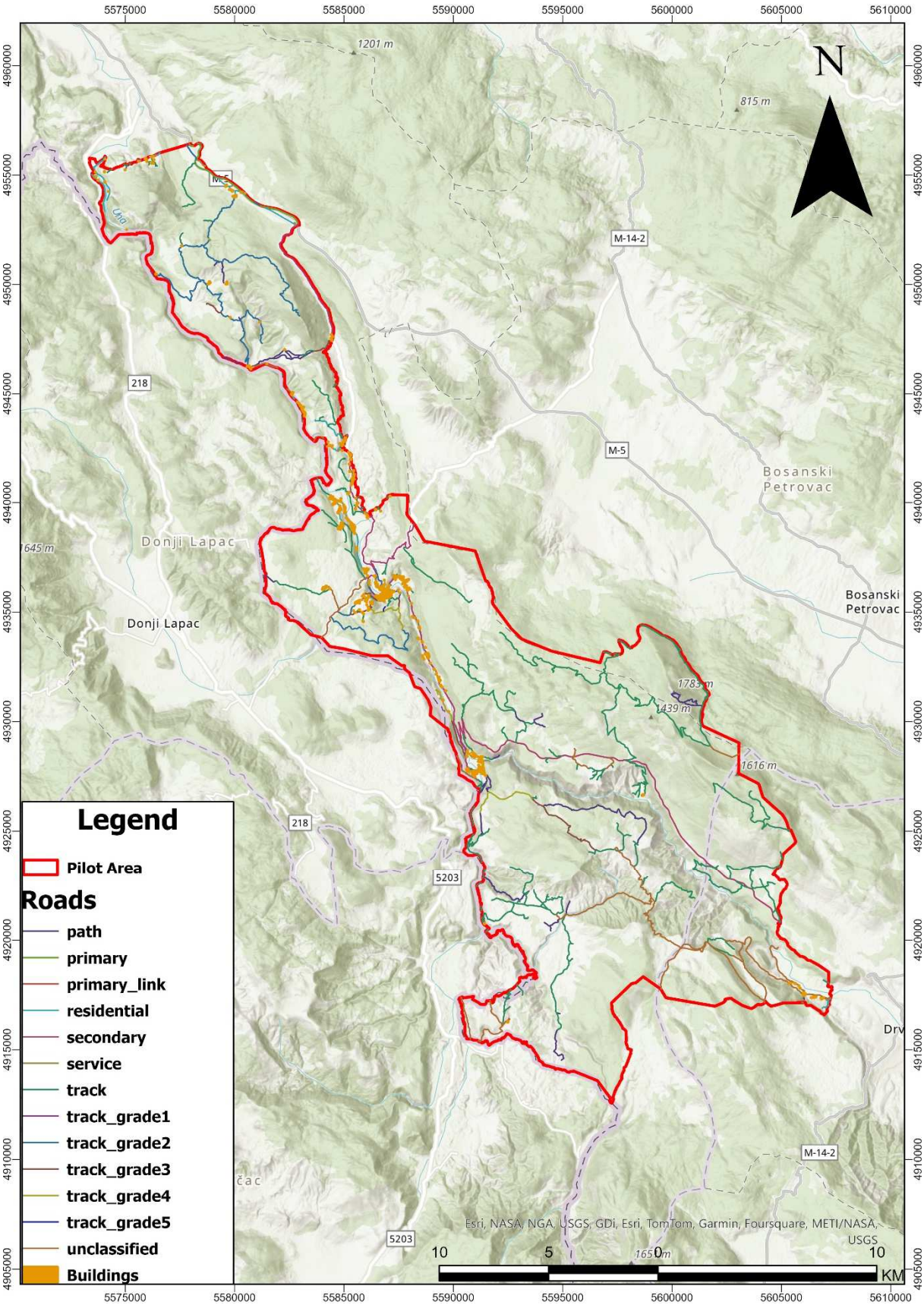

Figure 128. Roads and buildings map of the pilot area in Bosnia and Herzegovina.

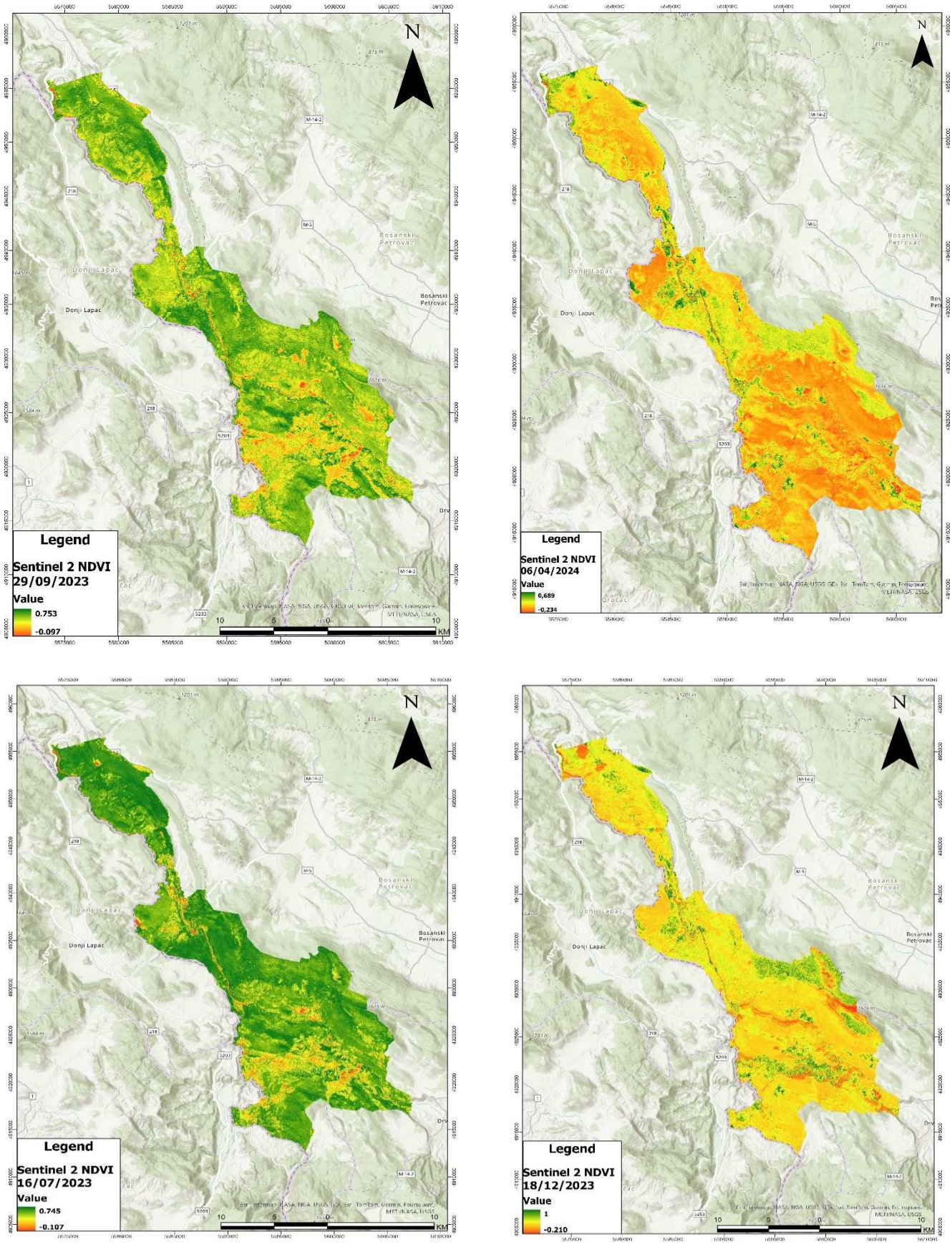

Figure 129. NDVI maps that cover all four seasons for the pilot area of Bosnia and Herzegovina. The autumn NDVI map is displayed at the top left, the spring NDVI map at the top right, the summer NDVI map at the bottom left, and the winter NDVI map at the bottom right.

- **Sentinel 2 images**

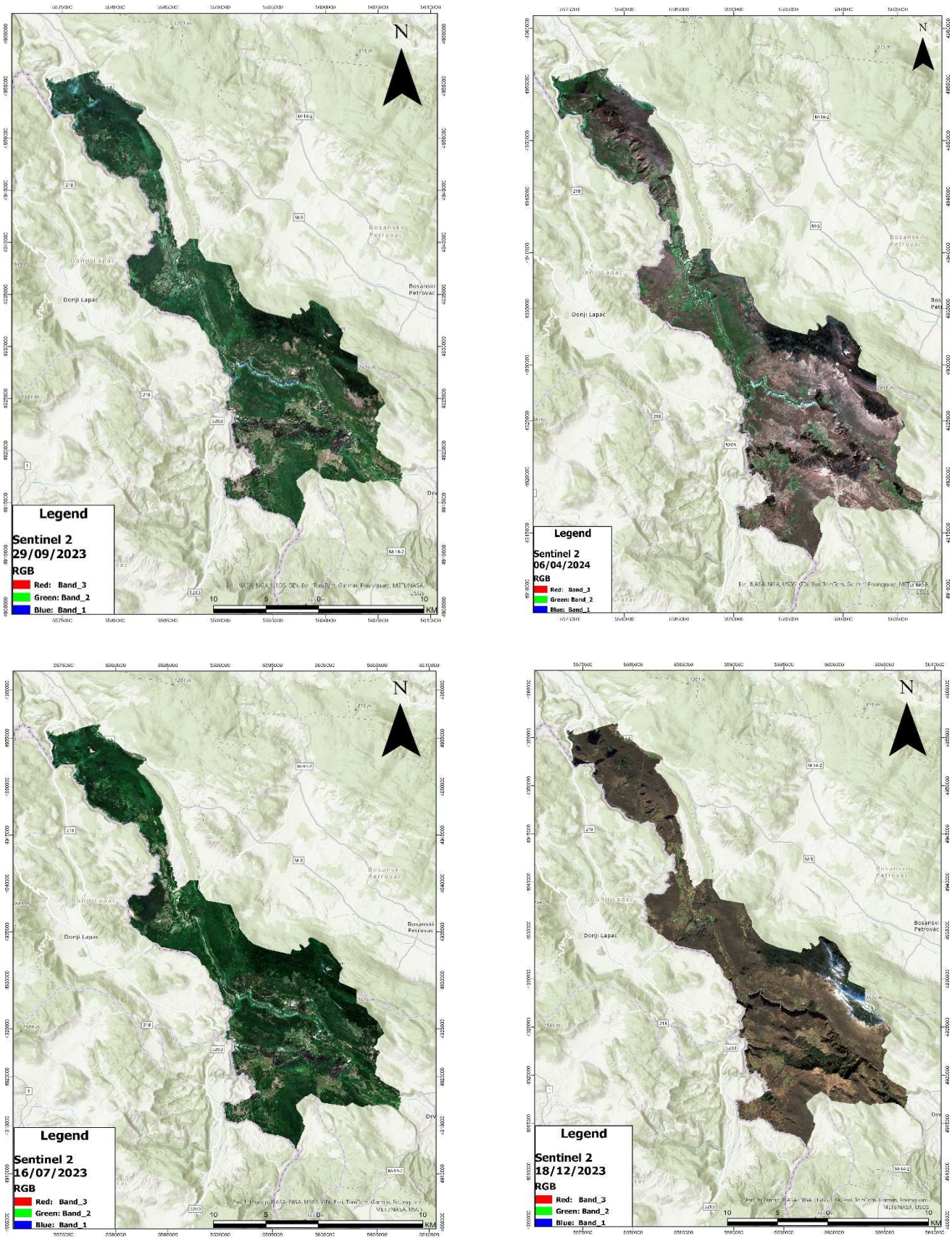

Figure 130. Sentinel 2 satellite images (true color combination) that cover all four seasons for the pilot area of Bosnia and Herzegovina. The autumn Sentinel 2 image is displayed at the top left, the spring one at the top right, the summer one at the bottom left, and the winter one at the bottom right.

- **Planet image**

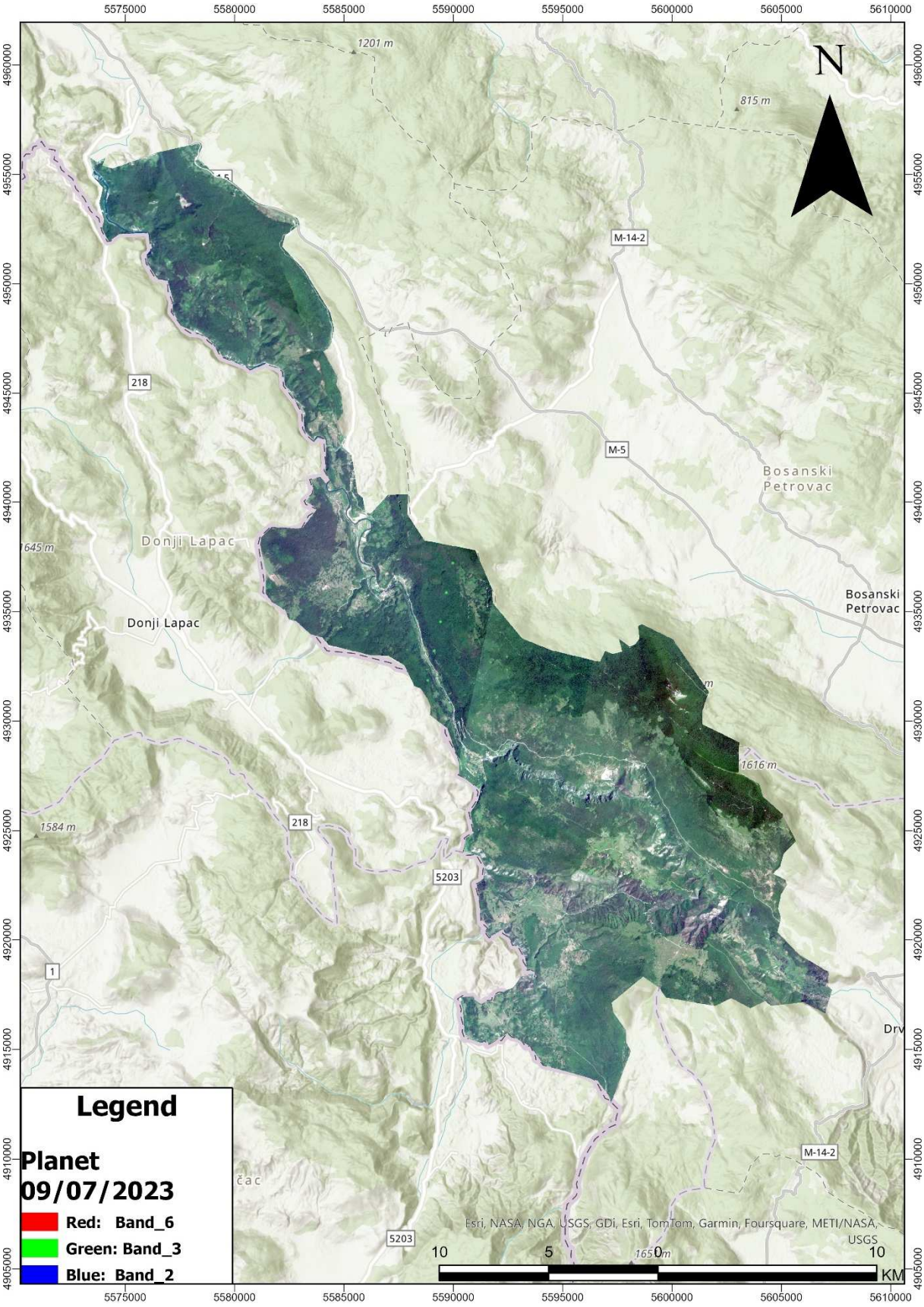

Figure 131. Planet image captured during summer for the pilot area of Bosnia and Herzegovina.

4. Fuel Mapping Methodological Approach

Fuel mapping will be done using Object-Based Image Analysis (OBIA), which is a technique used in remote sensing for image classification and analysis. Unlike traditional pixel-based approaches, OBIA groups pixels into meaningful image objects based on their spectral characteristics. These objects, or segments, are then classified and analyzed according to predefined rules and criteria set by the user. The initial step of OBIA involves creating objects based on the spectral similarity of adjacent pixels. The level of uniformity within each object is determined by the user through an appropriate scale parameter (Bock et al., 2005). Typically, in the final stage of classification, neighboring objects of the same class are merged.

OBIA, as implemented in the software eCognition, offers several advantages over traditional pixel-based methods when applied to High Spatial Resolution data. It effectively addresses within-class variability, and since classification occurs at the object level rather than the pixel level, it allows the use of various shape, texture, and context characteristics in the classification process (Kim et al., 2009; Rittl et al., 2013). Additionally, OBIA prevents the pixelated (salt and pepper) appearance often seen in pixel-based approaches, and the final classification results can be seamlessly integrated into a vector-GIS for further analysis. (Bock et al., 2005).

Another advantage of OBIA, compared to alternative pixel-based methods, is that in the same analysis data with different spatial resolutions can be integrated. Furthermore, ancillary spatial data, such as the ones presented in the previous chapters can also be integrated in the analysis in order to improve the final spatial and thematic accuracy of the produced data. For the needs of the current project Sentinel 2 and Planet data will be integrated. The former, have high spectral resolutions and they probably constitute the best data for large scale mapping, at no cost. The latter have a much better spatial resolution, so they allow a better delimitation of the segments. The combination of the two types of images has been proved extremely effective in fuel and vegetation mapping. Various classifiers will be tested and evaluated for their accuracy, while the entire classification process will be assisted by ground truth data that will be collected by PP9 and all pilot partners. The classification is applied through a set of rules as shown in Figure 132.

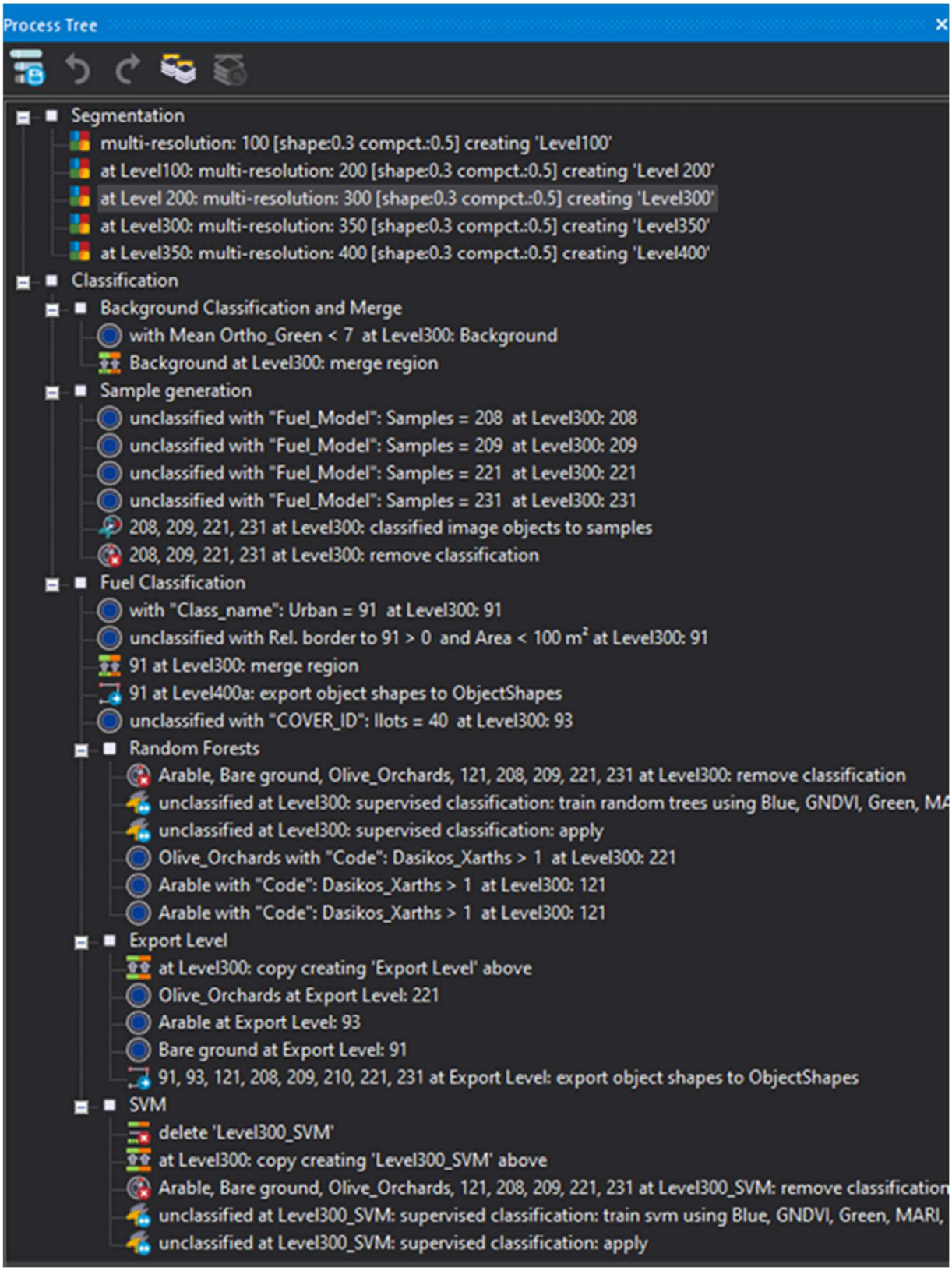

Figure 132. OBIA Classification Algorithm

5. Fire Risk Assessment Methodological Approach

An in-depth analysis of fire risk assessment is essential for this project and therefore should be included in this paper. The Fire Danger Index (FDI) developed by Xofis et al. (2020a, b) will be utilized, incorporating two key components of the fire regime: fuel availability and burnability, and anthropogenic activities. Additionally, it includes the pyric history to indicate an area's potential vulnerability. Fuel availability will be assessed through a combination of remote sensing data, field data on vegetation structure, and compositional characteristics. Anthropogenic activities will be factored into the FDI by considering the proximity to the nearest road or settlement. The pyric history will be integrated by collecting data from local forest services and converting it into a Raster GIS format.

The FlamMap model can be utilized to simulate fire behavior. FlamMap is a One-dimensional fire simulation model that estimates fire behavior under uniform weather conditions. It calculates key components of fire behavior, including fireline intensity, rate of spread, flame height, and crown fire activity. Although FlamMap does not account for ignition points or changing weather conditions during a fire event, it is a powerful tool commonly used to estimate fire risk based on vegetation and topographic characteristics (Calkin et al. 2010). In this context, it is more suitable for this study compared to other simulators like FARSITE, as it allows for the identification of areas with a high potential for high-intensity fires under appropriate weather conditions. Fire behavior simulation using FlamMap generates a number of different parameters of fire behavior including fireline intensity (often called Byram's intensity), rate of spread, flame length e.t.c. Fireline intensity describes the heat release per meter of fire front and is calculated by the following equation which is an adjustment of the original equation developed by Byram:

$I=0.007\ H*W*R$

Where:

I=Fireline intensity in Kw/m

H=Heat yield in cal/g

W=Fuel loading in tonnes/ha

R=Rate of spread in m/min

Fireline intensity estimates will be rescaled to a range between 0 and 1 to create the Fire Intensity (FI) component of the Fire Danger Index (FDI)

formula (1). Rate of Spread (ROS) is also a crucial component of fire behavior, as it significantly influences the time needed for an ignition to develop into a large, difficult-to-suppress wildfire. Preliminary analysis in two study areas revealed that fireline intensity and rate of spread are significantly and positively correlated, with a correlation of approximately 60%. However, certain land cover types, such as grasslands and meadows, exhibit low energy release due to their low fuel load but still have a high ROS. In a complex landscape mosaic like the pilot area of Croatia and the broader Mediterranean region, these land cover types pose a high fire hazard because they increase the likelihood of a wildfire spreading rapidly into nearby areas with high fuel load and high potential for intense fires. Given that the FDI's purpose is to identify areas most vulnerable to high-intensity wildfires and to improve the organization of suppression forces, the ROS is included as a separate component in the FDI formula with a relatively low weight, despite already being a part of the fireline intensity equation. ROS values were also rescaled to a range between 0 and 1 to form the ROS component of the FDI formula (1).

$$FDI=0.5*FI+0.2*ROS+0.2*HI+0.1*PH \quad (1)$$

This formula also incorporates two additional critical components of fire risk: the Human Index (HI) and the Pyric History Index (PH), both serving as proxies for fire ignition probability. The HI captures the fire risk will be associated with human activities, using the distance to roads as a proxy. Values range from 0, for areas 200 meters or more away from roads, to 1 for areas in immediate proximity, as closer distances have been linked to higher ignition frequency (Ricota et al. 2018; Catry et al. 2009). The PH, while not directly related to fire hazard, since past fires may reduce fuel load and thus fire intensity, provides insights into fire patterns linked to specific land uses and locations. For example, in the eastern Mediterranean, where free-range pastoralism is common, deliberate fires set by shepherds to improve grazing conditions create a pattern of clustered past fires, indicating higher fire risk areas. Although these fires are typically low-intensity due to their occurrence in autumn and in low-fuel areas, they still pose a risk of spreading to more flammable ecosystems. Including the PH index helps identify areas with specific patterns of past fires. The PH will be calculated using ignition data, applying a Kernel Density Estimation Function to convert point data into a raster file, with values from 0 (far from past ignition points) to 1 (close to past ignition points). The resulting FDI ranges from 0 to 1, with higher values indicating greater fire hazard.

The fire risk assessment is closely tied to accurately mapping the biomass, which includes the fuel component. Therefore, precise mapping of fuel dispersion is crucial. The initial step in this process involves identifying the fuel models present in the study area. Using field-collected data, each of the samples will be assigned a fuel model that best represents its biomass characteristics. Based on field observations, collected data, and international literature on Mediterranean vegetation types, fuel models will be determined.

Ancillary data will be utilized to delineate agricultural and urban areas, while the tree cover density data will also be used. The classification process will be supported by ground truth data that will be collected. Additionally, sample data will be gathered through the visual inspection of VHR (Very High Resolution) aerial photographs. Various classifiers will be tested for their effectiveness in identifying the selected fuel models. The performance of each classifier will be evaluated based on its efficiency in accurately reproducing the training set.

The classification will happen through the use of the object-based image analysis (OBIA) and also the Canopy Height Model (CHM) for each polygon will also be utilized while Canopy Base Height (CBH) will be assigned to each polygon based on the nearest sampled point and Crown Bulk Density will be computed in arc fuels. Consequently, five raster datasets will be produced, which are essential for implementing fire simulations.

The generated raster data, along with the Digital Elevation Model (DEM), the aspect model and the slope model, will be utilized in the fire simulation model FlamMap (Finney, 2006) to estimate potential Fireline Intensity and fire Rate of Spread. The study aims to evaluate fire hazard in the area in a spatially explicit manner under conditions favoring high-intensity fires. Recent major fires in the Eastern Mediterranean region, such as in Evros, Greece, occurred during the summer of 2023, the hottest on record for the area, marked by three consecutive heatwaves from June to August and wind patterns conducive to fire spread and intensity (Founta & Giannakopoulos, 2009; Tolika et al., 2009). Given the likelihood of such extreme weather events becoming more frequent in the future rather than remaining exceptionally rare, fire behavior simulations should be conducted under an extreme scenario with wind speeds of 35 km/h, assuming a prevailing south wind during summer. Fuel moisture parameters will be set at 3%, 4%, 5%, 30%, and 60% for 1-hour, 10-hour, 100-hour, live-woody, and live-herbaceous fuels, respectively.

6. Weather forecast data

For the characterisation of the project's study areas, an in-depth search was made of the available weather forecast datasets covering the whole EU Mediterranean area. The dataset to be used was selected according to the following criteria:

- Geographical coverage: the dataset should possibly cover all the study areas included in the partner countries. The use of a unique dataset for the entire area would allow a harmonisation of the data both in terms of data acquisition methods and for the climatic variables considered;
- Geometric resolution: the dataset should have sufficient geometric resolution (pixel size) to express the local variability of the weather-climate data;
- Climatic variables available in the dataset, both to be able to better characterise the areas of interest from a climatic point of view, and for the variables to be such that they can be used for a possible subsequent processing of the FWI (Canadian Forest Fire Weather Index);
- Availability of forecast data: the climate dataset had to be able to provide the forecast data for the next day, so that the calculation of FWI could take place the day before for the following day in such a way as to function as a "fire danger" warning system on the basis of the weather trend;
- Data quality: Recognition of the dataset by international bodies of meteorological data studies, and use of the dataset by local authorities and organisations were taken into account;
- Availability of an open API (Application Programming Interface) service, in order to be able to integrate such data within FRED platform programmatically.

The selected weather forecast datasets are those provided by the Meteo Italian Supercomputing Portal - MISTRAL (https://www.mistralportal.it/), a project co-funded by the EU aimed to build an Italian open weather data platform to provide national and international citizens, public administrations, and private organizations with weather data from observational networks, historical and real-time analysis and forecasts. Since 2021, the European Centre for Medium-Range Weather Forecasts (ECMWF) extracts regional observational data available in real-time from the MISTRAL Meteo-Hub. These data are used by ECMWF in the assimilation phase for numerical forecast models, thus increasing the observational database used until now. The use of observational data by ECMWF testifies to the added

value that regional observational weather data acquire through sharing on Meteo-Hub.

More specifically, MISTRAL offers two types of datasets of interest to FRED:

- **COSMO-5M** (COSMO at 5km – Mediterranean Region), a numerical integration of the forecast model called COSMO with a 5 km grid covering the whole Mediterranean Europe, thus including all FRED pilot areas. It includes two runs per day (00 and 12 UTC) of 18-hour assimilation (including the repetition of the last 6 hours of the previous run) and two runs per day (00 and 12 UTC) of 72-hour forecast and
- **COSMO-2I** (COSMO at 2.2km – Italy area), another numerical integration of the forecast COSMO model with a 2.2 km grid which covers not only the entire Italian territory, but also part of the countries facing the Adriatic Sea. In particular, all FRED pilot areas are covered by this dataset with the only exception of Portuguese one. It also represents a numerical integration of the COSMO forecast model. The procedure includes two runs per day (00 and 12 UTC) of 48-hour forecasts.

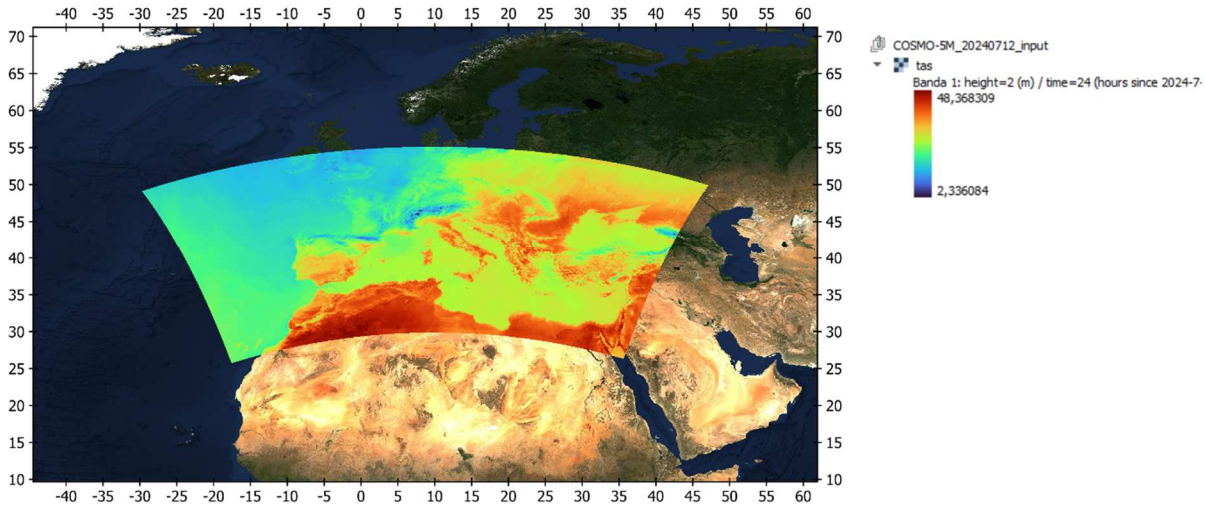

Figure 133. COSMO-5M: Forecasted Air temperature (°C) at noon on 12 July, 2024.

To get an idea of the geographical coverage of COSMO-5M weather forecast dataset, look at the Figure 133.

6.1. How to download the MISTRAL forecast data using the APIs

The forecast datasets for every day of the last week and for two runs per day are released as open data in the GRIB (General Regularly distributed Information in Binary form) format, a WMO (World Meteorological Organisation) standard format. To download them, users can directly use the following Meteo-Hub APIs:

- To get the list of all GRIB files for a specific dataset:

```
GET https://meteohub.mistralportal.it/api/datasets/{dataset_name}/opendata
```

where the query parameter `dataset_name` is the name of the dataset of which the packages list is referred (e.g., `COSMO-2I` or `COSMO-5M`).

- To ask for download a specific GRIB file (whose filename is known):

```
GET https://meteohub.mistralportal.it/api/opendata/{filename}
```

where the query parameter `filename` is the name of the package to download (e.g., `data-20240526T190845Z-93c81644-a741-4981-b293-02f2ae2a56ee.grib`)

- To ask for download one or more GRIB files related to a specific dataset, a specific reference date and/or a specific run (without knowing the filename):

```
GET
https://meteohub.mistralportal.it/api/opendata/{dataset_name}/download?reft
ime={reference_date}&run={run}
```

where the query parameter `dataset_name` is the name of the dataset of which the packages download is requested (e.g., `COSMO-2I` or `COSMO-5M`), the `reference_date` parameter can be expressed with the following data formats: YYYYMMDD or YYYY-mm-dd where YYYY stays for year, mm for month and dd for day (e.g., `20240526` or `2024-05-26`), and finally the `run` parameter in the time format HH:MM, where HH stays for hour and MM stays for minutes (e.g., `12:00`). The time for run parameter is intended as UTC.

No authentication is required to use these previously described APIs, unless the request of open data download refers to a dataset with restricted access. Source: https://www.mistralportal.it/user-guide/#jump-api (accessed 11/07/2024).

6.2. Meteorological variables of interest

Among the meteorological variables included in the COSMO-5M and COSMO-2I datasets, there are the following hourly forecast data:

- Air temperature [°C] at 2 m;
- Dew point temperature [°C] at 2 m;

- u-component of wind [m/s] at 10 m;
- v-component of wind [m/s] at 10 m;
- Total precipitation [kg/m^2].

These forecast data could be used to calculate the relative humidity, the wind speed, as well as the 24 h-cumulated precipitation at noon, which together with the air temperature at noon are the input meteorological variables for the calculation of the FWI, unless the initial condition.

6.3. How to retrieve the FWI input parameters from MISTRAL data

To retrieve the input meteorological variables for the FWI calculation it is necessary to extract and process the preliminary variables from the GRIB file. For instance, in Windows Subsystem for Linux (WSL), we can download the data of our interest (e.g., COSMO-2I forecast data related to 21/06/2024, run at 12:00) by executing the following API:

```
wget --content-disposition \
"https://meteohub.mistralportal.it/api/opendata/COSMO-
2I/download?reftime=20240621&run=12:00"
```

To extract the input data for the calculation of FWI on the day following the day of the forecast, the use of specialized packages and libraries as ecCodes, CDO and xclim is recommended. To this aim, we can create a Conda environment (e.g., `mistral-env`) and install the requirements:

```
# Create and activate a conda environment
conda create -n mistral-env
conda activate mistral-env

# Install packages
conda install -c conda-forge python-eccodes cdo xclim gdal
```

it is possible to execute the following bash script (e.g., `grib2nc.sh`):

```
#!/usr/bin/env bash

# input parameters
GRIB=$1
PREFIX=$2
DATA_FOLDER=data

mkdir -p $DATA_FOLDER
cd $DATA_FOLDER

echo Filtering GRIB messages into separate GRIB files...
grib_copy $GRIB -w stepRange=24 "[shortName]_[stepRange].grib"

echo Converting 2m temperature...
cdo -f nc \
```

```
    -setattribute,tas@standard_name="air_temperature",tas@long_name="noon
temperature",tas@units="degC",tas@cell_method="time: point" \
    -subc,273.15 \
    -chname,var11,tas \
    2t_24.grib temp.nc

echo Calculating 10m wind speed...
grib_copy -M 10u_24.grib 10v_24.grib wind_components.grib
cdo -f nc \
    -setattribute,u10@standard_name="eastward_wind",u10@long_name="u-
component of wind at
10m",u10@units="km/h",v10@standard_name="northward_wind",v10@long_name="v-
component of wind at 10m",v10@units="km/h" \
    -mulc,3.6 \
    -chname,var33,u10,var34,v10 \
    wind_components.grib wind_components.nc
xclim -v -i wind_components.nc -o wind.nc wind_speed_from_vector --uas u10
--vas v10

# filter total precipitation
grib_copy -w shortName=tp,stepRange=0-1/1-2/2-3/3-4/4-5/5-6/6-7/7-8/8-9/9-
10/10-11/11-12/12-13/13-14/14-15/15-16/16-17/17-18/18-19/19-20/20-21/21-
22/22-23/23-24 $GRIB tp_0-24.grib

echo Calculating 24h total precipitation...
cdo -f nc \
    -setattribute,pr@standard_name="precipitation_flux",pr@long_name="24-
hour precipitation",pr@units="mm/d",pr@cell_method="time: sum(interval: 1
day aggregation: sum)" \
    -chname,var61,pr \
    -shifttime,30minutes \
    -daysum \
    -shifttime,11hours \
    tp_0-24.grib prec.nc

echo Calculating relative humidity...
cdo -f nc \
    -setattribute,tas@standard_name="air_temperature",tas@long_name="noon
air temperature",tas@units="degK",tas@cell_method="time:
point",tdps@standard_name="dew_point_temperature",tdps@long_name="noon dew
point temperature",tdps@units="degK",tdps@cell_method="time: point" \
    -chname,var11,tas,var17,tdps \
    temperatures.grib temperatures.nc
xclim -v -i temperatures.nc -o rh.nc hurs_fromdewpoint --tas tas --tdps
tdps --method 'sonntag90'

echo Merging NetCDF files...
cdo -O merge temp.nc wind.nc prec.nc rh.nc ${PREFIX}_input.nc

# clean temporary data
rm tp*.grib *_24.grib temp*.* wind*.* prec.nc rh.nc lat*.nc out*.nc *.txt
```

```
# Run the grib2nc.sh script
./grib2nc.sh ~/mistral/data/data-20240621T175426Z-e55f2100-81ad-4e19-8019-
2624acf5366e.grib COSMO-2I_20240622
```

The Coordinate System (CS) in which the gridded forecast data are represented is a rotated latitude longitude CS with the following Well-Known Text (WKT):

```
GEOGCRS["Coordinate System imported from GRIB file",
    BASEGEOGCRS["Coordinate System imported from GRIB file",
        DATUM["unnamed",
            ELLIPSOID["Sphere",6367470,0,
                LENGTHUNIT["metre",1,
                    ID["EPSG",9001]]]],
        PRIMEM["Greenwich",0,
            ANGLEUNIT["degree",0.0174532925199433,
                ID["EPSG",9122]]]],
    DERIVINGCONVERSION["Pole rotation (GRIB convention)",
        METHOD["Pole rotation (GRIB convention)"],
        PARAMETER["Latitude of the southern pole (GRIB convention)",-47,
            ANGLEUNIT["degree",0.0174532925199433,
                ID["EPSG",9122]]],
        PARAMETER["Longitude of the southern pole (GRIB convention)",10,
            ANGLEUNIT["degree",0.0174532925199433,
                ID["EPSG",9122]]],
        PARAMETER["Axis rotation (GRIB convention)",0,
            ANGLEUNIT["degree",0.0174532925199433,
                ID["EPSG",9122]]]],
    CS[ellipsoidal,2],
        AXIS["latitude",north,
            ORDER[1],
            ANGLEUNIT["degree",0.0174532925199433,
                ID["EPSG",9122]]],
        AXIS["longitude",east,
            ORDER[2],
            ANGLEUNIT["degree",0.0174532925199433,
                ID["EPSG",9122]]]]
```

Save the WKT as text file (e.g., `grib_cs.wkt`) in the same folder containing data. Finally, it is possible to use the `gdalwarp` utility program of the GDAL library to transform the forecast data from the rotated lat-lon CS to another CS (e.g., geographic lat-lon, EPSG:4326) and convert data to another format (e.g., GeoTIFF), as follows:

```
# Air temperature (degC) at noon
gdalwarp -tr 0.02 0.02 -s_srs grib_cs.wkt -t_srs EPSG:4326 NETCDF:"COSMO-
2I_20240622_input.nc":tas COSMO-2I_20240622_temperature.tif

# Wind speed (km/h) at noon
gdalwarp -tr 0.02 0.02 -s_srs grib_cs.wkt -t_srs EPSG:4326 NETCDF:"COSMO-
2I_20240622_input.nc":sfcWind COSMO-2I_20240622_wind_speed.tif

# 24h-cumulated precipitation (mm) at noon
```

```
gdalwarp -tr 0.02 0.02 -s_srs grib_cs.wkt -t_srs EPSG:4326 NETCDF:"COSMO-
2I_20240622_input.nc":pr COSMO-2I_20240622_24h_precipitation.tif

# Relative humidity (%) at noon
gdalwarp -tr 0.02 0.02 -s_srs grib_cs.wkt -t_srs EPSG:4326 NETCDF:"COSMO-
2I_20240622_input.nc":hurs COSMO-2I_20240622_relative_humidity.tif
```

The COSMO-2I Air temperature and Relative humidity at noon are represented in Figure 134, while 24-h precipitation and Wind speed at noon in Figure 135.

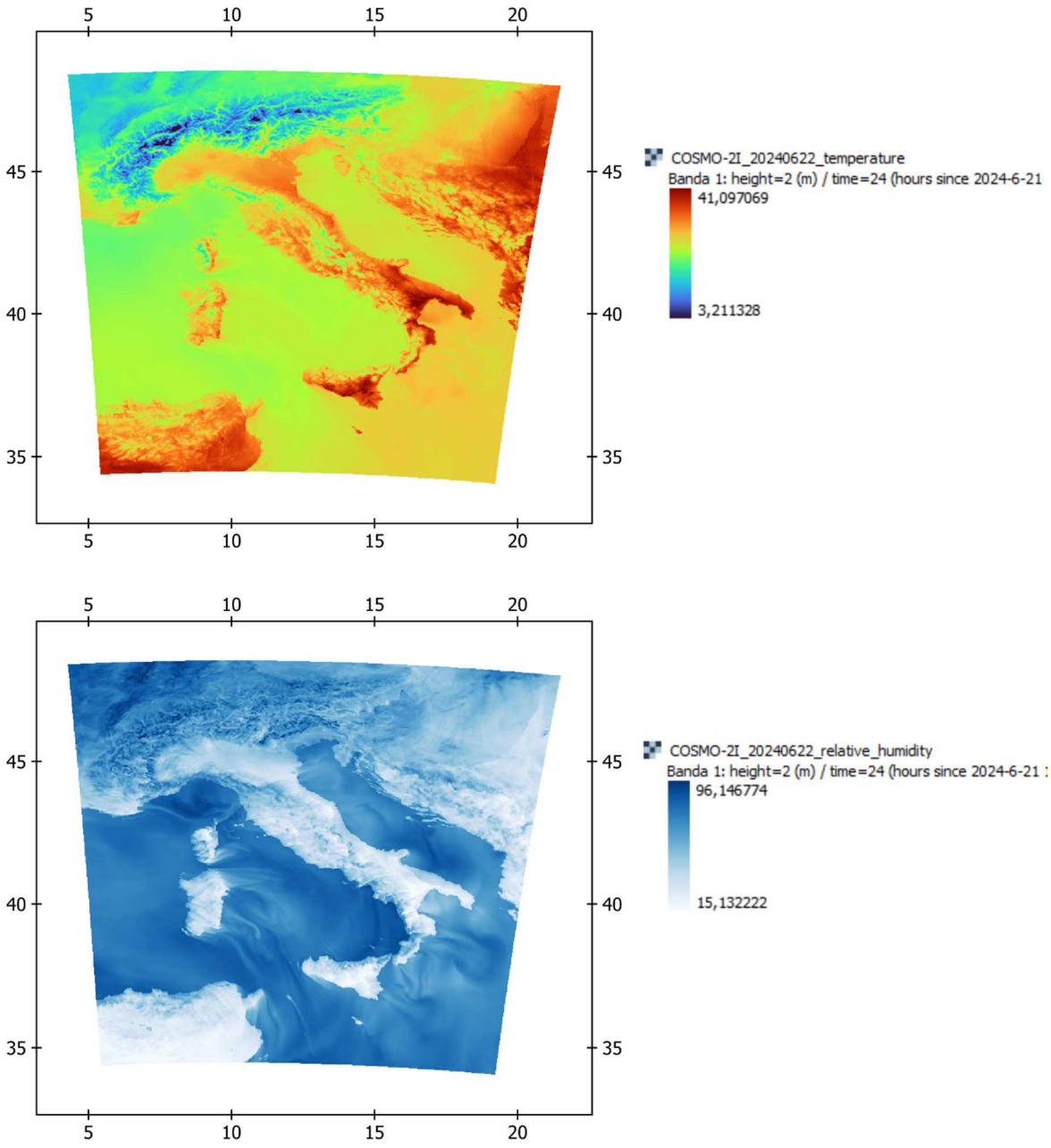

Figure 134. COSMO-2I: Air temperature and Relative humidity forecasted at noon on 22 June, 2024.

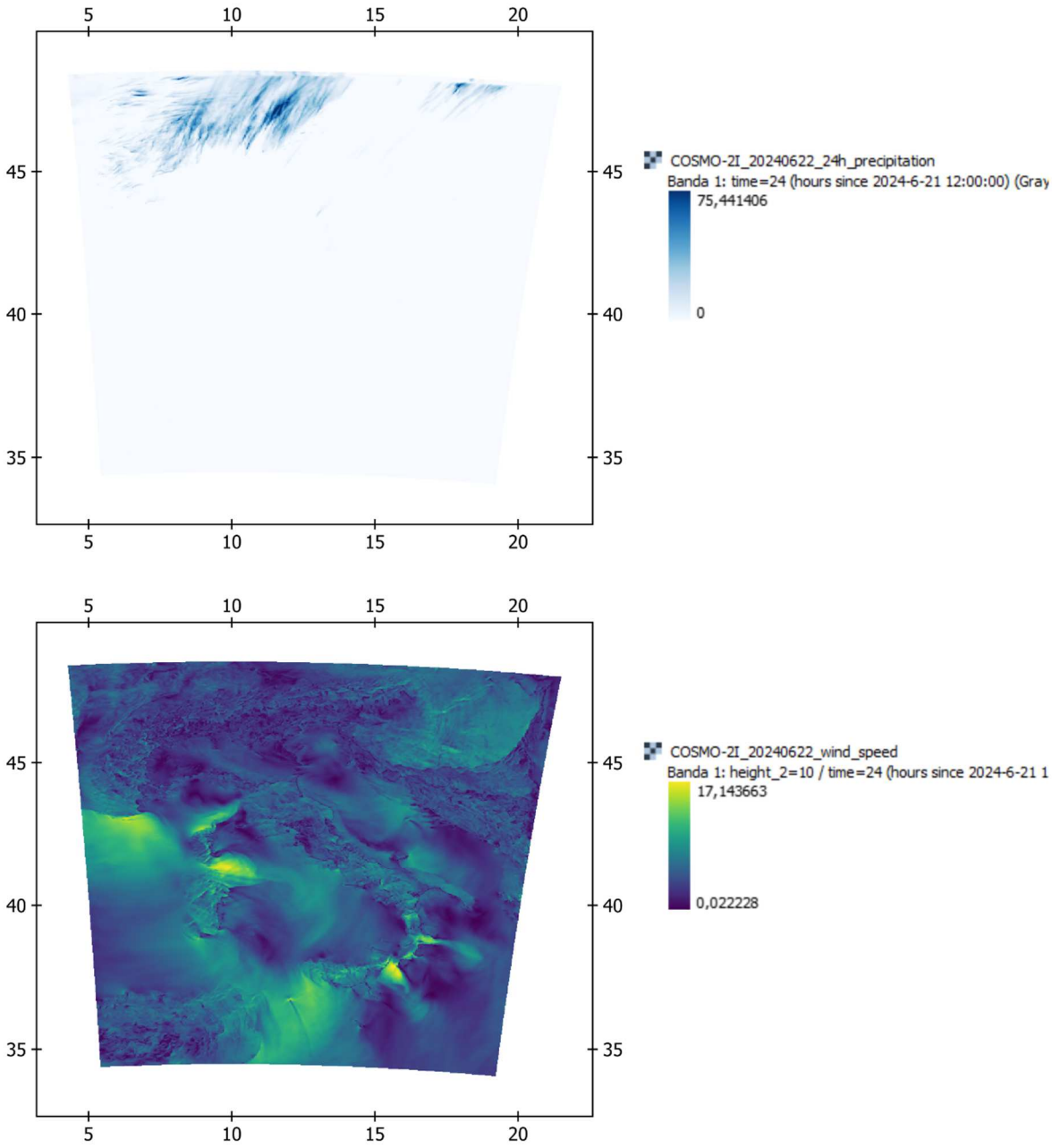

Figure 135. COSMO-2I: Air temperature and Relative humidity forecasted at noon on 22 June, 2024.

References

1. Alexander, L. V., Zhang, X., Peterson, T. C., Caesar, J., Gleason, B., Tank, A. K., ... & Collins, D. (23). Coauthors, 2006: Global observed changes in daily climate extremes of temperature and precipitation. J Geophys Res 111, D05109.
2. Alpert, P., Ben-Gai, T., Baharad, A., Benjamini, Y., Yekutieli, D., Colacino, M., ... & Manes, A. (2002). The paradoxical increase of Mediterranean extreme daily rainfall in spite of decrease in total values. Geophysical Research Letters,29(11), 31-1.
3. Arnell, N.W., Liu, C., Compagnucci, R., da Cunha, L., Hanaki, K., Howe, C., Mailu, G., Shiklomanov, I., Stakhiv, E., 2001. Hydrology and water resources. In: McCarthy, J.J., Canziani, O.F., Leary, N.A., Dokken, D.J., White, K.S. (Eds.) (2001). IPCC Climate Change 2001: Impacts, Adaptation & Vulnerability, The Third Assessment Report of Working Group II of the Intergovernmental Panel on Climate Change (IPCC), 1000. Cambridge University Press, Cambridge, UK, pp. 133-191.
4. Barros, V. R., Doyle, M.E., Camilloni, I.A. (2008). Precipitation trends in southeastern South America: relationship with ENSO phases and with low-level circulation. Theoretical and Applied Climatology, 93(1-2), 19-33.
5. Bartolini, G., Morabito, M., Crisci, A., Grifoni, D., Torrigiani, T., Petralli, M., ... & Orlandini, S. (2008). Recent trends in Tuscany (Italy) summer temperature and indices of extremes. Int J Climatol 28(13), 1751-1760.
6. Begert, M., Schlegel, T., Kirchhofer, W. (2005). Homogeneous temperature and precipitation series of Switzerland from 1864 to 2000. Int. J. Climat., 25(1), 65-80.
7. Benestad, R.E., Melsom, A. (2002). Is there a link between the unusually wet autumns in southeastern Norway and sea-surface temperature anomalies? Climate Research, 23(1), 67-79.
8. Boccolari, M., Malmusi, S. (2013). Changes in temperature and precipitation extremes observed in Modena, Italy. Atmos Res 122, 16-31.
9. Bock, M., Xofis, P., Rossner, G., Wissen, M., Mitchley, J. Object oriented methods for habitat mapping in multiple scales: Case studies from Northern Germany and North Downs, GB. J. Nat. Conserv. 2005, 13, 75–89.
10. Bono, E., La Loggia, G., Noto, L.V. (2005). Spatial interpolation methods based on the use of elevation data. Geophysical Research Abstracts 7, 08893.
11. Brath, A., Castellarin, A., Montanari, A. (1999). Detecting non stationarity in extreme rainfall data observed in Northern Italy. Proceedings of EGS – Plinius Conference on Mediterranean Storms, Maratea, 219-231.
12. Broecker, W. S. (1975). Climate change: are we on the brink of a pronounced global warming? Science 188:460-463.
13. Brunetti, M., Buffoni, L., Mangianti, F., Maugeri, M., & Nanni, T. (2004). Temperature, precipitation and extreme events during the last century in Italy. Global Planet Change 40(1), 141.
14. Brunetti, M., Maugeri, M., Monti, F., & Nanni, T. (2006). Temperature and precipitation variability in Italy in the last two centuries from homogenised instrumental time series. Int J Climatol 26(3), 345-381.-149.
15. Brunetti, M., Maugeri, M., Monti, F., Nanni, T. (2006). Temperature and precipitation variability in Italy in the last two centuries from homogenised instrumental time series. Int. J. Climat., 26(3), 345-381.

16. Burn, D.H., Hag Elnur, M.A. (2002). Detection of hydrologic trends and variability. Journal of hydrology, 255(1), 107-122.

17. Calkin, D.E., Ager, A.A., Gilbertson-Day, J. Wildfire risk and hazard: procedures for the first approximation. Gen. Tech. Rep. RMRS-GTR-235. Fort Collins, CO: U.S. Department of Agriculture, Forest Service, Rocky Mountain Research Station. 2010, 62 p.

18. Caloiero, T., Buttafuoco, G., Coscarelli, R., & Ferrari, E. (2015). Spatial and temporal characterization of climate at regional scale using homogeneous monthly precipitation and air temperature data: an application in Calabria (southern Italy). Hydrology Research 46(4), 629-646.

19. Catry, F.X., Rego, F.C., Bacao, F., Moreira, F. Modelling and mapping wildfire ignition risk in Portugal, Int. J. Wildland Fire 2009, 18, 921-931.

20. Chen, I.C., Hill, J.K., Ohlemüller, R., Roy, D.B., Thomas, C.D. (2011). Rapid range shifts of species associated with high levels of climate warming. Science, 333(6045), 1024-1026.

21. Cheung, W.H., Senay, G.B., Singh, A. (2008). Trends and Spatial Distribution of Annual and Seasonal Rainfall in Ethiopia. Int. J. Climatol., 28, 1723-1734.

22. Clark, W. A., Hosking, P. L. (1986). Statistical methods for geographers. John Wiley & Sons Inc.

23. Dai, A., Fung, I.Y., Del Genio, A.D. (1997). Surface observed global land precipitation variations during 1900–1988. J. Clim. 10, 2943-2962.

24. Davison, A.C., Hinkley, D.V. (1997). Bootstrap Methods and their Applications, Cambridge Series in Statistical and Probabilistic Mathematics.

25. De Luis, M.D., Raventós, J., González-Hidalgo, J.C., Sánchez, J.R., Cortina, J. (2000). Spatial analysis of rainfall trends in the region of Valencia (East Spain). Int. J. Climat., 20(12), 1451-1469.

26. De Michele, C., Montanari, A.,mRosso, R. (1998). The effects of non-stationarity on the evaluation of critical design storms. Wat. Sci. Tech., 37(11), 187–193.

27. Domonkos, P., Kyselý, J., Piotrowicz, K., Petrovic, P., & Likso, T. (2003). Variability of extreme temperature events in south–central Europe during the 20th century and its relationship with large-scale circulation. Int J Climatol 23(9), 987-1010.

28. Donat, M.G., Alexander, L.V., Yang, H., Durre, I., Vose, R., Dunn, R.J.H., ... & Hewitson, B. (2013). Updated analyses of temperature and precipitation extreme indices since the beginning of the twentieth century: the HadEX2 dataset. J Geophys Res Atmos, 118(5), 2098-2118.

29. Douglas, E.M., Vogel, R.M., Kroll, C.N. (2000). Trends in floods and low flows in the United States: impact of spatial correlation. Journal of Hydrology, 240(1), 90-105.

30. Easterling, D.R., Horton, B., Jones, P.D., Peterson, T.C., Karl, T.R., Parker, D.E., ... & Folland, C.K. (1997). Maximum and minimum temperature trends for the globe. Science 277(5324), 364-367.

31. Efron, B. (1979). Bootstrap methods: another look at the jackknife. The annals of Statistics, 1-26.

32. El Kenawy, A., López-Moreno, J.I., Vicente-Serrano, S.M. (2012). Trend and variability of surface air temperature in northeastern Spain (1920–2006): linkage to atmospheric circulation. Atmos Res 106, 159-180.

33. Esteban-Parra, M.J., Rodrigo, F.S., Castro-Diez, Y. (1998). Spatial and temporal patterns of precipitation in Spain for the period 1880–1992. Int. J. Climat., 18(14), 1557-1574.

34. Field, C.B., Barros, V.R., Mach, K., Mastrandrea, M. (2014). Climate change 2014: impacts, adaptation, and vulnerability. Contribution of working group II to the fifth assessment report of the Intergovernmental Panel on Climate Change, Cambridge University Press.

35. Fienberg, S.E. (1994). The analysis of cross-classified categorical data, 2nd edn. Cambridge, Massachusetts: The MIT Press.

36. Finkel, J.M., Katz, J.I. (2017). Changing US Extreme Temperature Statistics. arXiv preprint arXiv:1701.05224. Submitted to Int J Climatol.

37. Finney M.A. (2006) An Overview of FlamMap Fire Modeling Capabilities. USDA Forest Service Proceedings RMRS-P-41. 2006.

38. Fioravanti, G., Piervitali, E., & Desiato, F. (2016). Recent changes of temperature extremes over Italy: an index-based analysis. Theor Appl Climatol 123(3-4), 473-486.

39. Founda, D., Giannakopoulos, C., (2009). The exceptionally hot summer of 2007 in Athens,Greece—a typical summer in the future climate? Global Planetary Change, 67, 227–236.

40. Garbrecht, J., Van Liew, M., Brown, G.O. (2004). Trends in precipitation, streamflow, and evapotranspiration in the Great Plains of the United States. Journal of Hydrologic Engineering, 9(5), 360-367.

41. Gianfilippo, M., Giovanni, F., Marcello, M., Onofrio, L., Enrico, P., Silvia, F., Davide, A., Raoul, R., Marco di, F., Renato, S., 2023. Country report for Slovenia, in San-Miguel-Ayanz et al. (Eds), Forest Fires in Europe, Middle East and North Africa 2022, Publications Office of the European Union, Luxembourg, doi:10.2760/348120, JRC135226.

42. González-Hidalgo, J. C., Lopez-Bustins, J. A., Štepánek, P., Martin-Vide, J., & de Luis, M. (2009). Monthly precipitation trends on the Mediterranean fringe of the Iberian Peninsula during the second-half of the twentieth century (1951–2000). Int. J. Climat., 29(10), 1415-1429.

43. González-Hidalgo, J.C., Brunetti, M., De Luis, M. (2010). Precipitation trends in Spanish hydrological divisions, 1946-2005. Climate research, 43(3), 215.

44. González-Hidalgo, J.C., De Luis M, Raventos, J., Sanchez, J.R. (2003) Daily rainfall trend in the Valencia region of Spain. Theor. Appl. Climatol. 75: 117–130.

45. Guhathakurta, P., Rajeevan, M. (2008). Trends in the rainfall pattern over India. Int. J. Climat., 28(11), 1453-1469.

46. Hänsel, S., Petzold, S., Matschullat, J. (2009). Precipitation trend analysis for central eastern Germany 1851–2006. In Bioclimatology and Natural Hazards (pp. 29-38). Springer Netherlands.

47. Hansen, J., Johnson, D., Lacis, A., Lebedeff, S., Lee, P., Rind, D., Russell, G. (1981). Climate impact of increasing atmospheric carbon dioxide. Science 213(4511), 957-966.

48. Harris, I., Osborn, T.J., Jones, P. & Lister, D.H. (2020). Version 4 of the CRU TS monthly high-resolution gridded multivariate climate dataset. Sci Data 7,109. https://rdcu.be/b3nUI

49. Hartmann, D.L., Klein Tank, A.M.G., Rusticucci, M., Alexander, L.V., Brönnimann, S., Charabi, Y., Dentener, F.J., Dlugokencky, E.J., Easterling, D.R., Kaplan, A., Soden, B.J., Thorne, P.W., Wild M., Zhai, P.M. (2013): Observations: Atmosphere and Surface. In: Climate Change 2013: The Physical Science Basis. Contribution of Working Group I to the Fifth Assessment Report of the Intergovernmental Panel on Climate Change [Stocker, T.F., D. Qin, G.-K. Plattner, M. Tignor, S.K. Allen, J. Boschung, A. Nauels, Y. Xia, V. Bex and P.M. Midgley (eds.)]. Cambridge University Press, Cambridge, United Kingdom and New York, NY, USA.

50. Haylock, M. R., Peterson, T. C., Alves, L. M., Ambrizzi, T., Anunciação, Y. M. T., Baez, J., ... & Vincent, L. A. (2006). Trends in total and extreme South American rainfall in 1960-2000 and links with sea surface temperature. Journal of climate, 19(8), 1490-1512.

51. Haylock, M., Nicholls, N. (2000). Trends in extreme rainfall indices for an updated high quality data set for Australia, 1910-1998. Int. J. Climatol., 20(13), 1533-1541.

52. Held, I.M., Soden, B.J. (2000). Water vapor feedback and global warming 1. Annual review of energy and the environment, 25(1), 441-475.

53. Helsel, D.R., Hirsch, R.M. (1992). Statistical methods in water resources (Vol. 49). Elsevier.
54. Hirsch, R. M., Slack, J. R., Smith, R. A. (1982). Techniques of trend analysis for monthly water quality data. Water Resour Res, 18(1), 107-121.
55. Hirsch, R.M., Alexander, R.B., & Smith, R.A. (1991). Selection of methods for the detection and estimation of trends in water quality. Water Resour Res, 27(5), 803-813.
56. Hirsch, R.M., Slack, J.R. (1984). A nonparametric trend test for seasonal data with serial dependence. Water Resources Research, 20(6), 727-732.
57. Hoerling, M., Hurrell, J., Eischeid, J., Phillips, A. (2006). Detection and attribution of twentieth-century northern and southern African rainfall change. Journal of climate, 19(16), 3989-4008.
58. Huld, T. A., Šúri, M., Dunlop, E. D., & Micale, F. (2006). Estimating average daytime and daily temperature profiles within Europe. Environ Modell Softw, 21(12), 1650-1661.
59. Hulme, M., Osborn, T.J., Johns, T.C. (1998). Precipitation sensitivity to global warming: comparisons of observations with HadCM2 simulations. Geophys. Res. Lett. 25, 3379–3382.
60. IPCC, 2013. Summary for Policymakers. In: Stocker, T.F., Qin, D., Plattner, G.-K., Tignor, M., Allen, S.K., Boschung, J., Nauels, A., Xia, Y., Bex, V., Midgley, P.M. (Eds.), Climate Change 2013: The Physical Science Basis. Contribution of Working Group I to the Fifth Assessment Report of the Intergovernmental Panel on Climate Change. Cambridge University Press, Cambridge, United Kingdom; New York, New York, USA.
61. IPCC, 2013. Summary for Policymakers. In: Stocker, T.F., Qin, D., Plattner, G.-K., Tignor, M., Allen, S.K., Boschung, J., Nauels, A., Xia, Y., Bex, V., Midgley, P.M. (Eds.), Climate Change 2013: The Physical Science Basis. Contribution of Working Group I to the Fifth Assessment Report of the Intergovernmental Panel on Climate Change. Cambridge University Press, Cambridge, United Kingdom; New York, New York, USA.
62. Jain, S. K., Kumar, V. (2012). Trend analysis of rainfall and temperature data for India. Current Science (Bangalore), 102(1), 37-49.
63. Jeffrey, S.J., Carter, J.O., Moodie, K.B., & Beswick, A.R. (2001). Using spatial interpolation to construct a comprehensive archive of Australian climate data. Environ Modell Softw, 16(4), 309-330.
64. João, M., João, P., Paula, M., Miguel, C., 2023. Country report for Slovenia, in San-Miguel-Ayanz et al. (Eds), Forest Fires in Europe, Middle East and North Africa 2022, Publications Office of the European Union, Luxembourg, doi:10.2760/348120, JRC135226.
65. Jones, P.D., Moberg, A. (2003). Hemispheric and large-scale surface air temperature variations: An extensive revision and an update to 2001. J Climate 16(2), 206-223.
66. Jošt, J., 2023. Country report for Slovenia, in San-Miguel-Ayanz et al. (Eds), Forest Fires in Europe, Middle East and North Africa 2022, Publications Office of the European Union, Luxembourg, doi:10.2760/348120, JRC135226.
67. Karl, T.R., Knight, R.W. (1998). Secular trends of precipitation amount, frequency, and intensity in the United States. Bulletin of the American Meteorological society, 79(2), 231-241.
68. Karl, T.R., Meehl, G.A., Peterson, T.C., Kunkel, K.E., Gutowski, W.J., Easterling D.R. (2008). Executive summary in weather and climate extremes in a changing climate. Regions of focus: North America, Hawaii, Caribbean, and U.S. Pacific Islands, report, edited by T. R. Karl et al., U.S. Clim. Change Sci. Program and Subcomm. on Global Change Res., Washington, D. C.
69. Karpouzos, D.K., Kavalieratou, S., Babajimopoulos, C. (2010). Trend analysis of precipitation data in Pieria Region (Greece). European Water, 30, 31-40.
70. Kendall, M.G. (1962). Rank Correlation Methods. 3rd ed. Hafner. Publishing Company, New York.

71. Kim, M., Madden, M., Warner, T. Forest type mapping using object-specific texture measures from multispectral Ikonos imagery: Segmentation quality and image classification issues. Photogramm. Eng. Remote Sens. 2009, 75, 819–829.

72. Klein Tank, A.M.G., Wijngaard, J.B., Können, G.P., Böhm, R., Demarée, G., Gocheva, A., ... & Petrovic, P. (2002). Daily dataset of 20th-century surface air temperature and precipitation series for the European Climate Assessment. Int J Climatol 22(12), 1441-1453.

73. Klein Tank, A.M.G., Wijngaard, J.B., Können, G.P., Böhm, R., Demarée, G., Gocheva, A., ... & Petrovic, P. (2002). Daily dataset of 20th-century surface air temperature and precipitation series for the European Climate Assessment. Int. J. Climat., 22(12), 1441-1453.

74. Kostopoulou, E., & Jones, P. D. (2005). Assessment of climate extremes in the Eastern Mediterranean. Meteorol Atmos Phys 89(1-4), 69-85.

75. Kruger, A.C., Shongwe, S. (2004). Temperature trends in South Africa: 1960–2003. Int J Climatol 24(15), 1929-1945.

76. Kutiel, H., Maheras, P. (1998) Variations in the temperature regime across the Mediterranean during the last century and their relationship with circulation indices. Theor Appl Climatol, 61, 39-53.

77. LaDochy, S., Medina, R., Patzert, W. (2007). Recent California climate variability: spatial and temporal patterns in temperature trends. Clim Res 33(2), 159-169.

78. Lettenmaier, D.P., Wood, E.F., Wallis, J.R. (1994). Hydro-climatological trends in the continental United States, 1948-88. Journal of Climate, 7(4), 586-607.

79. Liebmann, B., Kiladis, G.N., Vera, C.S., Saulo, A.C., Carvalho, L.M. (2004). Subseasonal variations of rainfall in South America in the vicinity of the low-level jet east of the Andes and comparison to those in the South Atlantic convergence zone. Journal of Climate, 17(19), 3829-3842.

80. Livezey, R.E., Chen, W.Y. (1983). Statistical field significance and its determination by Monte Carlo techniques. Monthly Weather Review, 111(1), 46-59.

81. Longobardi, A., Villani, P. (2010). Trend analysis of annual and seasonal rainfall time series in the Mediterranean area. Int. J. Climat., 30(10), 1538-1546.

82. López-Moreno, JI., Vicente Serrano, SM., Angulo-Martínez, M.,Begueria, S., Kenawy, A. (2010). Trends in daily precipitation on the northeastern.

83. Lu, H., Jing, W., Zhao, J., Liu, X., Huang, Z. (2014). Characteristics of the Temporal Variation in Temperature and Precipitation in China's Lower Yellow River Region. Advances in Meteorology, 2014.

84. Luo, Y., Wang, Z., Liu, X., Zhang, M. (2014). Spatial and Temporal Variability of Precipitation in Haihe River Basin, China: Characterization and Management Implications. Advances in Meteorology, 2014.

85. Maheras, P., Tolika, K., Anagnostopoulou, C., Vafiadis, M., Patrikas, I., & Flocas, H. (2004). On the relationships between circulation types and changes in rainfall variability in Greece. Int. J. Climat., 24(13), 1695-1712.

86. Mann, H.B. (1945). Nonparametric tests against trend. Econometrica: Journal of the Econometric Society, 245-259.

87. Martínez, M.D., Serra, C., Burgueño, A., Lana, X., 2010. Time trends of daily maximum and minimum temperatures in Catalonia (NE Spain) for the period 1975–2004. Int J Climatol 30, 267–290.

88. Milijenko, D., Ante, K., Siniša P., 2023. Country report for Croatia, in San-Miguel-Ayanz et al. (Eds), Forest Fires in Europe, Middle East and North Africa 2022, Publications Office of the European Union, Luxembourg, doi:10.2760/348120, JRC135226.

89. New, M., Hewitson, B., Stephenson, D.B., Tsiga, A., Kruger, A., Manhique, A., ... & Lajoie, R. (2006). Evidence of trends in daily climate extremes over southern and west Africa. J Geophys Res Atmos (1984–2012), 111(D14).

90. Norrant, C., Douguédroit, A. (2006). Monthly and daily precipitation trends in the Mediterranean (1950–2000). Theoretical and Applied Climatology, 83(1-4), 89-106.

91. Oliver, J.E. (1980). Monthly precipitation distribution: a comparative index. The Professional Geographer, 32(3), 300-309.

92. Pagliara, S., Viti, C., Gozzini, B., Meneguzzo, F., Crisci, A. (1998). Uncertainties and trends in extreme rainfall series in Tuscany, Italy: Effects on urban drainage network design. Wat. Sci. Tech., 37(11), 195–202.

93. Palmieri, S., Siani, A.M., D'Agostino, A. (1991). Climate fluctuations and trends in Italy within the last 100 years. In Annales geophysicae (Vol. 9, No. 12, pp. 769-776). Copernicus.

94. Phillips, D.L., Marks, D.G. (1996). Spatial uncertainty analysis: propagation of interpolation errors in spatially distributed models. Ecol Model 91(1-3), 213-229.

95. Piao, S., Liu, H., Shen, Z., Peng, J., Zhang, Y., Niu, S., ... & Tan, J. (2017). Global Change and Terrestrial Ecosystems. In The Geographical Sciences During 1986-2015 (pp. 205-232). Springer Singapore.

96. Piervitali, E., Colacino, M., Conte, M. (1998). Rainfall over the Central-Western Mediterranean basin in the period 1951-1995. Part I: Precipitation trends. Nuovo cimento della Società italiana di fisica. C, 21(3), 331-344.

97. Plummer, N., Lin, Z., Torok, S. (1995). Trends in the diurnal temperature range over Australia since 1951. Atmos Res 37(1-3), 79-86.

98. Polemio, M., Casarano, D. (2008). Climate change, drought and groundwater availability in southern Italy. Geological Society, London, Special Publications, 288(1), 39-51.

99. Qian, W., Lin, X. (2005). Regional trends in recent precipitation indices in China. Meteorology and Atmospheric Physics, 90(3-4), 193-207.

100. Ricotta, C., Bajocco, S., Guglietta, D., Conedera, M. (2018). Assessing the Influence of Roads on Fire Ignition: Does Land Cover Matter? Fire, 1, 24.

101. Rittl, T., Cooper, M., Heck, R.J., Ballester, M.V.R. (2013). Object-based method outperforms per-pixel method for land cover classification in a protected area of the Brazilian Atlantic rainforest region. Pedosphere, 23, 290–297.

102. Rodrigo, F.S., Trigo, R.M. (2007). Trends in daily rainfall in the Iberian Peninsula from 1951 to 2002. Int. J. Climat., 27(4), 513-529.

103. San-Miguel-Ayanz, J., Durrant, T., Boca, R., Maianti, P., Liberta`, G., Jacome Felix Oom, D., Branco, A., De Rigo, D., Suarez-Moreno, M., Ferrari, D., Roglia, E., Scionti, N., Broglia, M., Onida, M., Tistan, A. and Loffler, P., (2023). Forest Fires in Europe, Middle East and North Africa 2022, Publications Office of the European Union, Luxemburg, doi:10.2760/348120, JRC135226.

104. Sharma, C. S., Panda, S. N., Pradhan, R. P., Singh, A., Kawamura, A. (2016). Precipitation and temperature changes in eastern India by multiple trend detection methods. Atmos Res 180, 211-225.

105. Solomon, S., et al. (2007), Technical summary, in Climate Change 2007: The Physical Science Basis. Contribution of Working Group I to the Fourth Assessment Report of the Intergovernmental Panel on Climate Change, edited by S. Solomon et al., pp. 19–91, Cambridge Univ. Press, Cambridge, U. K.

106. Sonali, P., Kumar, D. N. (2013). Review of trend detection methods and their application to detect temperature changes in India. J Hydrol, 476, 212-227.

107. Taylor, W.A. (2000). Change-point analysis: a powerful new tool for detecting changes. preprint, available as http://www.variation.com/cpa/tech/changepoint.html.

108. Tolika, K., Maheras, P., Tegoulias, I., (2009). Extreme temperatures in Greece during 2007: could this be a “return to the future”? Geophysical Research Letters, 36, 1–5.

109. Toreti, A., Desiato, F. (2008). Changes in temperature extremes over Italy in the last 44 years. Int J Climatol 28(6), 733-745.

110. Trenberth, K. E., Smith, L., Qian, T., Dai, A., & Fasullo, J. (2007). Estimates of the global water budget and its annual cycle using observational and model data. J Hydrometeorol 8(4), 758-769.

111. Vaes, G., Willems, P., Berlamont, J. (2002). 100 years of Belgian rainfall: Are there trends? Water Sci. Technol., 45, 55-61.

112. Ventura, F., Pisa, P. R., Ardizzoni, E. (2002). Temperature and precipitation trends in Bologna (Italy) from 1952 to 1999. Atmos Res 61(3), 203-214.

113. Vincent, L.A., Peterson, T.C., Barros, V.R., Marino, M.B., Rusticucci, M., Carrasco, G., ... & Grimm, A.M. (2005). Observed trends in indices of daily temperature extremes in South America 1960-2000. J Climate, 18(23), 5011-5023.

114. Viola, F., Liuzzo, L., Noto, L. V., Lo Conti, F., La Loggia, G. (2013). Spatial distribution of temperature trends in Sicily. Int J Climatol 34(1), 1-17.

115. Vose, R. S., Easterling, D. R., & Gleason, B. (2005). Maximum and minimum temperature trends for the globe: An update through 2004. Geophys Research Lett 32(23).

116. WMO (ed.). 1992. International meteorological vocabulary, Volume WMO/OMN/BMO-No.182. Secretariat of the World Meteorological Organization.

117. Xoplaki, E., Gonzalez-Rouco, J.F., Luterbacher, J., Wanner, H. (2003). Mediterranean summer air temperature variability and its connection to the large-scale atmospheric circulation and SSTs. Climate Dynamics, 20(7-8), 723-739.

118. Yue, S., Wang, C.Y. (2002). Applicability of prewhitening to eliminate the influence of serial correlation on the Mann-Kendall test. Water Resources Research, 38(6), 4-1.

119. Zhai, P., Zhang, X., Wan, H., Pan, X. (2005). Trends in total precipitation and frequency of daily precipitation extremes over China. J Climate 18(7), 1096-1108.

120. Zhou, L., Dai, A., Dai, Y., Vose, R. S., Zou, C. Z., Tian, Y., & Chen, H. (2009). Spatial dependence of diurnal temperature range trends on precipitation from 1950 to 2004. Climate Dynamics, 32(2-3), 429-440.